HISTONE DYNAMICS IN DNA DAMAGE AND REPAIR

INAUGURALDISSERTATION

zur

Erlangung der Würde eines Doktors der Philosophie

vorgelegt der

Philosophisch-Naturwissenschaftlichen Fakultät

der Universität Basel

von

Michael Hermann Hauer

aus Deutschland

Basel, 2019

Genehmigt von der Philosophisch-Naturwissenschaftlichen Fakultät

auf Antrag von

Prof. Dr. Susan M. Gasser

Prof. Dr. Tom Owen-Hughes

Basel, den 23 Mai 2017

Prof. Dr. Martin Spiess

Dekan

CONTENTS

THESIS SUMMARY

The overall perspective of my PhD project was to uncover the mechanisms that generate DNA damage-dependent chromatin mobility and to identify the players implicated in this process. To tackle this problem, I investigated the physical characteristics and composition of chromatin under DNA damaging conditions. I see my PhD project divided into two mayor themes:

(I) Identifying physical chromatin changes under DNA damaging conditions (mainly using microscopic assays)

(II) Addressing changes in chromatin protein composition upon DNA damage and DNA damage checkpoint activation (using Western blot analysis, genome-wide nucleosome mapping, microscopy and quantitative mass spectrometry)

This thesis consists of six chapters. **Chapter 1** introduces the structure and function of chromatin and shows how it changes in response to DNA damage. **Chapter 2** gives an in-depth overview about the function of chromatin remodeling enzymes during DNA double-strand break repair. **Chapters 3-5** summarize my main scientific contributions. In **Chapter 6**, I discuss the findings of my work, draw conclusions and present future prospectives.

My main project led to the finding that remodeling enzymes trigger chromatin mobility in response to DNA damage by a mechanism that involves the proteasomal degradation of nucleosomes. Nucleosomes are essential for proper chromatin organization and the maintenance of genome integrity. Histones are post-translationally modified and often evicted at sites of DNA breaks, facilitating recruitment of repair factors. Whether such chromatin changes are localized or genome-wide has been a question of debate. Using a range of quantitative methods, we show that histone levels drop by 20-40% in response to DNA damage, due to eviction from chromatin by the INO80 remodeler and degradation by the proteasome. Chromatin decompaction and increased fiber flexibility accompany histone degradation, but also occur in the absence of damage when histone levels are reduced by other means. As a result, recombination rates and DNA repair focus turnover are enhanced. Thus, we propose that a generalized reduction in nucleosome occupancy is an integral part of the DNA damage response, providing mechanisms for enhanced chromatin mobility and homology search.

This thesis includes the following publications:

Peer-reviewed publications

Gonzalez-Sandoval, A., B. D. Towbin, V. Kalck, D. S. Cabianca, D. Gaidatzis, **M. H. Hauer**, L. Geng, L. Wang, T. Yang, X. Wang, K. Zhao and S. M. Gasser (2015). "Perinuclear Anchoring of H3K9-Methylated Chromatin Stabilizes Induced Cell Fate in C. elegans Embryos." Cell 163(6): 1333-1347.

Hauer, M. H., A. Seeber, V. Singh, R. Thierry, R. Sack, A. Amitai, M. Kryzhanovska, J. Eglinger, D. Holcman, T. Owen-Hughes and S. M. Gasser (2017). "Histone degradation in response to DNA damage enhances chromatin dynamics and recombination rates." Nat Struct Mol Biol 24(2): 99-107.

Review articles and editorials

Hauer, M.*, Seeber, A.*, and Gasser, S.M. (2013). Nucleosome remodelaers in double-strand break repair. Current Opinion in Genetics & Development 23, 174-184.

Gerhold, C. B., **M. H. Hauer** and S. M. Gasser (2015). "INO80-C and SWR-C: guardians of the genome." J Mol Biol 427(3): 637-651.

*equal contribution

CHAPTER 1: INTRODUCTION TO HISTONE DYNAMICS IN DNA DAMAGE AND REPAIR

Chromatin structure

Nucleosomes: The building blocks of chromatin

The organization of genomic DNA into chromatin is common amongst all eukaryotes, with its principles of architecture being conserved from yeast to man. The most basic and repeating unit of chromatin is the nucleosome which is formed by 146 base pairs (bp) of DNA that wrap around an octameric core of histone proteins (**Fig. 1a**). A canonical nucleosome is composed of the four core histones H2A, H2B, H3 and H4. Histones are small, positively charged proteins containing both an N-terminal histone tail and a central histone fold domain (HFD). The hydrophobic HFD serves as dimerization module prompting the formation of H2A-H2B and H3-H4 dimers, whereas a positively charged histone surface stabilizes histone-DNA interactions (for review, see (Malik and Henikoff 2003); (Khorasanizadeh 2004) and (Talbert, Ahmad et al. 2012)). Canonical nucleosome core particles contain two H3-H4 and two H2A-H2B dimers, forming an inner $(H3\text{-}H4)_2$ tetrameric core flanked by two separate 2x(H2A-H2B) dimers (Luger, Mader et al. 1997). In contrast to this compact core, the flexible and lysine-rich histone tails extend away from the nucleosome core particle.

These core histones are among the most highly conserved proteins in all eukaryotes (Malik and Henikoff 2003) and their evolutionary origin can be tracked back to archaea (Sandman, Krzycki et al. 1990) where, in the case of *M. fervidus*, tetrameric, nucleosome-like histone structures were found to bind and compact DNA (Pereira, Grayling et al. 1997). Within each histone type the primary amino acid sequence is highly conserved across species, yet the level of conservation among all histone variants is most apparent with respect to the secondary and tertiary protein structure of the HFD (Arents and Moudrianakis 1995) which defines the common nominator for all histones.

Next to histones, high mobility group proteins are the second most abundant proteins found on chromatin (for review see (Travers 2003) and (Bianchi and Agresti 2005)). Small, highly charged proteins, they have a variety of different functions ranging from the establishment of proper chromatin architecture to the control of transcriptionally active and inactive chromatin regions. There are three major families of HMG proteins: HMGA, HMGN, HMGB. HMGA proteins contain an AT hook and bind to AT rich DNA sequences. HMGN proteins bind inside nucleosomes. HMGB proteins contain

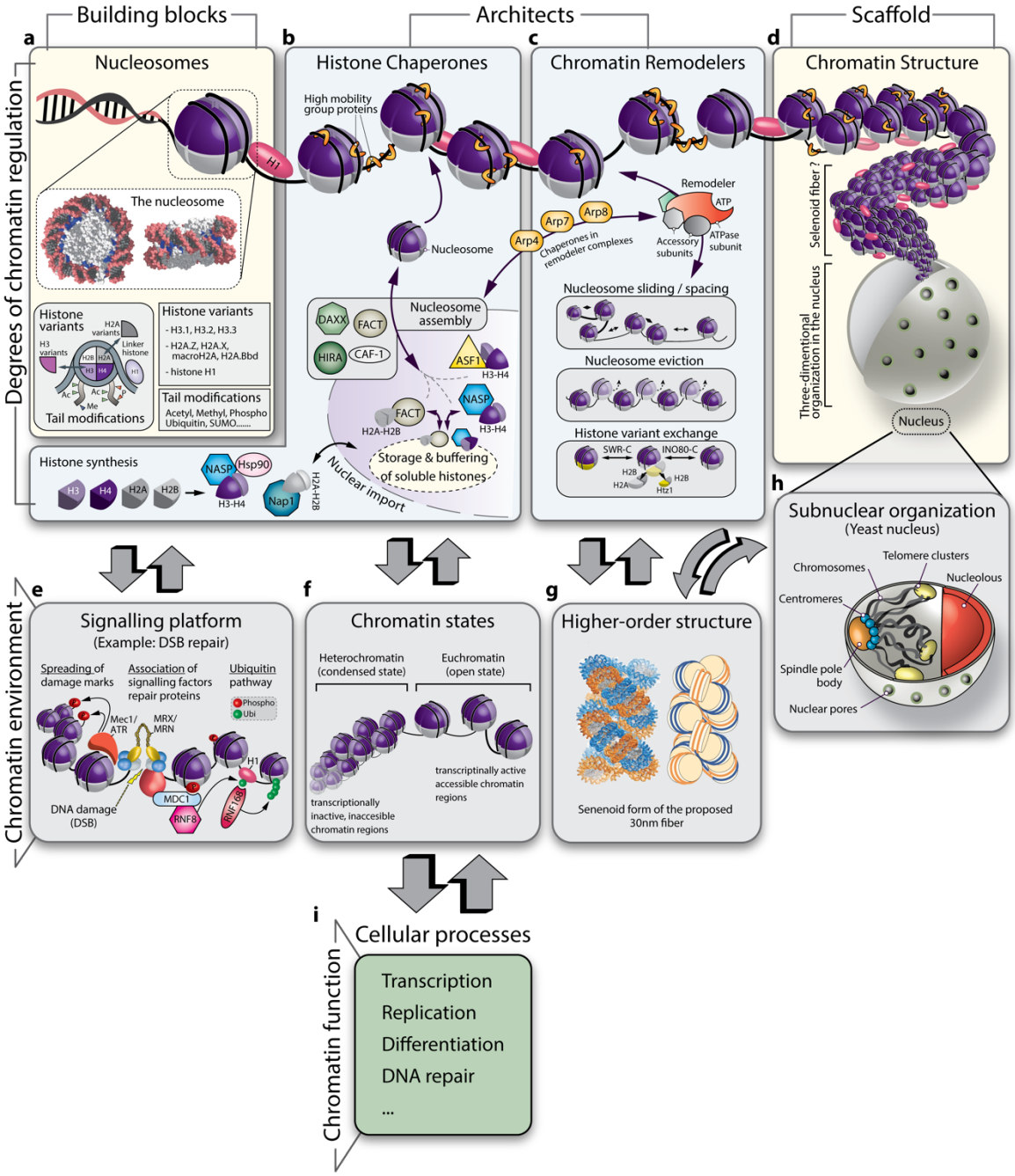

Figure 1 Chromatin structure and function. (**a**) Overview of nucleosomes as the building blocks of chromatin. Nucleosomes come in many different "flavors" owing to a multitude of histone variants and histone tail modifications. (**b**) Illustrates the role of histone chaperones in protecting newly synthesized histones and assembling them into nucleosomes. (**c**) Chromatin remodeling complexes and their role in organizing nucleosomes along DNA. (**d**) Chromatin adopts a scaffold structure. Chromatin has roles during (**e**) DSB repair, forms (**f**) different states of compaction and fold into (**g**) higher-order structures. (**h**) Chromatin organization and subcompartmentalization of the yeast nucleus. (**i**) Different degrees of chromatin compaction and its local environment impact a variety of cellular processes

HMG boxes, 80 amino acid domains that bind to the minor groove of DNA (Bianchi and Agresti 2005, Malarkey and Churchill 2012). HMGB1 has well studied roles in enhancing transcription (Celona, Weiner et al. 2011). Yeast has two HMGB homologues called Nhp6 A and B (non-histone protein) (Stillman 2010).

Histone variants

Despite the high level of conservation among core histones, nucleosomes can come in many different flavors owing to the existence of additional, non-canonical histone variants and the vast combinatorial variety of post-translational modifications (PTMs) (**Fig. 1a**, reviewed in (Campos and Reinberg 2009)). Lower eukaryotes like the budding yeast *Saccharomyces cerevisiae*, express a single version of each inner-core (H3, H4) and outer-core (H2A, H2B) histone alongside with two non-canonical histone variants Htz1 and Hho1. Their counterparts in higher eukaryotes, H2A.Z and H1, are highly conserved. H1 is a special histone as it lacks the HDF domain and serves as a unique structural linker histone. While the exact role of Hho1 in yeast remains somewhat enigmatic, H1 is an abundant component of higher eukaryotic chromatin, where it associates with the linker DNA between nucleosomes (**Fig. 1**). This impacts chromatin structure, compaction and folding (Panday and Grove 2017). In contrast to H1, all other histone variants retain the typical HFD, but differ in other aspects of amino acid sequence. Few H2B and H4 variants exist, while there are multiple H2A and H3 variants: H2A.Z is an abundant H2A variant found throughout chromatin where it accumulates at +1 nucleosome in promoter regions (Guillemette, Bataille et al. 2005, Li, Eirin-Lopez et al. 2005, Raisner, Hartley et al. 2005, Albert, Mavrich et al. 2007), and, to a lesser extent, throughout gene bodies. The pattern of H2A.Z positioning over coding regions and near gene promoters clearly highlights its role in transcriptional regulation, which is well documented in both yeast and mammalian cells (Rando and Winston 2012). In addition to the role in transcription, various reports implicate H2A.Z or Htz1 in DNA repair pathways (Kalocsay, Hiller et al. 2009, Morillo-Huesca, Clemente-Ruiz et al. 2010). Notably, yeast *htz1* deletion alleles are hypersensitive to DNA damaging agents (Kalocsay, Hiller et al. 2009). This hypersensitivity probably reflects indirect effects on transcriptional as well as direct effects on repair. Besides H2A.Z, mammals, flies and worms express H2A.X, another H2A variant. H2A.X does not significantly differ from the canonical H2A except for an additional C-terminal motif. H2A.X is found uniformly along chromatin, and its most prominent feature is that it can be phosphorylated on a C-terminal serine residue in response to DNA damage. In humans, H2A.X phosphorylation occurs at serine S139 generating γH2A.X, while in yeast the canonical H2A contains a serine at S129 that serves the same role, generating γH2A (Rogakou, Pilch et al. 1998, Downs, Lowndes et al. 2000). Two additional H2A variants, macroH2A and H2A.Bbd (Barr body deficient), are found exclusively in mammals. H2A.Bbd

expression is restricted to brain tissue and testes where its function remains largely unknown (Campos and Reinberg 2009). Both macroH2A and H2A.Bbd fail to fully accommodate within the nucleosome particle. Therefore, they are believed to confer a more open nucleosomal state (Zhou, Fan et al. 2007) (Luger, Dechassa et al. 2012). Interestingly, macroH2A was found to bind chromatin in a Poly(ADP-ribose) (PAR)-dependent manner (Timinszky, Till et al. 2009, Khurana, Kruhlak et al. 2014) and accumulate at DNA double-strand breaks (DSBs) as well as UV damaged sites (Xu, Xu et al. 2012).

With respect to histone H3, three different variants (H3.1, H3.2 and H3.3) are found in all higher eukaryotes, where H3.1 and H3.2 are synthetized and loaded during DNA replication. In contrast, the histone variant H3.3 is expressed and deposited into chromatin throughout the cell cycle in a transcription-independent manner (Gurard-Levin, Quivy et al. 2014)). Yeast only use one histone H3.3-like variant for both pathways. Finally, centromere-specific H3 variants (CenpA in humans and Cse4 in budding yeast) define centromeric regions for proper chromosome function and segregation.

Histone post-translational modifications

Histone variants play an important role in diversifying nucleosome structure, providing a means to modulate nucleosome composition and compaction along the genome (**Fig. 1a**). They respond to the genomic context, while generating a nucleosomal context. An additional layer of nucleosome modifications is achieved by post-translationally modifying histone tails, in particular the N-terminal tails of histones H3 and H4 (Campos and Reinberg 2009) and (Zentner and Henikoff 2013). Based on their mode of action, the impact of histone PTMs on chromatin structure can be divided into three categories: intrinsic, extrinsic or effector-mediated. Intrinsic effects directly influence physical nucleosome stability by altering histone-histone or histone-DNA interactions. This depends on the localization of the modified residue within the nucleosome core particle. Histone PTMs that act extrinsically on chromatin change inter-nucleosomal contacts and thereby affect higher order chromatin structure and organization. The effector-mediated impact describes chromatin changes which arise though the recruitment and action of chromatin-modifying proteins to histone PTMs. In all cases, histone modifying enzymes like acetyltransferases (HATs) and methyltransferases (HMTs) catalyze the covalent attachment of acetyl and methyl moieties to lysine residues. This neutralizes positive charges and regulates the association of chromatin binding proteins.

Many experiments, ranging from early chromatin fractionation (Hebbes, Clayton et al. 1994) to genome-wide ChIP-sequencing (Wang, Zang et al. 2008), have identified highly repetitive and transcriptionally silent heterochromatin as a hypoacetylated domain. Depending on different subtypes of

heterochromatin, the histones can be further enriched for either H3 lysine 9 di- or tri-methylation (H3K9me2/3), which recruits heterochromatin protein 1 (HP1), or for H3K27me3, which recruits the Polycomb repressive complex 1 (PRC1) (Nielsen, Oulad-Abdelghani et al. 2001, Jacobs and Khorasanizadeh 2002, Fischle, Wang et al. 2003). Transcriptionally silent heterochromatin generally also assumes a specific spatial distribution within the nuclear space. Repressive, H3K9me3-enriched chromatin is associated with the nuclear envelope, forming lamin associated domains (LADs). In humans, lamina association may be achieved through direct interactions of HP1 with integral lamin B-type receptors or through binding of barrier-to-autointegration factor (BAF) to LEM-domain proteins (Towbin, Gonzalez-Sandoval et al. 2013)). In embryos of the nematode *C. elegans,* a nuclear envelope protein and direct H3K9me3 reader called CEC-4, bridges between heterochromatin and the inner nuclear membrane (Gonzalez-Sandoval, Towbin et al. 2015).

Taken together, these hallmarks of heterochromatin confer a closed chromatin state which protects vulnerable parts of the genome from rearrangements by preventing illegitimate transcription or deleterious recombination events (reviewed in Zeller and Gasser, in prep.). In contrast, euchromatin generally excludes H3K9 methylation. Indeed, transcriptionally active regions are found in a hyperacetylated state which promotes chromatin unfolding and favors binding of the transcription machinery. Transcribed genes show an enrichment of H4K16ac and H3K4me3 within their 5' region whereas H3K36me3 accumulates towards the 3' end of the gene (Hebbes, Clayton et al. 1994). Such active modifications keep gene bodies open for transcription factor binding and the successful assembly of the transcription machinery.

Histone modifications also have important functions at sites of DNA lesions after genotoxic events. The most prominent modification is the phosphorylation of histone variant H2A.X on its C-terminal serine by the checkpoint kinases ATR and ATM (Mec1 and Tel1 in yeast) (Rogakou, Pilch et al. 1998, Downs, Lowndes et al. 2000). After initial phosphorylation, γH2A.X spreads from the site of damage creating a positive feedback loop which recruits various repair factors and amplifies DNA damage checkpoint (DDC) signaling. H2A.X is not the only histone modified by PTMs in response to DNA damage. Specific H4 acetylation and methylation events occur (H4K16ac, H4K20me), together with histone H1 and H2B ubiquitylation. Both are known to function during the DNA damage response (DDR). Acetylation of H4K16 in response to DNA damage is carried out by the HATs TIP60 and MOF (Murr, Loizou et al. 2006, Sharma, So et al. 2010). Whereas MOF regulates global levels of H4K16Ac with important roles in replication, TIP60 localizes to DSBs and modifies H4K16 in a site specific manner (Akhtar and Becker 2000). Interestingly, depletion of either MOF or TIP60 shows defects in DSB repair. E3 ubiquitin ligases bear similar functions at sites of DNA damage. At the site of a DSB, the heterodimeric

RNF20-40 complex monoubiquitinates H2BK120. This coincides with RNF8 E3 ligase-mediated ubiquitination of Histone H1. RNF168, another ubiquitin ligase, subsequently binds to ubiquitinated H1 and targets H2AK13 and K15. Ubiquitination events carried out by the combined function of RNF8/RNF168 favor the recruitment of 53BP1, a protein channeling DSB repair through non-homologous end joining (NHEJ), by protecting from resection. In contrast, H4K16ac together with monoubiquitinated H2BK120 was shown to promote chromatin relaxation and facilitates the recruitment of factors that promote resection and repair by homologous recombination (HR) (Schwertman, Bekker-Jensen et al. 2016))

Taken together, histone PTMs work alongside histone variants to define nucleosome structure and orchestrate repair within chromatin. Histone modifications can partition the genome into domains of different epigenetic states, with nucleosomes at the base of genome organization, as the building block of chromatin (**Fig. 1a**). Following this hierarchy of genomic organization from DNA into chromatin fibers, it is clear that a highly regulated enzymatic machinery must exist to orchestrate the assembly and disassembly of histones into nucleosomes, their deposition and proper placement along the DNA fiber. Two large protein families of histone chaperones and nucleosome remodeling complexes carry out the majority of these "architectural" tasks. These are discussed in the next paragraph.

Histone chaperones and nucleosome remodelers: The architects of chromatin

Once histones are synthesized in the cytoplasm, they are immediately bound by dedicated histone chaperones (**Fig. 1b**). As a consequence, free histones are basically non-existent in a cellular context. If not incorporated into chromatin, histones reside in a chaperone-associated form that either shields their hydrophobic histone-histone (Natsume, Eitoku et al. 2007) or buffers their charged surface (Andrews, Chen et al. 2010) preventing improper nucleosome assembly, unspecific binding to DNA and unscheduled histone degradation. Chaperones have overlapping as well as unique roles in histone binding, buffering and transfer (De Koning, Corpet et al. 2007) and (Gurard-Levin, Quivy et al. 2014)). In brief, mammalian NASP (nuclear autoantigenic sperm protein) binds to canonical H3-H4 dimers protecting them from degradation and regulating their transfer into the nucleus. Nap 1 (Nucleosome-assembly protein 1) carries out similar functions as NASP, but acts on H2A-H2B dimers. While NASP and Asf1 (anti-silencing function 1) have overlapping roles in buffering soluble pools of canonical H3-H4 within the nucleus, the FACT (facilitates chromatin transcription) complex associates with H2A-H2B dimers and plays a major role in safeguarding histones before and after the passage of transcription polymerases. The CAF-1 (chromatin assembly factor 1) complex has a unique function in regulating H3.1-H4 assembly into nucleosomes during replication. In contrast, DAXX (death domain–associated protein) and HIRA

(histone regulator A) coordinate H3.3-H4 dimer assembly independent of new DNA synthesis, often in a transcription coupled manner.

Following the assembly of histones into chromatin-bound nucleosomes, the level of nucleosome packaging and the access of DNA binding proteins to specific sequence motifs can be altered by chromatin remodeling complexes (remodelers) (**Fig. 1c**). Remodelers do not assemble new nucleosomes from histone dimers, yet they often work in concert with or subsequent to chaperones. Remodelers contain subunits that bind histones, such as the actin related proteins Arp4, Arp5, Arp7, Arp8 and Arp9 in *S. cerevisiae,* which bridge between chaperone function and remodeler action (**Fig. 1bc**). Remodelers also contain a catalytic subunit that harbors a large Swi2/Snf2 (switch/sucrose non-fermenting) ATPase. This subunit uses the energy of ATP hydrolysis to exchange histone variants as well as evict, slide and space nucleosomes along DNA. Such actions regulate gene transcription, DNA replication, repair and chromatin structure genome-wide (Clapier and Cairns 2009) and (Seeber, Hauer et al. 2013)). Except for human Alc1 (amplified in liver cancer 1) and Fun30 (yeast function unknown protein 30, SMARCAD1 in humans), the majority of Snf2 ATPases act as part of large macromolecular assemblies. Each catalytically active ATPase is surrounded by different auxiliary subunits, including DNA helicases, histone modifying enzymes, histone mark readers, actin related proteins and actin itself. Some of these subunits are shared among remodeling complexes, others are unique. An in-depth overview on chromatin remodeler composition and function with a focus on DNA damage and repair is given in **Chapter 2** as well as in (Clapier and Cairns 2009).

Higher-order chromatin folding and subnuclear organization

While the role of the nucleosome as the basic repeating unit of chromatin is clear (**Fig. 1d**), there is a continuing debate whether or not interphase chromatin is organized into a solenoid helix, that was called the 30nm fiber (**Fig. 1g**). In the 30 nm fiber folding model, regularly spaced nucleosomal arrays of the 10nm fiber level (primary structure) are folded into a 30nm fiber (secondary structure), which itself can be subjected to larger-scale configurations (tertiary structure) through long range chromatin interactions. This higher-order structure defines the way chromatin occupies the nuclear space (Zhou, Fan et al. 2007). The formation of a 30nm fiber requires the selective binding of nucleosomes that are in close proximity to each other on the DNA strand, and generally histone modifications, linker lengths and linker histones themselves (e.g. H1) determine whether a "one start" solenoid or a "two start" zigzag helix is formed (Dorigo, Schalch et al. 2004, Schalch, Duda et al. 2005, Robinson, Fairall et al. 2006, Li and Reinberg 2011). In contrast to the 30nm fiber model which is largely based on the folding of the nucleosomal fiber in vitro, other studies argue based on in vivo measurements, that interphase chromatin is a mesh of 10nm fibers (beads on a string) (Eden Fussner 2010). Thus, an alternative model proposes that interphase nucleosomes

exist in a highly disordered, interdigitated state that prevents the formation of 30nm fibers (Zhou, Fan et al. 2007, Maeshima and Eltsov 2008, Luger, Dechassa et al. 2012). Similar to the 30nm fiber model, the state of interdigitation is thought to be regulated by nucleosome spacing, nucleosome composition and other chromatin associated proteins (Luger, Dechassa et al. 2012). Thus, the existence of secondary and tertiary structural elements in vivo remains controversial. Nonetheless, it is clear that modifying the plasticity and the dynamics of chromatin can have dramatic effects on DNA metabolism.

Beyond the higher order folding of the chromatin fiber, chromatin domains and chromosomes themselves are ordered within the nuclear space. In yeast, chromosomes assume a Rabl conformation (**Fig. 1h**), through which all centromeres cluster at one point, near the membrane-embedded spindle pole body (SPB), while telomeres are anchored at other sites around the nuclear rim (Gotta, Laroche et al. 1996, Bystricky, Laroche et al. 2005, Duan, Andronescu et al. 2010). Furthermore, the highly repetitive and transcribed rDNA is found in a single, crescent shaped nucleolus in yeast, which defines yet another subnuclear compartment. Apart from spatially organizing chromosomes, nuclear position can also have far reaching effects on transcription (Taddei, Van Houwe et al. 2006) and DNA repair (Nagai, Dubrana et al. 2008, Oza, Jaspersen et al. 2009).

Chromatin dynamics during DSB repair

All cells, post-mitotic or proliferating, are challenged by thousands of DNA damaging events every day. Damage is induced by exogenous (radiation, radiomimetic cancer drugs or toxins) as well as endogenous (free radicals from cell internal metabolism) agents (Lindahl and Barnes 2000, Jackson and Bartek 2009)). One of the most common sources of exogenous damage to which we are exposed every day is solar ultraviolet (UV) light. When the high energy from short wavelength UV rays is released on the DNA backbone, thymidine base dimers are formed. Such bulky DNA adducts can be bypassed by translesion synthesis (TLS) or efficiently repaired through a process called nucleotide excision repair (NER). If left unresolved, such adducts pose a barrier to replicative or transcription polymerases and can cause the formation of single-stranded (SSBs) as well as double-stranded (DSBs) DNA breaks. The same threat applies to endogenous replication stress which is caused through excessive DNA base damage or by a lack of free nucleotides for de-novo DNA synthesis. When replication forks collapse, both SSB and DSB formation has been observed. In contrast to breaks which are formed through cellular processes, ionizing radiation (IR) or radiomimetic drugs like Zeocin (also known as Bleomycin) can more directly induce SSBs and DSBs (Povirk, Wubter et al. 1977).

DNA damage checkpoint activation and homology directed DSB repair

Given the diversity of DNA lesions possible, a large array of specialized repair pathways has evolved, employing a multitude of repair proteins, some dedicated to unique types of repair, and others serving multiple pathways. Common to most genomic insults is the activation of the DNA damage response pathway (DDR). It is initiated by a highly conserved kinase signaling cascade called the DNA damage checkpoint (DDC) (**Fig. 2a**). Following damage sensing and activation of a central DDC checkpoint kinase, downstream transducer proteins, some of which are also kinases, initiate and fine-tune repair pathway choice and recovery. A DSB can trigger one of two major repair pathways. Non-homologous end joining (NHEJ), which ligates the free DNA ends back together, or homologous recombination (HR) which copies information from a DNA template (the sister chromatid or an ectopic donor) to repair the break (Heyer, Ehmsen et al. 2010) and (Symington and Gautier 2011)). Post-mitotic mammalian cells prevalently use NHEJ, whereas replicative cells show a substantial, albeit low level of HR. Yeast spend much of their lifetime in S- or G2-phase which makes HR the preferred pathway for DSB repair. While NHEJ can be error prone and introduce small insertions or deletions (INDELs), HR faithfully restores the original sequence information. If HR is not mediated by an intact sister chromatid, but by the homologous chromosome, it is possible that a diploid cell might lose its heterozygous state (LOH).

A DSB repaired by HR is first bound by the damage sensing MRX/MRN complex which activates the key checkpoint kinases Mec1/ATR and Tel1/ATM (**Fig. 2c**). Transducer proteins (Rad9/53BP1, MDC1) help to transmits the damage signal to downstream effector kinases (Rad53/CHK2, CHK1) and trigger full DDC activation. This response spreads within the entire nucleus and stimulates the recruitment of repair proteins to the sites of DNA damage. Early repair factors like helicases (Sgs1/BLM) disentangle DNA to facilitate resection by the exonucleases Sae2/CtIP, EXO1 and DNA2. Helicase action highlights the fact that DNA structure needs to change during repair. This becomes especially important during HR directed DSB repair as it requires both the access to the lesion as well as to the homologous templates for later D-loop formation, strand invasion and successful repair.

Nucleosomes can obstruct repair factor access (**Fig. 2c**). To overcome this barrier, several chromatin remodeling complexes like INO80-C, SWR1-C/SRCAP-C and RSC are recruited to DSB sites (Morrison, Highland et al. 2004, van Attikum, Fritsch et al. 2004, Chai, Huang et al. 2005). Remodelers shift nucleosomes, exchange histone variants or evict whole nucleosomes. This is thought to increase chromatin accessibility for repair. For instance, INO80-C binds to H2A.Z containing nucleosomes where it exchanges H2A.Z-H2B dimers for canonical H2A-H2B (Papamichos-Chronakis, Watanabe et al. 2011). The reverse action is catalyzed by SWR1-C which incorporates H2A.Z–H2B dimers into nucleosomes in

a stepwise and unidirectional fashion (Luk, Ranjan et al. 2010). While INO80 and RSC have well studies roles in DSB repair, many other remodelers function on similar pathways. Another remodeler that has recently been implicated in DSB repair is Fun30 and its human homologue SMARCAD1. Both proteins were shown to promote Exo1 and Dna2-mediated long-range resection through chromatin (Chen, Cui et al. 2012, Costelloe, Louge et al. 2012, Eapen, Sugawara et al. 2012). In vivo, Fun30 acts as a bone fide remodeler, being able to catalyze histone dimer exchanges and nucleosome re-positioning (Awad, Ryan et al. 2010). In yeast, Fun30 binding to DSBs has recently been shown to depend on an interaction network including the damage scaffold protein Dpb11/TopBP1 and the 9-1-1 complex (Bantele, Ferreira et al. 2017). Furthermore, Fun30 has important roles in deactivating the DNA damage checkpoint after repair (Chen, Cui et al. 2012, Eapen, Sugawara et al. 2012). An extensive overview on remodeler action during DSB repair is given in **Chapter 2**.

Extensive resection creates long 3' single stranded (ss) DNA overhangs flanking the break. Overhangs are subsequently bound and protected by the ssDNA binding complex RPA. Widespread RPA binding feeds back into the DDC through accumulation of additional Mec1/ATR. In both yeast and mammals this is accompanied by γH2A (γH2A.X in mammals) phosphorylation; a mark which helps Mec1/ATR spreading. This further highlights the fact that chromatin serves as a signaling platform during DSB repair (**Fig. 2c**).

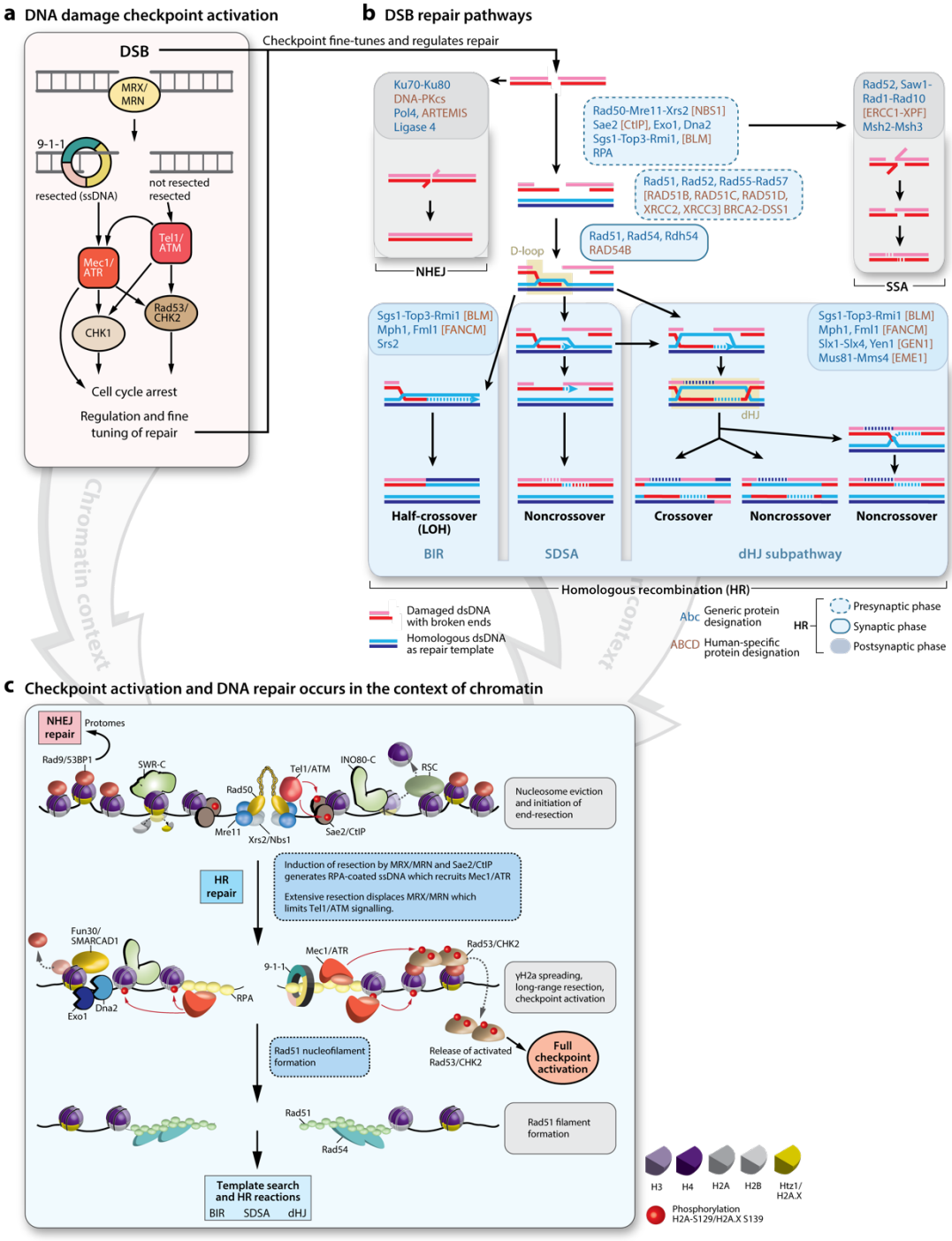

Figure 2 Checkpoint activation and DSB repair in the context of chromatin. (**a**) Proteins involved in DNA damage checkpoint activation in response to a DSB. Mammalian proteins are capitalized. (**b**) DSB repair pathways. Blue protein names refer to yeast proteins corresponding mammalian names are in brackets and brown. Proteins without a yeast homologue are brown with no bracket. Dashed lines indicate DNA synthesis. DSBs can be repaired by at least three pathways: non-homologous end joining (NHEJ), single-strand annealing (SSA) and homologous recombination (HR). Adapted from (Heyer, Ehmsen et al. 2010). (**c**) Both the DNA damage checkpoint and DSB repair need to integrate into chromatin. The key steps and the main players during HR directed DSB repair are listed. The first panel highlights early steps after DSB occurrence. The second panel illustrates DSB processing and spreading of the DDC signal. The last panel shows the Rad51 nucleofilament before homology search and later strand invasion and repair.

Rad51 nucleofilament formation follows RPA binding and is initiated through Rad52-dependent displacement of RPA. The nucleofilament then engages in a physical search for its homologous template which can be the sister chromatid if replication has already occurred, or an ectopic, non-sister donor sequence. This process of homology search has long been considered as one of the central mechanisms which would require chromatin movement. Physically moving DNA within the nucleus requires structural changes within chromatin. Thus, both damage signaling and repair needs to be integrated within chromatin. Chromosomes undergo spatial organization and compartmentalization within the nucleus. Thus, an inherently difficult task is presented to homology directed repair if the donor template is spatially distant or even in another subcompartment of the nucleus. Cells solve this dilemma through controlled relocalization events and by increasing the physical mobility of damaged DNA within the nucleus - both processes are thought to promote homology search and repair and will be discussed in detail.

DSB repair within the nuclear space – a matter of position

The 16 yeast chromosomes assume a Rabl conformation within the interphase nucleus. Both their terminal ends and their central regions undergo clustering and subcompartmentation. Telomeres come together in 4-5 foci at the nuclear periphery. Centromeres also cluster spatially at the inner nuclear membrane through microtubules that link the centromere to the yeast centrosome equivalent, called the spindle pole body (SPB) (**Fig. 1h**)(Bystricky, Laroche et al. 2005, Duan, Andronescu et al. 2010). Whereas in species with an open mitosis the centrosome-kinetochore link is set up only in mitosis, in budding yeast, which has a closed mitosis, short MTs link chromosomes to the SPB throughout the cell cycle. The SUN (Sad1-Unc-84-related) domain protein Mps3 and the acidic Esc1 protein are integral parts of the inner nuclear membrane and independently anchor telomeres to suppress subtelomeric recombination (Schober, Ferreira et al. 2009). However, telomere positon is dynamic and when they become critically short, they are released from their peripheral anchor for telomerase-dependent elongation (Ferreira, Luke et al. 2011). This observation, together with the notion that Rad52 foci, are preferentially found internally (Bystricky, Van Attikum et al. 2009) led to the general hypothesis that canonical homologous recombination is favored within the interior of the nucleus while the periphery suppresses recombination and favors alternative repair pathways (Horigome, Bustard et al. 2016). Nuclear compartmentalization is conserved among species and different chromosomes occupy distinct regions within the nucleus. Furthermore, in all species known, heterochromatin domains cluster together (Taddei and Gasser 2012)).

The main gate that controls traffic in and out of the nucleus is the nuclear pore complex (NPC). It consists of more than 30 different protein species which form subcomplexes that are arranged in an eight-fold symmetry and penetrate the outer and inner nuclear membrane (Bukata, Parker et al. 2013). The

Nup84 subcomplex has been identified to serve as a binding site for persistent DSBs (Nagai, Dubrana et al. 2008, Kalocsay, Hiller et al. 2009, Oza, Jaspersen et al. 2009) which occur at collapsed replication forks (Nagai, Dubrana et al. 2008, Su XA 2015), in subtelomereic regions (Therizols, Fairhead et al. 2006) or can be artificially induced by endonuclease expression (**Fig. 3**) (Nagai, Dubrana et al. 2008, Oza, Jaspersen et al. 2009). It was further noted that DSBs localize to another type of inner nuclear membrane protein - the SUN domain protein Mps3 in budding yeast. This is equally true in the fission yeast *Schizosaccharomyces pombe* where DSBs associate with Sad1, a member of the LINC (linker of nucleoskeleton and cytoskeleton) complex. Studies by the Gasser and King laboratories have investigated the requirements for DSB binding to Nup84 and/or Mps3 and identified the factors which distinguish them (Horigome, Oma et al. 2014, Swartz, Rodriguez et al. 2014). The association of DSBs with Nup84 was further shown to occur independent of the cell cycle phase and required neither the chromatin remodeler INO80C nor the recombinase activity of Rad51. Hence, extensive resection of the break was dispensable (Horigome, Oma et al. 2014). In contrast, Mps3 or Sad1 binding happened uniquely in S/G2 phase and was dependent on resection. Here, binding to Mps3 further required both INO80 remodeling function and Rad51 activity. Importantly, direct targeting of SWR1 via LexA fusions shifted chromatin to the nuclear periphery even in the absence of DNA damage (Yoshida, Shimada et al. 2010, Horigome, Oma et al. 2014). SWR1 mediated Htz1 (H2A.Z) incorporation was necessary for both binding to pores and Mps3. Horigome *et al.,* moreover, used a functional assay that scored for sister chromatid exchange and showed that mutations in the two binding sites have additive repair defects. This suggested that sequestration at Mps3 and the nuclear pore regulate different DSB repair outcomes.

Previous work indicated that the Slx5/Slx8 SUMO-targeted ubiquitin ligase (STUbL) interacts with nuclear pores both in yeast (Nagai, Dubrana et al. 2008) and the fly *Drosophila melanogaster* (Ryu, Spatola et al. 2015). In addition, several studies identified Slx5/Slx8 as a suppressor for gross chromosomal rearrangement (GCR) events (Zhang, Roberts et al. 2006, Nagai, Dubrana et al. 2008). Combined with the notion that STUbLs contain SUMO-interacting motifs (SIMs) (Sarangi and Zhao 2015) and the fact that repair proteins of many different pathways are SUMOylated (Cremona, Sarangi et al. 2012, Psakhye and Jentsch 2012) it became obvious to test whether SUMO ligases contribute to the relocation of damage to the nuclear envelope. The question arose whether Slx5/Slx8 has an active role in relocating DSBs or instead processes them at the periphery? Four recent studies (Ryu, Spatola et al. 2015, Su XA 2015, Churikov, Charifi et al. 2016, Horigome, Bustard et al. 2016) have addressed this question

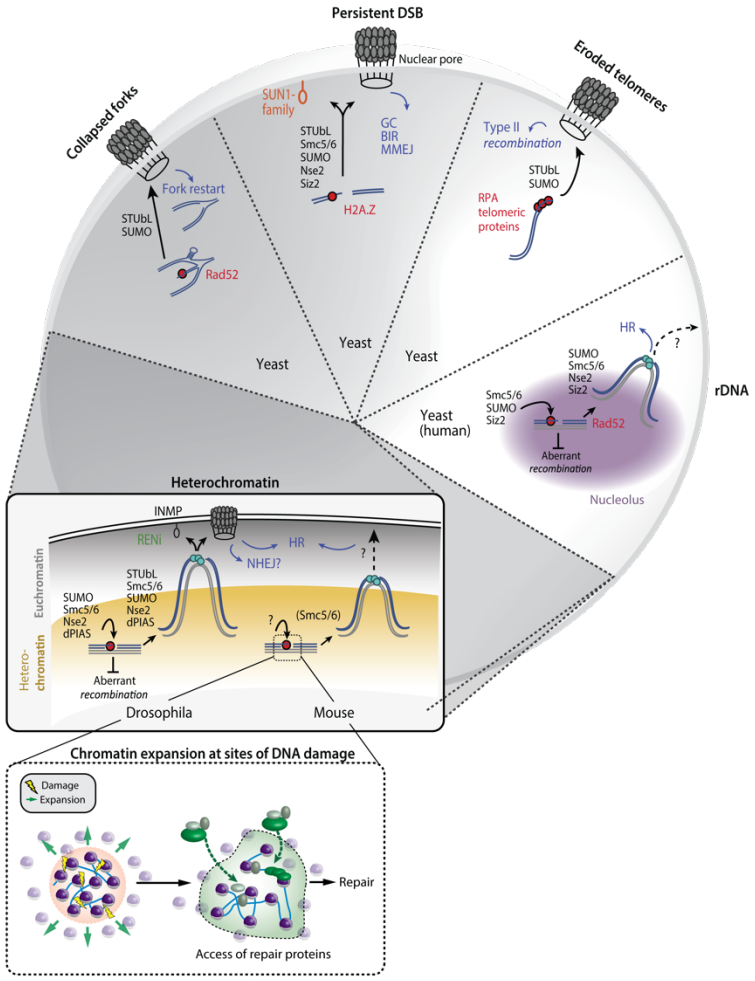

Figure 3 Relocalization pathways and signaling mechanisms in yeast, *Drosophila* and humans. Adopted from (Amaral, Ryu et al. 2017). The models show how different types of DNA damage are relocated to the nuclear periphery - either to nuclear pores or other anchors within the inner nuclear membrane. Collapsed replication forks, persistent DSBs and eroded telomeres all shift to nuclear pores with different requirements. A two-step pathway was identified for DSBs in heterochromatic domains. Here, breaks first move outside of the heterochromatic domain and then towards the nuclear periphery. The differences and similarities in this pathway is illustrated for *Drosophila* and mice. The lowest panel in the figure indicates how chromatin expansion at the site of a DSB could increase repair factor access to promote efficient repair.

at induced DSBs, eroded telomeres, and collapsed replication forks in budding yeast and Drosophila (Seeber and Gasser 2016)). In yeast, polySUMOylation mediated by the E3 ligases Siz2 and Mms21 targeted Slx5/Slx8 to persistent breaks in G1 phase with both Slx5 and Slx8 being indispensable for damage relocation to nuclear pores. In contrast, monoSUMOylation during S phase was sufficient to shift resected breaks to Mps3. Here, relocation occurred independently of Slx5/Slx8. Functionally, Slx5/Slx8-dependent DSB binding to pores appears to favor repair by ectopic break-induced replication (BIR) and/or imprecise end-joining. In a parallel study by the Chiolo laboratory using *Drosophila* cells, it was

shown that DSBs in heterochromatin, which are known to accumulate at the outer rim of heterochromatic domains (Chiolo, Minoda et al. 2011) (**Fig. 3**), shifted further towards the nuclear periphery (Ryu, Spatola et al. 2015). While relocation events followed the same SUMOylation and STUbL dependencies as in yeast, binding differed since it occurred both at nuclear pores and the fly Mps3 homologues Koi and Spag4 (Chiolo, Minoda et al. 2011).

Whereas these two studies focused on induced DSBs, similar work was pursued by the Geli and Lisby laboratories which focused on the molecular requirements for the relocation of eroded telomeres to the nuclear periphery. Shortened telomeres arise from replicative ageing-related telomerase loss (Churikov, Charifi et al. 2016) (**Fig. 3**). Once critically short, they become unprotected and elicit Mec1-dependent checkpoint activation and growth arrest (Hector, Ray et al. 2012). Most of the cells die or remain arrested, but some survivors can escape by rearranging their telomeres through rare recombination events (Zakian 1999). Churikov *et al.* found that critically shortened telomeres are relocated to the NPC in a SUMO-dependent pathway very similar to that observed at DSBs in yeast and *Drosophila*. The shift of eroded telomeres to the NPC involved Slx5-Slx8-dependent targeting of poly-SUMOylated proteins and is proposed to facilitate telomere repair events either through de-SUMOylation or proteasomal degradation events (Churikov, Charifi et al. 2016).

Collectively, these studies defined a conserved and SUMOylation-dependent pathway which shifts damage from a subnuclear context to a peripheral anchor – either being the NPCs or the inner nuclear membrane protein Mps3/SUN1. In this context, relocation is thought to favor alternative repair pathways whereas failure to move appears to be detrimental for the recovery from the insult.

Repair in heterochromatic domains: Where DSB relocation integrates with chromatin structure

Apart from shifting damage to the nuclear periphery, DSB relocation events have been observed in the context of heterochromatin. Heterochromatic regions consist of highly repetitive sequences which are prone to non-allelic, ectopic recombination. Illegitimate recombination events can cause translocations, duplications and deletions often found in human diseases such as cancer and infertility (Pearson, Nichol Edamura et al. 2005). To preserve genome integrity, repair within these regions needs to be tightly regulated. Compared to HR, NHEJ in repetitive DNA is potentially less problematic as small insertions or deletions would not affect the overall function of tandem repeats as severely as genes. Thus, the question remained whether heterochromatic DSBs are repaired either by NHEJ, HR or both. Furthermore, it was not known whether the highly compacted and rigid heterochromatic domains would need to be expanded in response to DNA damage to allow repair protein access. Studies on the spatial dynamics of DSB repair

in the context of heterochromatin greatly benefitted from the organization of heterochromatic regions in a distinct domain within the nucleus, a phenomenon conserved from yeast to man.

In yeast and humans, the highly transcribed and repetitive rDNA elements cluster together in a prominent subnuclear domain – the nucleolus. This site of ribosome biosynthesis separates from the rest of the genetic material and displays heterochromatic properties. An early study in yeast found that induced DSBs in the rDNA context need to shift their position and move towards the outside of the nucleolar volume in order to be processed for homologous recombination (Torres-Rosell, Sunjevaric et al. 2007). Nucleolar exclusion depended on Rad52 SUMOylation by the Smc5/6-Mms21 SUMO ligase complex and is thought to prevent illegitimate recombination events within the clustered rDNA repeats. Consequently, mutations which abrogated this shift caused rDNA hyperrecombination and genome instability (Torres-Rosell, Sunjevaric et al. 2007). Recently, two reports showed remarkable conservation of this pathway in human cells (Harding, Boiarsky et al. 2015, van Sluis and McStay 2015). In both studies, persistent DSB in the rDNA reorganized within the nucleolus shifted away from this repetitive compartment, exactly as had been described in yeast (Torres-Rosell, Sunjevaric et al. 2007, Harding, Boiarsky et al. 2015, van Sluis and McStay 2015). This coincided with ATM-dependent inhibition of RNA polymerase I, an important step to prevent collision between the repair and transcription machineries. Harding *et al.* additionally found that NHEJ was the prevalent pathway allowing transcriptional restart if repair could occur quickly (Harding, Boiarsky et al. 2015).

Pericentric and centromeric repeats in humans and flies are also organized in a heterochromatic subcompartment within the nucleus, and the Karpen laboratory made the interesting observation that pericentric DSB repair happened with striking similarities to the rDNA situation in flies. Namely, irradiation-induces DSBs in heterochromatin were relocated before they could be repaired by HR (Chiolo, Minoda et al. 2011). Whereas proteins involved in early resection events were rapidly recruited to the breaks, recombination steps that involved Rad51 mediated strand invasion only occurred after the shift (Chiolo, Minoda et al. 2011). Break relocation itself depended on checkpoint and resection proteins whereas the Smc5/6 SUMO E3 ligase complex was required to exclude Rad51 from heterochromatic domains and prevent abnormal recombination (Chiolo, Minoda et al. 2011). As described above, the Chiolo lab now extended this *Drosophila* study, showing that pericentromeric DSBs further undergo SUMOylation dependent anchoring to the NPC or at inner nuclear membrane proteins after having relocated to the edge of the heterochromatic domains (INMPs) (Ryu, Spatola et al. 2015). This appears to be an essential step before Rad51 recruitment could occur to promote HR repair.

Most of the studies discussed so far uniquely addressed HR repair of heterochromatic DSB and found that it happened only after breaks had relocated away from the repressive compartment (Torres-Rosell, Sunjevaric et al. 2007, Ayoub, Jeyasekharan et al. 2008, Chiolo, Minoda et al. 2011, Jakob, Splinter et al. 2011, Harding, Boiarsky et al. 2015, Ryu, Spatola et al. 2015, van Sluis and McStay 2015). Moreover, a subset of these studies reported repair kinetics in the context of heterochromatin to be significantly slower as in euchromatin (Chiolo, Minoda et al. 2011, Ryu, Spatola et al. 2015). When Harding *et al.* compared the kinetics of HR and NHEJ specifically in heterochromatin, these two major repair pathways showed further temporal variation (Harding, Boiarsky et al. 2015). On the one hand, the general impact of NHEJ in heterochromatin repair is questioned and on the other hand it raises questions concerning the exact timeframe of both HR or NHEJ in repetitive genomic regions. Two recent studies refine previous findings and provide answers to both questions (Janssen, Breuer et al. 2016, Tsouroula, Furst et al. 2016). Jannsen and colleagues used an in vivo system to induce heterochromatic or euchromatic single DSBs in *Drosophila* and followed their repair kinetics in space and time. Their results recapitulated the spatio–temporal dynamics of irradiation induced breaks (Chiolo, Minoda et al. 2011, Ryu, Spatola et al. 2015). Yet, live cell imaging together with sequence analysis of repair products revised earlier findings by showing that DSBs in euchromatin and heterochromatin follow strikingly similar repair kinetics and employ both NHEJ and HR (Janssen, Breuer et al. 2016). The spatial uncoupling of DSB repair pathways (NHEJ vs. HR) in mammalian heterochromatin was addressed by the Soutoglou laboratory and provided answers to how repair varies in different heterochromatic compartments (Tsouroula, Furst et al. 2016). Sophisticated microscopy techniques were used to track the repair of CRISPR-Cas9-induced, pericentric or centromeric DSBs during different stages of cell cycle. While pericentric breaks in G1 phase were repaired by NHEJ and remained positionally stable, HR during S/G2 could only occur after breaks had relocated to the edge of the pericentric domain. Centromeric breaks behaved differently and all repair events underwent heterochromatic exclusion. DSB relocation was further found to depend on DNA resection followed by Rad51/BRCA2 binding and DSB stabilization to prevent repair by another, deleterious recombination pathway called single-strand annealing (SSA) (Tsouroula, Furst et al. 2016).

In conclusion, these results emphasize the general importance of spatially separating HR mediated repair events from highly repetitive sequences. In heterochromatic regions, a SUMOylation and StUBL dependent pathway shifts damage away from the repeats such that DSBs are physically isolated from other ectopic sequences, a mechanism most likely preventing aberrant recombination. While the functional importance and the key players of this process have been fairly well described, the question remains whether highly compacted and inaccessible heterochromatic domains undergo additional structural changes in response to DNA damage. This hypothesis becomes tempting as changing chromatin structure

after DNA insults would both provide a basis for the observed long-range shifts of broken DNA as well as increase the access of repair proteins to the lesions.

Chromatin unfolds in response to DNA damage

Heterochromatin is highly compacted and inaccessible. This restrictive chromatin nature mainly relies on densely packaged nucleosomes, repressive histone marks (H3K9me3, H3K27me3) and other heterochromatin binding proteins such as HP1 and KAP-1 (Goodarzi, Noon et al. 2008, Polo, Kaidi et al. 2010). Since both NHEJ and HR reactions still need to occur close to or within heterochromatin, it was proposed that the accessibility of such domains must increase in response to DNA damage. Several studies have proven this hypothesis just and show that DNA damage indeed causes heterochromatin to unfold. In human fibroblasts or mouse NIH3T3 cells, chromatin relaxation in response to IR happened as a result of ATM-dependent KAP-1 phosphorylation and its subsequent loss from heterochromatin (Ziv, Bielopolski et al. 2006, Goodarzi, Noon et al. 2008, Beucher, Birraux et al. 2009, Goodarzi, Kurka et al. 2011, Woodbine, Brunton et al. 2011, Lee, Goodarzi et al. 2012). Interestingly, CHD3 (Goodarzi, Kurka et al.), a remodeler involved in chromatin compaction and gene repression (Denslow and Wade 2007) also dissociated upon KAP-1 phosphorylation. Comparable events were seen after treatment with tert-butyl hydroperoxide (TBH), an agent which confers oxidative damage (Woodbine, Brunton et al. 2011). Moreover, the yeast remodeler enzyme SWI/SNF facilitated Rad51 and Rad54 dependent strand invasion by alleviating heterochromatic constraints during recombinational repair in vitro (Sinha, Watanabe et al. 2009). In *Drosophila*, both checkpoint kinases ATM and ATR are required for global heterochromatin expansion which triggers DSB relocation together with an increase in the access of HR factors like Rad51 (Chiolo, Minoda et al. 2011, Ryu, Spatola et al. 2015). While heterochromatin relaxation equally occurs at site-specific, CRISPR-Cas9-induced DSBs in mice NIH3T3 cells, it was found that the the compacted state at pericentric or centromeric regions was neither refractory to RAD51 nor to KU80 (Tsouroula, Furst et al. 2016). Furthermore, RAD51 recruitment patterns were not altered after forced heterochromatin relaxation either through treatment with the deacetylase inhibitor Trichostatin A (TSA) or by tethering of the transcriptional activator VP64 (Tsouroula, Furst et al. 2016). The question whether heterochromatin expansion is functionally linked to relocation and whether it needs to occur before a DSB can be moved towards the edge of repressive domains is therefore currently under dispute. Tsouroula *et al.* further observed that heterochromatin expansion did neither cause KAP-1 alleviation nor a reduction in the heterochromatin-associated repressive mark H3K9me3 (Tsouroula, Furst et al. 2016). Surprisingly, H3K9 methylation even increased around DSBs. This is to some extent in line with observations previously made by the Misteli laboratory (Burgess, Burman et al. 2014). Here, laser-irradiation caused rapid chromatin

expansion but was followed by a localized compaction. The re-compaction was found to be important for checkpoint signaling but not for repair which suggests that specific chromatin configurations regulate different aspects of the DDR (Burgess, Burman et al. 2014). Furthermore, unfolding and compaction might happen at different time-scales after DNA damage indicating a blockage to certain factors while allowing the access of others. The exact mechanism that causes heterochromatin to unfold in response to DNA damage, and the extent to which re-compaction is integral to the DDR in human and mouse cells remains subject to further investigation.

Chromatin compaction in telomeres is also investigated in mammalian systems. Telomeres are structures with long TTAGG repeats that extend over many kilobases and end in a 3' ssDNA overhang which, if left unprotected, appears like a resected DSB ready for recombination. The shelterin complex (comprised of TRF1, TRF2 and other proteins) binds to telomeric ends and bends them into a protective form called "t-loop". T-loop formation blocks ATM binding which prevents DDR activation and illegitimate recombination events (Marcomini and Gasser 2015)). It has further been proposed that shelterin might mediate chromatin compaction at telomere ends as another means to prevent aberrant DNA damage signaling (Bandaria, Qin et al. 2016). Since DDR signaling is not strictly inhibited by chromatin compaction (Ziv, Bielopolski et al. 2006, Goodarzi, Noon et al. 2008) and chromatin re-compaction can, in some cases, even amplify DDC signaling (Burgess, Burman et al. 2014), it was difficult to predict a priori whether chromatin compaction could protect telomeres from DDR signaling. Bandaria *et al.* used super-resolution microscopy in HeLa cells and showed that the shelterin complex together with telomeric DNA organizes human telomeres into compact globular structures. Interestingly, knockdown of individual shelterin subunits or mutations that interfered with its assembly caused a 10-fold increase in telomere volume which was indicative for chromatin unfolding and directly linked to the accumulation of DDR signals at telomeres. This suggests that DNA compaction reduces the access of DDR factors at telomeres, hence termed the "telomere compaction model" (Bandaria, Qin et al. 2016).

Two recent studies now challenge this idea (Timashev, Babcock et al. 2017, Vancevska, Douglass et al. 2017). Super-resolution STROM microscopy in HeLa cells depleted for TRF1, TRF2 or both (Vancevska, Douglass et al. 2017) or in mouse cells (Timashev, Babcock et al. 2017) showed that accumulation of DDR markers like γH2A.X or 53BP1 at telomeres can occur without widespread chromatin decompaction (Timashev, Babcock et al. 2017, Vancevska, Douglass et al. 2017). In both cases, the knockdown of shelterin factors only affected the size of a small DDR-positive telomere subset, consistent with an increase in TTAGG fish signal. This is indicative of a previously known 53BP1-dependent clustering of dysfunctional telomeres. Whereas these studies neither exclude nor definitely

prove the possibility that a compacted chromatin state protects telomeres from aberrant DDR signaling (Parks and Stone 2017)), they do contribute to our understanding of telomere protection and the function of chromatin compaction in DDR signaling.

DNA damage is not restricted to heterochromatin or telomeres but occurs everywhere in the genome. As a consequence, the barrier of nucleosomes which confer global chromatin compaction needs to be overcome to allow repair factor binding. Accordingly, chromatin decondensation was found to be a universal prerequisite to promote repair of different DNA lesions including base damage, SSBs and DSBs. UV light causes base damage which is repaired by a process called nucleotide excision repair (NER). In this pathway, the detection of DNA lesions is stimulated by the damaged DNA-binding protein 2 (DDB2), a member of the cullin-RING ubiquitin ligase (CRL4) complex (Marteijn, Lans et al. 2014)). ZRF1, another NER protein, stabilizes the CRL4 complex at damaged sites (Gracheva, Chitale et al. 2016) and DICER processed non-coding RNAs were also found to assist in repair (Francia, Michelini et al. 2012, Wei, Ba et al. 2012). Fluorescence microscopy experiments in hamster AO3 cells showed that DDB2 elicits the unfolding of large chromatin structures at UV-induced damage sites in an ATP-dependent manner (Luijsterburg, Lindh et al. 2012). Interestingly, this agreed with a DDB2- and PARP1-dependent reduction in core histone density around the lesion (Luijsterburg, Lindh et al. 2012). Furthermore, the direct targeting of DDB2, ZRF1 or DICER to chromatin by a LacI fusion protein allowed the unfolding of chromatin even in the absence of DNA damage (Adam, Dabin et al. 2016, Chitale and Richly 2017). Under these conditions, DICER and ZRF1 function were shown to depend on PARP1 while the catalytic activity of DICER was dispensable (Chitale and Richly 2017).

Chromatin decompaction is also observed at DSBs which repair via NHEJ or HR. In human U2OS cells, PARP1 was shown to recruit the CHD2 remodeler to multiphoton micro-irradiation induced DSBs through a poly(ADP-ribose)[PAR]-binding domain. CHD2 triggered rapid chromatin expansion and the deposition of histone variant H3.3 (Luijsterburg, de Krijger et al. 2016). This was further required to assemble the NHEJ complex at broken chromosomes and promote efficient DSB repair (Luijsterburg, de Krijger et al. 2016). Another microscopy-based study used a molecular flow assay to measure chromatin compaction around irradiation induced DSBs (Hinde, Kong et al. 2014). By analyzing the flow of EGFP molecules into chromatin before and after DSB induction, Hinde *et al.* found that DNA damage induces a transient decrease in chromatin compaction which in turn facilitated NHEJ repair factor (Ku70) recruitment to the lesions (Hinde, Kong et al. 2014).

Similar effects were recently shown to occur during homology directed DSB repair in yeast. A study by the Gasser and Holcman laboratories used improved time-lapse imaging regimes and super-resolution microscopy to follow the spatial occupancy of chromatin in response to DNA a at site-specific DSB (Amitai, Seeber et al. 2017). Amitai and colleagues found that INO80-dependent chromatin expansion also occurred at site specific DSBs and further used mathematical polymer models which predicted that chromatin unfolding would favor DSB extrusion from compacted domains (Amitai, Seeber et al. 2017). These predictions held true during in vivo experiments and could explain how DSBs are excluded from the nucleolar volume for HR repair (Amitai, Seeber et al. 2017).

In summary, both mammalian and yeast chromatin unfolds and, in some cases, re-compacts in response to DNA damage. This is true for heterochromatic and euchromatic domains and potentially regulates different repair reactions and safeguards genome stability by modulating repair factor access. To some extent, telomere protection follows the same principles. Interestingly, all of these findings indicate large-scale changes in chromatin structure. However, the mechanism by which DNA relocates cannot be simply explained by chromatin expansion and other pathways must be at play to physically move broken DNA from one compartment to the next. This tempting hypothesis has found prove in a number of different studies which show how broken DNA increases its mobility within the nucleus with implications in HR repair both in yeast and mammalian cells (Dion, Kalck et al. 2012, Mine-Hattab and Rothstein 2012, Seeber, Dion et al. 2013, Lottersberger, Karssemeijer et al. 2015, Amitai, Seeber et al. 2017, Hauer, Seeber et al. 2017).

Chromatin mobility: On the move with native and broken DNA

A number of experiments over the past 20 years has shown that chromatin is not a static entity in yeast, flies, mice and humans, but undergoes defined movements within the nuclear space (Marshall, Straight et al. 1997, Bornfleth, Edelmann et al. 1999, Heun, Laroche et al. 2001, Vazquez, Belmont et al. 2001, Chubb, Boyle et al. 2002, Neumann, Dion et al. 2012) (Dion and Gasser 2013, Seeber and Gasser 2016). The majority of these movements showed sub-diffusive behavior (Weber, Theriot et al. 2010, Albert, Mathon et al. 2013, Amitai, Toulouze et al. 2015) indicating that chromatin could roam only within a restricted volume which was significantly smaller than that of the nucleus. This argued that internal forces must constrain chromatin movement (Marshall, Straight et al. 1997, Heun, Laroche et al. 2001, Vazquez, Belmont et al. 2001, Chubb, Boyle et al. 2002, Gasser, Hediger et al. 2004, Bystricky, Laroche et al. 2005). The mobility of a locus was indeed ATP-dependent in vivo (Marshall, Straight et al. 1997, Heun, Laroche et al. 2001, Levi, Ruan et al. 2005) and strongly influenced by the interaction with fixed elements at the

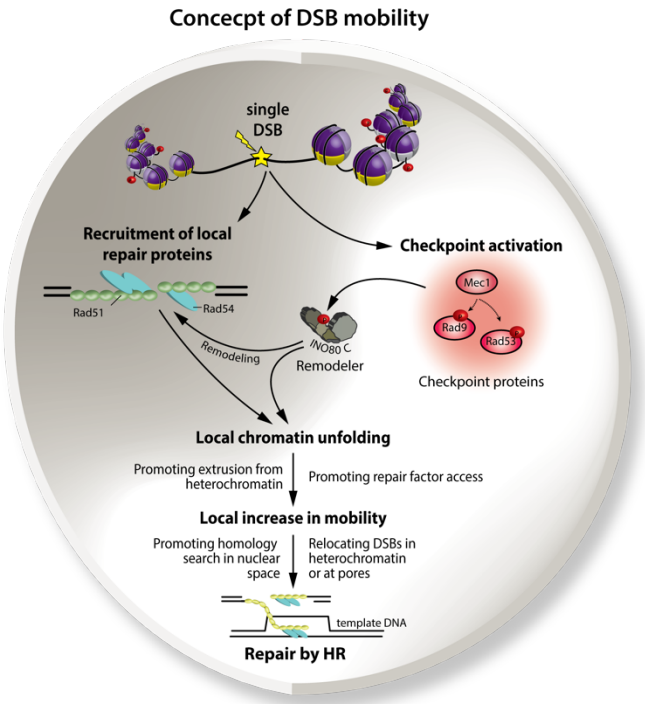

Figure 4 The concepts of local DSB mobility. The formation of a DSB activates the DNA damage checkpoint. The key checkpoint kinase Mec1 phosphorylates downstream effector proteins (Rad9 and Rad53) as well as chromatin remodeling complexes (INO80-C). If the DSB is repaired by HR, local repair proteins process the lesion and lead to the formation of the Rad51 nucleofilament which will enter homology search and engage in recombinational repair. Chromatin locally unfolds at the break site. This likely promotes extrusion from heterochromatic domains and increases the access of repair factors. Furthermore, DSBs become more mobile. This is thought to facilitate the homology search through nuclear space and promote relocation events to the nuclear periphery. Both the DNA damage checkpoint and chromatin remodelers have been implicated in DSB mobility.

nuclear envelope such as pores (Verdaasdonk, Vasquez et al. 2013, Horigome, Oma et al. 2014), the inner nuclear membrane protein Esc1 (Gasser, Hediger et al. 2004) or the spindle pole body (SPB) (Verdaasdonk, Vasquez et al. 2013, Strecker, Gupta et al. 2016, Lawrimore, Barry et al. 2017). Exemplary studies forced Silent Information Regulator (SIR) complex assembly on ectopic plasmids which shifted them to the nuclear envelope and abolished movement (Gasser, Hediger et al. 2004, Bupp, Martin et al. 2007). In contrast, circularizing the endogenous *LYS2* locus into a 16 kb ring which caused the constraint movement of *LYS2* to become freely diffusive after pop-out (Gasser, Hediger et al. 2004) argued for an additional source of drag that is posed on chromatin by the continuity and inherent flexibility of the chromatin fiber itself. Experiments which compared chromatin flexibility and the degree of movement at different loci along the genome enforced this notion (Verdaasdonk, Vasquez et al. 2013, Dickerson, Gierlinski et al. 2016). Furthermore, changing the local chromatin context directly impacted movement as seen in mobility changes after chromatin remodeler targeting (Neumann, Dion et al. 2012), the ablation of sister chromatid cohesion (Dion, Kalck et al. 2013), or forced nucleosome reduction from DNA (Bouck

and Bloom 2007, Verdaasdonk, Vasquez et al. 2013, Hauer, Seeber et al. 2017). Finally, INO80-dependent eviction of nucleosomes at the PHO5 locus in the absence of phosphate increases the movement of an appropriately tagged locus (Neumann, Dion et al. 2012). The notion that damaged chromatin underwent large structural changes and that DSBs were physically shifted either away from heterochromatic compartments (see previous paragraphs) or towards the nuclear periphery, made it tempting to test whether chromatin mobility would also change in response to DNA damage.

Investigations into this hypothesis have indeed shown that chromatin movement increases in response to DNA damage both at the site of an induced DSB (**Fig. 4**)(Dion, Kalck et al. 2012, Mine-Hattab and Rothstein 2012) and genome-wide at undamaged sites when multiple DSBs were present in the genome (Mine-Hattab and Rothstein 2012, Seeber, Dion et al. 2013, Hauer, Seeber et al. 2017). In both cases, the INO80 remodeler and proteins of the DDC were required for the increased mobility (Dion, Kalck et al. 2012, Mine-Hattab and Rothstein 2012, Seeber, Dion et al. 2013, Amitai, Seeber et al. 2017). Similar dependencies have recently been shown for mammalian cells where IR triggered an 53BP1 and ATM kinase dependent increase in locus movement (Lottersberger, Karssemeijer et al. 2015). Earlier work from the de Lange laboratory had shown that uncapped telomeres (which lack components of the protective shelterin complex) undergo increased movement and correlated with elevated rates of telomere end-to-end fusions. Both telomere movement and end-to-end fusion depended on 53BP1 (Dimitrova, Chen et al. 2008). In a more recent work, enhanced mobility of dysfunctional telomeres was further linked to SUN-domain-containing proteins which stay in contact with the LINC complex that bridges the nucleoskeleton to the cytoskeleton (Lottersberger, Karssemeijer et al. 2015). Following this intriguing observation, the authors also identified a role for cytoskeleton-bound kinesins in telomere fusions and the repair of internal breaks, suggesting that an active, kinesin-driven movement of the nucleus or elements in the nuclear envelope affects DSB repair (Lottersberger, Karssemeijer et al. 2015). In budding yeast, DSB mobility was correlated with efficient HR (Dion, Kalck et al. 2012, Hauer, Seeber et al. 2017), whereas DSBs that exhibited increased movement in human cells were more likely to result in genomic translocations events (Roukos, Voss et al. 2013). This argues that enhanced mobility is a tightly controlled and programmed event rather than a side effect of the DDR.

DSB mobility is thought to enhance the search for a homologous donor sequence required for DSB repair by HR (Rudin and Haber 1988, Weiner, Zauberman et al. 2009, Neumann, Dion et al. 2012). This seem to be especially important if the sister chromatid is equally broken or absent and an ectopic template becomes essential for successful repair. Furthermore, DSBs need to be mobile for relocation away from the bulk of heterochromatic repeats (Torres-Rosell, Sunjevaric et al. 2007, Chiolo, Minoda et al. 2011,

Harding, Boiarsky et al. 2015, Ryu, Spatola et al. 2015, van Sluis and McStay 2015, Tsouroula, Furst et al. 2016). Another benefit of increasing the mobility of DSBs or telomeres locally and the genome globally is to disassociate illegitimate pairing events during HR or re-attach a lost end for NHEJ (Lottersberger, Karssemeijer et al. 2015). However, the mechanisms that generate enhanced chromatin mobility have remained elusive.

Histone loss and the cytoskeleton affect chromatin mobility

Until recently, little was known about the the mechanisms which drive chromatin mobility at site specific DSBs, genome-wide when multiple DSBs were present or at uncapped human telomeres (Torres-Rosell, Sunjevaric et al. 2007, Dion, Kalck et al. 2012, Mine-Hattab and Rothstein 2012, Seeber, Dion et al. 2013, Harding, Boiarsky et al. 2015, van Sluis and McStay 2015, Tsouroula, Furst et al. 2016). Recently, accumulating evidence shows that the movement observed at dysfunctional telomeres after the depletion of shelterin complex components can be linked to the cytoskeleton. Besides the implications of DDC checkpoint protein 53BP1 (Dimitrova, Chen et al. 2008, Lottersberger, Karssemeijer et al. 2015), increased mobility of uncapped telomeres could be reversibly inhibited by treating cells with the microtubule poison Taxol or Nocodazole (Lottersberger, Karssemeijer et al. 2015). Importantly, the same effect was seen upon knockout of the two LINC complex components SUN1 and SUN2 which indirectly link chromosomes to microtubules via nuclear-membrane-spanning KASH-domain Nesprin proteins. Interestingly, Taxol also reduced the movement of IR-induced damage foci (Lottersberger, Karssemeijer et al. 2015).

Another very recent study in mammalian cells used a high-throughput chromosome conformation capture assay (capture Hi-C) to investigate clustering of induced DSBs, yet another pathway that demands for chromatin mobility (Aymard, Aguirrebengoa et al. 2017). The results demonstrated that DSBs clustering occurred in actively transcribed regions and depended on both DDR proteins and cytoskeleton organizers; namely MRN, Formin 2 (FMN2, a nuclear actin organizer) and the LINC complex (Aymard, Aguirrebengoa et al. 2017). In summary, these studies imply that the forces applied by microtubules can be transduced to internal chromatin domains. In yeast, however, early experiments indicated a reverse effect and Nocodazole treatment was shown to increase the mobility of chromatin in the absence of damage (Marshall, Straight et al. 1997). This probably reflects the different roles of cytoskeletal filaments in yeast and man, as in budding yeast, subcellular organelles are more commonly positioned by actin filaments rather than by microtubules.

Intriguingly in yeast, the depletion of the KASH-like protein Csm4, a putative LINC complex component, similarly increased telomere movement, although most likely this was due to telomere

detachment (Spichal, Brion et al. 2016). Work from this laboratory further implicates the actin cytoskeleton in chromatin movement and showed that both cytoplasmic and nuclear actin contribute to locus motion, through a mechanism that appears to be independent of Csm4 (Spichal, Brion et al. 2016).. A recent study by the Gasser laboratory showed that the effect of the actin cytoskeleton on chromatin mobility is likely caused by actin-driven nuclear oscillations rather than through a direct effect on chromatin (Amitai, Seeber et al. 2017). Consequently, actin depolarization with the cytotoxic Latrunculin A reduced nuclear rotation but did not prevent DSB-induced movement (Amitai, Seeber et al. 2017). Within the eukaryotic nucleus, actin has been detected in its monomeric, globular "G" form. Intriguingly, actin directly interacts with Actin Related Protein (Arp) containing chromatin remodelers like INO80-C. Since INO80 is necessary for damage-associated mobility (Dion, Kalck et al. 2012, Seeber, Dion et al. 2013, Hauer, Seeber et al. 2017), Latrunculin A could interfere with mobility by abrogating INO80-C-mediated changes in the nucleosome packing.

Previous experiments showed that histone level homeostasis impacts cellular aging, DNA repair and genome stability. Aging yeast cells and human fibroblasts exhibit a substantial loss of Histone H3 and Histone H4 (Feser, Truong et al. 2010, O'Sullivan, Kubicek et al. 2010) (Oberdoerffer 2010). Notably, this reduction in human fibroblasts seems to correlate with prolonged DDR signaling arising from eroded telomeres (O'Sullivan, Kubicek et al. 2010). While histone overexpression is sufficient to extend the replicative lifespan in yeast (Feser, Truong et al. 2010) it also coincides with a hypersensitivity to DNA damaging agents (Liang, Burkhart et al. 2012). Furthermore, overexpressed histone proteins accumulate as a free pool in the nucleus and the DDC protein Rad53 was shown to mediate their proteasome dependent degradation (Gunjan and Verreault 2003, Singh, Gonzalez et al. 2012). Taken together with the important function of chromatin remodeling enzymes in DSB mobility, it is likely that endogenous histone levels could also play a major role in damage-induced chromatin mobility. Here, controlled histone reductions would both provide a mechanism for local and global chromatin mobility in response to DNA damage. This hypothesis is supported by polymer modeling which predicts both the expansion of chromatin and the loss of constraining forces that limit chromatin movement. Amatai *et al.* could recently validate these predictions in vivo and showed that local DSB mobility is concurrent with remodeler-dependent unfolding. (**Fig. 4**) (Amitai, Seeber et al. 2017). However, the mechanisms that underlie enhanced chromatin mobility have remained elusive. In this thesis, I show that nucleosome degradation triggered by remodelers and checkpoint proteins enhances chromatin movement and accessibility, and promotes efficient repair (**Chapter 4**).

Histones have to go: The fate of nucleosomes during DNA damage and repair

Several pioneering studies from the Verreault and Gunjan laboratories, have shown that changing histone level homeostasis can impact DNA damage sensitivity. Early work in yeast identified a Rad53-dependent surveillance mechanism that regulates histone protein levels with implications in DNA repair (Gunjan and Verreault 2003). In this study, histone H3 was was overexpressed from the galactose promoter. Consequently, excess histones accumulated in cells depleted for Rad53 (*rad53*Δ) resulted in slow growth, DNA damage sensitivity, and chromosome loss phenotypes (Gunjan and Verreault 2003, Liang, Burkhart et al. 2012). Interestingly, *rad53*Δ sensitivity to genotoxic agents was significantly suppressed by disruption of the *HHT2-HHF2* gene cluster (*hht2-hhf2*Δ) which reduced histone H3/H4 gene dosage. Equal benefits of reduced histone dosage have been reported at site-specific DSBs where *HHT2-HHF2* deletion conferred survival after cut induction, apparently through HR repair (Liang, Burkhart et al. 2012). Interestingly, *hht2-hhf2*Δ seemed to reduce the free pool of histones rather than the chromatin bound histone fraction (Gunjan and Verreault 2003, Liang, Burkhart et al. 2012). This was consistent with the observation that that Rad53 only targeted nonchromatin-bound histones for phosphorylation. Both free histones and proteins of the DDR have highly charged interfaces to interact with DNA. Furthermore, Rad53 has been shown to directly interact with histones (Gunjan and Verreault 2003). This led to the hypothesis that damage sensitivity caused by histone overexpression in *rad53*Δ cells could derive from excess histones binding to repair proteins and thus sequestering them away from the damage (Gunjan and Verreault 2003). Likewise, histone reduction would then promote survival after damage by increasing the amount of free repair proteins. Proteasomal degradation of histones in the Rad53 pathway was mediated by the E3 ligase Tom1 (Singh, Kabbaj et al. 2009, Singh, Gonzalez et al. 2012). The two ubiquitin conjugating enzymes (E2) Ubc4 and UBc5 interacted with Rad53 in vivo and could ubiquitinate histones *in vitro*. Interestingly Rad53-mediated histone H3 phosphorylation at tyrosine 99 was critical for the degradation of this histone (Singh, Kabbaj et al. 2009). Thereafter, a screen based on sensitivities to histone overexpression identified additional histone E3 ligases in this process (Singh, Gonzalez et al. 2012).

Reduced histone levels have equally been observed after replicative ageing in human fibroblasts (O'Sullivan, Kubicek et al. 2010) (Oberdoerffer 2010) and (Pal and Tyler 2016)). Replicative aged cells show decreased levels in both histone transcription and protein levels. Interestingly this effect seems to derive from a chronic checkpoint response triggered by telomere shortening in the course of aging (O'Sullivan, Kubicek et al. 2010). Similar degrees of age-related histone level reductions were seen in yeast (Feser, Truong et al. 2010). Notably, cell longevity could be increased by bringing histone amounts back to their native level (Feser, Truong et al. 2010). This shows interesting parallels to a recently identified

process in which transient histone gene repression coincided with the recovery of mammalian cells from apoptosis (Tang, Talbot et al. 2017). This process has been termed "anastasis" and raises the interesting hypothesis that transient histone level reductions could be beneficial for growth recovery through mechanisms yet to be identified (Tang, Talbot et al. 2017). In contrast, forcing nucleosome loss from DNA in vivo can be detrimental in certain situation. The Neefjes laboratory showed that the chemotherapeutic agent doxorubicin (a topoisomerase II [TopoII] inhibitor) caused histone eviction from open chromatin and contributed to chemotherapeutic effects (Pang, Qiao et al. 2013). Doxorubicin was found to bind to the minor groove of DNA via its amino sugar (Frederick, Williams et al. 1990) and probably compete for histone or HMG protein binding (Pang, Qiao et al. 2013). On one hand, this is beneficial as doxorubicin evicted yH2A.X from the lesions caused by TopoII inhibition, and thereby attenuated the DDC, driving cancer cells into apoptotic cell death. On the other hand, the observed histone loss could explain the detrimental secondary effects of doxorubicin on slowly proliferating heart tissue, a rather unwanted effect (Pang, Qiao et al. 2013). Furthermore, the Henikoff group showed that doxorubicin-induced topoisomerase inhibition results in increased nucleosome turnover and salt solubility within gene bodies and suggest that mainly DNA torsional stress contributes to the destabilization of nucleosomes (Teves and Henikoff 2014). Of course a complete block of histone synthesis has more drastic effects: it blocks the cell cycle (Kim, Han et al. 1988), increases centromere separation and spindle length (Bouck and Bloom 2007), makes chromatin more susceptible to radiation damage (Celona, Weiner et al. 2011), impairs chromosome bi-orientation during mitosis (Murillo-Pineda, Cabello-Lobato et al. 2014) and leads to a global up-regulation of transcription (Kim, Han et al. 1988, Celona, Weiner et al. 2011, Hu, Chen et al. 2014).

Taken together these results show how reductions in nucleosome occupancy along DNA can cause detrimental effects in certain scenarios. Interestingly, this raises the possibility of using chromatin modifying drugs/methods to increase the success of cancer therapy in chemotherapeutic combination treatments.

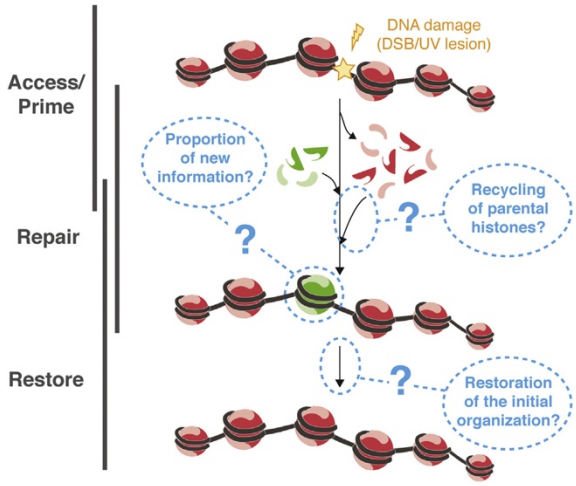

Figure 5 The prime-repair-restore model. Adopted from (Adam, Dabin et al. 2015). DNA damage (yellow star) triggers widespread chromatin changes, including a loss of pre-existing histones (red) at the damage site and the incorporation of new information (green) during the course of repair. The pattern of histone variants and associated PTMs after restorage differs from the original state. Future challenges and key questions in the field are marked by dashed blue circles.

Given that damage does not occur on naked DNA but in the context of chromatin, it is clear that repair must occur in accordance to the prime-repair-restore model (**Fig. 5**) (Soria, Polo et al. 2012). First, before a lesion can be repaired, it must firstly be made accessible to the repair machinery ("primed"). Secondly, repair needs to take place in the context of chromatin and finally, it is important to restore the chromatin/nucleosome context after repair. The repair and recovery from DNA damage has thus implications in both cell survival and epigenome maintenance (Soria, Polo et al. 2012, Adam, Dabin et al. 2015, Gerhold, Hauer et al. 2015). Histone degradation and mobilization after genomic insults and checkpoint activation is not restricted to DSBs and has been shown to occur both locally and globally in response to various DNA damaging agents. In that sense, the van Attikum laboratory has shown that chromatin remodeling alters nucleosome dynamics at IR induced DSBs as well as at sites of UV damage (Luijsterburg, Lindh et al. 2012, Luijsterburg, de Krijger et al. 2016). CHD2-dependent remodeling of chromatin around breaks in human U2OS cells relied on parylation which caused chromatin expansion and deposition of the histone variant H3.3 (Luijsterburg, de Krijger et al. 2016). Furthermore, fluorescence recovery after photobleaching (FRAP) microscopy revealed a DDB2 and PARP1 dependent loss of core histones from UV-damaged chromatin in hamster cells (Luijsterburg, Lindh et al. 2012). Apart from the importance of parylation in DDR signaling, ATM and NBS1 recruitment to I-PpoI induced DSBs was shown to cause localized disruption of nucleosomes in human MCF7 cells (Berkovich, Monnat et al. 2007). In this case, ChIP experiments were used to follow the levels of H2B at breaks (Berkovich, Monnat et al. 2007). A later study by the same laboratory followed the abundance of all core histones around I-PpoI sites (Goldstein, Derheimer et al. 2013). Break induction caused a selective loss of H2A and H2B, but not

of H3 nor H4. Interestingly, down-regulation of nucleolin, a protein with histone chaperone activity, abrogates nucleosome disruption, repair factor recruitment and the repair of the DSBs (Goldstein, Derheimer et al. 2013). Similar results were obtained with FRAP experiments at localized UV damage sites in different human cell lines (Dinant, Ampatziadis-Michailidis et al. 2013). In this case, selective H2A/H2B loss at the damaged sites depended on the Spt16, one of the two subunits of the histone chaperone FACT. Moreover, Spt16 was essential to restart transcription after repair (Dinant, Ampatziadis-Michailidis et al. 2013). Finally, it was shown that disrupting nucleosomes to allow access for repair was important for DSBs induced at the yeast mating type locus MAT, if the donor is heterochromatic. In a strain created by Hicks *et al.*, recombination-mediated repair of a DSB at MAT could only occur at the HML donor locus (Tsabar, Hicks et al. 2016). Notably, 60 minutes after cut induction, nucleosomes at the donor site were greatly reduced and coincided with homology-driven strand invasion (Rad51 accumulation) (Tsabar, Hicks et al. 2016). These observations indicate that chromatin accessibility needs to be increased both at the DSB site and the homologous template to allow for successful recombination.

In addition to these local effects, nucleosomes were found to be lost genome-wide in response to UV, IR or radiomimetic damage. Consistently, chromatin fractionation and salt extraction studies in human 293T cells showed that histones were destabilized and released from chromatin upon irradiation (Xu, Sun et al. 2010). This technique measured the degree of protein extractability from chromatin in response to damage. The authors found that the core histones H2B, H3 and H4, as well as the histone variant H2A.X became more extractable after damage. This IR-dependent destabilization was further found to be an active process requiring the ATPase activity of the p400 ATPase in the SWI/SNF complex and histone acetylation by the Tip60 acetyltransferase (Xu, Sun et al. 2010). Analysis of the human CUL4-DDB-ROC1 ubiquitin ligase showed substrate specificity to histones in vitro and further ubiquitinated H3 and H4 in response to global UV damage in vivo (Wang, Zhai et al. 2006). Ubiquitination weakened histone-histone interactions and caused nucleosome eviction. At this stage, it was not analyzed whether subsequent proteasomal degradation occurred (Wang, Zhai et al. 2006). In **Chapter 4**, I will discuss our finding which describes a global, proteasome-mediated degradation of all core histones in response to Zeocin damage (Hauer, Seeber et al. 2017).

References

Adam, S., J. Dabin, O. Chevallier, O. Leroy, C. Baldeyron, A. Corpet, P. Lomonte, O. Renaud, G. Almouzni and S. E. Polo (2016). "Real-Time Tracking of Parental Histones Reveals Their Contribution to Chromatin Integrity Following DNA Damage." Mol Cell **64**(1): 65-78.

Adam, S., J. Dabin and S. E. Polo (2015). "Chromatin plasticity in response to DNA damage: The shape of things to come." DNA Repair (Amst) **32**: 120-126.

Akhtar, A. and P. B. Becker (2000). "Activation of transcription through histone H4 acetylation by MOF, an acetyltransferase essential for dosage compensation in Drosophila." Mol Cell **5**(2): 367-375.

Albert, B., J. Mathon, A. Shukla, H. Saad, C. Normand, I. Leger-Silvestre, D. Villa, A. Kamgoue, J. Mozziconacci, H. Wong, C. Zimmer, P. Bhargava, A. Bancaud and O. Gadal (2013). "Systematic characterization of the conformation and dynamics of budding yeast chromosome XII." J Cell Biol **202**(2): 201-210.

Albert, I., T. N. Mavrich, L. P. Tomsho, J. Qi, S. J. Zanton, S. C. Schuster and B. F. Pugh (2007). "Translational and rotational settings of H2A.Z nucleosomes across the Saccharomyces cerevisiae genome." Nature **446**(7135): 572-576.

Amaral, N., T. Ryu, X. Li and I. Chiolo (2017). "Nuclear Dynamics of Heterochromatin Repair." Trends Genet **33**(2): 86-100.

Amitai, A., A. Seeber, S. M. Gasser and D. Holcman (2017). "Visualization of Chromatin Decompaction and Break Site Extrusion as Predicted by Statistical Polymer Modeling of Single-Locus Trajectories." Cell Rep **18**(5): 1200-1214.

Amitai, A., M. Toulouze, K. Dubrana and D. Holcman (2015). "Analysis of Single Locus Trajectories for Extracting In Vivo Chromatin Tethering Interactions." PLoS Computational Biology **11**(8): e1004433.

Andrews, A. J., X. Chen, A. Zevin, L. A. Stargell and K. Luger (2010). "The histone chaperone Nap1 promotes nucleosome assembly by eliminating nonnucleosomal histone DNA interactions." Mol Cell **37**(6): 834-842.

Arents, G. and E. N. Moudrianakis (1995). "The histone fold: a ubiquitous architectural motif utilized in DNA compaction and protein dimerization." Proc Natl Acad Sci U S A **92**(24): 11170-11174.

Awad, S., D. Ryan, P. Prochasson, T. Owen-Hughes and A. H. Hassan (2010). "The Snf2 homolog Fun30 acts as a homodimeric ATP-dependent chromatin-remodeling enzyme." J Biol Chem **285**(13): 9477-9484.

Aymard, F., M. Aguirrebengoa, E. Guillou, B. M. Javierre, B. Bugler, C. Arnould, V. Rocher, J. S. Iacovoni, A. Biernacka, M. Skrzypczak, K. Ginalski, M. Rowicka, P. Fraser and G. Legube (2017). "Genome-wide mapping of long-range contacts unveils clustering of DNA double-strand breaks at damaged active genes." Nat Struct Mol Biol **24**(4): 353-361.

Ayoub, N., A. D. Jeyasekharan, J. A. Bernal and A. R. Venkitaraman (2008). "HP1-beta mobilization promotes chromatin changes that initiate the DNA damage response." Nature **453**(7195): 682-686.

Bandaria, J. N., P. Qin, V. Berk, S. Chu and A. Yildiz (2016). "Shelterin Protects Chromosome Ends by Compacting Telomeric Chromatin." Cell **164**(4): 735-746.

Bantele, S. C., P. Ferreira, D. Gritenaite, D. Boos and B. Pfander (2017). "Targeting of the Fun30 nucleosome remodeller by the Dpb11 scaffold facilitates cell cycle-regulated DNA end resection." Elife **6**.

Berkovich, E., R. J. Monnat, Jr. and M. B. Kastan (2007). "Roles of ATM and NBS1 in chromatin structure modulation and DNA double-strand break repair." Nat Cell Biol **9**(6): 683-690.

Beucher, A., J. Birraux, L. Tchouandong, O. Barton, A. Shibata, S. Conrad, A. A. Goodarzi, A. Krempler, P. A. Jeggo and M. Lobrich (2009). "ATM and Artemis promote homologous recombination of radiation-induced DNA double-strand breaks in G2." EMBO J **28**(21): 3413-3427.

Bianchi, M. E. and A. Agresti (2005). "HMG proteins: dynamic players in gene regulation and differentiation." Current opinion in genetics & development **15**(5): 496-506.

Bornfleth, H., P. Edelmann, D. Zink, T. Cremer and C. Cremer (1999). "Quantitative motion analysis of subchromosomal foci in living cells using four-dimensional microscopy." Biophys J **77**(5): 2871-2886.

Bouck, D. C. and K. Bloom (2007). "Pericentric chromatin is an elastic component of the mitotic spindle." Curr Biol **17**(9): 741-748.

Bukata, L., S. L. Parker and M. A. D'Angelo (2013). "Nuclear pore complexes in the maintenance of genome integrity." Curr Opin Cell Biol **25**(3): 378-386.

Bupp, J. M., A. E. Martin, E. S. Stensrud and S. L. Jaspersen (2007). "Telomere anchoring at the nuclear periphery requires the budding yeast Sad1-UNC-84 domain protein Mps3." J Cell Biol **179**(5): 845-854.

Burgess, R. C., B. Burman, M. J. Kruhlak and T. Misteli (2014). "Activation of DNA damage response signaling by condensed chromatin." Cell Rep **9**(5): 1703-1717.

Bystricky, K., T. Laroche, G. van Houwe, M. Blaszczyk and S. M. Gasser (2005). "Chromosome looping in yeast: telomere pairing and coordinated movement reflect anchoring efficiency and territorial organization." J Cell Biol **168**(3): 375-387.

Bystricky, K., H. Van Attikum, M. D. Montiel, V. Dion, L. Gehlen and S. M. Gasser (2009). "Regulation of nuclear positioning and dynamics of the silent mating type loci by the yeast Ku70/Ku80 complex." Mol Cell Biol **29**(3): 835-848.

Campos, E. I. and D. Reinberg (2009). "Histones: annotating chromatin." Annu Rev Genet **43**: 559-599.

Celona, B., A. Weiner, F. Di Felice, F. M. Mancuso, E. Cesarini, R. L. Rossi, L. Gregory, D. Baban, G. Rossetti, P. Grianti, M. Pagani, T. Bonaldi, J. Ragoussis, N. Friedman, G. Camilloni, M. E. Bianchi and A. Agresti (2011). "Substantial histone reduction modulates genomewide nucleosomal occupancy and global transcriptional output." PLoS Biol **9**(6): e1001086.

Chai, B., J. Huang, B. R. Cairns and B. C. Laurent (2005). "Distinct roles for the RSC and Swi/Snf ATP-dependent chromatin remodelers in DNA double-strand break repair." Genes Dev **19**(14): 1656-1661.

Chen, X., D. Cui, A. Papusha, X. Zhang, C. D. Chu, J. Tang, K. Chen, X. Pan and G. Ira (2012). "The Fun30 nucleosome remodeller promotes resection of DNA double-strand break ends." Nature **489**(7417): 576-580.

Chiolo, I., A. Minoda, S. U. Colmenares, A. Polyzos, S. V. Costes and G. H. Karpen (2011). "Double-Strand Breaks in Heterochromatin Move Outside of a Dynamic HP1a Domain to Complete Recombinational Repair." Cell **144**(5): 732-744.

Chitale, S. and H. Richly (2017). "DICER and ZRF1 contribute to chromatin decondensation during nucleotide excision repair." Nucleic Acids Res.

Chubb, J. R., S. Boyle, P. Perry and W. A. Bickmore (2002). "Chromatin motion is constrained by association with nuclear compartments in human cells." Curr Biol **12**(6): 439-445.

Churikov, D., F. Charifi, N. Eckert-Boulet, S. Silva, M. N. Simon, M. Lisby and V. Geli (2016). "SUMO-Dependent Relocalization of Eroded Telomeres to Nuclear Pore Complexes Controls Telomere Recombination." Cell Rep **15**(6): 1242-1253.

Clapier, C. R. and B. R. Cairns (2009). "The biology of chromatin remodeling complexes." Annu Rev Biochem **78**: 273-304.

Costelloe, T., R. Louge, N. Tomimatsu, B. Mukherjee, E. Martini, B. Khadaroo, K. Dubois, W. W. Wiegant, A. Thierry, S. Burma, H. van Attikum and B. Llorente (2012). "The yeast Fun30 and human SMARCAD1 chromatin remodellers promote DNA end resection." Nature **489**(7417): 581-584.

Cremona, C. A., P. Sarangi, Y. Yang, L. E. Hang, S. Rahman and X. Zhao (2012). "Extensive DNA damage-induced sumoylation contributes to replication and repair and acts in addition to the mec1 checkpoint." Mol Cell **45**(3): 422-432.

De Koning, L., A. Corpet, J. E. Haber and G. Almouzni (2007). "Histone chaperones: an escort network regulating histone traffic." Nat Struct Mol Biol **14**(11): 997-1007.

Denslow, S. A. and P. A. Wade (2007). "The human Mi-2/NuRD complex and gene regulation." Oncogene **26**(37): 5433-5438.

Dickerson, D., M. Gierlinski, V. Singh, E. Kitamura, G. Ball, T. U. Tanaka and T. Owen-Hughes (2016). "High resolution imaging reveals heterogeneity in chromatin states between cells that is not inherited through cell division." BMC Cell Biol **17**(1): 33.

Dimitrova, N., Y. C. M. Chen, D. L. Spector and T. de Lange (2008). "53BP1 promotes non-homologous end joining of telomeres by increasing chromatin mobility." Nature **456**(7221): 524-U551.

Dinant, C., G. Ampatziadis-Michailidis, H. Lans, M. Tresini, A. Lagarou, M. Grosbart, A. F. Theil, W. A. van Cappellen, H. Kimura, J. Bartek, M. Fousteri, A. B. Houtsmuller, W. Vermeulen and J. A. Marteijn (2013). "Enhanced chromatin dynamics by FACT promotes transcriptional restart after UV-induced DNA damage." Mol Cell **51**(4): 469-479.

Dion, V. and S. M. Gasser (2013). "Chromatin movement in the maintenance of genome stability." Cell **152**(6): 1355-1364.

Dion, V., V. Kalck, C. Horigome, B. D. Towbin and S. M. Gasser (2012). "Increased mobility of double-strand breaks requires Mec1, Rad9 and the homologous recombination machinery." Nat Cell Biol **14**(5): 502-509.

Dion, V., V. Kalck, A. Seeber, T. Schleker and S. M. Gasser (2013). "Cohesin and the nucleolus constrain the mobility of spontaneous repair foci." EMBO Rep **14**(11): 984-991.

Dorigo, B., T. Schalch, A. Kulangara, S. Duda, R. R. Schroeder and T. J. Richmond (2004). "Nucleosome arrays reveal the two-start organization of the chromatin fiber." Science **306**(5701): 1571-1573.

Downs, J. A., N. F. Lowndes and S. P. Jackson (2000). "A role for Saccharomyces cerevisiae histone H2A in DNA repair." Nature **408**(6815): 1001-1004.

Duan, Z., M. Andronescu, K. Schutz, S. McIlwain, Y. J. Kim, C. Lee, J. Shendure, S. Fields, C. A. Blau and W. S. Noble (2010). "A three-dimensional model of the yeast genome." Nature **465**(7296): 363-367.

Eapen, V. V., N. Sugawara, M. Tsabar, W. H. Wu and J. E. Haber (2012). "The Saccharomyces cerevisiae chromatin remodeler Fun30 regulates DNA end resection and checkpoint deactivation." Mol Cell Biol **32**(22): 4727-4740.

Eden Fussner, R. W. C. a. D. P. B.-J. (2010). "Living without 30 nm chromatin fibers." Trends in Biochemical Sciences **36**(1): 1-6.

Ferreira, H. C., B. Luke, H. Schober, V. Kalck, J. Lingner and S. M. Gasser (2011). "The PIAS homologue Siz2 regulates perinuclear telomere position and telomerase activity in budding yeast." Nat Cell Biol **13**(7): 867-874.

Feser, J., D. Truong, C. Das, J. J. Carson, J. Kieft, T. Harkness and J. K. Tyler (2010). "Elevated histone expression promotes life span extension." Mol Cell **39**(5): 724-735.

Fischle, W., Y. Wang, S. A. Jacobs, Y. Kim, C. D. Allis and S. Khorasanizadeh (2003). "Molecular basis for the discrimination of repressive methyl-lysine marks in histone H3 by Polycomb and HP1 chromodomains." Genes Dev **17**(15): 1870-1881.

Francia, S., F. Michelini, A. Saxena, D. Tang, M. de Hoon, V. Anelli, M. Mione, P. Carninci and F. d'Adda di Fagagna (2012). "Site-specific DICER and DROSHA RNA products control the DNA-damage response." Nature **488**(7410): 231-235.

Frederick, C. A., L. D. Williams, G. Ughetto, G. A. van der Marel, J. H. van Boom, A. Rich and A. H. Wang (1990). "Structural comparison of anticancer drug-DNA complexes: adriamycin and daunomycin." Biochemistry **29**(10): 2538-2549.

Gasser, S. M., F. Hediger, A. Taddei, F. R. Neumann and M. R. Gartenberg (2004). "The function of telomere clustering in yeast: the circe effect." Cold Spring Harb Symp Quant Biol **69**: 327-337.

Gerhold, C. B., M. H. Hauer and S. M. Gasser (2015). "INO80-C and SWR-C: guardians of the genome." J Mol Biol **427**(3): 637-651.

Goldstein, M., F. A. Derheimer, J. Tait-Mulder and M. B. Kastan (2013). "Nucleolin mediates nucleosome disruption critical for DNA double-strand break repair." Proc Natl Acad Sci U S A **110**(42): 16874-16879.

Gonzalez-Sandoval, A., B. D. Towbin, V. Kalck, D. S. Cabianca, D. Gaidatzis, M. H. Hauer, L. Geng, L. Wang, T. Yang, X. Wang, K. Zhao and S. M. Gasser (2015). "Perinuclear Anchoring of H3K9-Methylated Chromatin Stabilizes Induced Cell Fate in C. elegans Embryos." Cell **163**(6): 1333-1347.

Goodarzi, A. A., T. Kurka and P. A. Jeggo (2011). "KAP-1 phosphorylation regulates CHD3 nucleosome remodeling during the DNA double-strand break response." Nat Struct Mol Biol **18**(7): 831-839.

Goodarzi, A. A., A. T. Noon, D. Deckbar, Y. Ziv, Y. Shiloh, M. Lobrich and P. A. Jeggo (2008). "ATM signaling facilitates repair of DNA double-strand breaks associated with heterochromatin." Mol Cell **31**(2): 167-177.

Gotta, M., T. Laroche, A. Formenton, L. Maillet, H. Scherthan and S. M. Gasser (1996). "The clustering of telomeres and colocalization with Rap1, Sir3, and Sir4 proteins in wild-type Saccharomyces cerevisiae." J Cell Biol **134**(6): 1349-1363.

Gracheva, E., S. Chitale, T. Wilhelm, A. Rapp, J. Byrne, J. Stadler, R. Medina, M. C. Cardoso and H. Richly (2016). "ZRF1 mediates remodeling of E3 ligases at DNA lesion sites during nucleotide excision repair." J Cell Biol **213**(2): 185-200.

Guillemette, B., A. R. Bataille, N. Gevry, M. Adam, M. Blanchette, F. Robert and L. Gaudreau (2005). "Variant histone H2A.Z is globally localized to the promoters of inactive yeast genes and regulates nucleosome positioning." PLoS Biol **3**(12): e384.

Gunjan, A. and A. Verreault (2003). "A Rad53 kinase-dependent surveillance mechanism that regulates histone protein levels in S. cerevisiae." Cell **115**(5): 537-549.

Gurard-Levin, Z. A., J. P. Quivy and G. Almouzni (2014). "Histone chaperones: assisting histone traffic and nucleosome dynamics." Annu Rev Biochem **83**: 487-517.

Harding, S. M., J. A. Boiarsky and R. A. Greenberg (2015). "ATM Dependent Silencing Links Nucleolar Chromatin Reorganization to DNA Damage Recognition." Cell Rep **13**(2): 251-259.

Hauer, M. H., A. Seeber, V. Singh, R. Thierry, R. Sack, A. Amitai, M. Kryzhanovska, J. Eglinger, D. Holcman, T. Owen-Hughes and S. M. Gasser (2017). "Histone degradation in response to DNA damage enhances chromatin dynamics and recombination rates." Nat Struct Mol Biol **24**(2): 99-107.

Hebbes, T. R., A. L. Clayton, A. W. Thorne and C. Crane-Robinson (1994). "Core histone hyperacetylation co-maps with generalized DNase I sensitivity in the chicken beta-globin chromosomal domain." EMBO J **13**(8): 1823-1830.

Hector, R. E., A. Ray, B. R. Chen, R. Shtofman, K. L. Berkner and K. W. Runge (2012). "Mec1p associates with functionally compromised telomeres." Chromosoma **121**(3): 277-290.

Heun, P., T. Laroche, K. Shimada, P. Furrer and S. M. Gasser (2001). "Chromosome dynamics in the yeast interphase nucleus." Science **294**(5549): 2181-2186.

Heyer, W. D., K. T. Ehmsen and J. Liu (2010). "Regulation of homologous recombination in eukaryotes." Annu Rev Genet **44**: 113-139.

Hinde, E., X. Kong, K. Yokomori and E. Gratton (2014). "Chromatin dynamics during DNA repair revealed by pair correlation analysis of molecular flow in the nucleus." Biophys J **107**(1): 55-65.

Horigome, C., D. E. Bustard, I. Marcomini, N. Delgoshaie, M. Tsai-Pflugfelder, J. A. Cobb and S. M. Gasser (2016). "PolySUMOylation by Siz2 and Mms21 triggers relocation of DNA breaks to nuclear pores through the Slx5/Slx8 STUbL." Genes Dev **30**(8): 931-945.

Horigome, C., Y. Oma, T. Konishi, R. Schmid, I. Marcomini, M. H. Hauer, V. Dion, M. Harata and S. M. Gasser (2014). "SWR1 and INO80 chromatin remodelers contribute to DNA double-strand break perinuclear anchorage site choice." Mol Cell **55**(4): 626-639.

Hu, Z., K. Chen, Z. Xia, M. Chavez, S. Pal, J. H. Seol, C. C. Chen, W. Li and J. K. Tyler (2014). "Nucleosome loss leads to global transcriptional up-regulation and genomic instability during yeast aging." Genes Dev **28**(4): 396-408.

Jackson, S. P. and J. Bartek (2009). "The DNA-damage response in human biology and disease." Nature **461**(7267): 1071-1078.

Jacobs, S. A. and S. Khorasanizadeh (2002). "Structure of HP1 chromodomain bound to a lysine 9-methylated histone H3 tail." Science **295**(5562): 2080-2083.

Jakob, B., J. Splinter, S. Conrad, K. O. Voss, D. Zink, M. Durante, M. Lobrich and G. Taucher-Scholz (2011). "DNA double-strand breaks in heterochromatin elicit fast repair protein recruitment, histone H2AX phosphorylation and relocation to euchromatin." Nucleic Acids Res **39**(15): 6489-6499.

Janssen, A., G. A. Breuer, E. K. Brinkman, A. I. van der Meulen, S. V. Borden, B. van Steensel, R. S. Bindra, J. R. LaRocque and G. H. Karpen (2016). "A single double-strand break system reveals repair dynamics and mechanisms in heterochromatin and euchromatin." Genes Dev **30**(14): 1645-1657.

Kalocsay, M., N. J. Hiller and S. Jentsch (2009). "Chromosome-wide Rad51 spreading and SUMO-H2A.Z-dependent chromosome fixation in response to a persistent DNA double-strand break." Mol Cell **33**(3): 335-343.

Khorasanizadeh, S. (2004). "The nucleosome: from genomic organization to genomic regulation." Cell **116**(2): 259-272.

Khurana, S., M. J. Kruhlak, J. Kim, A. D. Tran, J. Liu, K. Nyswaner, L. Shi, P. Jailwala, M. H. Sung, O. Hakim and P. Oberdoerffer (2014). "A macrohistone variant links dynamic chromatin compaction to BRCA1-dependent genome maintenance." Cell Rep **8**(4): 1049-1062.

Kim, U. J., M. Han, P. Kayne and M. Grunstein (1988). "Effects of histone H4 depletion on the cell cycle and transcription of Saccharomyces cerevisiae." EMBO J **7**(7): 2211-2219.

Lawrimore, J., T. M. Barry, R. M. Barry, A. C. York, D. M. Cook, K. Akialis, J. Tyler, P. Vasquez, E. Yeh and K. Bloom (2017). "Microtubule dynamics drive enhanced chromatin motion and mobilize telomeres in response to DNA damage." Mol Biol Cell.

Lee, D. H., A. A. Goodarzi, G. O. Adelmant, Y. Pan, P. A. Jeggo, J. A. Marto and D. Chowdhury (2012). "Phosphoproteomic analysis reveals that PP4 dephosphorylates KAP-1 impacting the DNA damage response." EMBO J **31**(10): 2403-2415.

Levi, V., Q. Ruan, M. Plutz, A. S. Belmont and E. Gratton (2005). "Chromatin dynamics in interphase cells revealed by tracking in a two-photon excitation microscope." Biophys J **89**(6): 4275-4285.

Li, A., J. M. Eirin-Lopez and J. Ausio (2005). "H2AX: tailoring histone H2A for chromatin-dependent genomic integrity." Biochem Cell Biol **83**(4): 505-515.

Li, G. and D. Reinberg (2011). "Chromatin higher-order structures and gene regulation." Curr Opin Genet Dev **21**(2): 175-186.

Liang, D., S. L. Burkhart, R. K. Singh, M. H. Kabbaj and A. Gunjan (2012). "Histone dosage regulates DNA damage sensitivity in a checkpoint-independent manner by the homologous recombination pathway." Nucleic Acids Res **40**(19): 9604-9620.

Lindahl, T. and D. E. Barnes (2000). "Repair of endogenous DNA damage." Cold Spring Harb Symp Quant Biol **65**: 127-133.

Lottersberger, F., R. A. Karssemeijer, N. Dimitrova and T. de Lange (2015). "53BP1 and the LINC Complex Promote Microtubule-Dependent DSB Mobility and DNA Repair." Cell **163**(4): 880-893.

Luger, K., M. L. Dechassa and D. J. Tremethick (2012). "New insights into nucleosome and chromatin structure: an ordered state or a disordered affair?" Nat Rev Mol Cell Biol **13**(7): 436-447.

Luger, K., A. W. Mader, R. K. Richmond, D. F. Sargent and T. J. Richmond (1997). "Crystal structure of the nucleosome core particle at 2.8 angstrom resolution." Nature **389**(6648): 251-260.

Luijsterburg, M. S., I. de Krijger, W. W. Wiegant, R. G. Shah, G. Smeenk, A. J. de Groot, A. Pines, A. C. Vertegaal, J. J. Jacobs, G. M. Shah and H. van Attikum (2016). "PARP1 Links CHD2-Mediated Chromatin Expansion and H3.3 Deposition to DNA Repair by Non-homologous End-Joining." Mol Cell **61**(4): 547-562.

Luijsterburg, M. S., M. Lindh, K. Acs, M. G. Vrouwe, A. Pines, H. van Attikum, L. H. Mullenders and N. P. Dantuma (2012). "DDB2 promotes chromatin decondensation at UV-induced DNA damage." J Cell Biol **197**(2): 267-281.

Luk, E., A. Ranjan, P. C. Fitzgerald, G. Mizuguchi, Y. Huang, D. Wei and C. Wu (2010). "Stepwise histone replacement by SWR1 requires dual activation with histone H2A.Z and canonical nucleosome." Cell **143**(5): 725-736.

Maeshima, K. and M. Eltsov (2008). "Packaging the genome: the structure of mitotic chromosomes." J Biochem **143**(2): 145-153.

Malarkey, C. S. and M. E. Churchill (2012). "The high mobility group box: the ultimate utility player of a cell." Trends Biochem Sci **37**(12): 553-562.

Malik, H. S. and S. Henikoff (2003). "Phylogenomics of the nucleosome." Nat Struct Biol **10**(11): 882-891.

Marcomini, I. and S. M. Gasser (2015). "Nuclear organization in DNA end processing: Telomeres vs double-strand breaks." DNA Repair (Amst) **32**: 134-140.

Marshall, W. F., A. Straight, J. F. Marko, J. Swedlow, A. Dernburg, A. Belmont, A. W. Murray, D. A. Agard and J. W. Sedat (1997). "Interphase chromosomes undergo constrained diffusional motion in living cells." Curr Biol **7**(12): 930-939.

Marteijn, J. A., H. Lans, W. Vermeulen and J. H. Hoeijmakers (2014). "Understanding nucleotide excision repair and its roles in cancer and ageing." Nat Rev Mol Cell Biol **15**(7): 465-481.

Mine-Hattab, J. and R. Rothstein (2012). "Increased chromosome mobility facilitates homology search during recombination." Nat Cell Biol **14**(5): 510-517.

Morillo-Huesca, M., M. Clemente-Ruiz, E. Andujar and F. Prado (2010). "The SWR1 histone replacement complex causes genetic instability and genome-wide transcription misregulation in the absence of H2A.Z." PLoS One **5**(8): e12143.

Morrison, A. J., J. Highland, N. J. Krogan, A. Arbel-Eden, J. F. Greenblatt, J. E. Haber and X. Shen (2004). "INO80 and gamma-H2AX interaction links ATP-dependent chromatin remodeling to DNA damage repair." Cell **119**(6): 767-775.

Murillo-Pineda, M., M. J. Cabello-Lobato, M. Clemente-Ruiz, F. Monje-Casas and F. Prado (2014). "Defective histone supply causes condensin-dependent chromatin alterations, SAC activation and chromosome decatenation impairment." Nucleic Acids Res **42**(20): 12469-12482.

Murr, R., J. I. Loizou, Y. G. Yang, C. Cuenin, H. Li, Z. Q. Wang and Z. Herceg (2006). "Histone acetylation by Trrap-Tip60 modulates loading of repair proteins and repair of DNA double-strand breaks." Nat Cell Biol **8**(1): 91-99.

Nagai, S., K. Dubrana, M. Tsai-Pflugfelder, M. B. Davidson, T. M. Roberts, G. W. Brown, E. Varela, F. Hediger, S. M. Gasser and N. J. Krogan (2008). "Functional targeting of DNA damage to a nuclear pore-associated SUMO-dependent ubiquitin ligase." Science **322**(5901): 597-602.

Natsume, R., M. Eitoku, Y. Akai, N. Sano, M. Horikoshi and T. Senda (2007). "Structure and function of the histone chaperone CIA/ASF1 complexed with histones H3 and H4." Nature **446**(7133): 338-341.

Neumann, F. R., V. Dion, L. R. Gehlen, M. Tsai-Pflugfelder, R. Schmid, A. Taddei and S. M. Gasser (2012). "Targeted INO80 enhances subnuclear chromatin movement and ectopic homologous recombination." Genes Dev **26**(4): 369-383.

Nielsen, A. L., M. Oulad-Abdelghani, J. A. Ortiz, E. Remboutsika, P. Chambon and R. Losson (2001). "Heterochromatin formation in mammalian cells: interaction between histones and HP1 proteins." Mol Cell **7**(4): 729-739.

O'Sullivan, R. J., S. Kubicek, S. L. Schreiber and J. Karlseder (2010). "Reduced histone biosynthesis and chromatin changes arising from a damage signal at telomeres." Nat Struct Mol Biol **17**(10): 1218-1225.

Oberdoerffer, P. (2010). "An age of fewer histones." Nat Cell Biol **12**(11): 1029-1031.

Oza, P., S. L. Jaspersen, A. Miele, J. Dekker and C. L. Peterson (2009). "Mechanisms that regulate localization of a DNA double-strand break to the nuclear periphery." Genes Dev **23**(8): 912-927.

Pal, S. and J. K. Tyler (2016). "Epigenetics and aging." Sci Adv **2**(7): e1600584.

Panday, A. and A. Grove (2017). "Yeast HMO1: Linker Histone Reinvented." Microbiol Mol Biol Rev **81**(1).

Pang, B., X. Qiao, L. Janssen, A. Velds, T. Groothuis, R. Kerkhoven, M. Nieuwland, H. Ovaa, S. Rottenberg, O. van Tellingen, J. Janssen, P. Huijgens, W. Zwart and J. Neefjes (2013). "Drug-induced histone eviction from open chromatin contributes to the chemotherapeutic effects of doxorubicin." Nat Commun **4**: 1908.

Papamichos-Chronakis, M., S. Watanabe, O. J. Rando and C. L. Peterson (2011). "Global regulation of H2A.Z localization by the INO80 chromatin-remodeling enzyme is essential for genome integrity." Cell **144**(2): 200-213.

Parks, J. W. and M. D. Stone (2017). "Single-Molecule Studies of Telomeres and Telomerase." Annu Rev Biophys.

Pearson, C. E., K. Nichol Edamura and J. D. Cleary (2005). "Repeat instability: mechanisms of dynamic mutations." Nat Rev Genet **6**(10): 729-742.

Pereira, S. L., R. A. Grayling, R. Lurz and J. N. Reeve (1997). "Archaeal nucleosomes." Proc Natl Acad Sci U S A **94**(23): 12633-12637.

Polo, S. E., A. Kaidi, L. Baskcomb, Y. Galanty and S. P. Jackson (2010). "Regulation of DNA-damage responses and cell-cycle progression by the chromatin remodelling factor CHD4." EMBO J **29**(18): 3130-3139.

Povirk, L. F., W. Wubter, W. Kohnlein and F. Hutchinson (1977). "DNA double-strand breaks and alkali-labile bonds produced by bleomycin." Nucleic Acids Res **4**(10): 3573-3580.

Psakhye, I. and S. Jentsch (2012). "Protein group modification and synergy in the SUMO pathway as exemplified in DNA repair." Cell **151**(4): 807-820.

Raisner, R. M., P. D. Hartley, M. D. Meneghini, M. Z. Bao, C. L. Liu, S. L. Schreiber, O. J. Rando and H. D. Madhani (2005). "Histone variant H2A.Z marks the 5' ends of both active and inactive genes in euchromatin." Cell **123**(2): 233-248.

Rando, O. J. and F. Winston (2012). "Chromatin and transcription in yeast." Genetics **190**(2): 351-387.

Robinson, P. J., L. Fairall, V. A. Huynh and D. Rhodes (2006). "EM measurements define the dimensions of the "30-nm" chromatin fiber: evidence for a compact, interdigitated structure." Proc Natl Acad Sci U S A **103**(17): 6506-6511.

Rogakou, E. P., D. R. Pilch, A. H. Orr, V. S. Ivanova and W. M. Bonner (1998). "DNA double-stranded breaks induce histone H2AX phosphorylation on serine 139." J Biol Chem **273**(10): 5858-5868.

Roukos, V., T. C. Voss, C. K. Schmidt, S. Lee, D. Wangsa and T. Misteli (2013). "Spatial dynamics of chromosome translocations in living cells." Science **341**(6146): 660-664.

Rudin, N. and J. E. Haber (1988). "Efficient repair of HO-induced chromosomal breaks in Saccharomyces cerevisiae by recombination between flanking homologous sequences." Mol Cell Biol **8**(9): 3918-3928.

Ryu, T., B. Spatola, L. Delabaere, K. Bowlin, H. Hopp, R. Kunitake, G. H. Karpen and I. Chiolo (2015). "Heterochromatic breaks move to the nuclear periphery to continue recombinational repair." Nat Cell Biol **17**(11): 1401-1411.

Sandman, K., J. A. Krzycki, B. Dobrinski, R. Lurz and J. N. Reeve (1990). "HMf, a DNA-binding protein isolated from the hyperthermophilic archaeon Methanothermus fervidus, is most closely related to histones." Proc Natl Acad Sci U S A **87**(15): 5788-5791.

Sarangi, P. and X. Zhao (2015). "SUMO-mediated regulation of DNA damage repair and responses." Trends Biochem Sci **40**(4): 233-242.

Schalch, T., S. Duda, D. F. Sargent and T. J. Richmond (2005). "X-ray structure of a tetranucleosome and its implications for the chromatin fibre." Nature **436**(7047): 138-141.

Schober, H., H. Ferreira, V. Kalck, L. R. Gehlen and S. M. Gasser (2009). "Yeast telomerase and the SUN domain protein Mps3 anchor telomeres and repress subtelomeric recombination." Genes Dev **23**(8): 928-938.

Schwertman, P., S. Bekker-Jensen and N. Mailand (2016). "Regulation of DNA double-strand break repair by ubiquitin and ubiquitin-like modifiers." Nat Rev Mol Cell Biol **17**(6): 379-394.

Seeber, A., V. Dion and S. M. Gasser (2013). "Checkpoint kinases and the INO80 nucleosome remodeling complex enhance global chromatin mobility in response to DNA damage." Genes Dev **27**(18): 1999-2008.

Seeber, A. and S. M. Gasser (2016). "Chromatin organization and dynamics in double-strand break repair." Curr Opin Genet Dev **43**: 9-16.

Seeber, A., M. Hauer and S. M. Gasser (2013). "Nucleosome remodelers in double-strand break repair." Curr Opin Genet Dev **23**(2): 174-184.

Sharma, G. G., S. So, A. Gupta, R. Kumar, C. Cayrou, N. Avvakumov, U. Bhadra, R. K. Pandita, M. H. Porteus, D. J. Chen, J. Cote and T. K. Pandita (2010). "MOF and histone H4 acetylation at lysine 16 are critical for DNA damage response and double-strand break repair." Mol Cell Biol **30**(14): 3582-3595.

Singh, R. K., M. Gonzalez, M. H. Kabbaj and A. Gunjan (2012). "Novel E3 ubiquitin ligases that regulate histone protein levels in the budding yeast Saccharomyces cerevisiae." PLoS One **7**(5): e36295.

Singh, R. K., M. H. Kabbaj, J. Paik and A. Gunjan (2009). "Histone levels are regulated by phosphorylation and ubiquitylation-dependent proteolysis." Nat Cell Biol **11**(8): 925-933.

Sinha, M., S. Watanabe, A. Johnson, D. Moazed and C. L. Peterson (2009). "Recombinational repair within heterochromatin requires ATP-dependent chromatin remodeling." Cell **138**(6): 1109-1121.

Soria, G., S. E. Polo and G. Almouzni (2012). "Prime, repair, restore: the active role of chromatin in the DNA damage response." Mol Cell **46**(6): 722-734.

Spichal, M., A. Brion, S. Herbert, A. Cournac, M. Marbouty, C. Zimmer, R. Koszul and E. Fabre (2016). "Evidence for a dual role of actin in regulating chromosome organization and dynamics in yeast." J Cell Sci **129**(4): 681-692.

Stillman, D. J. (2010). "Nhp6: a small but powerful effector of chromatin structure in Saccharomyces cerevisiae." Biochimica et Biophysica Acta (BBA)-Gene Regulatory Mechanisms **1799**(1): 175-180.

Strecker, J., G. D. Gupta, W. Zhang, M. Bashkurov, M. C. Landry, L. Pelletier and D. Durocher (2016). "DNA damage signalling targets the kinetochore to promote chromatin mobility." Nat Cell Biol **18**(3): 281-290.

Su XA, D. V., Gasser SM, Freudenreich CH (2015). "Regulation of recombination at yeast nuclear pores controls repair and triplet repeat stability." GENES & DEVELOPMENT(29): 1006–1017.

Swartz, R. K., E. C. Rodriguez and M. C. King (2014). "A role for nuclear envelope-bridging complexes in homology-directed repair." Mol Biol Cell **25**(16): 2461-2471.

Symington, L. S. and J. Gautier (2011). "Double-strand break end resection and repair pathway choice." Annual review of genetics **45**: 247-271.

Taddei, A. and S. M. Gasser (2012). "Structure and function in the budding yeast nucleus." Genetics **192**(1): 107-129.

Taddei, A., G. Van Houwe, F. Hediger, V. Kalck, F. Cubizolles, H. Schober and S. M. Gasser (2006). "Nuclear pore association confers optimal expression levels for an inducible yeast gene." Nature **441**(7094): 774-778.

Talbert, P. B., K. Ahmad, G. Almouzni, J. Ausio, F. Berger, P. L. Bhalla, W. M. Bonner, W. Z. Cande, B. P. Chadwick, S. W. Chan, G. A. Cross, L. Cui, S. I. Dimitrov, D. Doenecke, J. M. Eirin-Lopez, M. A. Gorovsky, S. B. Hake, B. A. Hamkalo, S. Holec, S. E. Jacobsen, K. Kamieniarz, S. Khochbin, A. G. Ladurner, D. Landsman, J. A. Latham, B. Loppin, H. S. Malik, W. F. Marzluff, J. R. Pehrson, J. Postberg, R. Schneider, M. B. Singh, M. M. Smith, E. Thompson, M. E. Torres-Padilla, D. J. Tremethick, B. M. Turner, J.

H. Waterborg, H. Wollmann, R. Yelagandula, B. Zhu and S. Henikoff (2012). "A unified phylogeny-based nomenclature for histone variants." Epigenetics Chromatin **5**: 7.

Tang, H. M., C. C. Talbot, Jr., M. C. Fung and H. L. Tang (2017). "Molecular signature of anastasis for reversal of apoptosis." F1000Res **6**: 43.

Teves, S. S. and S. Henikoff (2014). "Transcription-generated torsional stress destabilizes nucleosomes." Nat Struct Mol Biol **21**(1): 88-94.

Therizols, P., C. Fairhead, G. G. Cabal, A. Genovesio, J. C. Olivo-Marin, B. Dujon and E. Fabre (2006). "Telomere tethering at the nuclear periphery is essential for efficient DNA double strand break repair in subtelomeric region." J Cell Biol **172**(2): 189-199.

Timashev, L. A., H. Babcock, X. Zhuang and T. de Lange (2017). "The DDR at telomeres lacking intact shelterin does not require substantial chromatin decompaction." Genes Dev **31**(6): 578-589.

Timinszky, G., S. Till, P. O. Hassa, M. Hothorn, G. Kustatscher, B. Nijmeijer, J. Colombelli, M. Altmeyer, E. H. Stelzer, K. Scheffzek, M. O. Hottiger and A. G. Ladurner (2009). "A macrodomain-containing histone rearranges chromatin upon sensing PARP1 activation." Nat Struct Mol Biol **16**(9): 923-929.

Torres-Rosell, J., I. Sunjevaric, G. De Piccoli, M. Sacher, N. Eckert-Boulet, R. Reid, S. Jentsch, R. Rothstein, L. Aragon and M. Lisby (2007). "The Smc5-Smc6 complex and SUMO modification of Rad52 regulates recombinational repair at the ribosomal gene locus." Nat Cell Biol **9**(8): 923-931.

Towbin, B. D., A. Gonzalez-Sandoval and S. M. Gasser (2013). "Mechanisms of heterochromatin subnuclear localization." Trends Biochem Sci **38**(7): 356-363.

Travers, A. A. (2003). "Priming the nucleosome: a role for HMGB proteins?" EMBO reports **4**(2): 131-136.

Tsabar, M., W. M. Hicks, O. Tsaponina and J. E. Haber (2016). "Re-establishment of nucleosome occupancy during double-strand break repair in budding yeast." DNA Repair (Amst) **47**: 21-29.

Tsouroula, K., A. Furst, M. Rogier, V. Heyer, A. Maglott-Roth, A. Ferrand, B. Reina-San-Martin and E. Soutoglou (2016). "Temporal and Spatial Uncoupling of DNA Double Strand Break Repair Pathways within Mammalian Heterochromatin." Mol Cell **63**(2): 293-305.

van Attikum, H., O. Fritsch, B. Hohn and S. M. Gasser (2004). "Recruitment of the INO80 complex by H2A phosphorylation links ATP-dependent chromatin remodeling with DNA double-strand break repair." Cell **119**(6): 777-788.

van Sluis, M. and B. McStay (2015). "A localized nucleolar DNA damage response facilitates recruitment of the homology-directed repair machinery independent of cell cycle stage." Genes Dev **29**(11): 1151-1163.

Vancevska, A., K. M. Douglass, V. Pfeiffer, S. Manley and J. Lingner (2017). "The telomeric DNA damage response occurs in the absence of chromatin decompaction." Genes Dev **31**(6): 567-577.

Vazquez, J., A. S. Belmont and J. W. Sedat (2001). "Multiple regimes of constrained chromosome motion are regulated in the interphase Drosophila nucleus." Curr Biol **11**(16): 1227-1239.

Verdaasdonk, J. S., P. A. Vasquez, R. M. Barry, T. Barry, S. Goodwin, M. G. Forest and K. Bloom (2013). "Centromere tethering confines chromosome domains." Mol Cell **52**(6): 819-831.

Wang, H., L. Zhai, J. Xu, H. Y. Joo, S. Jackson, H. Erdjument-Bromage, P. Tempst, Y. Xiong and Y. Zhang (2006). "Histone H3 and H4 ubiquitylation by the CUL4-DDB-ROC1 ubiquitin ligase facilitates cellular response to DNA damage." Mol Cell **22**(3): 383-394.

Wang, Z., C. Zang, J. A. Rosenfeld, D. E. Schones, A. Barski, S. Cuddapah, K. Cui, T. Y. Roh, W. Peng, M. Q. Zhang and K. Zhao (2008). "Combinatorial patterns of histone acetylations and methylations in the human genome." Nat Genet **40**(7): 897-903.

Weber, S. C., J. A. Theriot and A. J. Spakowitz (2010). "Subdiffusive motion of a polymer composed of subdiffusive monomers." Phys Rev E Stat Nonlin Soft Matter Phys **82**(1 Pt 1): 011913.

Wei, W., Z. Ba, M. Gao, Y. Wu, Y. Ma, S. Amiard, C. I. White, J. M. Rendtlew Danielsen, Y. G. Yang and Y. Qi (2012). "A role for small RNAs in DNA double-strand break repair." Cell **149**(1): 101-112.

Weiner, A., N. Zauberman and A. Minsky (2009). "Recombinational DNA repair in a cellular context: a search for the homology search." Nat Rev Microbiol **7**(10): 748-755.

Woodbine, L., H. Brunton, A. A. Goodarzi, A. Shibata and P. A. Jeggo (2011). "Endogenously induced DNA double strand breaks arise in heterochromatic DNA regions and require ataxia telangiectasia mutated and Artemis for their repair." Nucleic Acids Res **39**(16): 6986-6997.

Xu, C., Y. Xu, O. Gursoy-Yuzugullu and B. D. Price (2012). "The histone variant macroH2A1.1 is recruited to DSBs through a mechanism involving PARP1." FEBS Lett **586**(21): 3920-3925.

Xu, Y., Y. Sun, X. Jiang, M. K. Ayrapetov, P. Moskwa, S. Yang, D. M. Weinstock and B. D. Price (2010). "The p400 ATPase regulates nucleosome stability and chromatin ubiquitination during DNA repair." J Cell Biol **191**(1): 31-43.

Yoshida, T., K. Shimada, Y. Oma, V. Kalck, K. Akimura, A. Taddei, H. Iwahashi, K. Kugou, K. Ohta, S. M. Gasser and M. Harata (2010). "Actin-related protein Arp6 influences H2A.Z-dependent and -independent gene expression and links ribosomal protein genes to nuclear pores." PLoS Genet **6**(4): e1000910.

Zakian, S.-C. T. a. V. A. (1999). "Telomere-Telomere Recombination Is an Efficient Bypass Pathway for Telomere Maintenance in *Saccharomyces cerevisiae*." Molecular and cellular biology **19**: 8083–8093.

Zentner, G. E. and S. Henikoff (2013). "Regulation of nucleosome dynamics by histone modifications." Nat Struct Mol Biol **20**(3): 259-266.

Zhang, C., T. M. Roberts, J. Yang, R. Desai and G. W. Brown (2006). "Suppression of genomic instability by SLX5 and SLX8 in Saccharomyces cerevisiae." DNA Repair (Amst) **5**(3): 336-346.

Zhou, J., J. Y. Fan, D. Rangasamy and D. J. Tremethick (2007). "The nucleosome surface regulates chromatin compaction and couples it with transcriptional repression." Nat Struct Mol Biol **14**(11): 1070-1076.

Ziv, Y., D. Bielopolski, Y. Galanty, C. Lukas, Y. Taya, D. C. Schultz, J. Lukas, S. Bekker-Jensen, J. Bartek and Y. Shiloh (2006). "Chromatin relaxation in response to DNA double-strand breaks is modulated by a novel ATM- and KAP-1 dependent pathway." Nat Cell Biol **8**(8): 870-876.

CHAPTER 2: NUCLEOSOME REMODELERS IN DOUBLE-STRAND BREAK REPAIR

Seeber, A.*, **Hauer, M**.*, and Gasser, S.M. (2013). Nucleosome remodelers in double-strand break repair. Current Opinion in Genetics & Development 23, 174-184. * Equal contribution

Author contributions: M.H., A.S. and S.M.G. wrote the manuscript. M.H. and A.S. designed the figures. All the authors discussed the data and participated in the preparation of the manuscript.

Gerhold, C. B., **M. H. Hauer** and S. M. Gasser (2015). "INO80-C and SWR-C: guardians of the genome." J Mol Biol 427(3): 637-651.

Author contributions: C.B.G. and S.M.G. wrote the manuscript. M.H. designed the figures and assisted in the final assembly of the article. All the authors discussed the data and participated in the preparation of the manuscript.

Summary

This chapter highlights the importance of nucleosome remodelers in DNA repair and provides an in-depth overview on INO80 and SWR-1 remodeling complex function. It consists of two parts based on the review articles shown here.

Remodelers form a conserved class of proteins harboring a Swi2/Snf2 ATPase that uses the energy from ATP hydrolysis to change the local state of chromatin by exchanging histone variants, ejecting octamers and sliding/spacing nucleosomes. These actions regulate gene transcription, DNA replication, repair and chromatin structure genome-wide. The first part of this chapter discusses the roles of yeast and mammalian chromatin remodeling complexes in DSB repair pathways. We provide side by side comparisons of remodeler subunit conservation and their respective roles in DNA damage repair. In addition, we highlight the importance of chromatin remodeling in regulating damage-provoked local and global chromatin mobility. The second part of this chapter specifically discusses the roles of INO80-C and SWR1 as "Guardians of the Genome". Both remodelers possess important functions in DSB relocation events, cell cycle regulation, damage repair and were implicated in cancer.

Available online at www.sciencedirect.com

SciVerse ScienceDirect

Current Opinion in Genetics & Development

Nucleosome remodelers in double-strand break repair

Andrew Seeber[1,2,4], Michael Hauer[1,3,4] and Susan M Gasser[1,2]

ATP-dependent nucleosome remodelers use ATP hydrolysis to shift, evict and exchange histone dimers or octamers and have well-established roles in transcription. Earlier work has suggested a role for nucleosome remodelers such as INO80 in double-strand break (DSB) repair. This review will begin with an update on recent studies that explore how remodelers are recruited to DSBs. We then examine their impact on various steps of repair, focusing on resection and the formation of the Rad51-ssDNA nucleofilament. Finally, we will explore new studies that implicate remodelers in the physical movement of chromatin in response to damage.

Addresses
[1] Friedrich Miescher Institute for Biomedical Research, Maulbeerstrasse 66, CH-4058 Basel, Switzerland
[2] University of Basel, Faculty of Natural Sciences, Klingelbergstrasse 50, CH-4056 Basel, Switzerland
[3] University of Tuebingen, Interfaculty Institute for Cell Biology, Department of Molecular Biology, Auf der Morgenstelle 15, D-72076 Tuebingen, Germany

Corresponding author: Gasser, Susan M (susan.gasser@fmi.ch)
[4] These authors contributed equally to this work.

Current Opinion in Genetics & Development 2013, **23**:xx–yy

This review comes from a themed issue on **Genome architecture and expression**

Edited by **Genevieve Almouzni** and **Frederick Alt**

0959-437X/$ – see front matter,

http://dx.doi.org/10.1016/j.gde.2012.12.008

Introduction

In eukaryotic cells, the genomic DNA is wrapped around histone proteins to form a compact nucleosomal fiber. This form of chromatin is bound and protected by a variety of factors, yet is nonetheless susceptible to environmentally induced damage. Once damaged, repair and checkpoint signaling machineries recruit chromatin modifying enzymes to render damaged DNA accessible to repair. This is mediated both by enzymes that modify histones and by ATP-dependent nucleosome remodelers that can shift, evict and exchange histone dimers or octamers, facilitating the different steps of the repair process. Histone modifications coordinate repair with other DNA-based functions, such as transcription and replication. Recent work also suggests that nucleosome remodelers enhance micromovement [1•] and possibly evict proteins that inhibit the repair process [2••]. Finally, the re-establishment of the initial chromatin structure requires histone chaperones and various modifying enzymes that deposit or remove acetyl-groups, methyl-groups and ubiquitin from histone tails [3]. It is likely that active nucleosome remodeling is required as well for proper recovery after repair.

All remodelers of the SWI2/SNF2 family contain related, large catalytic ATPase subunits. A new phylogenetic analysis has replaced the classical grouping (SWI/SNF, ISWI, CHD and INO80) of the various remodelers, splitting them into six major families, namely the Snf2-like, Swr1-like, SMARCAL1, Rad54-like, Rad5/16-like and ERCC6/SSO1653-like [4] (Table 1). SWI/SNF members of the Snf2-like family contain a bromodomain which binds acetylated histone tails. ISWI remodelers have HAND, SANT and SLIDE domains involved in DNA binding in the context of nucleosomes. The Snf2-like family also includes CHD remodelers, which contain a tandem chromodomain that mediates binding to methylated histones. INO80 complexes fall into the Swr1-like class, which has a characteristic insert in the middle of the ATPase domain, and contain a RuvB-like DNA helicase, Rvb1/2 in yeast or TIP49a,b in mammals. Most remodeling complexes harbor a number of additional subunits, among them actin and actin related proteins (Arps), some of which are shared, others unique to specific remodelers (Table 1) [5].

Previous work had shown that mutation or down-regulation of some remodeler subunits renders cells hypersensitive to DNA damage [6]. This phenotype, however, can stem from effects either on transcription, replication, or the repair pathway itself. To study the direct involvement of chromatin remodelers in double strand break (DSB) repair, chromatin immunoprecipitation (ChIP) and fluorescent imaging studies have monitored whether or not a given ATP-dependent nucleosome remodeler was recruited to a unique DSB or to a zone of laser-induced damage. These approaches have implicated many remodelers directly in steps of repair, and most frequently in repair by homologous recombination (HR), but more recently, also by non-homologous end joining (Table 2). Given the broader effect of remodelers on chromatin composition, we will hereafter refer to them as chromatin remodelers, rather than nucleosome remodelers. In this review, we provide an overview about the various roles that remodeling complexes play during DSB repair. Crucial to understand is how remodelers are initially recruited to DSBs, how they impact the various steps of repair and how they affect the formation of the Rad51-ssDNA nucleofilament. Recent studies also implicate chromatin remodelers in changing the physical movement of DNA in response to damage.

Please cite this article in press as: Seeber A, et al.: Nucleosome remodelers in double-strand break repair, Curr Opin Genet Dev (2013), http://dx.doi.org/10.1016/j.gde.2012.12.008

Table 1

Composition and classification of nucleosome remodelers in *S. cerevisiae* and Human.

Grouping			Organism							
Family	Subfamily & Composition		*S. cerevisiae*				Human			
Swr1 like	Ino80	Complex	**INO80**				**INO80**			
		ATPase	Ino80				hINO80			
		Orthologous subunits	Rvb1*, Rvb2*				TIP49A*, TIP49B*			
			Arp4*, Arp5*, Arp8, Act1				BAF53a*, ARP5, ARP8			
			Taf14							
			Ies2				hIES2			
			Ies6				hIES6			
		Unique	Ies1, Ies3-5, Nhp10				Amida, NFRKB, MCRS1, FLJ90652, FLJ20309			
	Swr1	Complex	**SWR1**				**SRCAP**		**TRRAP/Tip60**	
		ATPase	Swr1				SRCAP		p400	
		Orthologous subunits	Rvb1*, Rvb2*				Tip49a*, Tip49b*		Tip49a*, Tip49b*	
			Arp4*, Arp6, Act1				BAF53a*, Arp6		BAF53a*, Actin	
			Yaf9				GAS41*		GAS41*	
			Swc4/Eaf2				DMAP1*		DMAP1*	
			Swc2/Vps72				YL-1*		YL-1*	
			Bdf1						BRD8/TRCp120	
			H2AZ, H2B				H2AZ, H2B			
			Swc6/Vps71				Znf-HIT1			
		Unique	Swc3,5,7						Tip60, MRG15, MRGX, FLJ11730, MRGBP, EPC1,EPC-like, ING3	
	Etl1	Complex	**FUN30**				**SMARCAD1**			
		ATPase	Fun30				SMARCD1			
		Subunits	Not identified				Not identified			
Snf2 like	Mi-2	Complex	**No homolog**				**NuRD**			
		ATPase					CHD3/Mi-2α CHD4/Mi-2β			
		Subunits					MBD2,MBD3, MTA1-3, HDAC1-2, RbAp46 or 48, p66α, p66β			
	Chd1	Complex	**CHD1**				**CHD1**			
		ATPase	Chd1				CHD1			
		Subunits	monomeric				monomermic			
	Alc1	**Complex**	**No homolog**				**ALC1**			
		ATPase					ALC1			
		Subunits					Not identified			
	Snf2	Complex	**SWI/SNF**		**RSC**		**BAF**		**PBAF**	
		ATPase	Swi2/Snf2		Sth1		BRG1/SMARCA4 or hBRM/SMARCA2		BRG1	
		Orthologous subunits					BAF250a/ARID1A or BAF250b/ARID1B or			
					Rsc1, Rsc2, Rsc4		BAF180*, BAF200/ARID2*		BAF180*, BAF200/ARID2*	
			Swi3		Rsc8		BAF155/SMARCC1* and/or BAF170/SMARCC2*		BAF155/SMARCC1* and/or BAF170/SMARCC2*	
			Swp73		Rsc6		BAF60a/SMARCD1*		BAF60a/SMARCD1*	
			Arp7*, Arp9*		Arp7*, Arp9*		BAF53a*		BAF53a*	
			Snf5		Sfh1		BAF47/hSNF5/SMARCB1*		BAF47/hSNF5/SMARCB1*	
							BAF57/SMARCE1*		BAF57/SMARCE1*	
							β-actin*		β-actin*	
		Unique	Swi1/Adr6, Swp82, Taf14, Snf6, Snf11		Rsc3, Rsc5, Rsc7, Rsc9, Rsc10, Rsc30, Htl1, Lbd7, Rtt102		BAF45a or BAF45d			
	Iswi	Complex	**ISW1a**	**ISW1b**		**ISW2**	**ACF**	**CHRAC**		**NURF**
		ATPase	Isw1*	Isw1*		Isw2	hSNF2H			hSNF2L
		Orthologous subunits				Itc1	WCRF180/ hACF1*	WCRF180/ hACF1*		BPTF
						Dpb4		hCHRAC17		RbAp46
						Dls1		hCHRAC15		RbAp48
		Unique	Ioc3	Ioc2, Ioc4						
Rad54 like	Rad54	Complex	**Rad54**				**Rad54**			
		ATPase	Rad54				Rad54			

*Subunits shared within different remodeling complexes of the same organism.

Recruitment of chromatin remodelers to a DSB

The INO80 nucleosome remodeler is recruited to DSBs in both yeast and man. In yeast, the INO80 complex is made up of 15 subunits including Ino80, Rvb1/2, Arp5/8, Arp4, Act1, Nhp10 and Ies3. Its recruitment to DSBs in yeast requires an interaction with phosphorylated H2A (γH2A); mutation of the phosphoacceptor site on yeast H2A reduced INO80 binding at an induced DSB [7]. The subunits implicated in this interaction are Nhp10 and Ies3

Please cite this article in press as: Seeber A, et al.: Nucleosome remodelers in double-strand break repair, Curr Opin Genet Dev (2013), http://dx.doi.org/10.1016/j.gde.2012.12.008

Table 2

A summary of [chromatin remodelers], the relevant subunit and key findings reported in this review

Family & Subunits				Remodeler subunit functions addressed in this review			
Grouping[4]		Name of Remodeling complex	Core Subunits [4,5]	Remodeler complex function/Remarks	Subunit (organism)	(Proposed) function of subunit during DNA damage repair	Ref.
Family	Sub family						
Swr1 like	Ett1	Fun30	non identified	In budding yeast, Fun30 promotes long range DNA end resection & regulates centromere function. In fission yeast, Fft3 acts as a protector of heterochromatic regions.	Fun30(*Sce*)	A novel remodeling enzyme with higher activity in histone dimer exchange than nucleosome repositioning. Promotes long range DNA end resection and checkpoint adaptation through removal of Rad9. Regulates the function and architecture of centromeric chromatin via nucleosome remodeling and blocking of transcription over centromeres.	[38] [2,42] [40]
		Fft3/Fun30	non identified		Fft3 (*Spo*)	Localizes at known insulator elements, protecting centromeres and subtelomeres from euchromatin spreading. Fft3 controls the identity of heterochromatic regions.	[41]
	SMARCAD1	non identified		Closest homolog to yeast Fun30 with roles in the maintenance of silent chromatin and novel functions in DNA end resection and repair	SMARCAD1 (*Hsa*)	Role in DNA end resection, knockdowns result in homologous recombination and RPA foci formation defects.	[42]
Ino80	INO80	15		INO80 has been studied for many years in yeast, plants and humans. It plays a role in many steps of DSB repair via homologous recombination; implications have been made in resection, nucleofilament formation and the dynamics of a DSB fiber.	Arp4 (*Sce*)	Arp4 is lost upon Arp8 deletion and it physically associates with γH2A, promoting INO80 recruitment to the site of a DSB.	[7,63]
					ARP5 (*Hsa*)	Mammalian ARP5 shuttles between the cytoplasm and the nucleus, promoting initial H2A.X phosphorylation and INO80 binding to γ-H2A.X upon damage.	[11]
					Arp5 (*Ath*)	Arp5 is essential in plants to promote resistance to DNA damaging agents.	[12]
					ARP8 (*Hsa*)	Major role in recruiting INO80 to sites of damage, independent of H2A.X phosphorylation. Novel findings link ARP8 to RPA foci formation and ssDNA accumulation, implying a role in resection.	[10,35]
					Arp8 (*Sce*)	Stabilizes Arp4 and Act1 in INO80. Increases the processivity and rate of recombination rate of a locus when targeted onto chromatin. Promotes Rad51 recruitment to sites of damage in haploid cells.	[1,7,8, 47,63]
					Nhp10 (*Sce*)	Required for Arp4 dependent interaction of INO80 with γH2A.	[7]
					Ies3 (*Sce*)	Promotes γH2A dependent recruitment of INO80 to DSBs (lost from the complex in *nhp10Δ*).	[7]
					Act1 (*Sce*)	Like Arp4, is lost upon deletion of Arp8.	[7,63]
	Swr1	Swr1	19	Among other roles, the yeast SWR1 remodeling complex deposits H2A.Z (Htz1 in yeast) at DSBs by catalyzing the replacement of H2A–H2B dimers with H2A.Z–H2B dimers. This reaction occurs stepwise and in an unidirectional manner.			[13]
		TTRAP/Tip60	22		P400(*Hsa*)	The catalytic subunit P400 can exchange H2A.Z onto nucleosomes at DSBs. Incorporation of H2A.Z along with other modifications subsequently facilitates loading of brca1 complexes.	[17]
	Ino80, Swr1	INO80, SRCAP TTRAP/Tip60	15,13,22	TIP49a/b acts as a part of many human remodeling complexes with potential roles in DNA repair	TIP49a; TIP49b (*Hsa*)	The yeast homolog Rvb1/Rvb2 unwinds DNA at 3′ ssDNA overhangs, implying a role in processing resected ends. Promotes RAD51 foci accumulation at DSBs by relaxing chromatin and making it accessible for the repair machinery.	[37,45, 46]
Snf2 like	Mi-2	NuRD	12	The NuRD complex has a well established role in deacetylating chromatin, promoting repressive states and regulating development *in vitro*as well as remodeling nucleosomes *in vitro*. Its function during DNA damage repair can vary with the composition of the complex (CHD3 or CHD4 containing).	CHD3(*Hsa*)	Acts as a heterochromatin factor and is released via ATM dependent KAP1 phosphorylation upon damage. Loss of CHD3 leads to chromatin decondensation and genomic instability.	[31]
					CHD4 (*Hsa*)	Is recruited to sites of DNA damage (PARylation dependent) where it promotes Ubiquitination of histones and thereby the recruitment of BRCA1 and RNF168. CHD4 has a function in G2/M checkpoint maintenance.	[28,64] [28]
	Alc1	ALC1/CHD1L	1	ALC1 was identified as a novel, CHD1-like (CHD1L) remodeler. Its recruitment to breaks is adenosine 5′-diphosphate (ADP)-ribose (PAR) dependent.	ALC1(*Hsa*)	ALC1 re-positions nucleosomes in-vitro. Interacts with NHEJ proteins, probably priming breaks for repair by NHEJ.	[28-30]
	Snf2	RSC	18	The yeast RSC complex is known to prime the DSB site for repair by mobilizing nucleosomes and loading Mre11. Novel results implicate RSC in DNA end resection, even though cells depleted for RSC are still proficient in SSA.			[2,34,6 5]
		SWI/SNF	11	Yeast SWI/SNF has broad roles in regulating transcription, mitotic exit and activation of yeast replication origins. In higher eukaryotes, SWI/SNF remodeler complexes localize to DSBs and play distinct roles in repair events as well as regulating the damage response checkpoint.	BAF170(*Hsa*)	Mediates SWI/SNF recruitment to DSB sites after damage in an ATM/ATR phosphorylation dependent manner (enhanced by BRIT1/MCPH1). Impacts the DNA damage checkpoint through interaction with p53 and the acetyl transferase CBP. Required to propagate γH2A.Xvia its interaction with H3K14-Indication of a novel, cooperative activation loop with H3 HAT Gcn5 upon DNA damage	[23] [21,66, 67]
					BRG1(*Hsa*)		
					hBRM(*Hsa*)	In contrast to BAF170, this alternative SWI/SNF catalytic subunit plays no role in regulating the DNA damage response.	[66]
Rad54 like	Rad54	Rad54	1	Rad54 is not a classic SNF2 remodeling enzyme but able to slide and remodel nucleosomes *in vitro*. Rad54 plays a major role in middle to late steps during homologous recombination and was recently implicated in regulating the dynamics of a DNA DSB fiber.	Rad54 yeast & human	Facilitates strand invasion and slides nucleosomes *in vitro*. Stabilizes the Rad51 ssDNA nucleofilament. Promotes homologous recombination.	[50,51, 59]
					Rad54(*Sce*) Rad54(*Hsa*)	Essential for the increased movement and nuclear search volume of an Ise1 induced DSB. Recruitment to DSBs is independent of ATP usage but dissociation from chromatin and the relocalization of damage foci to the nuclear periphery requires ATP hydrolysis.	[50] [47]

Please cite this article in press as: Seeber A, et al.: Nucleosome remodelers in double-strand break repair, Curr Opin Genet Dev (2013), http://dx.doi.org/10.1016/j.gde.2012.12.008

(a subunit which is lost upon deletion of *NHP10*) [8], and Arp4, with Arp4 having been shown to physically associate with γH2A [9]. The story appears to be different in mammals, where INO80 is recruited to laser-induced sites of damage independently of γH2A.X, but in a manner sensitive to loss of Arp8 [10]. shRNA against other INO80 subunits did not have an effect on recruitment, but it should be noted that the INO80 subunits studied were only reduced to levels ranging from 20% to 40% of wild-type levels. It remains possible that other INO80 subunits play a role in the recruitment to DSBs, but that the shRNA knock-down was not sufficient to impair binding at the break. Another mammalian study shows that Arp5 interacts with γH2A.X and promotes its initial phosphorylation [11]. In the same vein, a new report using *Arabidopsis* shows that Arp5 is required to prevent sensitivity to DNA damaging agents, highlighting the importance of this subunit [12]. Collectively these findings argue that in higher eukaryotes the initial recruitment of INO80 is mediated by Arp8, while Arp5 subsequently interacts with and facilitates the spread of γH2AX.

Also recruited by interaction with γH2A.X is the INO80-related yeast remodeler SWR1 (p400 or SRCAP in man). The SWR1 remodeler has been shown to deposit H2A.Z (Htz1 in yeast), a conserved variant of H2A, by catalyzing the replacement of H2A–H2B dimers with H2A.Z–H2B dimers in a stepwise and unidirectional manner [13]. H2A.Z is found enriched near the TSS of genes, as well as in some heterochromatic regions. A number of papers implicate H2A.Z or Htz1 in repair pathways [14] and, not surprisingly, mutants in Swr1 or Swr1 complex components are sensitive to DNA damaging agents [15,16]. In mammalian cells, H2A.Z can be exchanged onto nucleosomes at DSBs by TRRAP/TIP60's p400 ATPase domain, the recruitment of which depends on γH2A.X, as in yeast [36]. At the DSB, H2A.Z exchange is required for the acetylation of histone H4 by TIP60, and for histone ubiquitination by RNF8. H2A.Z then ultimately leads to enhanced Ku recruitment, favoring repair by NHEJ, whereas its absence, leads to extensive resection and inaccurate repair [17•].

The SWI/SNF remodeling complex has also been shown to be recruited to DSBs [18], although the mechanism of recruitment is unknown, particularly in yeast. In one report, a null mutant of the yeast SWI/SNF subunit Snf2 did not result in enhanced sensitivity to UV or ionizing radiation (IR) [19], while in other yeast backgrounds *SNF2* or *SNF5* deletions rendered cells susceptible to either HU or bleomycin treatment [18]. Indeed, in this paper, SWI/SNF2 subunits could be detected at DSBs by ChIP one hour after damage induction [18]. What SWI/SNF achieves at DSBs in yeast is unclear, as it appears to be dispensable for HR if the donor sequence is euchromatic. On the other hand, SWI/SNF was shown to be necessary for the eviction of heterochromatin factors (Sir3) from donor sequences *in vitro* [20]. This occurs during mating type switching, which requires invasion of the resected DNA strands from *MAT* into silent chromatin at *HM* loci.

In humans, the SWI/SNF complex contains one of two catalytic subunits, BRG1 or BRM, along with many BRG1/BRM associated factors (BAFs) [5]. A recent study proposed a positive feedback loop, in which the histone acetyl transferase (HAT) GCN5 binds to γH2A.X upon damage, acetylating adjacent H3 molecules, which would be recognized by the bromodomain of BRG1. SWI/SNF is then thought to facilitate access to the damage extending phosphorylation of H2A.X and thus more acetylation [21•]. However, other HATs, such as Tip60, p300 and CBP have been shown to work with SWI/SNF at DSBs in NHEJ [22].

In a more general way, DSBs undergo a series of dependent events which involve ubiquitination, acetylation of H3K14 and finally the acetylation-dependent recruitment and active remodeling by the SWI/SNF subunit BRG1.

In one study, SWI/SNF was shown to be recruited to neocarzinostatin induced DSBs in a manner promoted by BRIT1/MCPH1, an early DNA damage response protein. This entailed the ATR/ATM dependent phosphorylation of the SWI/SNF subunit, BAF170. Chromatin cannot relax as monitored by MNase sensitivity assays upon BRIT/MCPH1 depletion, which coincides with defects in both HR and NHEJ in mammalian cells [23].

In conclusion, human SWI/SNF has previously unappreciated roles in promoting the early spread of γH2A.X and histone acetylation at DSBs. Whether NHEJ and HR pathways have a differential dependence on SWI/SNF is not yet clear.

Repressive Snf2-like remodeling complexes of the Mi-2 and CHD class (such as CHD1 and NuRD complexes) are unique in the sense that their catalytic subunits contain a characteristic N-terminal tandem chromodomain, which directs them to methylated histones. This domain, at least for Chd1, regulates its ATPase motor dynamics [24•]. CHD1 and NuRD have clear roles in transcriptional regulation, histone dynamics and gene silencing [5], whereas their impact on DSB repair is only starting to be revealed.

In mammalian cells, shRNA knockdowns of NuRD subunits, CHD4 or MTA2, resulted in increased levels of spontaneous damage and persistent p53 activation [25•]. CHD4 also promotes ubiquitination of histones, which correlates with recruitment of BRCA1 and RNF168 and maintenance of the G2/M checkpoint. Further studies

Please cite this article in press as: Seeber A, et al.: Nucleosome remodelers in double-strand break repair, Curr Opin Genet Dev (2013), http://dx.doi.org/10.1016/j.gde.2012.12.008

showed that the NuRD components CHD4 and MTA1 are recruited to sites of IR-induced DNA damage. This recruitment takes place in a previously unappreciated, polyadenosine 5′-diphosphate (ADP)-ribose (PARylation)-dependent manner, but is independent of H2A.X phosphorylation [26•,27••]. It was also shown that components of the Polycomb Repressive Complex 1 (PRC1), such as MEL-18, are recruited to DSBs in a PARylation-dependent manner, and that PARylation is required to exclude nascent RNA as well as RNA polymerase II from regions of laser induced damage [27••]. Thus PARylation and NuRD recruitment appear to repress transcription at breaks. Speculation on the role of heterochromatin proteins in DSB repair is discussed elsewhere [3]. PARylation is also crucial for the recruitment of another human Snf2-like chromatin remodeler, ALC1, also known as CHD1L. ALC1 is targeted to sites of phleomycin-induced damage through its interaction with poly-ADP ribose. ALC1 overexpression delays or impedes repair, based on the comet assay. It is thought that ALC1 may promote NHEJ through its physical interactions with Ku70, XRCC1, DNA-PKcs and the histone chaperone APLF. Its interaction with subunits of the RPA complex may also suggest a role in HR, or another pathway of repair requiring DNA resection [28–30].

Finally, the related NuRD complex ATPase, CHD3, was shown to be lost from lesions induced in KAP-1-enriched heterochromatic domains [26•]. This effect is regulated by ATM dependent phosphorylation of KAP-1 at Ser824. Once KAP-1 is phosphorylated (pKAP-1), its direct interaction with CHD3 is disrupted, resulting in CHD3 loss from the domain. The ensuing chromatin relaxation is thought to promote DNA accessibility of heterochromatic regions, thereby facilitating repair [31••,32]. This is consistent with the role proposed for CHD3 and MI-2 in promoting chromatin compaction and gene repression [33].

The closest yeast equivalent to mammalian CHD3, CHD4 and ALC1 ATPases is the monomeric Chd1 remodeler (Table 1). Computational studies showed that yeast and other lower eukaryotes lack KAP-1-like proteins and PAR, and so far there have been no recent studies that link yeast Chd1 to DSB repair. In summary, these results identify ALC1 and CHD4 as active factors in genome maintenance that recruit DNA damage response factors, possibly favoring repair, while the related CHD3-containing NuRD remodeler complex needs to be lost from heterochromatic sites in order to aid repair. This suggests that the chromatin context of the DNA damage strongly influences which remodeler is important for subsequent repair events. Furthermore, depending on whether the situation calls for NHEJ-mediated or HR-mediated repair, resection may either need to be attenuated or promoted by remodeling complexes.

Role of chromatin remodelers in resection

The Swr1-like remodeler INO80 [7] and the Snf2-like remodeler RSC [34] were the first chromatin remodeling complexes to be associated with resection (for an in depth analysis see [6]). A recent study on mammalian INO80 and one of its subunits, Arp8, shows the importance of INO80 in RPA filament formation after damage [35•]. This is consistent with its previously demonstrated role in resection in yeast [36]. We note that, TIP49a,b which is part of the human INO80, SCRAP and TTRAP/Tip60 complexes [5] and yeast Rvb1/Rvb2 of INO80 and SWR1, have been shown to be ATP-dependent helicases that unwind DNA at 3′ ssDNA overhangs of at least 30 nucleotides in length, in a 3′ to 5′ direction [37]. These *in vitro* findings suggest that complexes containing TIP49a,b (or Rvb1/Rvb2) may be generally involved in processing resected DNA ends.

Fun30 is a poorly characterized chromatin remodeler of the Etl1 Snf2-like nucleosome remodeler family [4,38,39••]. The previous best described role of Fun30 was the protection of centromeres by maintaining the integrity of centromeric chromatin [40,41]. Three new studies highlight the role of Fun30 in Sgs1 and Exo1 dependent long-range resection at a DSB [2,40,42••]. Fun30 appears to be the most important chromatin remodeler for long-range resection in yeast, although this role is partially redundant with that of INO80 and RSC near the DSB [2]. This also appears to hold true in mammals for SMARCAD1, the closest human homologue of Fun30 [42••]. Intriguingly, Fun30 becomes partly dispensable when recruitment of the checkpoint mediator Rad9 is ablated. Rad9 inhibits resection at DSBs [43,44] thus favoring NHEJ over HR. Fun30 is proposed to remove Rad9 (Figure 1) and thus promote resection and HR [2,39••]. Consistently, when Fun30 is deleted, Rad9 spreads outwards from the DSB, presumably antagonizing resection [2]. This paper also offers evidence indicating that CHD1, SWR1, Rad54 and ISW1 remodeling factors do not play any significant role in resection, though Rad54 is epistatic with Fun30 with respect to its damage sensitivity [2].

Cells without intact INO80, SWR1 and RSC are still proficient in single-strand annealing (SSA), a repair mechanism that requires extensive resection to repair a DSB. However, *fun30Δ* strains are defective in repair by SSA, highlighting the importance of this protein's involvement in long range resection [2,39••]. Importantly, Fun30 does not seem to be involved in strand invasion or in later steps of HR. However, like *rdh54Δ* strains, *fun30Δ* strains are defective in adaptation to a single DSB, due to the hyperactivation of Mec1 (ATR kinase) through Mre11 [39••]. These papers have now added Fun30 to the list of DNA damage response factors, although little is known about the complex(es) it forms.

Please cite this article in press as: Seeber A, et al.: Nucleosome remodelers in double-strand break repair, Curr Opin Genet Dev (2013), http://dx.doi.org/10.1016/j.gde.2012.12.008

Figure 1

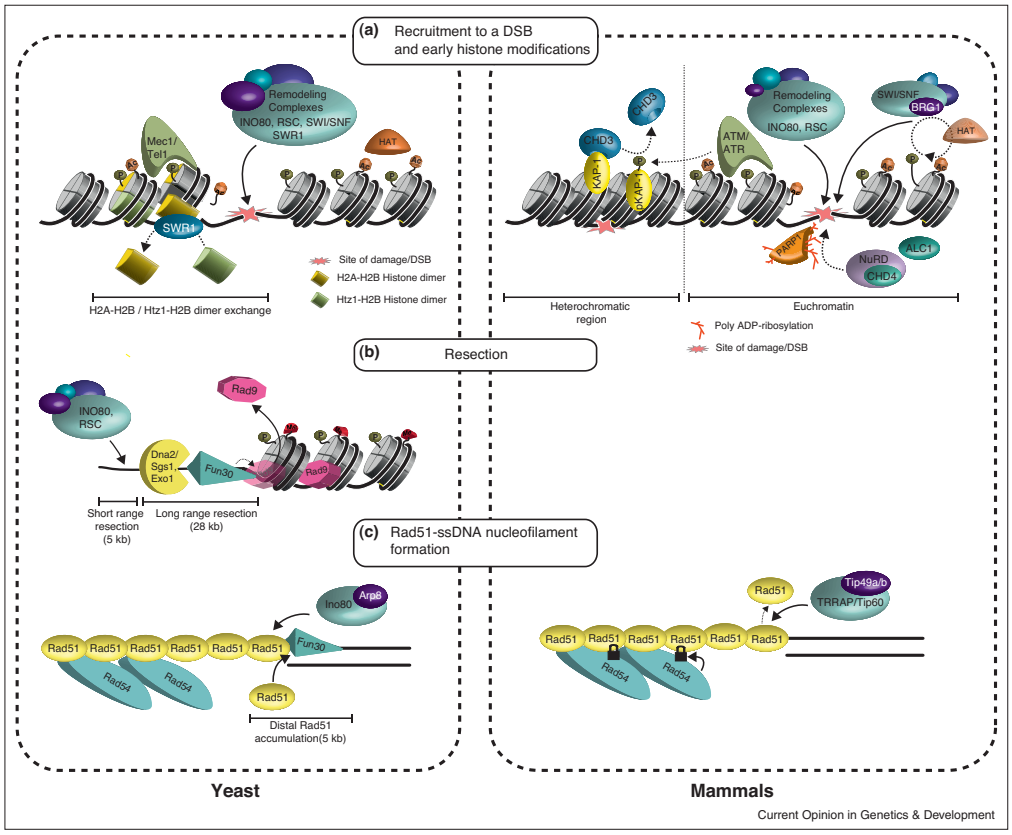

Chromatin remodeling at different steps during HR. **(a)** Formation of a DSB activates the DNA damage response followed by an orchestrated localization of repair factors to the site of damage, priming it for repair. The events occurring in budding yeast are on the left and those in mammals on the right. One of the first steps during DSB repair is the acetylation of histones, combined with phosphorylation by checkpoint kinases. The combination recruits chromatin remodeling complexes to the site of damage. Upon binding, remodelers change the local occupancy and histone composition of nucleosomes around the DSB, facilitating the accessibility for subsequent repair factors. In mammals both acetylation and the recruitment of remodelers associated with transcriptional repression is documented. In heterochromatic regions the CHD3-containing NuRD complex is evicted from heterochromatin. This may facilitate the opening of these compacted chromatin regions. PARylation is also important in recruiting NuRD complex components such as CHD4 and ALC1 (CHD1L) near the lesion. **(b)** The next step in HR requires resection of the dsDNA at the break site, generating a 3′ overhang. RSC and INO80 have a role in short range resection while Fun30 is essential for long range resection. Following DSB formation, Fun30 accumulates at distal sites from the break, removing the resection barrier imposed by Rad9 binding. Once Rad9 is removed, the exonucleases Dna2/Sgs1 and Exo1 can produce long ssDNA overhangs. **(c)** Following resection, the ssDNA binding protein Rad51 is loaded onto DNA and forms the ssDNA nucleofilament. Rad54 stabilizes the Rad51 filament. In haploid yeast cells, Arp8 within the INO80 complex is required for efficient accumulation of Rad51 at DSBs. In mammals Tip49a,b in the human TRRAP/Tip60 promotes Rad51 focus formation at DSBs.

Rad51-ssDNA filament formation

After resection, one of the next steps in HR is the formation of a Rad51 filament along the ssDNA strand. This is facilitated by a number of remodelers. For example when Fun30 is deleted, Rad51 levels at distal sites from a DSB (5 kb) are greatly reduced and accumulate slowly over time. Even though basal protein levels are reduced, this defect in recruitment and accumulation is not seen within proximal sites to the DSB (1 kb) [2].

The same holds true for Tip49a-depleted or Tip49b-depleted human cells where Rad51 focus accumulation

Please cite this article in press as: Seeber A, et al.: Nucleosome remodelers in double-strand break repair, Curr Opin Genet Dev (2013), http://dx.doi.org/10.1016/j.gde.2012.12.008

is strongly reduced in response to IR, rendering cells sensitive to damaging agents. Indeed, the amount of soluble Rad51 accumulates, and the level of chromatin-bound Rad51 decreases, upon Tip49a/b depletion. The authors also show that relaxing chromatin before DSB induction, using sodium butyrate to provoke hyperacetylation, restores the number of Rad51 foci to wild-type levels, possibly achieving the same opening of chromatin as that effected by the Tip49/TRRAP/Tip60 complex [45,46]. Alternatively, SRCAP may be involved. One model proposes that the role of Tip49 within the TTRAP–Tip60 complex is to relax chromatin by acetylation, enabling the access of the repair machinery at the break site. Mammalian INO80 does not seem to be important for the recruitment of Rad51, but rather affects the recruitment of early repair proteins such as 53BP1, which may antagonize HR [35•]. In contrast, in haploid yeast Rad51 recruitment to an irreparable DSB is diminished in *arp8*Δ cells [47]. We note that when a donor is present and the DSB was repairable by HR in yeast, as in the mammalian study, INO80 mutants did not show a defect in Rad51 recruitment [48]. Given that yeast Rad51 activity is enhanced in diploids, it may be that Arp8 becomes dispensable in diploid cells for Rad51-filament formation [49].

Rad54 also plays a role in stabilizing Rad51 ssDNA filaments [50,51]. Evidence from a new mammalian study indicates that Rad54 dependent accumulation of Rad51 does not require the ATPase domain of Rad54, although ATP hydrolysis is required for the dissociation of Rad54 from the filament. Following IR induced damage over five hours, the authors observed an increase in the number of Rad54-GFP foci at the nuclear periphery. After another five hours the number of foci at the periphery dropped to the same levels as at the beginning of the experiment. In a Rad54-GFP ATPase mutant, the number of foci at the periphery continued to accumulate over the course of the experiment. The authors interpret this effect as relocation of a DSB to the nuclear periphery. However, this result could also indicate that DSBs are repaired faster in internal regions (euchromatin) than at the periphery (heterochromatin), or that foci persist longer in less accessible peripheral heterochromatin [52••]. Finally, displacement of yeast heterochromatin factors by the SWI/SNF remodeler complex was shown to promote Rad51 mediated joint-molecule formation and Rad54 dependent strand invasion, priming the DSB for repair by HR *in vitro* [20]. Taken together, these observations support the model that SWI/SNF ATPases facilitate Rad51 focus formation while Rad54 promotes filament assembly.

Dynamics of the DSB fiber

The least understood step in HR is homology search [53] (Figure 2). This process implies that a DSB scans the nucleus for its homologous template, in order to anneal and finally carry out repair by recombination. Undamaged chromatin moves within the nucleus, but it is constrained by the continuity of the chromatin fiber [54]. Both sides of a break remain linked by the MRN/MRX complex, yet changes in chromatin structure could change the persistence length of the chromatin fiber [1]. Recently it was tested whether the mobility of a DNA locus changes upon DSB induction and the impact of such movement on HR-mediated repair. Two studies in budding yeast have shown that DNA bearing a DSB in S-phase cells moves through a nuclear volume approximately 4-times larger than that of undamaged DNA [55••,56••]. Similarly, in mammalian cells the mobility of IR induced foci was found to increase over that of undamaged chromatin [57•]. While yeast and man share this phenomenon, a small increase in radius of constraint in yeast can enhance access to more than 60% of the genome, while in mammalian cells the same radius of movement might only mean that damage shifts from a compacted domain of chromatin to an open space nearby, without accessing a large part of the genome.

In support of the idea that chromatin mobility enhances HR, it was shown that the decreased chromatin mobility scored in a *rad9*Δ strains, correlated with lower rates of heteroduplex formation, when the donor sequence sits on a nonhomologous chromosome [55••]. The ATR homologue Mec1 was also implicated in the increased mobility of the DSB [55••].

One way in which random chromatin movement can be increased is through the removal of nucleosomes, which might increase the flexibility of a compacted chromatin fiber. In support of this model, work from the Gasser laboratory showed that the targeting of INO80 increased chromatin mobility in a manner dependent on its ATPase activity. At the *PHO5* promoter the increased movement could be correlated with nucleosome displacement by INO80 [1]. Consistently, the enhanced movement scored at an induced DSB was partially reduced in an *arp8*Δ strain [1], while the loss of Rad51 or of Rad54's ATPase activity completely eliminated damage-induced chromatin mobility [55••]. Since Rad51 helps recruit Rad54, and Rad54 in turn stabilizes the Rad51-ssDNA fiber, it is unclear whether the Rad54 ATPase action or the creation of the Rad51-ssDNA filament, or both enhance movement [55••].

Rad54 remodels chromatin [58] in a manner that correlates both with its dsDNA translocation activity, and its ATPase activity [50,51]. Thus, Rad54 may actively slide nucleosomes away from the resected DSB [59], which could, based on the action of other chromatin remodelers, increase the radius of the random walk movement of the DSB, due to reduced constraint on the damaged chromatin fiber. Interestingly, Rad54 molecules in human do not need their ATPase domains to associate

Please cite this article in press as: Seeber A, et al.: Nucleosome remodelers in double-strand break repair, Curr Opin Genet Dev (2013), http://dx.doi.org/10.1016/j.gde.2012.12.008

Figure 2

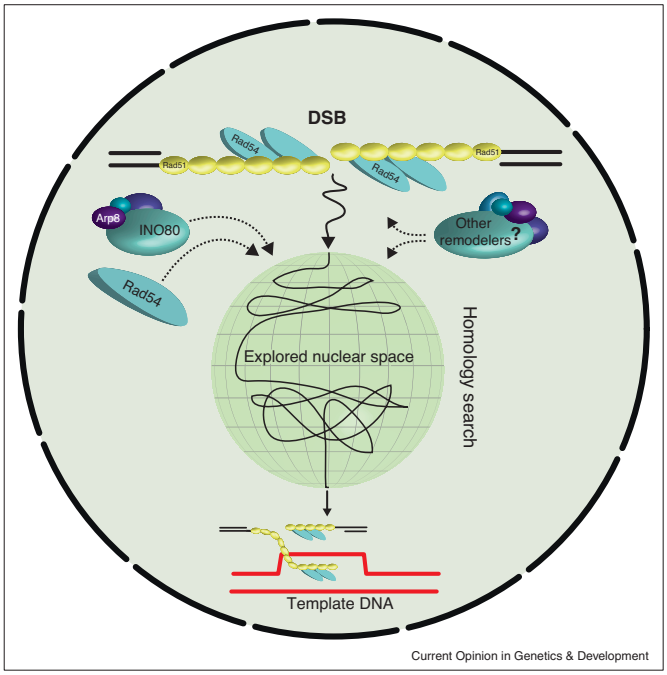

A speculative role of chromatin remodelers in homology search. In order to repair a lesion by HR, the homologous template needs to be identified and bound. The homologous template can be the sister chromatid after replication, although in special cases, repair occurs with ectopic homologous sequences. Several studies suggest that the efficiency of homology search is rate-limiting for DSB repair by HR with ectopic donors [53,62]. Upon damage, DSBs become more mobile, which may facilitate the homology search through nuclear space. This increase in mobility is dependent on the ATPase activities of INO80 and Rad54, both of which can remodel nucleosomes. Other chromatin remodeling complexes may also be involved in homology search dynamics.

with DSBs, and lack of ATPase activity inhibits its turnover at sites of damage, as shown by FRAP [52••]. Thus, it could also be the release of Rad54 that enhances movement of the resected break. In mammalian cells, but not in yeast, hINO80 binds to and promotes the expression of the *RAD54* gene, which suggests that INO80 may also have indirect effects in DSB repair. Indeed, enhanced expression of Rad54 can complement the DNA repair defect of human Ino80-deficient cells [60].

The specific mechanism of how remodelers increase chromatin mobility is still an open question. Multiple effects, including release from anchoring molecules, reduced persistence length, or the effect of the ATPase itself, are all possibilities. Some insight may be gained by identifying and comparing the effects of different remodeler subtypes in regard to chromatin mobility.

Conclusions

Up to this point only a few studies of chromatin remodelers in damage have scored defects in repair that could be traced unambiguously to the remodeler's activity at the site of damage. This may in part reflect redundancy in the function of chromatin remodelers, but may also simply arise from the fact that the appropriate read-outs were not yet monitored. Many unanswered questions remain. It is still unclear why so many chromatin remodeling factors are recruited to double-strand breaks. It is unclear how chromatin remodelers increase mobility of chromatin, why some damage shows movement while other do not, and what the impact of chromatin mobility is on repair. What role do remodelers play in the late stages of HR or in the restoration of chromatin after repair? The literature currently implicates histone chaperones in this step leaving the role for remodelers largely open [3]. The fate of nucleosomes during the DNA damage response is

Please cite this article in press as: Seeber A, et al.: Nucleosome remodelers in double-strand break repair, Curr Opin Genet Dev (2013), http://dx.doi.org/10.1016/j.gde.2012.12.008

an open question. Certainly, there has to be nucleosome eviction during resection to form an overhang for HR. The possibility remains that half nucleosomes remain bound, although it is unlikely that the Rad51 fiber contains nucleosomes. Improved methods for quantifying histone abundance at sites of damage would help to resolve this question. The fact that many cancers have mutations in subunits of chromatin remodeling complexes [61] indicates that these enzymes remain an unexplored source of diagnostic targets to help screen for diseases that stem from genomic instability.

Acknowledgments

The Gasser laboratory is supported by the Novartis Research Foundation, the Marie Curie networks Image-DDR and Nucleosome 4D, and the Swiss National Science Foundation. We thank H. Ferreira, V. Dion and F. Clarke for constructive advice on the writing.

References and recommended reading

Papers of particular interest, published within the period of review, have been highlighted as:

- • of special interest
- •• of outstanding interest

1. • Neumann FR, Dion V, Gehlen LR, Tsai-Pflugfelder M, Schmid R, Taddei A, Gasser SM: **Targeted INO80 enhances subnuclear chromatin movement and ectopic homologous recombination**. *Genes Dev* 2012, **26**:369-383.
The authors show that targeting the INO80 complex to a locus increases its mobility within the yeast nucleus. This was correlated with higher rates of spontaneous gene conversion, and with nucleosome eviction at the *PHO5* promoter. The increase in mobility at a DSB is Arp8-dependent. The authors propose a model where by nucleosome eviction increases chromatin mobility by enhancing the flexibility of the chromatin fiber.

2. •• Chen X, Cui D, Papusha A, Zhang X, Chu CD, Tang J, Chen K, Pan X, Ira G: **The Fun30 nucleosome remodeller promotes resection of DNA double-strand break ends**. *Nature* 2012, **489**:576-580.
One of three important studies on the role of Fun30 in double-strand break repair. Here the authors highlight Fun30 as nucleosome remodeler that promotes resection of DSBs through a mechanism that seems to promote the removal of Rad9. They also show the relative roles of the RSC and INO80 remodeling complexes in resection.

3. Soria G, Polo Sophie E, Almouzni G: **Prime, repair, restore: the active role of chromatin in the DNA damage response**. *Mol Cell* 2012, **46**:722-734.

4. Flaus A, Martin DM, Barton GJ, Owen-Hughes T: **Identification of multiple distinct Snf2 subfamilies with conserved structural motifs**. *Nucleic Acids Res* 2006, **34**:2887-2905.

5. Clapier CR, Cairns BR: **The biology of chromatin remodeling complexes**. *Annu Rev Biochem* 2009, **78**:273-304.

6. Chambers AL, Downs JA: **The RSC and INO80 chromatin-remodeling complexes in DNA double-strand break repair**. *Prog Mol Biol Transl Sci* 2012, **110**:229-261.

7. van Attikum H, Fritsch O, Hohn B, Gasser SM: **Recruitment of the INO80 complex by H2A phosphorylation links ATP-dependent chromatin remodeling with DNA double-strand break repair**. *Cell* 2004, **119**:777-788.

8. Morrison AJ, Highland J, Krogan NJ, Arbel-Eden A, Greenblatt JF, Haber JE, Shen X: **INO80 and γ-H2AX interaction links ATP-dependent chromatin remodeling to DNA damage repair**. *Cell* 2004, **119**:767-775.

9. Downs JA, Allard S, Jobin-Robitaille O, Javaheri A, Auger A, Bouchard N, Kron SJ, Jackson SP, Cote J: **Binding of chromatin-modifying activities to phosphorylated histone H2A at DNA damage sites**. *Mol Cell* 2004, **16**:979-990.

10. Kashiwaba S, Kitahashi K, Watanabe T, Onoda F, Ohtsu M, Murakami Y: **The mammalian INO80 complex is recruited to DNA damage sites in an ARP8 dependent manner**. *Biochem Biophys Res Commun* 2010, **402**:619-625.

11. Kitayama K, Kamo M, Oma Y, Matsuda R, Uchida T, Ikura T, Tashiro S, Ohyama T, Winsor B, Harata M: **The human actin-related protein hArp5: nucleo-cytoplasmic shuttling and involvement in DNA repair**. *Exp Cell Res* 2009, **315**:206-217.

12. Kandasamy MK, McKinney EC, Deal RB, Smith AP, Meagher RB: **Arabidopsis actin-related protein ARP5 in multicellular development and DNA repair**. *Dev Biol* 2009, **335**:22-32.

13. Luk E, Ranjan A, Fitzgerald PC, Mizuguchi G, Huang Y, Wei D, Wu C: **Stepwise histone replacement by SWR1 requires dual activation with histone H2A.Z and canonical nucleosome**. *Cell* 2010, **143**:725-736.

14. Bao YH: **Chromatin response to DNA double-strand break damage**. *Epigenomics* 2011, **3**:307-321.

15. Kalocsay M, Hiller NJ, Jentsch S: **Chromosome-wide Rad51 spreading and SUMO-H2A.Z-dependent chromosome fixation in response to a persistent DNA double-strand break**. *Mol Cell* 2009, **33**:335-343.

16. Morillo-Huesca M, Clemente-Ruiz M, Andujar E, Prado F: **The SWR1 histone replacement complex causes genetic instability and genome-wide transcription misregulation in the absence of H2A.Z**. *PLoS ONE* 2010, **5**:e12143.

17. • Xu Y, Ayrapetov MK, Xu C, Gursoy-Yuzugullu O, Hu Y, Price BD: **Histone H2A.Z controls a critical chromatin remodeling step required for DNA double-strand break repair**. *Mol Cell* 2012, **48**:723-733.
Convincing evidence is put forth for a functional role of H2A.Z deposition by p400 and subsequent acetylation by Tip60 in mammals at dSBs in mammalian cells, Incorporation of H2A.Z along with acetylation of H4 facilitates relaxation of chromatin and allows for subsequent modifications such as ubiquitination and loading of KU to mediate repair by NHEJ.

18. Chai B, Huang J, Cairns BR, Laurent BC: **Distinct roles for the RSC and Swi/Snf ATP-dependent chromatin remodelers in DNA double-strand break repair**. *Genes Dev* 2005, **19**:1656-1661.

19. Shen X, Mizuguchi G, Hamiche A, Wu C: **A chromatin remodelling complex involved in transcription and DNA processing**. *Nature* 2000, **406**:541-544.

20. Sinha M, Watanabe S, Johnson A, Moazed D, Peterson CL: **Recombinational repair within heterochromatin requires ATP-dependent chromatin remodeling**. *Cell* 2009, **138**:1109-1121.

21. • Lee HS, Park JH, Kim SJ, Kwon SJ, Kwon J: **A cooperative activation loop among SWI/SNF, gamma-H2AX and H3 acetylation for DNA double-strand break repair**. *EMBO J* 2010, **29**:1434-1445.
The authors provide evidence of a positive feedback loop between SWI/SNF, H3 acetylation and phosphorylation of H2A.X, facilitating DSB repair.

22. Ogiwara H, Ui A, Otsuka A, Satoh H, Yokomi I, Nakajima S, Yasui A, Yokota J, Kohno T: **Histone acetylation by CBP and p300 at double-strand break sites facilitates SWI/SNF chromatin remodeling and the recruitment of non-homologous end joining factors**. *Oncogene* 2011, **30**:2135-2146.

23. Peng G, Yim EK, Dai H, Jackson AP, Burgt I, Pan MR, Hu R, Li K, Lin SY: **BRIT1/MCPH1 links chromatin remodelling to DNA damage response**. *Nat Cell Biol* 2009, **11**:865-872.

24. • Hauk G, McKnight JN, Nodelman IM, Bowman GD: **The chromodomains of the Chd1 chromatin remodeler regulate DNA access to the ATPase motor**. *Mol Cell* 2010, **39**:711-723.
This study solved the crystal structure of yeast Chd1 and proposes a model where the chromodomains of Chd1 allow it to distinguish between nucleosomes and naked DNA by controlling access to its ATPase motor.

25. • Smeenk G, Wiegant WW, Vrolijk H, Solari AP, Pastink A, van Attikum H: **The NuRD chromatin-remodeling complex regulates signaling and repair of DNA damage**. *J Cell Biol* 2010, **190**:741-749.
Knockdown of *MTA2* or *CHD4*, which encode components of the NuRD complex, leads to accumulation of DNA damage as well as sensitivity to IR. CHD4 stimulates RNF8/RNF168 dependent ubiquitin conjugates, and promotes DSB repair and checkpoint activation in response to IR.

Please cite this article in press as: Seeber A, et al.: Nucleosome remodelers in double-strand break repair, Curr Opin Genet Dev (2013), http://dx.doi.org/10.1016/j.gde.2012.12.008

26. Polo SE, Kaidi A, Baskcomb L, Galanty Y, Jackson SP: **Regulation**
• **of DNA-damage responses and cell-cycle progression by the chromatin remodelling factor CHD4**. *EMBO J* 2010, **29**:3130-3139.
CHD4 promotes DSB repair and cell survival after damage as well as acting as a regulator of G1/S cell cycle progression by controlling p53 deacetylation.

27. Chou DM, Adamson B, Dephoure NE, Tan X, Nottke AC, Hurov KE,
•• Gygi SP, Colaiacovo MP, Elledge SJ: **A chromatin localization screen reveals poly (ADP ribose)-regulated recruitment of the repressive polycomb and NuRD complexes to sites of DNA damage**. *Proc Natl Acad Sci U S A* 2010, **107**:18475-18480.
The authors find that components of mammalian Polycomb Repressive Complex 1 (PRC1), such as MEL-18, like MTA1 and CHD4 of the NuRD complex, are recruited to sites of laser induced damage in a PARP dependent manner. They show that exclusion of nascent transcripts as well as RNA polymerase II from sites of laser induced damage was dependent on PARP. They propose a model whereby PARP promotes transcriptional repression at sites of DNA damage.

28. Ahel D, Horejsi Z, Wiechens N, Polo SE, Garcia-Wilson E, Ahel I, Flynn H, Skehel M, West SC, Jackson SP *et al.*: **Poly(ADP-ribose)-dependent regulation of DNA repair by the chromatin remodeling enzyme ALC1**. *Science* 2009, **325**:1240-1243.

29. Ahel I, Ahel D, Matsusaka T, Clark AJ, Pines J, Boulton SJ, West SC: **Poly(ADP-ribose)-binding zinc finger motifs in DNA repair/checkpoint proteins**. *Nature* 2008, **451**:81-85.

30. Gottschalk AJ, Timinszky G, Kong SE, Jin J, Cai Y, Swanson SK, Washburn MP, Florens L, Ladurner AG, Conaway JW *et al.*: **Poly(ADP-ribosyl)ation directs recruitment and activation of an ATP-dependent chromatin remodeler**. *Proc Natl Acad Sci U S A* 2009, **106**:13770-13774.

31. Goodarzi AA, Kurka T, Jeggo PA: **KAP-1 phosphorylation**
•• **regulates CHD3 nucleosome remodeling during the DNA double-strand break response**. *Nat Struct Mol Biol* 2011, **18**:831-839.
The authors show that the mammalian remodeler CHD3 is lost from heterochromatin upon damage following the phosphorylation of KAP-1 by ATM. Loss of CHD3 results in chromatin relaxation which could help facilitate repair in heterochromatic regions, by antagonizing chromatin compaction.

32. Goodarzi AA, Noon AT, Deckbar D, Ziv Y, Shiloh Y, Lobrich M, Jeggo PA: **ATM signaling facilitates repair of DNA double-strand breaks associated with heterochromatin**. *Mol Cell* 2008, **31**:167-177.

33. Denslow SA, Wade PA: **The human Mi-2//NuRD complex and gene regulation**. *Oncogene* 2007, **26**:5433-5438.

34. Shim EY, Hong SJ, Oum JH, Yanez Y, Zhang Y, Lee SE: **RSC mobilizes nucleosomes to improve accessibility of repair machinery to the damaged chromatin**. *Mol Cell Biol* 2007, **27**:1602-1613.

35. Gospodinov A, Vaissiere T, Krastev DB, Legube G, Anachkova B,
• Herceg Z: **Mammalian Ino80 mediates double-strand break repair through its role in DNA end strand resection**. *Mol Cell Biol* 2011, **31**:4735-4745.
Here the authors show that mammalian INO80 is required for efficient DSB repair. They show that 53BP1 but not Rad51 focus formation is impaired upon human Ino80 depletion. This led them to investigate the role of INO80 in early steps of repair and they find that the complex mediates 5′–3′ resection of DSB ends.

36. van Attikum H, Fritsch O, Gasser SM: **Distinct roles for SWR1 and INO80 chromatin remodeling complexes at chromosomal double-strand breaks**. *EMBO J* 2007, **26**:4113-4125.

37. Papin C, Humbert O, Kalashnikova A, Eckert K, Morera S, Kas E, Grigoriev M: **3′- to 5′ DNA unwinding by TIP49b proteins**. *FEBS J* 2010, **277**:2705-2714.

38. Awad S, Ryan D, Prochasson P, Owen-Hughes T, Hassan AH: **The Snf2 homolog Fun30 acts as a homodimeric ATP-dependent chromatin-remodeling enzyme**. *J Biol Chem* 2010, **285**:9477-9484.

39. Eapen VV, Sugawara N, Tsabar M, Wu WH, Haber JE: **The**
•• ***Saccharomyces cerevisiae* chromatin remodeler Fun30 regulates DNA end-resection and checkpoint deactivation**. *Mol Cell Biol* 2012, **32**:4727-4740.
One of three important studies on the role of Fun30 in double strand break repair. The authors show that Fun30 promotes 5′ to 3′ resection of DSBs. Deletion of *FUN30* results in a ~3.3 fold reduction in the speed of resection. They also show that Fun30 is important for the adaptation of DNA damage checkpoint arrested cells with an unrepaired DSB to resume cell cycle progression.

40. Durand-Dubief M, Will WR, Petrini E, Theodorou D, Harris RR, Crawford MR, Paszkiewicz K, Krueger F, Correra RM, Vetter AT *et al.*: **SWI/SNF-like chromatin remodeling factor Fun30 supports point centromere function in *S. cerevisiae***. *PLoS Genet* 2012, **8**:e1002974.

41. Stralfors A, Walfridsson J, Bhuiyan H, Ekwall K: **The FUN30 chromatin remodeler, Fft3, protects centromeric and subtelomeric domains from euchromatin formation**. *PLoS Genet* 2011, **7**:e1001334.

42. Costelloe T, Louge R, Tomimatsu N, Mukherjee B, Martini E,
•• Khadaroo B, Dubois K, Wiegant WW, Thierry A, Burma S *et al.*: **The yeast Fun30 and human SMARCAD1 chromatin remodellers promote DNA end resection**. *Nature* 2012, **489**:581-584.
One of three important studies on the role of Fun30 in double strand break repair. In addition to showing that yeast Fun30 plays a role in resection these authors show that the closest human homologue, SMARCAD1 also is recruited to and plays a role in repair of DSBs.

43. Lazzaro F, Sapountzi V, Granata M, Pellicioli A, Vaze M, Haber JE, Plevani P, Lydall D, Muzi-Falconi M: **Histone methyltransferase Dot1 and Rad9 inhibit single-stranded DNA accumulation at DSBs and uncapped telomeres**. *EMBO J* 2008, **27**:1502-1512.

44. Lydall D, Weinert T: **Yeast checkpoint genes in DNA damage processing: implications for repair and arrest**. *Science* 1995, **270**:1488-1491.

45. Gospodinov A, Tsaneva I, Anachkova B: **RAD51 foci formation in response to DNA damage is modulated by TIP49**. *Int J Biochem Cell Biol* 2009, **41**:925-933.

46. Murr R, Loizou JI, Yang YG, Cuenin C, Li H, Wang ZQ, Herceg Z: **Histone acetylation by Trrap–Tip60 modulates loading of repair proteins and repair of DNA double-strand breaks**. *Nat Cell Biol* 2006, **8**:91-99.

47. Tsukuda T, Fleming AB, Nickoloff JA, Osley MA: **Chromatin remodelling at a DNA double-strand break site in *Saccharomyces cerevisiae***. *Nature* 2005, **438**:379-383.

48. Tsukuda T, Lo YC, Krishna S, Sterk R, Osley MA, Nickoloff JA: **INO80-dependent chromatin remodeling regulates early and late stages of mitotic homologous recombination**. *DNA Repair (Amst)* 2009, **8**:360-369.

49. Morgan EA, Shah N, Symington LS: **The requirement for ATP hydrolysis by *Saccharomyces cerevisiae* Rad51 is bypassed by mating-type heterozygosity or RAD54 in high copy**. *Mol Cell Biol* 2002, **22**:6336-6343.

50. Mazin AV, Mazina OM, Bugreev DV, Rossi MJ: **Rad54, the motor of homologous recombination**. *DNA Repair (Amst)* 2010, **9**:286-302.

51. Ceballos SJ, Heyer WD: **Functions of the Snf2/Swi2 family Rad54 motor protein in homologous recombination**. *Biochim Biophys Acta* 2011, **1809**:509-523.

52. Agarwal S, van Cappellen Wa, Guénolé A, Eppink B, Linsen SEV,
•• Meijering E, Houtsmuller A, Kanaar R, Essers J: **ATP-dependent and independent functions of Rad54 in genome maintenance**. *J Cell Biol* 2011, **192**:735-750.
The authors show that human Rad54 is required for the timely accumulation of Rad51 at DSBs that is independent of Rad54's ATPase activity. They also show that Rad54's ATPase activity is required for the redistribution of DSB repair sites within the nucleus.

53. Gehlen LR, Gasser SM, Dion V: **How broken DNA finds its template for repair: a computational approach**. *Prog Theor Phys Suppl* 2011, **191**:20.

54. Gartenberg MR, Neumann FR, Laroche T, Blaszczyk M, Gasser SM: **Sir-mediated repression can occur independently of chromosomal and subnuclear contexts**. *Cell* 2004, **119**:955-967.

Please cite this article in press as: Seeber A, et al.: Nucleosome remodelers in double-strand break repair, Curr Opin Genet Dev (2013), http://dx.doi.org/10.1016/j.gde.2012.12.008

55. •• Dion V, Kalck V, Horigome C, Towbin BD, Gasser SM: **Increased mobility of double-strand breaks requires Mec1, Rad9 and the homologous recombination machinery**. *Nat Cell Biol* 2012, **14**:502-509.
This study along with that of Mine-Hattab and Rothstein shows that a DSB is more mobile than its undamaged counterpart. A nick induced by collision of the replication fork with protein adduct does not increase in mobility. Dion *et al.* show that the chromatin remodeler Rad54, and specifically its ATPase activity, are required for increased chromatin mobility upon damage, as is Rad9 and Mec1. The rate of heteroduplex formation with an ectopic donor is reduced in a *rad9* mutant.

56. •• Mine-Hattab J, Rothstein R: **Increased chromosome mobility facilitates homology search during recombination**. *Nat Cell Biol* 2012, **14**:510-517.
This study shared many of the same findings as Dion *et al.*, but performed the study in diploid yeast cells. Increased mobility depends in part on Sae2. Importantly, Mine-Hattab and Rothstein show that not only a DSB but also a non-homologous, undamaged chromosomal locus increases in mobility when cells incur damage.

57. • Krawczyk PM, Borovski T, Stap J, Cijsouw T, ten Cate R, Medema JP, Kanaar R, Franken NA, Aten JA: **Chromatin mobility is increased at sites of DNA double-strand breaks**. *J Cell Sci* 2012, **125**:2127-2133.
Here the authors show that DSB foci are more mobile than undamaged chromatin. They also show that drugs such as Curcumin or azacitidine, which affect chromatin structure, can reduce mobility.

58. Zhang Z, Fan HY, Goldman JA, Kingston RE: **Homology-driven chromatin remodeling by human RAD54**. *Nat Struct Mol Biol* 2007, **14**:397-405.

59. Alexeev A, Mazin A, Kowalczykowski SC: **Rad54 protein possesses chromatin-remodeling activity stimulated by the Rad51-ssDNA nucleoprotein filament**. *Nat Struct Biol* 2003, **10**:182-186.

60. Park EJ, Hur SK, Kwon J: **Human INO80 chromatin-remodelling complex contributes to DNA double-strand break repair via the expression of Rad54B and XRCC3 genes**. *Biochem J* 2010, **431**:179-187.

61. Luijsterburg MS, van Attikum H: **Chromatin and the DNA damage response: the cancer connection**. *Mol Oncol* 2011, **5**:349-367.

62. Wilson JH, Leung WY, Bosco G, Dieu D, Haber JE: **The frequency of gene targeting in yeast depends on the number of target copies**. *Proc Natl Acad Sci U S A* 1994, **91**:177-181.

63. Shen X, Ranallo R, Choi E, Wu C: **Involvement of actin-related proteins in ATP-dependent chromatin remodeling**. *Mol Cell* 2003, **12**:147-155.

64. Larsen DH, Poinsignon C, Gudjonsson T, Dinant C, Payne MR, Hari FJ, Rendtlew Danielsen JM, Menard P, Sand JC, Stucki M *et al.*: **The chromatin-remodeling factor CHD4 coordinates signaling and repair after DNA damage**. *J Cell Biol* 2010, **190**:731-740.

65. Oum JH, Seong C, Kwon Y, Ji JH, Sid A, Ramakrishnan S, Ira G, Malkova A, Sung P, Lee SE *et al.*: **RSC facilitates Rad59-dependent homologous recombination between sister chromatids by promoting cohesin loading at DNA double-strand breaks**. *Mol Cell Biol* 2011, **31**:3924-3937.

66. Naidu SR, Love IM, Imbalzano AN, Grossman SR, Androphy EJ: **The SWI/SNF chromatin remodeling subunit BRG1 is a critical regulator of p53 necessary for proliferation of malignant cells**. *Oncogene* 2009, **28**:2492-2501.

67. Park JH, Park EJ, Hur SK, Kim S, Kwon J: **Mammalian SWI/SNF chromatin remodeling complexes are required to prevent apoptosis after DNA damage**. *DNA Repair (Amst)* 2009, **8**:29-39.

Please cite this article in press as: Seeber A, et al.: Nucleosome remodelers in double-strand break repair, Curr Opin Genet Dev (2013), http://dx.doi.org/10.1016/j.gde.2012.12.008

Review

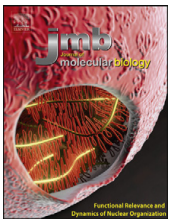

INO80-C and SWR-C: Guardians of the Genome

Christian-Benedikt Gerhold[1], **Michael H. Hauer**[1] **and Susan M. Gasser**[1,2]

1 - Friedrich Miescher Institute for Biomedical Research, *Maulbeerstrasse 66, CH-4058 Basel, Switzerland*
2 - University of Basel Faculty of Natural Sciences, *Klingelbergstrasse 50, CH-4056 Basel, Switzerland*

Correspondence to Susan M. Gasser: *susan.gasser@fmi.ch*
http://dx.doi.org/10.1016/j.jmb.2014.10.015
Edited by E. Soutoglou

Abstract

The double membrane of the eukaryotic nucleus surrounds the genome, constraining it to a nuclear sphere. Proteins, RNA protein particles and artificial chromosome rings diffuse rapidly and freely throughout the nucleoplasm, while chromosomal loci show subdiffusive movement with varying degrees of constraint. *In situ* biochemical approaches and live imaging studies have revealed the existence of nuclear subcompartments that are enriched for specific chromatin states and/or enzymatic activities. This sequestration is thought to enhance the formation of heterochromatin, particularly when factors of limited abundance are involved. Implicit in the concept of compartmentation is the idea that chromatin is able to move from one compartment to another. Indeed, in budding yeast, gene activation, repression and the presence of persistent DNA double-strand breaks each has been shown to provoke subnuclear relocalization of chromatin. In some cases, movement has been linked to the action of ATP-dependent chromatin remodeling complexes, more specifically to the Snf2-related ATPase-containing complexes, SWR-C and INO80-C. Here we examine how these multi-subunit remodelers contribute to chromatin-based processes linked to the DNA damage response. We review recent evidence that supports a role for yeast SWR-C and INO80-C in determining the subnuclear position of damaged domains and finally, we recap the multiple ways in which these remodelers contribute to genomic integrity.

Introduction

Despite its small size, the budding yeast nucleus is a well-organized cellular compartment, in which chromosome position is at least partially determined by the interaction of landmark chromosomal domains, such as telomeres and centromeres, with the nuclear envelope [1,2]. Telomeres cluster at the nuclear rim tethered by telomere-specific factors, while centromeres are linked by microtubules—even in interphase—to the membrane-embedded spindle pole body. Despite the flexibility of the chromatin fiber, various techniques have shown that intra-chromosomal contacts are more frequent than inter-chromosomal contacts [3–5], suggesting that yeast chromosomes also occupy "territories", much like those proposed for larger vertebrate nuclei by Cremer and Cremer [6]. Consistently, the smallest yeast chromosomes, such as chromosome III, fold back allowing contact between right and left telomeres in a loose, whole chromosome loop [7,8]. Other telomeres appear to cluster stochastically, with chromosome arm length playing a more important role in partner choice than sequence composition [9]. In addition to telomeres, heritably silenced loci colocalize with telomeres at the nuclear envelope [10], while active genes distribute more randomly. Silencing factors themselves (Sir3 and Sir4) play a role in both clustering [11] and perinuclear anchoring [12–14], as they interact with anchorage sites at the nuclear membrane, namely Mps3 [15,16] and Esc1 [14,17]. Nuclear pores provide further organization at the nuclear rim, contacting poised promoters or active genes through either SAGA (*S*pt/*A*da/*G*cn5 *a*cetyltransferase) or the mRNA-binding complex THO-TREX [18].

0022-2836/

The enrichment of heterochromatin along the inner face of the nuclear envelope is a conserved feature of all eukaryotic nuclei, except for a few differentiated mammalian cell types [19]. Whereas the association of promoters with nuclear pores may also be conserved across species, the impact of this interaction is unclear. In contrast, the functional relevance of the association of DNA double-strand breaks (DSBs) and very short telomeres with the inner face of the nuclear pore is clear [20,21]. Pore protein mutations render yeast cells highly sensitive to DNA damaging agents, particularly in strains in which homologous recombination (HR) is impaired [20,22,23]. Given that nuclear pores are preferred sites of SUMO metabolism and that a large number of proteins are sumoylated in response to DNA damage [24,25], the functional impact of pore association may well reflect the sumoylation associated with specific repair pathways. For instance, the pore-associated SUMO-dependent ubiquitin ligase Slx5/Slx8 plays a role in recombination-mediated repair [26–28].

Despite the multiple anchorage points mentioned above, most yeast chromatin is in constant motion. Its movement, which can be monitored by fluorescence time-lapse microscopy, is best described as a constrained random walk [13,29,30], whose dynamics vary with intracellular ATP levels and the cell cycle [13,29,31,32]. An average yeast locus in open chromatin in G1 phase, distal from chromosome ends, has a radius of constraint of ~0.65 μm, which drops to ~0.35 μm in S phase, representing roughly 30% and 15% of the nuclear volume, respectively. The degree of movement is dependent on many parameters, including the status of the local chromatin, linkage of sister chromatids through cohesin and the distance of the tag from a landmark anchorage site [2,12,33,34].

Recent results implicate two nucleosome remodelers (INO80-C and SWR-C) in regulating this chromatin mobility and in the association of DNA damage with perinuclear sites [30,35–37]. It is thus relevant to review chromatin dynamics in terms of local nucleosome composition, chromatin compaction and the precise position of the locus within the nuclear sphere. Remarkably, INO80-C and SWR-C nucleosome remodelers are implicated in all three aspects of chromatin dynamics, particularly during the DNA damage response (DDR).

Chromatin Compaction and Spatial Constraint

Three overlapping mechanisms contribute to subnuclear chromatin localization. The first reflects an order imposed by enzymatic functions inherent to the nucleus and often arises from large protein complexes that interact, leading to a clustering of their DNA substrates (e.g., replication foci). The second is the result of sequence-specific anchorage, that is, interactions of chromatin with less mobile structures (e.g., pores, SPB, nucleoli). The third is the impact of the chromatin fiber itself, namely, its compaction and continuity, which means that one locus can impact both the position and the mobility of its neighbor. Not only at silenced regions but also in general, yeast chromatin is highly compacted, having a 40- to 80-fold higher compaction ratio than B-form DNA [38,39]. This ratio is, of course, even higher in mammalian cells. Nonetheless, chromatin must be accessible for DNA binding factors that regulate replication, transcription, recombination and repair. Thus, dynamic modulation of chromatin states is a key regulatory principle for nearly every DNA-based reaction.

Initial evidence that chromatin mobility and compaction are interdependent came from measurements of chromatin mobility monitored by fluorescence correlated spectroscopy or two-photon standing wave fluorescence photobleaching [40]. With this, the Bardeen group showed that short-range chromatin mobility *in vivo* was variable and reflected DNA–histone interaction. Notably, mobility increased when DNA–histone interactions were weakened in higher salt concentrations and decreased upon specific photocrosslinking of histones [40]. This link between nucleosomal stability and chromatin mobility is consistent with later studies described below, which showed that the nucleosome remodeler INO80-C increased the movement of chromatin to which it was bound [30].

By tracking fluorescently tagged chromosomal loci with time-lapse microscopy and plotting mean squared displacement, one can extract quantitative parameters of chromatin mobility, most commonly, the radius of constraint (Rc), which defines the area within which a particle is free to diffuse. While the Rc values for non-repetitive, open chromatin domains in fly, human or yeast cells are very comparable, their apparent diffusion coefficients (*D*) range from 1.25×10^{-4} $\mu m^2/s$ (5p14) in man to 1.8×10^{-3} $\mu m^2/s$ (*LYS2*) in yeast [29,31,41]. Different types of motion can also be distinguished: smaller, saltatory movements <0.2 μm that occur constantly, and larger, more rapid movements (i.e., >0.5 μm in a 10.5-s interval [31]). The smaller movements are observed for internal sequences and repressed domains at the nuclear periphery. Active, internal loci on the other hand also show larger steps. Even more irregular is the movement associated with DSBs, which can be tracked through the binding of the HR factor Rad52 [42,43]. In this case, both diffusion coefficients and Rc increase, purportedly as part of a homology search process. Specifically, a particular undamaged locus with Rc = 0.46 μm in S phase (12% of the nuclear volume), increased to 0.70 μm (47%) after induction of a DSB and initial processing of the end to bind Rad52 [42]. The increase may in part reflect the loss of cohesion between sister chromatids,

for the release of cohesin from replicated sisters was shown to augment the Rc value [34]. On the other hand, the loss or alteration of nucleosome modification or density that accompany DSB processing may also contribute to increased mobility.

Chromatin Dynamics during Cell Cycle

As mentioned above, the mobility of a chromosomal locus depends on two further criteria: cell cycle stage and its chromatin status. Studies in *Drosophila* spermatocytes revealed both random constrained movement over short-time windows and a long-range movement in S/G2 phase, which occurred over a much longer timescale. Moreover, a decrease in step size for rapid movements was recorded in late G2 spermatocytes just before entry into meiosis [32]. This drop in mobility correlated with a developmental change that is characterized by nuclear reorganization and a dramatic movement of bulk chromatin from a central region to three distinct perinuclear masses [44]. The decrease in chromatin movement scored for budding yeast origins of replication in S phase [31] is due at least in part to the loading of the cohesin ring, which links replicated sisters together [34]. Not only linkages in *trans* but also the linear continuity of the DNA strand in *cis* restricts chromatin mobility; the tracking of a 17-kb fluorescently tagged locus excised from a yeast chromosome showed rapid movement throughout the nucleoplasm (Rc = 0.95 μm), rather than its normal constraint (Rc = 0.65 μm) [13,30]. This freedom of movement would enhance contact between sequences, which is needed for the homology search step of DSB repair by HR. Studies with plasmid-borne donors argue that this search is indeed rate limiting in yeast [45]; thus, altered movement would be one way to favor a homology search beyond the replicated sister chromatid (Fig. 1).

Chromatin Remodelers and Chromatin Mobility

The enhanced subnuclear movement observed for DSBs argues that chromatin movement is not simply caused by Brownian motion but is a regulated cellular process that responds to enzymatic control (reviewed in Ref. [33]). For instance, the chromatin remodeler INO80-C is able to increase chromatin mobility when it is bound either at an artificial reporter or at the endogenous *PHO5* promoter [30], although in the latter case, increased mobility correlated with induced transcription, whereas in the former, it did not. Intriguingly, the targeting of either SWI/SNF or SWR-C chromatin remodelers (through lexA-Snf2, lexA-Swr1 or lexA-Arp6 fusions) to the same locus did not increase Rc values [30,37], while the tethering of the Rad54 ATPase domain did (M.H.H., unpublished results). Thus, it is not simply the presence of a large complex but the type of activity it exerts that impacts chromatin mobility. With 17 different Snf2-type ATPases in yeast and 53 in human [46], it is likely that different chromatin remodelers will play various and only partially redundant roles that alter the composition, structure and mobility of chromatin. The INO80-C result argues that, at least in some cases, the modulation of nucleosome organization impacts chromatin dynamics.

The Mobility of DNA DSBs

Induction of a targeted and irreparable DSB increases the mobility of the targeted locus compared with that of the same site undamaged [42,43]. Prior to the increase, there may be a transient drop in mobility that correlates with the initial steps of resection, lasting approximately 10 min [47]. The subsequent increase was shown to correlate with the efficiency of DNA repair by HR with an ectopic donor sequence, and the activity of Rad54, a remodeler ATPase required for strand exchange, contributed to the increase. Enhanced DSB movement was also dependent on the DDR, notably on the ATR kinase Mec1 and its coactivator Rad9 (which serves an equivalent role as BRCA1 or 53BP1 in man) [42]. In this respect, it is important to note that multiple subunits of Snf2 chromatin remodeling complexes including ISW1, ISW2, INO80-C, SWR-C, RSC and SWI/SNF undergo DNA damage-induced phosphorylation by Mec1 and Tel1 [48,49].

The DDR also modifies chromatin itself by phosphorylating H2A in yeast (H2A.X in mammals). This leads to an extensive modification of local chromatin composition, including acetylation, ubiquitination, potential H2A.Z deposition and eventually histone eviction, coincident with end resection (reviewed in Ref. [50]). It is difficult to sort out which of these modifications ultimately contributes to enhanced chromatin mobility, as the interplay between remodelers and their chromatin substrates at sites of DNA damage contributes to many aspects of DNA repair. Interestingly, the concerted activity of the DDR and remodelers is not restricted to the site of DNA damage. Checkpoint activation, even in the absence of damage, leads to a more generalized increase in chromatin mobility that was dependent on Mec1 and its downstream target kinase Rad53 [36,43] (Fig. 1).

The underlying phenomenon that allows for enhanced chromatin movement at breaks and non-damaged sites may reflect localized nucleosome remodeling, which can impact compaction and alter the long-range flexibility of the chromatin fiber. Indeed, *arp8* and *arp5* null mutants, which significantly hamper Ino80's ATPase activity [51,52], fully counteract the increase in mobility at genomic loci away from the DSB and partially reduce the mobility of the DSB itself [30,36]. The loss of the Swr1 ATPase, or of SWR-C cofactors, also compromised the enhanced mobility at

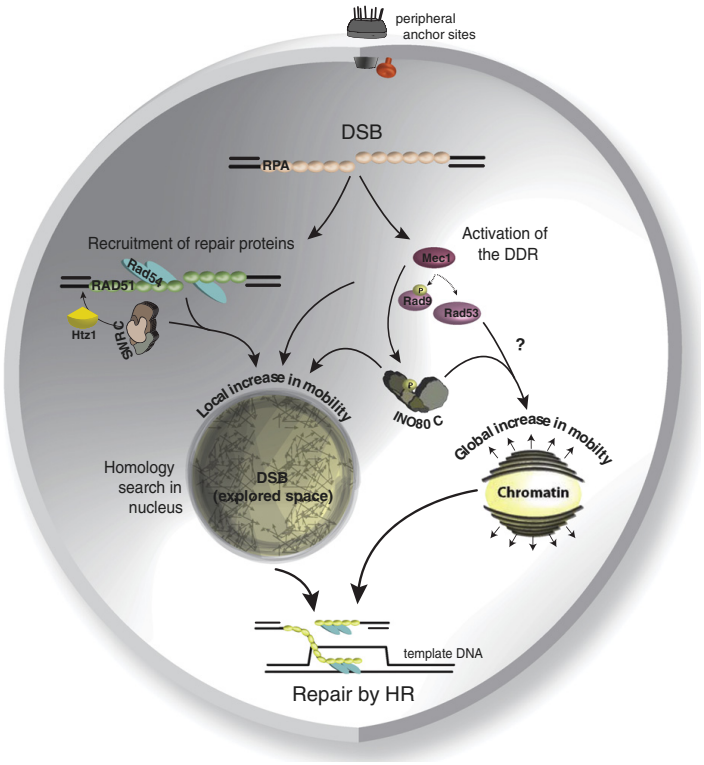

Fig. 1. Local and global chromatin mobility increase in response to DNA damage. DNA damage activates the DDR and checkpoint kinase Mec1 phosphorylates its downstream targets Rad53 and Rad9. Several subunits of INO80-C are also targeted by the Mec1-activated checkpoint response. Repair proteins Rad51 and Rad54 and checkpoint proteins Rad9 and Mec1 contribute to increased chromatin dynamics at the DSB. A general increase in chromatin movement at non-damaged sites ("global increase in mobility") requires Mec1, Rad53 and the INO80 complex. Both may facilitate contact between the DSB and ectopic sites of homology. The underlying mechanism that drives chromatin mobility remains unexplained.

the damaged locus, yet it did not affect movement at distal sites [36,37]. In common is the fact that changes in chromatin mobility are dependent on the initial ATR/Mec1 checkpoint kinase response, suggesting that chromatin alterations are part of a cell's physiological response to DNA damage. Importantly, the Mec1-induced effects appear to be mediated at least in part by INO80-C [36].

Relocating Difficult-to-Repair DNA Damage to the Nuclear Periphery

A second phenomenon observed in yeast that links nuclear organization to DNA repair concerns the relocation of difficult-to-repair DNA DSBs and collapsed replication forks to the nuclear envelope [20,53]. Both the Nup84 subcomplex of the nuclear pore and the SUN domain protein Mps3 are implicated as perinuclear binding sites for break association (reviewed in Ref. [54]). The relocalization event from the nucleoplasm to the periphery required activation of the DNA damage checkpoint and was affected by loss of the histone variant Htz1 (H2A.Z) [35], which implies a role for SWR-C in the process of DSB relocation. Indeed, both SWR-C and INO80-C were recently shown to contribute to the positioning of DSBs at the nuclear envelope [37] (Fig. 2). Specifically, the loss of Swr1 or Htz1 was shown to compromise the association of DSBs with either nuclear pores or with the membrane protein Mps3, while INO80-C promotes binding to Mps3 without affecting DSB relocation to pores [37]. The two binding sites are further distinguished by the phase of the cell cycle in which they

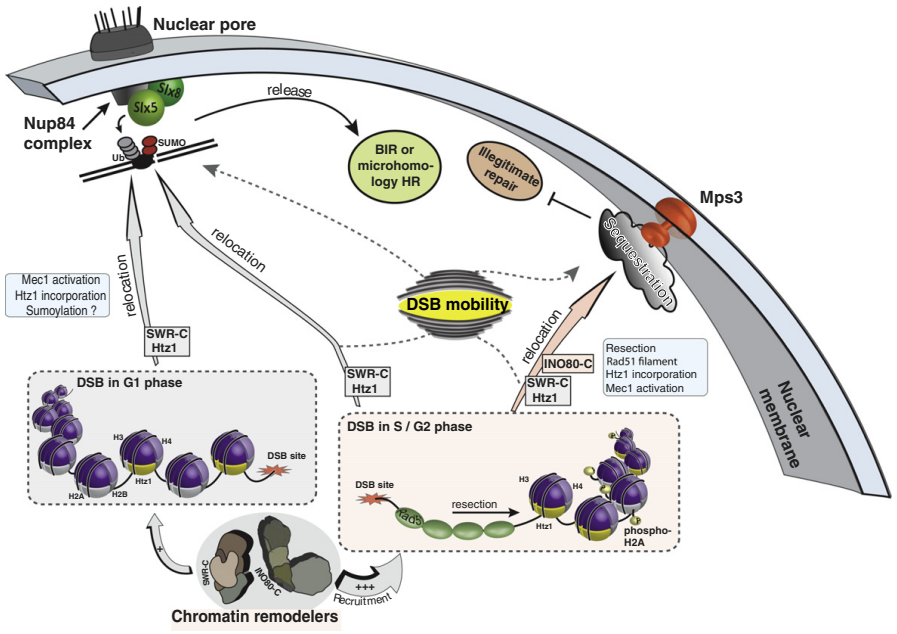

Fig. 2. SWR-C and INO80-C influence DSB relocation to nuclear pores or Mps3 with different requirements in G1 and S/G2 phases. DNA DSBs trigger an orchestrated localization of repair factors, including remodelers, such as SWR-C and INO80-C to the site of damage. The cell cycle phase appears to play an important role in remodeler targeting to the DSB as SWR-C and INO80-C are preferably recruited to the site of damage in S/G2 phase. Facilitated resection links chromatin remodeling to the HR repair pathway. Persistent DSBs that have no allelic donor relocate to the nuclear periphery where they contact either the Nup84 subcomplex of nuclear pores or the transmembrane SUN domain protein, Mps3. SWR-C and Htz1 (H2A.Z) are required for association of breaks with either pores or Mps3. INO80-C promotes DSB localization to Mps3 in a manner specific to S/G2 phase. Mps3 association of DSBs is Rad51 dependent and sequestration at Mps3 may suppress illegitimate recombination. Pore association links DSBs to Slx5/Slx8 (a SUMO-targeted ubiquitin ligase) for degradation of the sumoylated repair machinery, possibly triggering repair by alternative pathways, such as break-induced replication (BIR).

are functional: the association of persistent DSBs with Mps3 requires Rad51 and end resection, which occurs only in S phase cells, while DSB-pore association occurs as well in G1 phase.

The two binding sites appear to have different effects on the outcome of repair (Fig. 2). Sequestration of breaks or telomeres by Mps3 generally suppresses recombination events [16,53]. Hence, DSB relocalization to Mps3 after unsuccessful homology search may prevent illegitimate recombination. Association with the pore, on the other hand, favors non-canonical recombination, that is, recombination with sequences other than those on the homologous sister chromosome. Associated with the nuclear pore is the Slx5/Slx8 SUMO-targeted ubiquitin ligase, which ubiquitylates components of the sumoylated repair machinery, such as Rad52, and targets them for degradation [55]. This function may be necessary to allow alternative repair events, such as break-induced replication or microhomology-mediated recombination. Consistently, type II survivors of telomerase ablation, which survive thanks to imprecise recombination events between telomeric repeats, require Slx5/Slx8 activity [56,57]. On the other hand, Slx5/Slx8 was reported to inhibit Rad51-mediated (canonical) recombination events [55]. Even if the relevant targets of sumoylation and eventually ubiquitination remain unclear, the role of the nuclear pore in harboring SUMO-modulating enzymes that help cells survive DNA damage is undisputed [23,58]. Intriguingly, a recent study in *Caenorhabditis elegans* suggests that aspects of pore regulation of repair pathways—in this case, for translesion synthesis—may also be conserved across species [59].

The discovery that INO80-C and SWR-C play important roles in DSB relocalization, thereby affecting the long-range organization of chromatin in

the nucleus, is consistent with other recent results that implicate these multi-subunit chromatin remodelers in chromatin-associated processes elicited by DNA damage. Thus, we can view INO80-C and SWR-C as important guardians of the genome, each contributing to genomic integrity in a unique way.

Even though the ATPase and scaffold proteins Ino80 and Swr1 have similar domain architectures and share some common subunits, their overall topology, mode of nucleosome interaction and range of enzymatic activities vary significantly [52,60,61] (Fig. 3). Whereas SWR-C has been shown to incorporate the H2A.Z (Htz1) variant into nucleosomes [62–64], INO80-C is reported to evict unacetylated Htz1 from the genome [65] but also remodels, spaces or evicts whole nucleosomes [66–68]. Both remodelers contain a DNA helicase, Rvb1/Rvb2, apparently present as a double

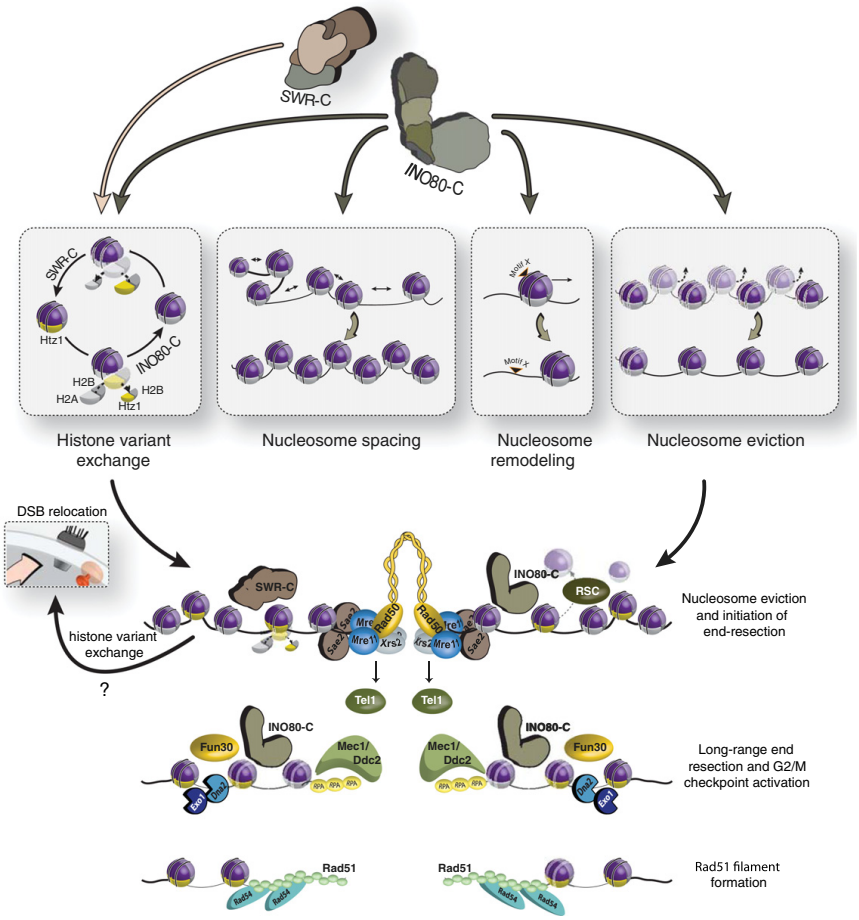

Fig. 3. SWR-C and INO80-C remodeling in DSB repair and damage-related processes. INO80-C and SWR-C mediate a number of remodeling activities. Histone variant exchange: INO80-C counteracts SWR-C-dependent Htz1 incorporation. Htz1 is essential for enhanced DSB mobility and DSB relocation to the nuclear periphery. Nucleosome spacing: INO80-C equally spaces nucleosomes to form regular arrays. Nucleosome remodeling: INO80-C slides nucleosomes to expose DNA sequences and features. Nucleosome eviction: INO80-C evicts whole nucleosomes from DNA, making it accessible to a variety of factors. At least some of these activities appear to be important for DSB repair, relocation and mobility. As depicted at the bottom, nucleosome eviction by several remodeling enzymes around the DSB appears to facilitate the accessibility for subsequent repair factors and promotes efficient processing and repair. See the text for details.

heterohexamer in INO80-C, and as a single heterohexamer in SWR-C [52,60]. The function of the Rvbs within these complexes remains largely unexplored.

It is also unclear what link, if any, exists between enhanced DSB mobility and the sequestration of DSBs at the nuclear periphery. Interestingly, in budding yeast, LexA targeting of Swr1, Arp6 or Htz1 is sufficient to shift a given locus (ARS607) to the nuclear membrane [37,69], yet the targeting of these proteins did not affect locus mobility. In contrast, the targeting of INO80-C subunits increased the mobility of an undamaged locus but did not alter its radial position [30].This suggests that random chromatin movement is not rate-limiting for DSB recruitment to pores or to Mps3. Indeed, *arp8*Δ or *rad51*Δ mutants have decreased DSB mobility, yet break relocation to the pore is intact [30,37,42]. It is important to note that the two events, enhanced mobility and pore sequestration, are kinetically distinct: movement seems to increase as soon as Mre11 and Rad52 bind, while DSBs accumulate at the nuclear periphery up to 2 hours after cleavage. Still it is likely that both events reflect chromatin changes at the level of the nucleosome.

It is not yet clear whether a general concept of damage-induced chromatin mobility is conserved in mammalian cells, as seemingly opposing results have been published (reviewed in Ref. [33]). In terms of DNA translocations, two models have been proposed: the 'contact-first model' requires two breaks that are in spatial proximity already prior to DNA damage [70,71], while DSBs in the 'breakage-first model' are able to scan the nuclear compartment to search for partners [72]. It is interesting to note that, in mouse fibroblasts, DSBs generally do not provoke enhanced movement, but the subpopulation of DNA DSBs that ultimately leads to translocations does indeed show enhanced mobility. This fulfills both the 'contact- and breakage-first hypotheses' [73]. Similar results were reported for DSBs induced by ionizing radiation and etoposide in human U2OS cells, which show a roughly 2-fold increase in Rc values, in a cell-cycle-dependent and an ATP-dependent manner [74,75]. Enhanced movement was also scored for uncapped telomeres in mammalian cells, yet mobility increase was 53BP1 dependent [76]. In the latter case, movement was proposed to enhance end joining, while in the former reports, it was suggested to facilitate HR. One testable hypothesis is that the movement, which promotes homology search, is actively suppressed in mammals. A failure to impair mammalian chromosomal break mobility might then lead to deleterious translocations or deletions. Intriguingly, the human SWI/SNF homologue BRM appears to favor precise NHEJ [77], possibly by impairing movement.

We note that human SWI/SNF complex (found in two related forms, called BAF and PBAF) has been identified to be the most frequently mutated chromatin regulatory complex in human cancer [78], suggesting that its mutation poses a serious threat to genomic stability. Moreover, PBAF, the human homologue of the yeast RSC remodeling complex, was shown to be important for both DSB-induced transcriptional silencing and the repair of a subset of DNA DSBs at early time points [79]. Therefore, it is possible that PBAF antagonizes mobility to favor rapid pathways of repair like NHEJ, and it may be opposed by the action of INO80-C.

INO80-C and SWR-C in DNA Repair and Replication

In budding yeast, both INO80-C and SWR-C were shown to be recruited to DSBs and to impact the repair process at different stages [80–82] (Fig. 3). While sharing many similarities in subunit composition, SWR-C and INO80-C have very distinct functions with regard to nucleosome remodeling. Both influence the genomic distribution of the histone variant Htz1: SWR-C deposits Htz1 in a stepwise manner, exchanging it for the canonical H2A, while INO80-C has been proposed to evict Htz1, particularly at non-promoter sites [65]. In addition and unlike SWR-C, INO80-C is able to slide, position and evict nucleosomes, regardless of their composition. This contributes to the regulation of a large number of genes (reviewed in Ref. [61]). Indeed, the catalytic Ino80 subunit and the Arp5 subunit map to many RNA pol II promoters that show changes in expression upon *ino80* deletion. In parallel, INO80-C is enriched at origins of replication and tRNA genes [83–85]. SWR-C, on the other hand, controls the expression of a restricted set of genes, largely through the deposition of Htz1 [86]. Both SWR-C and Htz1 are highly enriched immediately downstream of the transcriptional start site in budding yeast [87–89].

The link to DNA repair was first suggested by the strong hypersensitivity to DNA damaging agents scored for yeast cells that lack either Ino80 or Swr1. Loss of functional INO80-C leads to a pronounced sensitivity to hydroxyurea (HU) and methane methylsulfonate (MMS), with weaker sensitivity to ultraviolet light (UV) and ionizing radiation [66,90]. Yeast strains lacking Swr1 are also sensitive to HU or MMS [62], although HU sensitivity is much lower in *swr1*-deficient strains as compared to *ino80*-deficient strains. Intriguingly, *htz1*Δ single mutants are more sensitive to DNA damaging agents than *htz1*Δ*swr1*Δ double mutants [91], suggesting that SWR-C inflicts further damage or interferes with recovery from damage in the absence of Htz1.

Synthetic lethality screens have shown that the loss of INO80-C activity renders cells hypersensitive to the loss of genes involved in recombination, particularly in the presence of DNA damaging agents [92] (N. Hustedt and S.M.G., unpublished results). Coupled with the recruitment of INO80-C to an induced DSB [80,81], this argues for a direct role in DSB repair.

Similarly, SWR-C is rapidly recruited to DSBs, and *swr1* and *htz1* mutants also show synthetic sensitivity to DNA damaging agents in combination with factors involved in checkpoint activation and/or recombination [92] (N. Hustedt and S.M.G., unpublished results). Whereas INO80-C, along with RSC and Fun30, contributes to resection of the DSB, SWR-C appears not to be involved in resection under normal growth conditions [93,94]. Nonetheless, Swr1 recruitment to an induced DSB is both more rapid and more transient than that of Ino80, consistent with a role in early steps of DSB processing [93]. Its role may simply be to deposit Htz1. An important unresolved question concerns the events that trigger the recruitment of these remodelers to DNA damage.

The Recognition of DNA Damage by Remodelers

Although chromatin immunoprecipitation experiments showed that Mec1-dependent phosphorylation of histone H2A at serine 129 (H2A S129) (H2A.X S139 in mammals) was necessary for INO80-C and SWR-C recruitment to DNA breaks (reviewed in Ref. [50]), recent work argues that this effect is indirect. For unknown reasons, cells bearing an S129 mutation in histone H2A, eliminating the acceptor site for Mec1/Tel1 phosphorylation, accumulate in G1 phase. Intriguingly, remodeler recruitment to DSBs was also shown to be cell cycle dependent (higher in S and lower in G1); thus, the effect of the H2A S129 mutant is most likely indirect [82]. In addition to INO80-C and SWR-C, SWI/SNF, RSC and NuA4 accumulate at breaks weakly in G1 phase and much more robustly in G2 phase cells. Interestingly, γ-H2A.X (phospho-H2A) accumulation near the DSB was inversely correlated with remodeling enzyme enrichment being robust in G1 and less pronounced in G2/M. This correlates with the fact that the INO80-C remodeler is implicated in nucleosome eviction and the promotion of end resection at DSBs [82]. Finally, resection deficient yeast strains, that is, strains lacking Sgs1 and Exo1, showed a significant decrease of remodeler recruitment adjacent to the break, suggesting that either cross-talk between these factors and the remodelers or end resection itself plays a role in remodeler recruitment [82].

It is unclear which subunits of the remodelers directly recognize damaged sites. Interestingly, both SWR-C and INO80-C have subunits that bind single-strand and double-strand DNAs with fairly high affinity, albeit with little sequence specificity (reviewed in Ref. [61]). SWR-C accumulation immediately downstream of transcriptional start sites may well reflect the remodeler's affinity for non-nucleosomal DNA. On the other hand, Arp4, an integral subunit of INO80-C, SWR-C and NuA4, seems to bind to phosphorylated H2A (γ-H2A.X). For NuA4, this interaction activated its HAT activity and led to the acetylation of histones, contributing further to INO80-C and SWR-C recruitment to DSBs [95]. Another study implicated Nhp10, a non-essential subunit of INO80-C, in the interaction between INO80-C and γ-H2A.X [80]. Taf14 is another INO80-C subunit that is present in several complexes and may contribute to their recruitment to chromatin (M. Sopta, personal communication). Most likely, the combined affinities for DNA and modified histones contribute to the enhanced recruitment of remodeler complexes to DSBs.

Although γ-H2A.X may contribute to the recruitment of Arp4-containing chromatin modifiers, it also anti-correlates with their accumulation [82], suggesting that there may be a rapid eviction of γ-H2A.X-containing nucleosomes by the recruited remodelers. The same may be true for Htz1; we note that there are conflicting reports as to whether this variant increases or decreases at DSBs [35,93,96]. Most likely, Htz1-containing nucleosomes at the DSB are transiently deposited and rapidly lost, along with phosphorylated H2A, during the processing events that precede repair by HR.

Aiding or Avoiding Resection at DSBs

One of the first steps of DSB processing for HR involves resection of the DNA strands adjacent to the break (Fig. 3). This is achieved through either one of two resection pathways—that of Sgs1-Dna2 or of Exo1. The resection machinery dependent on Sgs1-Dna2 requires a nucleosome-free gap adjacent to the DSB. Resection by Exo1 is blocked by nucleosomes yet is stimulated by dynamic H2A.Z-H2B incorporation after DNA break induction, and consistently, SWR-C was found to facilitate Exo1 processing in HR [96]. Other laboratories failed to see effects of *swr1* mutants on resection [93,94]. Given that INO80-C helps evict H2A.Z and γ-H2A.X near DSBs [93], its role may be to facilitate resection dependent on Sgs1-Dna2.

In this respect, we note that some studies suggest that histones are lost as a consequence of resection rather than as a prerequisite for resection [97,98]. This suggests that remodelers fulfill tasks other than nucleosome eviction at the DSB, which favor or disfavor resection, and influence the outcome or pathway of repair. For instance, chromatin immunoprecipitation experiments showed that INO80-C subunits Arp8 and Nhp10 are important to retain Mec1 and Mre11 at the break site (indicative of resection), as well as yKu80 (which promotes NHEJ), while SWR-C contributes only to yKu retention [93]. Whereas the deletion of *swr1* and *arp8* had no effect on the repair of the *MAT* locus by gene conversion with *HM* loci [93], the remodeler mutants did have differential effects on NHEJ pathways: SWR-C promoted error-free NHEJ while INO80-C was found to have a modest effect on

error-prone NHEJ, which requires resection [93]. Moreover, deletion of SWR-C subunit Arp6 leads to a significant increase of spontaneous HR events, suggesting that SWR-C actively represses HR-mediated repair in yeast [99].

The data implicating INO80-C in repair are more extensive. Studies in *Arabidopsis thaliana* implicate INO80-C in ectopic (transposon) recombination events [100], and *arp8*-depleted diploid yeast cells were modestly defective in interhomolog DSB repair by HR [101]. Indeed, in *arp8*Δ cells, Rad51 is recruited to the DSB but the transfer to the homologous donor showed a marked delay, which correlates with a failure to displace nucleosomes at the donor locus [101]. Thus, it was argued that INO80-C contributes both to very early and very late stages of HR. Finally, *arp8*Δ strains were defective for DNA damage-induced sister chromatid recombination and inter-chromosomal recombination between heteroalleles, suggesting that widespread DNA damage might enhance INO80-C's contributions [99]. In this context, it is again relevant to mention that multiple INO80-C subunits are targets of Mec1 phosphorylation [48,49] and that a modification of its activity by phosphorylation may contribute to the defects revealed in various repair assays. Perhaps this explains the lack of effect seen by *ino80* mutation on recombination-mediated repair at *MAT*: this locus does not activate the checkpoint kinase Mec1 when it repairs the HO-induced cut by gene conversion with *HMR* or *HML*.

It is also important to note that *arp8*Δ strains may not reveal the full impact of INO80-C on repair, since yeasts lacking Arp8 are much less sensitive to DNA damaging agents than *ino80*Δ strains. Indeed, the lack of the Arp8 module (Arp8, Arp4 and actin) strongly hampers but does not impair the INO80-C remodeling reaction [52]. Unfortunately, in many strains, a complete *ino80* deletion is lethal. Further studies, preferably with a degron-inducible loss of function allele, will be needed to define the exact contribution of *INO80* to repair.

Conserved and Divergent Functions across Species

The INO80 subfamily of remodelers has an impact on genome stability throughout the eukaryotic kingdom, yet this conservation may not necessarily apply to specific roles in DSB repair. In mammalian cells, the more common repair pathway for DSB repair is NHEJ [102]. However, in mouse embryonic fibroblasts, INO80-C and its subunit YY1 are essential in HR-based repair and their deletion leads to DNA damage sensitivity. Additionally, loss of YY1 causes polyploidy and chromosomal aberrations [103]. In line with this finding, human and mouse INO80-C contribute to 5′–3′ strand resection [104] and mouse INO80-C was found to be required for the generation of single-stranded DNA for homology-directed DNA repair at telomeres [105].

Immunofluorescence experiments showed that human INO80-C is directed to the site of DNA damage in an Arp8-dependent manner, suggesting a direct role of mammalian INO80-C in DNA repair [106]. However, assessing the direct effects of human INO80-C in DNA repair might be difficult, as this chromatin remodeler also indirectly affects DNA repair by controlling the transcription of the repair genes Rad54B and XRCC3 [107]. It is unclear whether INO80 evicts H2A.Z in mammalian cells, as a H2A.Z chaperone has been recently reported, called ANP32E, which removes the histone variant across the genome and links H2A.Z to the p400/TIP60 complex [108].

The human counterpart of SWR-C, SRCAP, also incorporates H2A.Z-H2B dimers into nucleosomes [109]. Mutations in the human SRCAP protein can cause Floating-Harbor Syndrome, which is characterized by delayed osseous maturation, distinctive facial appearance, expressive language deficits and short stature [110]. Recent results show that, in HeLa cells, SRCAP contributes to cellular resistance to DSB-inducing agents and, as in yeast, is directly recruited to DSBs [111]. Intriguingly, SRCAP is able to form a complex with CtIP (*S. cerevisiae*: Sae2) and promotes accumulation of CtIP at DSBs, which is thought to cooperate with the MRN (*S. cerevisiae*: MRX) complex to stimulate the initiation of resection. Consistently, the same authors demonstrate that SRCAP facilitates DNA end resection, as well as the recruitment of replication protein A and the recombinase RAD51 [111]. In *A. thaliana*, mutations in SWR-C subunits also caused hypersensitivity to DNA damaging agents and correlated with impaired HR [112]. Whereas the damage hypersensitivity is conserved in budding yeast, *swr1*Δ and *arp6*Δ mutants lead instead to increased HR [91,99] and *swr1* null cells supported wild-type levels of Mre11 binding, end resection and checkpoint activation, in stark contrast to the phenotypes reported for SRCAP-depleted HeLa cells. Again further work is required to determine whether these discrepancies reflect the assays used or divergent roles for the H2A.Z (Htz1) in different species.

Involvement of INO80-C in Replication

The hypersensitivity of *S. cerevisiae ino80* deletion mutants to replication stress induced by HU depletion of nucleotides suggested a role of INO80-C in replication. Indeed, G1-arrested wild-type cells upregulate Ino80 expression upon release into HU-containing medium, and INO80-C is enriched at yeast origins of replication in an S-phase-specific manner, showing a genome-wide preference for early-firing over late-firing origins [83–85]. HU stalls replication forks due to a depletion of dNTPs and leads to a Mec1-dependent

checkpoint activation. Stabilizing polymerases at the stalled forks is essential for successful replication and cell survival. In two-dimensional gel analyses of stalled replication forks, a mutant *ino80* appeared to cause replication fork collapse [113], while *arp5*Δ and *arp8*Δ alleles did not but instead showed a dramatically impaired resumption of replication [83]. A genome-wide collapse of replication forks in the *ino80* mutant seems unlikely, given that the phosphorylation of H2A, indicative of DSBs arising from collapsed forks, was not significantly different between *ino80* and wild-type cells [85].

In contrast to HU, MMS induces S-phase-specific damage by base modification, provoking breaks or fork stalling that often require translesion synthesis for repair. Ubiquitination of the DNA replication processivity clamp proliferating nuclear antigen (PCNA) at K146 by Rad6-Rad18 is necessary to confer MMS damage tolerance during replication in the error-free damage avoidance pathway [114]. Within this pathway, Rad51 is recruited to the stalled replication fork in a Rad18-dependent and ub-PCNA-dependent manner [115]. A functional INO80 complex appears to be necessary for both Rad18 and Rad51 recruitments to MMS lesions and therefore also contributes to MMS resistance during replication [85]. The fact that ATPase activity of Ino80 is essential to recruit Rad18 and also Rad51 to stalled replication forks indicates that INO80-C also remodels nucleosomes and alters the chromatin landscape at damaged forks.

It will be interesting to explore how INO80-C and also SWR-C function in post-replicative repair or nucleosome assembly after replication, given that H3K56 acetylation both coincides with nucleosome reconstitution after passage of the replication fork (reviewed in Ref. [116]) and influences the enzymatic activity of SWR-C and INO80-C [117]. Not only the concerted action of INO80-C and SWR-C but also of other chromatin remodelers is likely to play a vital part in replication; notably, ISWI and INO80-C were also shown to function together to downregulate S phase checkpoint activity and ensure proper progression through S phase [118].

INO80-C and Nucleotide Excision Repair

Based on the findings that *ino80*Δ yeast strains are sensitive to replication blocking damage (induced by UV or MMS, for example), but not to ionizing radiation or camptothecin, it was suggested that INO80-C primarily functions during the replication of the genome [119]. However, the repair of methylated purines caused by MMS or UV-induced cyclobutyl pyrimidine dimers is not deficient in *ino80*Δ mutants [90,119]. Rather, INO80-C appears to function by facilitating the assembly of nucleotide excision repair (NER) factors and by restoring the chromatin state after NER of UV-induced damage. This may stem from the damage-induced interaction of INO80-C with Rad4-Rad23, a complex formed between the yeast XP-C homologue, Rad4, and Rad23, which bridges from the NER repair machinery to the proteasome [90,120]. Both Rad4 and Rad23 are necessary for NER due to the physical interaction of Rad23 with the 26S proteasome [121,122].

INO80-C and SWR-C in Checkpoint Pathways

INO80-C has been identified to be a Mec1 (ATR) and Tel1 (ATM) target in the DNA damage checkpoint response, with its subunit Ies4 being phosphorylated in the presence of DNA damage [48]. Ies4 phosphoacceptor site mutants do not significantly alter the repair of DNA damage but do modulate the checkpoint response [48]. An Ies4 phosphomimic mutant shows mild sensitivity to HU or MMS but no defects in other steps in HR- or NHEJ-mediated DSB repair, confirming that phospho-Ies4 is not directly involved in the repair process of DNA DSBs.

The phosphomimetic form of Ies4 does show an elevated checkpoint response in response to MMS and leads to a more pronounced cell cycle arrest. Impairing Ies4 phosphorylation had no evident impact on the checkpoint compared to wild-type cells but showed a strong synergistic lethality effect with the replication checkpoint factor Tof1 deletion mutant upon chronic exposure to HU. This suggest that INO80-C phosphorylation on subunit Ies4 is indeed critical during the DNA damage elicited by replication stress, even if it has no phenotype on its own [48]. There is no clear mechanism through which Ies4 phosphorylation could influence the remodeling activity of INO80-C although the protein is located close to the YEATS domain protein Taf14 within the Arp8 module of INO80-C [52]. Intriguingly, deletion of Nhp10 completely alleviates the DNA damage sensitivity of the phosphomimetic Ies4 mutations [48].

It is plausible that the Ies4 phosphoacceptor sites are redundant with other modifications induced by Mec1/Tel1 within INO80-C, given that Ies4 is among the non-conserved subunits in INO80-C. Indeed, a proteomic screen also identified Ies1 and Ino80 to be Mec1 and Tel1 targets [49] (N. Hustedt and S.M.G., personal communication). Since Ies1 does not associate with INO80-C in an *nhp10*Δ background [52], it would be possible that phosphorylation of at least Ies4 and Ies1 is jointly needed to modulate INO80 function upon checkpoint activation. In other words, checkpoint activation could be transmitted to INO80-C through the coordinate phosphorylation of both components (Ies1 and Ies4). In the INO80-C that lacks Nhp10, Ies1 may fail to be modulated, allowing Nhp10 deletion to suppress the DNA damage sensitivity of Ies4 phosphomimetic mutations.

The role of SWR-C in checkpoint activation is less well understood. The same proteomic screen that

identified Ies1 and Ino80 as new Mec1/Tel1 targets also shows that SWR-C subunits Bdf1 and Swr1 are phosphorylated upon checkpoint activation [49]. Therefore, it seems likely that also SWR-C plays a role in checkpoint-triggered processes. One hint that this may be the case comes from the observation that both SWR-C and INO80-C play a role in checkpoint adaptation. Checkpoint adaptation is a process that allows cells to escape an extended checkpoint arrest to re-enter the cell cycle with an unrepaired DSB. The components in this pathway seem to be at least partially conserved [123]. Budding yeast cells lacking Ino80, or expressing an ATPase deficient form of Ino80, are not able to overcome the checkpoint arrest. This correlates with a drop of H2A phosphorylation and increase of Htz1 incorporation surrounding the DSB. Interestingly, this effect can be counteracted by the additional deletion of Swr1. Therefore, INO80-C and SWR-C appear to have antagonistic functions in regulating checkpoint adaptation [124]. It is unclear whether SWR-C and INO80-C are involved in a novel pathway, possibly involving Htz1, or whether they act downstream of Ku70 or Rad51, two proteins previously implicated in the process.

Remodelers and Cancer

The role of chromatin remodelers in cancer is far from understood, but recent sequencing studies have made it clear that chromatin regulators play a vital part in maintaining the integrity of the genome. Not only are remodeler subunits found overexpressed or modulated in numerous types of cancer, but their correct interplay is crucial to maintain genome stability and prevent oncogenic transformation [78]. Human SWI/SNF or BAF has been identified to be the most frequently mutated chromatin regulatory complex in human cancer, suggesting that it is a potent tumor suppressor. In contrast to other known tumor suppressors or oncogenes that drive particular types of cancer, human SWI/SNF subunit genes were mutated in a wide range of cancers. Therefore, it is likely that SWI/SNF suppresses tumors on a very fundamental cellular level [78]. In the same study, it was shown that genes of SRCAP or TIP60 subunits were affected to a much lesser extent in the cancer genomes assessed, while INO80-C subunits were mutated only in a very small subset of cancers [78]. It would be interesting to probe for an imbalanced epigenetic landscape as a consequence of SWI/SNF mutations in cancer and to verify the factors that play havoc with chromatin composition.

Tumor suppressors such as SWI/SNF are usually difficult targets for cancer therapy, and therefore, it will be important to elucidate whether there are situations in which different remodelers antagonize each other, allowing for remodeler upregulation by inhibition of an opposing activity. On the other hand, given that BRG1 and BRM function as mutually exclusive subunits of human SWI/SNF, BRM could be a suitable target for SWI/SNF mutant cancer therapy in cancers that show paralogue insufficiency and dependence on the remaining ATPase subunit [125]. Paralogue insufficiency was also demonstrated in cancers for ARID1a and ARID1b, another subunit of the BRM/BRG1 complexes, suggesting that this too might be a potential target for inducing synthetic lethality in cancer cells [126].

The fact that multiple types of cancer show increased H3K56 acetylation suggests that the proper distribution of this specific post-translational modification is important for genomic integrity. In particular, this histone modification shows foci formation upon DNA damage that colocalize with sites of DNA repair [127]. Given the major impact of H3K56ac on the enzymatic activity of remodelers in yeast [117], there may be a misregulation of INO80-C and SRCAP (human SWR-C), or of TIP60, that contributes to genomic instability.

Finally, we note that many chromatin remodelers harbor subunits with a YEATS domain and several YEATS proteins in humans, such as GAS41, ENL and AF9, are linked to human cancers (reviewed in Ref. [128]). These proteins may be involved in the recruitment of remodelers to sites of damage or may modulate the Snf2 enzymatic activity that is necessary for maintenance of the epigenetic landscape under DNA damaging conditions. It is noteworthy that leukemias that specifically upregulate BAF (assembled around the BRG1 ATPase) require the complex for maintenance of the leukemia and that loss of BRG1 leads to immediate apoptosis and cell cycle arrest [129]. Given that BRG1 is dispensable for the long-term maintenance of hematopoietic stem cells, inhibitors that specifically block its function might be a promising avenue for a novel therapy against leukemia [129]. Finally it is also noteworthy that chromatin remodelers can be modulated by second messengers such as IP6 [130,131]. These small effector molecules may represent yet another means to modulate remodeler function, restoring the balance needed for genome stability by chemical intervention.

Acknowledgements

We thank Dr. Kenji Shimada, Dr. Vincent Dion, Dr. Jérôme Poli, Andrew Seeber and Dr. Chihiro Horigome for critical reading of the manuscript. We apologize to all those colleagues whose important work is not cited due to space limitations. The authors have been supported by a Research grants from the Human Frontiers Science Program and the Swiss National Science Foundation. Christian

Gerhold holds a FP7 Marie Curie Intra European Fellowship. Michael Hauer is supported by the Boehringer Ingelheim Foundation. The Gasser laboratory gratefully acknowledges the continued support of the Novartis Research Foundation.

Received 13 August 2014;
Received in revised form 13 October 2014;
Accepted 17 October 2014
Available online 30 October 2014

Keywords:
nuclear organization;
chromatin remodeling;
SWR-C;
INO80-C;
DNA repair

Abbreviations used:
DSB, double-strand break; HR, homologous recombination; HU, hydroxyurea; MMS, methane methylsulfonate; NER, nucleotide excision repair.

References

[1] Taddei A, Gasser SM. Structure and function in the budding yeast nucleus. Genetics 2012;192:107–29.
[2] Avsaroglu B, Bronk G, Gordon-Messer S, Ham J, Bressan DA, Haber JE, et al. Effect of chromosome tethering on nuclear organization in yeast. PLoS One 2014;9:e102474.
[3] Berger AB, Cabal GG, Fabre E, Duong T, Buc H, Nehrbass U, et al. High-resolution statistical mapping reveals gene territories in live yeast. Nat Methods 2008;5:1031–7.
[4] Rodley CD, Bertels F, Jones B, O'Sullivan JM. Global identification of yeast chromosome interactions using genome conformation capture. Fungal Genet Biol 2009;46:879–86.
[5] Duan Z, Andronescu M, Schutz K, McIlwain S, Kim YJ, Lee C, et al. A three-dimensional model of the yeast genome. Nature 2010;465:363–7.
[6] Cremer T, Cremer C. Chromosome territories, nuclear architecture and gene regulation in mammalian cells. Nat Rev Genet 2001;2:292–301.
[7] Dekker J, Rippe K, Dekker M, Kleckner N. Capturing chromosome conformation. Science 2002;295:1306–11.
[8] Bystricky K, Laroche T, van Houwe G, Blaszczyk M, Gasser SM. Chromosome looping in yeast: telomere pairing and coordinated movement reflect anchoring efficiency and territorial organization. J Cell Biol 2005;168:375–87.
[9] Schober H, Kalck V, Vega-Palas MA, Van Houwe G, Sage D, Unser M, et al. Controlled exchange of chromosomal arms reveals principles driving telomere interactions in yeast. Genome Res 2008;18:261–71.
[10] Gotta M, Laroche T, Formenton A, Maillet L, Scherthan H, Gasser SM. The clustering of telomeres and colocalization with Rap1, Sir3, and Sir4 proteins in wild-type *Saccharomyces cerevisiae*. J Cell Biol 1996;134:1349–63.
[11] Ruault M, De Meyer A, Loiodice I, Taddei A. Clustering heterochromatin: Sir3 promotes telomere clustering independently of silencing in yeast. J Cell Biol 2011;192:417–31.
[12] Hediger F, Neumann FR, Van Houwe G, Dubrana K, Gasser SM. Live imaging of telomeres: yKu and Sir proteins define redundant telomere-anchoring pathways in yeast. Curr Biol 2002;12:2076–89.
[13] Gartenberg MR, Neumann FR, Laroche T, Blaszczyk M, Gasser SM. Sir-mediated repression can occur independently of chromosomal and subnuclear contexts. Cell 2004;119:955–67.
[14] Taddei A, Hediger F, Neumann FR, Bauer C, Gasser SM. Separation of silencing from perinuclear anchoring functions in yeast Ku80, Sir4 and Esc1 proteins. EMBO J 2004;23:1301–12.
[15] Bupp JM, Martin AE, Stensrud ES, Jaspersen SL. Telomere anchoring at the nuclear periphery requires the budding yeast Sad1-UNC-84 domain protein Mps3. J Cell Biol 2007;179:845–54.
[16] Schober H, Ferreira H, Kalck V, Gehlen LR, Gasser SM. Yeast telomerase and the SUN domain protein Mps3 anchor telomeres and repress subtelomeric recombination. Genes Dev 2009;23:928–38.
[17] Andrulis ED, Zappulla DC, Ansari A, Perrod S, Laiosa CV, Gartenberg MR, et al. Esc1, a nuclear periphery protein required for Sir4-based plasmid anchoring and partitioning. Mol Cell Biol 2002;22:8292–301.
[18] Akhtar A, Gasser SM. The nuclear envelope and transcriptional control. Nat Rev Genet 2007;8:507–17.
[19] Solovei I, Wang AS, Thanisch K, Schmidt CS, Krebs S, Zwerger M, et al. LBR and lamin A/C sequentially tether peripheral heterochromatin and inversely regulate differentiation. Cell 2013;152:584–98.
[20] Nagai S, Dubrana K, Tsai-Pflugfelder M, Davidson MB, Roberts TM, Brown GW, et al. Functional targeting of DNA damage to a nuclear pore-associated SUMO-dependent ubiquitin ligase. Science 2008;322:597–602.
[21] Khadaroo B, Teixeira MT, Luciano P, Eckert-Boulet N, Germann SM, Simon MN, et al. The DNA damage response at eroded telomeres and tethering to the nuclear pore complex. Nat Cell Biol 2009;11:980–7.
[22] Therizols P, Fairhead C, Cabal GG, Genovesio A, Olivo-Marin JC, Dujon B, et al. Telomere tethering at the nuclear periphery is essential for efficient DNA double strand break repair in subtelomeric region. J Cell Biol 2006;172:189–99.
[23] Palancade B, Liu X, Garcia-Rubio M, Aguilera A, Zhao X, Doye V. Nucleoporins prevent DNA damage accumulation by modulating Ulp1-dependent sumoylation processes. Mol Biol Cell 2007;18:2912–23.
[24] Cremona CA, Sarangi P, Yang Y, Hang LE, Rahman S, Zhao X. Extensive DNA damage-induced sumoylation contributes to replication and repair and acts in addition to the mec1 checkpoint. Mol Cell 2012;45:422–32.
[25] Psakhye I, Jentsch S. Protein group modification and synergy in the SUMO pathway as exemplified in DNA repair. Cell 2012;151:807–20.
[26] Galanty Y, Belotserkovskaya R, Coates J, Jackson SP. RNF4, a SUMO-targeted ubiquitin E3 ligase, promotes DNA double-strand break repair. Genes Dev 2012;26:1179–95.
[27] Yin Y, Seifert A, Chua JS, Maure JF, Golebiowski F, Hay RT. SUMO-targeted ubiquitin E3 ligase RNF4 is required for the response of human cells to DNA damage. Genes Dev 2012;26:1196–208.
[28] Vyas R, Kumar R, Clermont F, Helfricht A, Kalev P, Sotiropoulou P, et al. RNF4 is required for DNA double-strand break repair *in vivo*. Cell Death Differ 2013;20:490–502.

[29] Marshall WF, Straight A, Marko JF, Swedlow J, Dernburg A, Belmont A, et al. Interphase chromosomes undergo constrained diffusional motion in living cells. Curr Biol 1997;7: 930–9.
[30] Neumann FR, Dion V, Gehlen LR, Tsai-Pflugfelder M, Schmid R, Taddei A, et al. Targeted INO80 enhances subnuclear chromatin movement and ectopic homologous recombination. Genes Dev 2012;26:369–83.
[31] Heun P, Laroche T, Shimada K, Furrer P, Gasser SM. Chromosome dynamics in the yeast interphase nucleus. Science 2001;294:2181–6.
[32] Vazquez J, Belmont AS, Sedat JW. The dynamics of homologous chromosome pairing during male *Drosophila* meiosis. Curr Biol 2002;12:1473–83.
[33] Dion V, Gasser SM. Chromatin movement in the maintenance of genome stability. Cell 2013;152:1355–64.
[34] Dion V, Kalck V, Seeber A, Schleker T, Gasser SM. Cohesin and the nucleolus constrain the mobility of spontaneous repair foci. EMBO Rep 2013;14:984–91.
[35] Kalocsay M, Hiller NJ, Jentsch S. Chromosome-wide Rad51 spreading and SUMO-H2A.Z-dependent chromosome fixation in response to a persistent DNA double-strand break. Mol Cell 2009;33:335–43.
[36] Seeber A, Dion V, Gasser SM. Checkpoint kinases and the INO80 nucleosome remodeling complex enhance global chromatin mobility in response to DNA damage. Genes Dev 2013;27:1999–2008.
[37] Horigome C, Oma Y, Konishi T, Schmid R, Marcomini I, Hauer M, et al. SWR1 and INO80 chromatin remodelers contribute to DNA double-strand break anchorage site choice at the nuclear periphery. Mol Cell 2014;55(4): 626–39.
[38] Guacci V, Hogan E, Koshland D. Chromosome condensation and sister chromatid pairing in budding yeast. J Cell Biol 1994;125:517–30.
[39] Bystricky K, Heun P, Gehlen L, Langowski J, Gasser SM. Long-range compaction and flexibility of interphase chromatin in budding yeast analyzed by high-resolution imaging techniques. Proc Natl Acad Sci USA 2004;101: 16495–500.
[40] Davis SK, Bardeen CJ. The connection between chromatin motion on the 100 nm length scale and core histone dynamics in live XTC-2 cells and isolated nuclei. Biophys J 2004;86:555–64.
[41] Chubb JR, Boyle S, Perry P, Bickmore WA. Chromatin motion is constrained by association with nuclear compartments in human cells. Curr Biol 2002;12:439–45.
[42] Dion V, Kalck V, Horigome C, Towbin BD, Gasser SM. Increased mobility of double-strand breaks requires Mec1, Rad9 and the homologous recombination machinery. Nat Cell Biol 2012;14:502–9.
[43] Mine-Hattab J, Rothstein R. Increased chromosome mobility facilitates homology search during recombination. Nat Cell Biol 2012;14:510–7.
[44] Cenci G, Rawson RB, Belloni G, Castrillon DH, Tudor M, Petrucci R, et al. UbcD1, a *Drosophila* ubiquitin-conjugating enzyme required for proper telomere behavior. Genes Dev 1997;11:863–75.
[45] Wilson JH, Leung WY, Bosco G, Dieu D, Haber JE. The frequency of gene targeting in yeast depends on the number of target copies. Proc Natl Acad Sci USA 1994;91:177–81.
[46] Flaus A, Martin DM, Barton GJ, Owen-Hughes T. Identification of multiple distinct Snf2 subfamilies with conserved structural motifs. Nucleic Acids Res 2006;34:2887–905.
[47] Saad H, Gallardo F, Dalvai M, Tanguy-le-Gac N, Lane D, Bystricky K. DNA dynamics during early double-strand break processing revealed by non-intrusive imaging of living cells. PLoS Genet 2014;10:e1004187.
[48] Morrison AJ, Kim J-A, Person MD, Highland J, Xiao J, Wehr TS, et al. Mec1/Tel1 phosphorylation of the INO80 chromatin remodeling complex influences DNA damage checkpoint responses. Cell 2007;130:499–511.
[49] Chen S-H, Albuquerque CP, Liang J, Suhandynata RT, Zhou H. A proteome-wide analysis of kinase-substrate network in the DNA damage response. J Biol Chem 2010; 285:12803–12.
[50] van Attikum H, Gasser SM. Crosstalk between histone modifications during the DNA damage response. Trends Cell Biol 2009;19:207–17.
[51] Shen X, Ranallo R, Choi E, Wu C. Involvement of actin-related proteins in ATP-dependent chromatin remodeling. Mol Cell 2003;12:147–55.
[52] Tosi A, Haas C, Herzog F, Gilmozzi A, Berninghausen O, Ungewickell C, et al. Structure and subunit topology of the INO80 chromatin remodeler and its interaction with the nucleosome. Cell 2013;154(6):1207–19.
[53] Oza P, Jaspersen SL, Miele A, Dekker J, Peterson CL. Mechanisms that regulate localization of a DNA double-strand break to the nuclear periphery. Genes Dev 2009;23:912–27.
[54] Bukata L, Parker SL, D'Angelo MA. Nuclear pore complexes in the maintenance of genome integrity. Curr Opin Cell Biol 2013;25:378–86.
[55] Burgess RC, Rahman S, Lisby M, Rothstein R, Zhao X. The Slx5-Slx8 complex affects sumoylation of DNA repair proteins and negatively regulates recombination. Mol Cell Biol 2007;27:6153–62.
[56] Azam M, Lee JY, Abraham V, Chanoux R, Schoenly KA, Johnson FB. Evidence that the *S. cerevisiae* Sgs1 protein facilitates recombinational repair of telomeres during senescence. Nucleic Acids Res 2006;34:506–16.
[57] Zhang C, Roberts TM, Yang J, Desai R, Brown GW. Suppression of genomic instability by SLX5 and SLX8 in *Saccharomyces cerevisiae*. DNA Repair (Amst) 2006;5: 336–46.
[58] Loeillet S, Palancade B, Cartron M, Thierry A, Richard GF, Dujon B, et al. Genetic network interactions among replication, repair and nuclear pore deficiencies in yeast. DNA Repair (Amst) 2005;4:459–68.
[59] Roerink SF, Koole W, Stapel LC, Romeijn RJ, Tijsterman M. A broad requirement for TLS polymerases eta and kappa, and interacting sumoylation and nuclear pore proteins, in lesion bypass during *C. elegans* embryogenesis. PLoS Genet 2012;8:e1002800.
[60] Nguyen VQ, Ranjan A, Stengel F, Wei D, Aebersold R, Wu C, et al. Molecular architecture of the ATP-dependent chromatin-remodeling complex SWR1. Cell 2013;154:1220–31.
[61] Nguyen VQ, Ranjan A, Stengel F, Wei D, Aebersold R, Wu C, et al. INO80 and SWR complexes: relating structure to function in chromatin remodeling. Trends Cell Biol 2014; 24(11):619–31.
[62] Mizuguchi G, Shen X, Landry J, Wu W-H, Sen S, Wu C. ATP-driven exchange of histone H2AZ variant catalyzed by SWR1 chromatin remodeling complex. Science 2004;303: 343–8.
[63] Luk E, Ranjan A, FitzGerald PC, Mizuguchi G, Huang Y, Wei D, et al. Stepwise histone replacement by SWR1 requires dual activation with histone H2A.Z and canonical nucleosome. Cell 2010;143:725–36.

[64] Ranjan A, Mizuguchi G, FitzGerald Peter C, Wei D, Wang F, Huang Y, et al. Nucleosome-free region dominates histone acetylation in targeting SWR1 to promoters for H2A.Z replacement. Cell 2013;154:1232–45.
[65] Papamichos-Chronakis M, Watanabe S, Rando OJ, Peterson CL. Global regulation of H2A.Z localization by the INO80 chromatin-remodeling enzyme is essential for genome integrity. Cell 2011;144:200–13.
[66] Shen X, Mizuguchi G, Hamiche A, Wu C. A chromatin remodelling complex involved in transcription and DNA processing. Nature 2000;406:541–4.
[67] Tsukuda T, Fleming AB, Nickoloff JA, Osley MA. Chromatin remodelling at a DNA double-strand break site in *Saccharomyces cerevisiae*. Nature 2005;438:379–83.
[68] Udugama M, Sabri A, Bartholomew B. The INO80 ATP-dependent chromatin remodeling complex is a nucleosome spacing factor. Mol Cell Biol 2011;31:662–73.
[69] Yoshida T, Shimada K, Oma Y, Kalck V, Akimura K, Taddei A, et al. Actin-related protein Arp6 influences H2A.Z-dependent and -independent gene expression and links ribosomal protein genes to nuclear pores. PLoS Genet 2010;6:e1000910.
[70] Soutoglou E, Dorn JF, Sengupta K, Jasin M, Nussenzweig A, Ried T, et al. Positional stability of single double-strand breaks in mammalian cells. Nat Cell Biol 2007;9:675–82.
[71] Nikiforova MN, Stringer JR, Blough R, Medvedovic M, Fagin JA, Nikiforov YE. Proximity of chromosomal loci that participate in radiation-induced rearrangements in human cells. Science 2000;290:138–41.
[72] Aten JA, Stap J, Krawczyk PM, van Oven CH, Hoebe RA, Essers J, et al. Dynamics of DNA double-strand breaks revealed by clustering of damaged chromosome domains. Science 2004;303:92–5.
[73] Roukos V, Voss TC, Schmidt CK, Lee S, Wangsa D, Misteli T. Spatial dynamics of chromosome translocations in living cells. Science 2013;341:660–4.
[74] Kruhlak MJ, Celeste A, Dellaire G, Fernandez-Capetillo O, Muller WG, McNally JG, et al. Changes in chromatin structure and mobility in living cells at sites of DNA double-strand breaks. J Cell Biol 2006;172:823–34.
[75] Krawczyk PM, Borovski T, Stap J, Cijsouw T, ten Cate R, Medema JP, et al. Chromatin mobility is increased at sites of DNA double-strand breaks. J Cell Sci 2012;125:2127–33.
[76] Dimitrova N, Chen YC, Spector DL, de Lange T. 53BP1 promotes non-homologous end joining of telomeres by increasing chromatin mobility. Nature 2008;456:524–8.
[77] Ui A, Ogiwara H, Nakajima S, Kanno S, Watanabe R, Harata M, et al. Possible involvement of LKB1-AMPK signaling in non-homologous end joining. Oncogene 2013;33:1640–8.
[78] Kadoch C, Hargreaves DC, Hodges C, Elias L, Ho L, Ranish J, et al. Proteomic and bioinformatic analysis of mammalian SWI/SNF complexes identifies extensive roles in human malignancy. Nat Genet 2013;45:592–601.
[79] Kakarougkas A, Ismail A, Chambers AL, Riballo E, Herbert AD, Kunzel J, et al. Requirement for PBAF in transcriptional repression and repair at DNA breaks in actively transcribed regions of chromatin. Mol Cell 2014;55:723–32.
[80] Morrison AJ, Highland J, Krogan NJ, Arbel-Eden A, Greenblatt JF, Haber JE, et al. INO80 and γ-H2AX interaction links ATP-dependent chromatin remodeling to DNA damage repair. Cell 2004;119:767–75.
[81] van Attikum H, Fritsch O, Hohn B, Gasser SM. Recruitment of the INO80 complex by H2A phosphorylation links ATP-dependent chromatin remodeling with DNA double-strand break repair. Cell 2004;119:777–88.
[82] Bennett G, Papamichos-Chronakis M, Peterson CL. DNA repair choice defines a common pathway for recruitment of chromatin regulators. Nat Commun 2013;4:2084.
[83] Shimada K, Oma Y, Schleker T, Kugou K, Ohta K, Harata M, et al. Ino80 chromatin remodeling complex promotes recovery of stalled replication forks. Curr Biol 2008;18:566–75.
[84] Vincent JA, Kwong TJ, Tsukiyama T. ATP-dependent chromatin remodeling shapes the DNA replication landscape. Nat Struct Mol Biol 2008;15:477–84.
[85] Falbo KB, Alabert C, Katou Y, Wu S, Han J, Wehr T, et al. Involvement of a chromatin remodeling complex in damage tolerance during DNA replication. Nat Struct Mol Biol 2009;16:1167–72.
[86] Krogan NJ, Keogh MC, Datta N, Sawa C, Ryan OW, Ding H, et al. A Snf2 family ATPase complex required for recruitment of the histone H2A variant Htz1. Mol Cell 2003;12:1565–76.
[87] Zhang H, Roberts DN, Cairns BR. Genome-wide dynamics of Htz1, a histone H2A variant that poises repressed/basal promoters for activation through histone loss. Cell 2005;123:219–31.
[88] Yen K, Vinayachandran V, Batta K, Koerber RT, Pugh BF. Genome-wide nucleosome specificity and directionality of chromatin remodelers. Cell 2012;149:1461–73.
[89] Yen K, Vinayachandran V, Pugh BF. SWR-C and INO80 chromatin remodelers recognize nucleosome-free regions near +1 nucleosomes. Cell 2013;154:1246–56.
[90] Sarkar S, Kiely R, McHugh PJ. The Ino80 chromatin-remodeling complex restores chromatin structure during UV DNA damage repair. J Cell Biol 2010;191:1061–8.
[91] Morillo-Huesca M, Clemente-Ruiz M, Andujar E, Prado F. The SWR1 histone replacement complex causes genetic instability and genome-wide transcription misregulation in the absence of H2A.Z. PLoS One 2010;5:e12143.
[92] Guenole A, Srivas R, Vreeken K, Wang ZZ, Wang S, Krogan NJ, et al. Dissection of DNA damage responses using multiconditional genetic interaction maps. Mol Cell 2013;49:346–58.
[93] van Attikum H, Fritsch O, Gasser SM. Distinct roles for SWR1 and INO80 chromatin remodeling complexes at chromosomal double-strand breaks. EMBO J 2007;26:4113–25.
[94] Chen X, Cui D, Papusha A, Zhang X, Chu CD, Tang J, et al. The Fun30 nucleosome remodeller promotes resection of DNA double-strand break ends. Nature 2012;489:576–80.
[95] Downs JA, Allard S, Jobin-Robitaille O, Javaheri A, Auger A, Bouchard N, et al. Binding of chromatin-modifying activities to phosphorylated histone H2A at DNA damage sites. Mol Cell 2004;16:979–90.
[96] Adkins NL, Niu H, Sung P, Peterson CL. Nucleosome dynamics regulates DNA processing. Nat Struct Mol Biol 2013;20:836–42.
[97] Shroff R, Arbel-Eden A, Pilch D, Ira G, Bonner WM, Petrini JH, et al. Distribution and dynamics of chromatin modification induced by a defined DNA double-strand break. Curr Biol 2004;14:1703–11.
[98] Chen C-C, Carson JJ, Feser J, Tamburini B, Zabaronick S, Linger J, et al. Acetylated lysine 56 on histone H3 drives chromatin assembly after repair and signals for the completion of repair. Cell 2008;134:231–43.
[99] Kawashima S, Ogiwara H, Tada S, Harata M, Wintersberger U, Enomoto T, et al. The INO80 complex is required for damage-induced recombination. Biochem Biophys Res Commun 2007;355:835–41.

[100] Fritsch O, Benvenuto G, Bowler C, Molinier J, Hohn B. The INO80 protein controls homologous recombination in *Arabidopsis thaliana*. Mol Cell 2004;16:479–85.
[101] Tsukuda T, Lo Y-C, Krishna S, Sterk R, Osley MA, Nickoloff JA. INO80-dependent chromatin remodeling regulates early and late stages of mitotic homologous recombination. DNA Repair 2009;8:360–9.
[102] Kim JS, Krasieva TB, Kurumizaka H, Chen DJ, Taylor AM, Yokomori K. Independent and sequential recruitment of NHEJ and HR factors to DNA damage sites in mammalian cells. J Cell Biol 2005;170:341–7.
[103] Wu S, Shi Y, Mulligan P, Gay F, Landry J, Liu H, et al. A YY1-INO80 complex regulates genomic stability through homologous recombination-based repair. Nat Struct Mol Biol 2007;14:1165–72.
[104] Gospodinov A, Vaissiere T, Krastev DB, Legube G, Anachkova B, Herceg Z. Mammalian Ino80 mediates double-strand break repair through its role in DNA end strand resection. Mol Cell Biol 2011;31:4735–45.
[105] Min JN, Tian Y, Xiao Y, Wu L, Li L, Chang S. The mINO80 chromatin remodeling complex is required for efficient telomere replication and maintenance of genome stability. Cell Res 2013. http://dx.doi.org/10.1038/cr.2013.113.
[106] Kashiwaba S-i, Kitahashi K, Watanabe T, Onoda F, Ohtsu M, Murakami Y. The mammalian INO80 complex is recruited to DNA damage sites in an ARP8 dependent manner. Biochem Biophys Res Commun 2010;402:619–25.
[107] Park EJ, Hur SK, Kwon J. Human INO80 chromatin-remodelling complex contributes to DNA double-strand break repair via the expression of Rad54B and XRCC3 genes. Biochem J 2010;431:179–87.
[108] Obri A, Ouararhni K, Papin C, Diebold ML, Padmanabhan K, Marek M, et al. ANP32E is a histone chaperone that removes H2A.Z from chromatin. Nature 2014;505:648–53.
[109] Ruhl DD, Jin J, Cai Y, Swanson S, Florens L, Washburn MP, et al. Purification of a human SRCAP complex that remodels chromatin by incorporating the histone variant H2A.Z into nucleosomes. Biochemistry 2006;45:5671–7.
[110] Hood RL, Lines MA, Nikkel SM, Schwartzentruber J, Beaulieu C, Nowaczyk MJ, et al. Mutations in SRCAP, encoding SNF2-related CREBBP activator protein, cause Floating-Harbor syndrome. Am J Hum Genet 2012;90:308–13.
[111] Dong S, Han J, Chen H, Liu T, Huen MS, Yang Y, et al. The human SRCAP chromatin remodeling complex promotes DNA-end resection. Curr Biol 2014;24:2097–110.
[112] Rosa M, Von Harder M, Aiese Cigliano R, Schlögelhofer P, Mittelsten Scheid O. The *Arabidopsis* SWR1 chromatin-remodeling complex is important for DNA repair, somatic recombination, and meiosis. Plant Cell Online 2013;25:1990–2001.
[113] Papamichos-Chronakis M, Peterson CL. The Ino80 chromatin-remodeling enzyme regulates replisome function and stability. Nat Struct Mol Biol 2008;15:338–45.
[114] Hoege C, Pfander B, Moldovan GL, Pyrowolakis G, Jentsch S. RAD6-dependent DNA repair is linked to modification of PCNA by ubiquitin and SUMO. Nature 2002;419:135–41.
[115] Branzei D, Vanoli F, Foiani M. SUMOylation regulates Rad18-mediated template switch. Nature 2008;456:915–20.
[116] Ransom M, Dennehey BK, Tyler JK. Chaperoning histones during DNA replication and repair. Cell 2010;140:183–95.
[117] Watanabe S, Radman-Livaja M, Rando OJ, Peterson CL. A histone acetylation switch regulates H2A.Z deposition by the SWR-C remodeling enzyme. Science 2013;340:195–9.
[118] Au TJ, Rodriguez J, Vincent JA, Tsukiyama T. ATP-dependent chromatin remodeling factors tune S phase checkpoint activity. Mol Cell Biol 2011;31:4454–63.
[119] Czaja W, Bespalov VA, Hinz JM, Smerdon MJ. Proficient repair in chromatin remodeling defective ino80 mutants of *Saccharomyces cerevisiae* highlights replication defects as the main contributor to DNA damage sensitivity. DNA Repair (Amst) 2010;9:976–84.
[120] Jiang Y, Wang X, Bao S, Guo R, Johnson DG, Shen X, et al. INO80 chromatin remodeling complex promotes the removal of UV lesions by the nucleotide excision repair pathway. Proc Natl Acad Sci 2010;107:17274–9.
[121] Schauber C, Chen L, Tongaonkar P, Vega I, Lambertson D, Potts W, et al. Rad23 links DNA repair to the ubiquitin/proteasome pathway. Nature 1998;391:715–8.
[122] Baek GH, Kim I, Rao H. The Cdc48 ATPase modulates the interaction between two proteolytic factors Ufd2 and Rad23. Proc Natl Acad Sci USA 2011;108:13558–63.
[123] Yoo HY, Kumagai A, Shevchenko A, Shevchenko A, Dunphy WG. Adaptation of a DNA replication checkpoint response depends upon inactivation of Claspin by the Polo-like kinase. Cell 2004;117:575–88.
[124] Papamichos-Chronakis M, Krebs JE, Peterson CL. Interplay between Ino80 and Swr1 chromatin remodeling enzymes regulates cell cycle checkpoint adaptation in response to DNA damage. Genes Dev 2006;20:2437–49.
[125] Hoffman GR, Rahal R, Buxton F, Xiang K, McAllister G, Frias E, et al. Functional epigenetics approach identifies BRM/SMARCA2 as a critical synthetic lethal target in BRG1-deficient cancers. Proc Natl Acad Sci USA 2014;111:3128–33.
[126] Helming KC, Wang X, Wilson BG, Vazquez F, Haswell JR, Manchester HE, et al. ARID1B is a specific vulnerability in ARID1A-mutant cancers. Nat Med 2014;20:251–4.
[127] Das C, Lucia MS, Hansen KC, Tyler JK. CBP/p300-mediated acetylation of histone H3 on lysine 56. Nature 2009;459:113–7.
[128] Schulze JM, Wang AY, Kobor MS. Reading chromatin: insights from yeast into YEATS domain structure and function. Epigenetics 2010;5:573–7.
[129] Buscarlet M, Krasteva V, Ho L, Simon C, Hebert J, Wilhelm B, et al. Essential role of BRG, the ATPase subunit of BAF chromatin remodeling complexes, in leukemia maintenance. Blood 2014;123:1720–8.
[130] Shen X, Xiao H, Ranallo R, Wu W-H, Wu C. Modulation of ATP-dependent chromatin-remodeling complexes by inositol polyphosphates. Science 2003;299:112–4.
[131] Steger DJ, Haswell ES, Miller AL, Wente SR, O'Shea EK. Regulation of chromatin remodeling by inositol polyphosphates. Science 2003;299:114–6.

CHAPTER 3: PERINUCLEAR ANCHORING OF H3K9-METHYLATED CHROMATIN IN C. ELEGANS EMBRYOS

Gonzalez-Sandoval, A., B. D. Towbin, V. Kalck, D. S. Cabianca, D. Gaidatzis, **M. H. Hauer**, L. Geng, L. Wang, T. Yang, X. Wang, K. Zhao and S. M. Gasser (2015). "Perinuclear Anchoring of H3K9 Methylated Chromatin Stabilizes Induced Cell Fate in C. elegans Embryos." Cell 163(6): 1333-1347.

Author contributions: Conceptualization, A.G.-S., B.D.T., and S.M.G.; Methodology, A.G.-S., B.D.T., and D.S.C.; Validation, A.G.-S., V.K., D.S.C.; Formal Analysis, D.G., M.H.H; Investigation, A.G.-S., B.D.T., V.K., D.S.C., M.H.H, L.G., L.W., T.Y., X.W.; Re- sources, K.Z.; Writing – Review & Editing, A.G.-S., B.D.T., D.S.C., S.M.G.; Supervision, K.Z., S.M.G.; Funding Acquisition, S.G.M.

Summary

This chapter discusses the mechanism of heterochromatin sequestration to the nuclear periphery in *C. elegans* embryos by the nuclear envelope protein CEC-4. The study by Gonzalez-Sandoval *et al.* further illustrates phenotypic effects on embryo development when dysregulation of the CEC-4 pathway occurs. Of special interest to this thesis is the semi-automated and pixel-classification driven image analysis workflow used to explore a subset of three-dimensional imaging data. We used it to unbiasedly measure the subnuclear position as well as spatial expansion of a fluorescently labeled, heterochromatic array in 3D space. After having successfully tested and published the principles of this technique, it was extensively used to address chromatin expansion in **Chapter 4**.

Article

Cell

Perinuclear Anchoring of H3K9-Methylated Chromatin Stabilizes Induced Cell Fate in *C. elegans* Embryos

Adriana Gonzalez-Sandoval,[1,2] Benjamin D. Towbin,[1,5] Veronique Kalck,[1] Daphne S. Cabianca,[1] Dimos Gaidatzis,[1,3] Michael H. Hauer,[1,2] Liqing Geng,[4] Li Wang,[4] Teddy Yang,[4] Xinghao Wang,[4] Kehao Zhao,[4] and Susan M. Gasser[1,2,*]

[1]Friedrich Miescher Institute for Biomedical Research, Maulbeerstrasse 66, CH-4058 Basel, Switzerland
[2]Faculty of Natural Sciences, University of Basel, Klingelbergstrasse 50/70, CH-4056 Basel, Switzerland
[3]Swiss Institute of Bioinformatics, CH-4058 Basel, Switzerland
[4]China Novartis Institute of Biomedical Research Co, Ltd. Bldg 3, Lane 3728 Jinke Road, Pudong New Area, Shanghai 201203, China
[5]Present address: Department of Molecular Cell Biology, The Weizmann Institute of Science, Rehovot 76100, Israel
*Correspondence: susan.gasser@fmi.ch
http://dx.doi.org/10.1016/j.cell.2015.10.066

SUMMARY

Interphase chromatin is organized in distinct nuclear sub-compartments, reflecting its degree of compaction and transcriptional status. In *Caenorhabditis elegans* embryos, H3K9 methylation is necessary to silence and to anchor repeat-rich heterochromatin at the nuclear periphery. In a screen for perinuclear anchors of heterochromatin, we identified a previously uncharacterized *C. elegans* chromodomain protein, CEC-4. CEC-4 binds preferentially mono-, di-, or tri-methylated H3K9 and localizes at the nuclear envelope independently of H3K9 methylation and nuclear lamin. CEC-4 is necessary for endogenous heterochromatin anchoring, but not for transcriptional repression, in contrast to other known H3K9 methyl-binders in worms, which mediate gene repression but not perinuclear anchoring. When we ectopically induce a muscle differentiation program in embryos, *cec-4* mutants fail to commit fully to muscle cell fate. This suggests that perinuclear sequestration of chromatin during development helps restrict cell differentiation programs by stabilizing commitment to a specific cell fate.

INTRODUCTION

Cues stemming from the spatial organization of chromatin are widely thought to influence the function of eukaryotic genomes. Indeed, chromatin assumes distinct patterns of distribution in the interphase nucleus in response to cell-type-specific gene expression (reviewed in Meister et al., 2011; Talamas and Capelson, 2015). Dense-staining heterochromatin and repressed tissue-specific genes are sequestered at the inner nuclear membrane (INM) in both plant and animal cells. In metazoans, an INM-associated network of the intermediate filament protein lamin and other associated proteins provides a scaffold that helps the interphase nucleus reform after mitosis (Nigg, 1992).

The chromatin that associates with the nuclear lamina (lamin-associated domains or LADs) is generally gene poor, transcriptionally silent, and enriched for repressive histone marks (Gerstein et al., 2010; Guelen et al., 2008; Ikegami et al., 2010; Pickersgill et al., 2006). Importantly, in *C. elegans* embryos the integrity of two histone methyltransferases (HMTs) that target histone H3K9, MET-2, and SET-25 was shown to be essential for the peripheral localization of heterochromatin (Towbin et al., 2012). Perturbed H3K9 methylation also partially compromised proper heterochromatin organization in mammalian cells (Kind et al., 2013; Pinheiro et al., 2012). However, no nuclear envelope protein has yet been identified that anchors H3K9-methylated chromatin specifically.

Studies of nuclear organization during the development of multicellular organisms or of embryonic stem cell (ESC) differentiation in vitro showed that perinuclear chromatin sequestration is a dynamic process that changes with cell-type-specific gene expression (Fussner et al., 2010; Harr et al., 2015; Meister et al., 2010; Peric-Hupkes et al., 2010). Important genetic studies of Solovei et al. (2013) showed that heterochromatin tethering in differentiated mammalian cells depends on two partially redundant pathways that reflect the sequential induction through development of lamin B receptor (LBR) and lamin A/C. In some mouse tissues both LBR and lamin A/C are expressed; in others, expression of only one is sufficient to ensure the conventional sequestration of heterochromatin at the INM. In the absence of both perinuclear components, heterochromatin accumulated at the nuclear core (Solovei et al., 2013).

Despite these genetic implications, it was unclear what bridges chromatin to LBR or lamin A/C. LBR has been shown to bind the chromodomain (CD) of Heterochromatin proteins 1α and γ (HP1α and HP1γ; (Ye and Worman, 1996), which are hallmarks of heterochromatin. But HP1α-containing chromocenters are not necessarily perinuclear, and HP1γ is bound to many euchromatic loci positioned away from INM (Minc et al., 1999). Moreover, complete ablation of HP1α or β in either pluripotent or differentiated ESCs does not change chromocenter positioning (Mattout et al., 2015). Mammalian LBR also binds histone H4K20me2 in vitro through its C-terminal Tudor domain (Hirano et al., 2012), yet H4K20me2 is

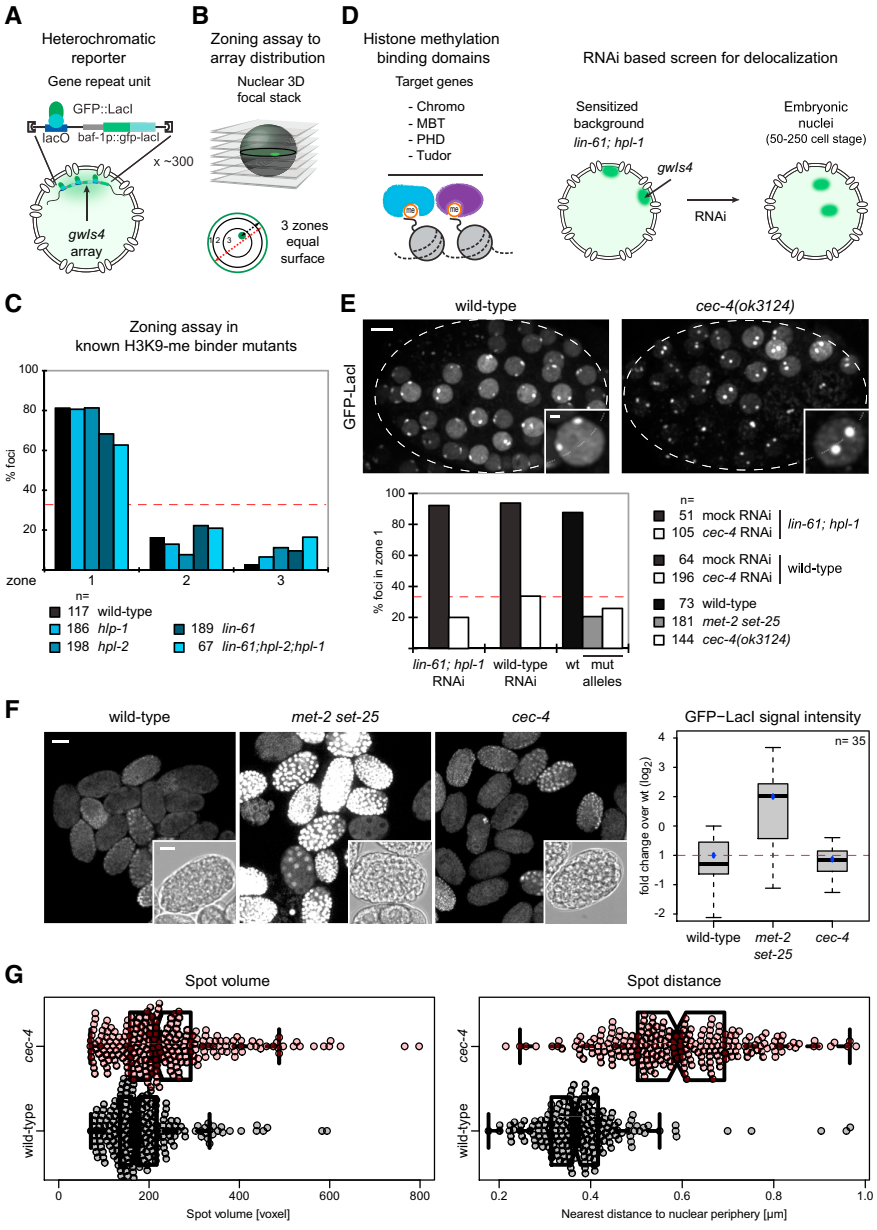

Figure 1. *cec-4* Is Required for Anchoring and Compaction of a Heterochromatic Array

(A) Heterochromatic transgene array *gwIs4 [baf-1p::GFP-lacI::let-858 3′UTR; myo-3p::RFP]* reporter.

(B) Zoning assay for array distribution. Radial position is determined relative to the INM, and values are binned into three concentric zones.

(legend continued on next page)

broadly distributed without enrichment on LADs (Barski et al., 2007).

Whereas mammalian lamins were reported to bind AT-rich DNA and histone dimers in vitro (reviewed in Wilson and Foisner, 2010), this affinity cannot account for selective heterochromatin binding. Nor is it explained by lamin A/C interaction with transcription factors or the barrier to autointegration factor (BAF), which may link specific promoters to lamins (Kubben et al., 2012; Meuleman et al., 2013). Similarly, the lamin associated Lap2β interacts with HDAC3 and the transcription factor cKrox, a ligand of GAGA motifs, leading to the repression and perinuclear anchoring of a subset of mammalian promoters (Zullo et al., 2012). Yet LADs extend far beyond promoters, coinciding instead with extensive domains of H3K9 methylation (Towbin et al., 2012).

Alternatively, nuclear lamins may act indirectly by providing a stable platform for the localization of other INM proteins (e.g., Lap2β, Emerin and Man1 [Brachner and Foisner, 2011]). Indeed, depletion of the *C. elegans* lamin, LMN-1, mislocalizes Emerin (EMR-1) and Man1 (LEM-2), and the worm Emerin in turn helps stabilize repressed muscle and neuronal genes at the INM in differentiated worm tissues (González-Aguilera et al., 2014). Yet neither Emerin nor Man1 bind heterochromatin directly. A similar indirect effect was ascribed to mammalian SAMP-1, an INM protein connected to LINC (linker of nucleo- and cytoskeleton) complex, whose loss compromises nuclear integrity and leads to Emerin, SUN-1, and Lamin A/C mislocalization (Gudise et al., 2011). Finally, loss of PRR14, a perinuclear HP1-binding protein, altered perinuclear attachment of H3K9-methylated domains in mammalian nuclei, yet led to general defects in nuclear structure, raising the question of indirect effect on DNA localization (Poleshko et al., 2013).

Here we exploit the power of RNAi screens in the nematode *C. elegans* to find a methyl-H3K9-specific perinuclear anchor for heterochromatin. We have individually downregulated genes that harbor characteristic histone methylation binding motifs and monitored changes in the perinuclear anchoring of heterochromatin in early embryos. We identified a previously uncharacterized *C. elegans* CD protein, CEC-4, as our only positive hit. CEC-4 localizes at the INM where it directly binds endogenous H3K9-methylated chromatin through its CD's aromatic cage. CEC-4 is not necessary for the transcriptional silencing of either endogenous genes or a heterochromatic reporter, although the methylation of H3K9 and its ligands HPL-2 and LIN-61 are. Despite this, a reproducible fraction of *cec-4* embryos were unable to maintain the muscle specification induced by a pulse of HLH-1 (MyoD) expression. We suggest that perinuclear sequestration of chromatin contributes to cell fate commitment under conditions of perturbed development.

RESULTS

CEC-4 Is a Chromodomain Factor that Anchors a Heterochromatic Array

To search for proteins involved in the anchoring of methylated H3K9 chromatin, we designed an RNAi screen with a fluorescent reporter for perinuclear heterochromatin positioning in *C. elegans* embryos. Our reporter is an integrated plasmid array, *gwIs4*, which expresses the GFP-LacI fusion protein under control of the ubiquitously active *baf-1* promoter. GFP-LacI binds a *lacO* site that occurs once per 3.5 kb (~300x), generating a fluorescent focus that binds the INM in embryonic nuclei (Figure 1A). The histones on the array are trimethylated on H3K9 and H3K27, but lack H3K4 methylation, and have reduced gene expression, thereby recapitulating conserved features of heterochromatin (Meister et al., 2010; Towbin et al., 2010). Array position is determined with a zoning assay in which radial distances from the spot to the nuclear periphery, scored in the focal plane in which the spot is the brightest, are binned into 3 zones of equal surface (Figure 1B). Deviation from 33% indicates nonrandom localization.

The *C. elegans* genome encodes 65 proteins that contain methyl-lysine/-arginine binding motifs, namely CD, MBT (malignant brain tumor), PHD (plant homeodomain) and Tudor domains (Table S1; reviewed in Taverna et al., 2007). This set of proteins includes HPL-1 and HPL-2, homologs of HP1, a highly conserved CD protein that binds methylated H3K9 to silence heterochromatin (Nestorov et al., 2013). HPL-1 co-localizes with the heterochromatic *gwIs4* array in worm embryos and appears to repress transcription in a promoter-specific manner working together with the H1 variant HIS-24 in larvae (Studencka et al., 2012a). HPL-2 binds H3K9me2/3 as well as H3K27me2/3 in vitro, and it is needed to repress large heterochromatic arrays in both embryos and germline cells, as well as to fine-tune other gene expression events (Couteau et al., 2002; Studencka et al., 2012b). A third H3K9me2/me3 ligand is the MBT-domain protein LIN-61, whose loss compromises vulva development, silencing of heterochromatic arrays, and a neuron-specific reporter in somatic cells (Koester-Eiserfunke and Fischle, 2011; Zheng et al., 2013). Remarkably, elimination of these known H3K9me ligands,

(C) Array distribution quantitation, as described in (B), in early embryos (50–250 cell stage) of indicated genotypes (Tables S1 and S3). Red line = random distribution of 33%.

(D) Design of candidate RNAi screen in *lin-61;hpl-1* deficient strain. L1 larvae subjected to RNAi for candidates listed in Table S3, and embryonic progeny screened for array delocalization.

(E) Z-projection of representative embryos bearing *gwIs4* in WT and *cec-4(ok3124)* strains. Insets: single nuclei. Scale bar, 5 or 2 μm, respectively. Array distribution, zone 1 data in early embryos as indicated, n = foci scored per condition. Pair-wise comparisons of mock RNAi and WT conditions with *cec-4* RNAi or mutant yielded p values < 0.001 by χ^2 test.

(F) Z-projection of GFP fluorescence in embryos of indicated genotype with *gwIs4*. Insets: bright field. Scale bar, 20 or 10 μm, respectively. Quantified signal intensity displayed as box plot in $\log_2$ scale, whiskers = 1st and 3rd quartiles. Black lines: median, blue dots: mean, red dashed line: baseline = mean of WT. n = embryos scored.

(G) 3D spot volume and distance from INM in WT and *cec-4(ok3124)* embryos. Notched box plots overlapping individual measurements as above. n = 209 and 237, respectively, from five embryos each; pair-wise comparisons with p-values < 0.001 by Student's t test.

See also Figure S1.

singly or in combination, had little impact on the perinuclear sequestration of the *gwIs4* heterochromatic array, although the mutants did lose transcriptional repression (Figure 1C; Towbin et al., 2012).

Conscious that anchor redundancy might be a concern, we downregulated other methyl-binding candidates by RNAi in *hpl-1;lin-61* double mutant embryos. Only one RNAi target, *cec-4,* which encodes an uncharacterized CD protein, affected the perinuclear anchoring of the heterochromatic reporter (Figures 1D and 1E). The percentage of heterochromatic foci in the outermost nuclear zone dropped from 92% to 20%, following *cec-4* RNAi (Figures 1E and S1B). Although *cec-3/eap-1* has been described as an H3K9me1-3 binder involved in neuron-specific gene expression (Greer et al., 2014; Zheng et al., 2013), *cec-3* RNAi had no impact on heterochromatin anchoring in our screen (data not shown).

The effect of *cec-4* RNAi on array position did not depend on the absence of LIN-61 or HPL-1, for the same RNAi in WT worms yielded identical array delocalization (Figures 1E and S1B). To rule out off-target effects of *cec-4* RNAi, we scored array position in embryos carrying the null mutant *cec-4(ok3124),* which lacks the 5′ UTR and first 2 exons (Figure S1A). The genetic ablation of *cec-4* phenocopied *cec-4* RNAi, yielding full array detachment from the INM, identical to that scored in embryos that lack H3K9 methylation; i.e., the *met-2 set-25* double mutant (Towbin et al., 2012). Thus, the CD-encoding *cec-4* gene is required, like H3K9-methylation, for the perinuclear anchoring of heterochromatic arrays in *C. elegans* early embryos.

We examined the effect of *cec-4* ablation on gene expression by quantifying the fluorescent intensity of GFP-LacI, which is expressed from a housekeeping promoter on the *gwIs4* array. Although the expression levels are strongly upregulated in *met-2 set-25* mutant, deletion of *cec-4* did not alter GFP-LacI expression in embryos (Figure 1F). Both H3K9me3 and the enzyme mediating this terminal modification, SET-25, remained enriched on the delocalized array in *cec-4* mutant embryos (Figures S1C and S1D), consistent with the observed transcriptional repression. We conclude that CEC-4-mediated anchoring is not essential for heterochromatic array repression. Nonetheless, coupled with the loss of anchoring we scored a significant decompaction of the reporter, upon release from the INM. Monitored by a quantitative 3D volume rendering protocol, we found that the mean volume expanded from about 192 to 239 voxels upon *cec-4* deletion (Figure 1G).

CEC-4 Localizes Intrinsically to the Nuclear Periphery

We next examined the subcellular localization of CEC-4. A mCherry-tagged version of *cec-4* was integrated as a site-specific, single-copy genomic insertion under control of its endogenous *cec-4* promoter and 3′UTR (Figure S2A). Confocal fluorescence microscopy of CEC-4-mCherry (CEC-4-mCh) showed that the protein forms a ring at the nuclear periphery at all embryonic stages (Figure 2A). This distribution persisted in larval and adult differentiated tissues and in the germline of adult worms (Figure 2D; data not shown). CEC-4 localization was independent of H3K9 methylation; the same perinuclear CEC-4-mCh ring was found in the *met-2 set-25* mutant, in which H3K9 is unmethylated and heterochromatin was delocalized and expressed (Figure 2C). Only in mitosis did CEC-4-mCh become dispersed (data not shown), much like lamins, which undergo phosphorylation by cyclinB/Cdk in mitosis (Nigg, 1992).

Quantification of fluorescence intensity of CEC-4-mCh in L1 larval stage showed protein level variation in a tissue-specific fashion. CEC-4 is weakly expressed in intestine, highly expressed in muscle, and is found at intermediate levels in almost every other tissue (Figure 2D). This unequal tissue-specific expression was not observed for an EMR-1 fusion construct designed and integrated in a similar manner (EMR-1-mCherry; Figures 2D and S2A).

To characterize CEC-4's nuclear rim pattern further, we imaged embryos at 100 nm resolution using super-resolution structured illumination microscopy (SR-SIM). The CEC-4-mCh ring resolved into a perinuclear, punctate pattern (Figure 2B), and counterlabeling of nuclear pores or LMN-1 (lamin) showed CEC-4 in the same concentric plane as lamin and is situated mostly between pores (Figure 2B). Lamin and CEC-4-mCh were in very close proximity, yet could be resolved as distinct foci (low yellow signal in red/green channel merge; Figure 2B), suggesting that CEC-4 might localize to the INM independently of lamin. Indeed, after treating these worms with *lmn-1* RNAi, CEC-4 perinuclear ring persisted (data not shown). The same was true after RNAi against Emerin, LEM-2, SUN-1, UNC-84, BAF-1, and all other known *C. elegans* INM components (Table S6).

We reasoned that if CEC-4 localizes independently of lamin, it might also associate with the nuclear envelope of budding yeast, which lacks lamin entirely (reviewed in Taddei and Gasser, 2012). Indeed, when expressed as a GFP fusion protein under control of the *GAL1* promoter, CEC-4-GFP formed a perinuclear ring at INM of yeast nuclei (Figure S2B). To map the domain that directs CEC-4 to the INM, we expressed complementary N- and C-terminal fragments of CEC-4, fused to GFP. Both yielded a diffuse nuclear distribution (Figure S2C), suggesting that the integrity of the holoprotein is necessary for INM enrichment (Figure S2C). Similar results were obtained with similar constructs expressed ectopically in *C. elegans* (data not shown). Finally, in yeast as in worms, ablation of known INM and pore basket proteins (Table S7) did not alter CEC-4-GFP localization. We therefore propose that either CEC-4 has an intrinsic affinity for the INM, or else it binds a conserved but uncharacterized membrane component.

CEC-4 Chromodomain Preferentially Binds Methylated H3K9

Based on sequence analysis, the CEC-4 CD (aa 82–141) shares 42% identity with mammalian HP1α CD and 33% with HPL-1/2 CDs, yet CEC-4 lacks the HP1-specific chromoshadow and RNA-binding hinge domains (Couteau et al., 2002). Protein comparison failed to reveal a strict homolog of CEC-4 in mammalian genomes, apart from the CD and a second conserved motif, here called PD (putative domain, aa 25–76), which is found in other CD-containing proteins (Figure 3A).

The CEC-4 CD has a canonical secondary structure like mammalian HP1 and Pc3 (Fischle et al., 2003b), with an aromatic cage containing two tyrosine residues that are predicted to recognize methylated lysine within the H3 ARK(S/T) motif. To characterize the specificity of CEC-4 CD binding, we expressed

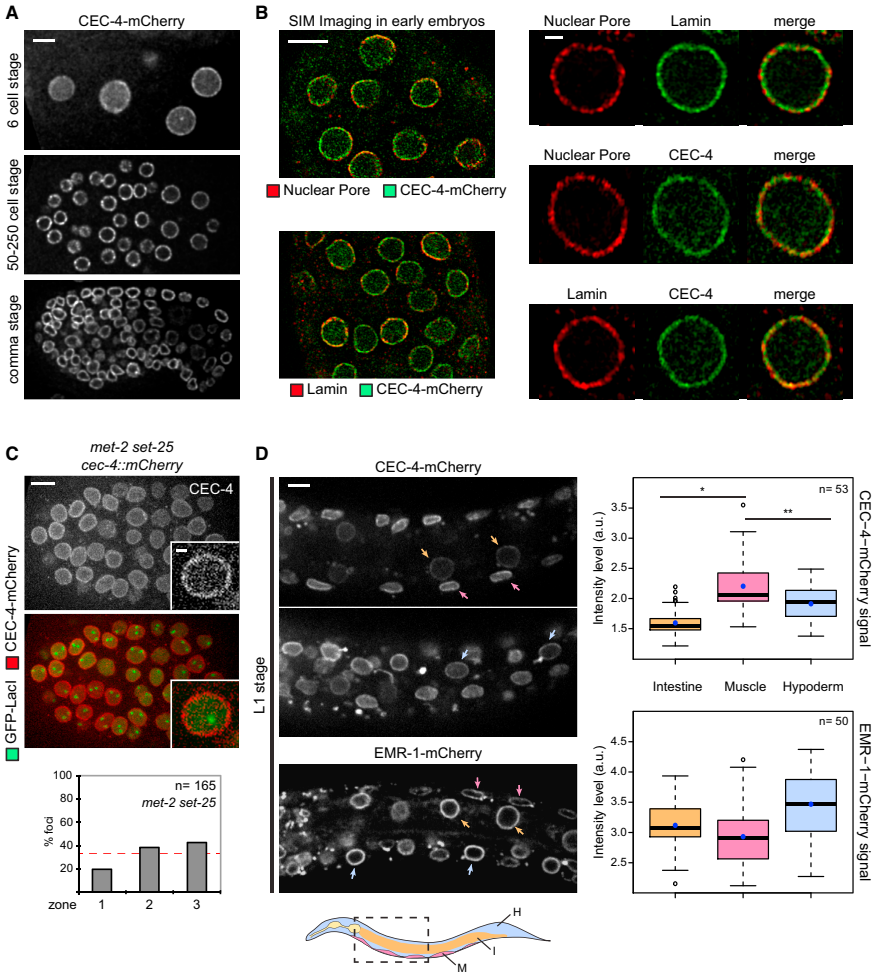

Figure 2. Perinuclear CEC-4 Localization Is Independent of H3K9 Methylation, and Varies from Tissue to Tissue

(A) Single plane images of indicated embryo stages expressing CEC-4-mCh.

(B) SR-SIM microscopy of CEC-4-mCh transgenic embryos, counterstained for nuclear pores, lamin or mCherry. Embryo sections and single nuclear planes shown.

(C) Z-projection of CEC-4-mCh in *met-2 set-25* mutant background; images of mCherry alone and merged with *gwIs4* GFP-LacI signal are shown. Insets: single plain nuclei. Quantification of array distribution, n = foci scored.

(D) Single plane confocal images of CEC-4- and EMR-1-mCh transgenic L1 larvae; scheme of L1 worm color-coded by tissue, M: muscle, I: intestine, H: hypoderm. Measured mCh signal intensity displayed as box plots in a.u. as in Figure 1. Black circles = outliers, n = number of nuclei per tissue; pair-wise comparisons for * and **p value < 0.001 in Wilcoxon test. Scale bar, 5 μm in whole/section embryos and larvae; 2μm in single nuclei/insets.

See also Figure S2.

and purified the WT CD-containing fragment of CEC-4 (CEC-4 CD; aa 25–141) and a mutated version of the same fragment (Y87A and Y111A; CEC-4 cd-2YA; Figures 3A and S3A), bearing point mutations that should disrupt the aromatic cage. Using magnetic beads coated with unmethylated (me0) or tri-methylated (me3) H3K9 peptide (aa 1–20+Cys), we found that the WT CEC-4 CD bound a H3K9me3 peptide specifically, while the CEC-4 cd-2YA mutant fragment did not (Figure 3B).

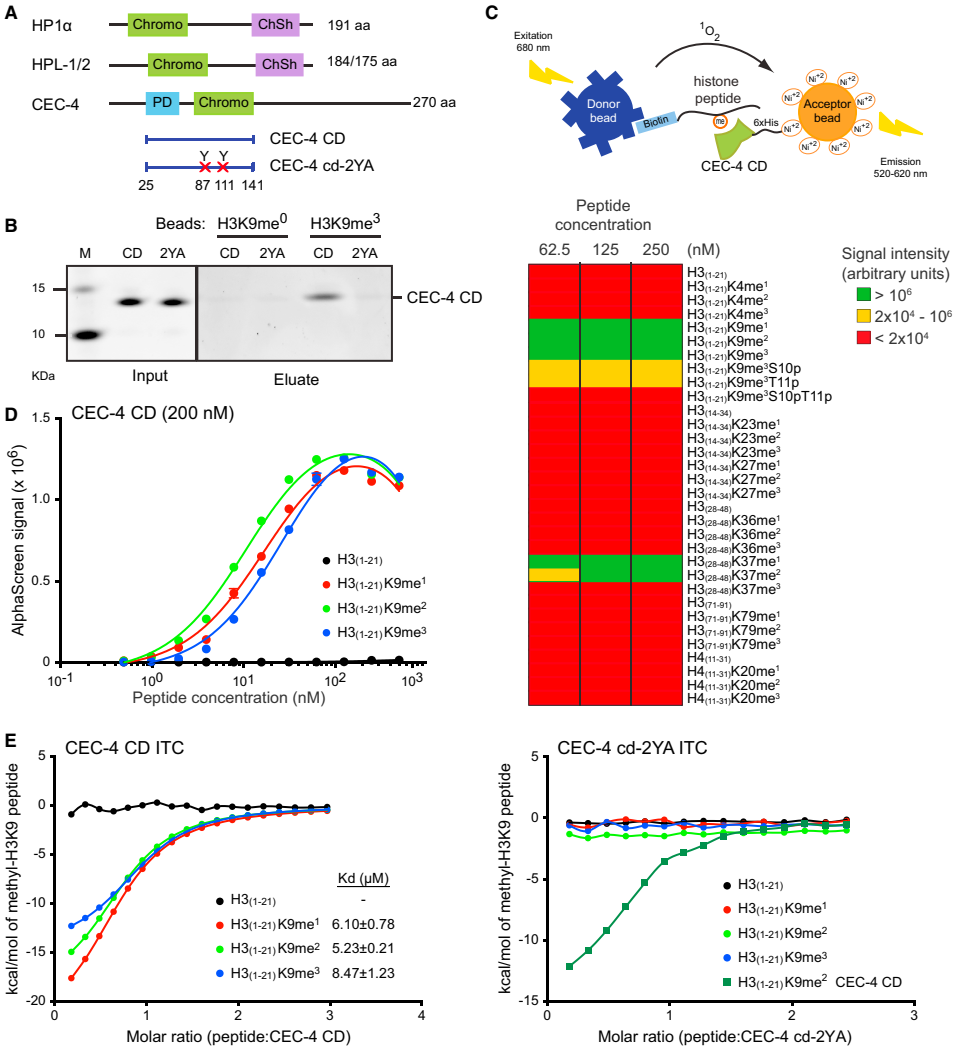

Figure 3. CEC-4 CD Binds Methylated H3K9 Peptides

(A) Schematic comparison of *H. sapiens* HP1α, *C. elegans* HPL-1/2 and CEC-4. CD (green), purple: chromoshadow (ChSh) domain, blue: conserved PD. Purified CEC-4 CD fragments in blue; red X = Y87A and Y111A mutations.

(B) Pull-down of recombinant His-tagged CEC-4 CD fragments (A) by unmodified or me3-H3K9 resin-immobilized peptides. Protein visualized by SYPRO Ruby staining.

(C) AlphaScreen scheme: donor and acceptor microbeads coated with 188 different biotinylated peptides and His-tagged CEC-4 CD, respectively. Interaction produces a fluorescent signal through singlet oxygen ($^1O_2$) transfer from donor to Ni^{+2} ions on acceptor beads. Three peptide concentrations tested with equal amounts of CEC-4 CD (200 nM). Color-coded results reflect signal intensity (see Table S4 for rest of library).

(D) Dose-response binding curves for indicated H3K9 peptides with CEC-4 CD in AlphaScreen assay.

(E) Quantitation of binding affinities of H3K9 peptides to CEC-4 CD and cd-2YA mutant determined by ITC. In (D) and (E) solid lines represent a nonlinear least-square fit using one-sided fitting equation.

See also Figures S3 and S4.

We evaluated CEC-4 CD specificity by scoring interaction with a range of modified and unmodified histone tail peptides in a quantitative chemiluminiscence assay (Alpha Screen; Taouji et al., 2009). We screened the ALTA Biosciences library, which contains 188 histone tail ligands each with a different epigenetic modification (Table S4; Figure 3C). Consistent with the pull-down assay, strong interaction signals were detected almost exclusively between CEC-4 CD and a peptide of histone H3 bearing me1-, me2-, or me3-K9. Intriguingly, CEC-4 affinity for H3K9me3-containing peptides was compromised by additionally phosphorylating S10 and/or T11 (Figure 3C and Table S4). Such modifications have been proposed to release HP1 from chromatin in mitosis (Fischle et al., 2003a).

The interaction of CEC-4 CD with methylated H3K9 was confirmed by serial dilutions of each peptide in the AlphaScreen (Figure 3D) and IC_{50} (half maximal inhibitory concentration) was determined by peptide displacement. CEC-4 CD bound to me1-, me-2, or me3-K9 H3 peptides with similar affinities (Figure S3C). We then measured binding energies using Isothermal Titration Calorimetry (ITC). Dissociation constants (Kd) for CEC-4 CD bound to the methylated H3K9 peptides ranged from 5 to 9 μM. There was a slight preference for me2 and no detectable binding to the unmodified H3 peptide (Figures 3E, S3D, and S4A). Similar Kd values have been reported for human, mouse, and *Drosophila* HP1 homologs (reviewed in Steffen et al., 2012). The interaction requires the characteristic aromatic cage of the CEC-4 CD, as CEC-4 cd-2YA gave only background level interaction (Figures 3E and S4A). We conclude that CEC-4 CD recognizes H3K9me1, me2, and me3. Its affinity for all three methyl-H3K9 forms is consistent with the fact that heterochromatic arrays remain peripherally sequestered in the *set-25* mutant, which has H3K9me1/me2, but no H3K9me3 (Towbin et al., 2012).

In addition to its strong affinity to H3K9me-peptides, we detected interaction of the CEC-4 CD with me1- or me-2 H3K37 (aa 28–48; Figures 3C and S3B; Table S4). Methylation of H3K37 has not been reported to occur in native *C. elegans* chromatin and was not detected in our own mass spectrometry of embryonic histones (data not shown; Towbin et al., 2012). To date, the only documented occurrence of H3K37me1 is in tandem with H3K36me1 at origins of replication in budding yeast, outside of S phase (Unnikrishnan et al., 2010). However, CEC-4 did not recognize H3K36me. In addition, CEC-4 CD had significantly lower affinity for H3K37me than for methylated H3K9 (Figures S3D, S3E, and S4B). Thus, the physiological relevance of this second binding site is unclear.

The CEC-4 CD Is Essential for Heterochromatin Anchoring in Embryos, but Is Redundant in Differentiated Tissues

The single-copy CEC-4-mCh fully restores array anchoring in the *cec-4* null mutant. It is enriched on the anchored heterochromatic reporter due to its affinity for H3K9me (Figures 4A and S2C). An identical integration construct bearing the aromatic cage mutations described above (CEC-4cd-2YA-mCh) did not complement for anchoring, nor did it bind to the array (Figure 4B). Thus, disruption of the CEC-4 CD aromatic cage is sufficient to disrupt the anchoring of heterochromatin at the INM in embryos and the binding of methylated H3K9 peptides in vitro. On the other hand, CD integrity is not involved in CEC-4 localization, given that CEC-4cd-2YA-mCh forms a perinuclear ring like WT CEC-4-mCh (Figure 4B).

In contrast to the situation in embryos, the ablation of *cec-4* did not provoke relocalization of the heterochromatic array in differentiated L1 larval tissues, such as intestine and hypoderm (Figure 4C). The same was observed in the *met-2 set-25* double mutant (Towbin et al., 2012). It appears, therefore, that compensatory or redundant mechanisms for anchoring heterochromatin are induced in the differentiated tissues of the L1 larva. It is unclear whether these mechanisms are fully independent of CEC-4 or if CEC-4 contributes to tissue-specific anchoring in a redundant manner (Figure 2D). Both the redundancy and tissue-specificity aspects are reminiscent of lamin A/C and LBR effects in mice (Solovei et al., 2013).

Loss of CEC-4 Alters the Spatial Distribution of Endogenous Chromosome Arms

Thus far integrated transgenic arrays were used as a surrogate for heterochromatin. To see if CEC-4 affects the distribution of endogenous chromatin, we performed LEM-2 chromatin immunoprecipitation coupled to deep sequencing (ChIP-seq) in WT and mutant embryos. *C. elegans* chromosomes are holocentric and lack pericentric satellite heterochromatin but are enriched for H3K9 methylation and repetitive elements along the distal arms of all autosomes and the left arm of chromosome X(Gerstein et al., 2010; Ikegami et al., 2010). Previous ChIP and lamin-Dam-ID studies had shown that chromosome arms are proximal to the INM in *C. elegans* embryos, larvae, and adults. Moreover, the loss of H3K9 methylation (*met-2 set-25*) was enough to compromise INM-anchoring of the repeat-rich autosomal arms (González-Aguilera et al., 2014; Ikegami et al., 2010; Towbin et al., 2012).

We used ChIP-seq to map LEM-2-binding along endogenous sequences in WT, *cec-4*, and *met-2 set-25* embryos. Euclidian distances were measured showing high similarity between replicas. Hierarchical clustering resolved WT LEM-2 ChIP as different from either mutant, while the *met-2 set-25* and *cec-4* mutants clustered together (Figure S5A). All input samples were very similar. Plotting the LEM-2 signals along the chromosomal sequences showed that distal arms lost anchoring in *cec-4* null embryos to the same degree as in the H3K9me-deficient *met-2 set-25* mutant (Figures 5A and S5B).

As expected, LEM-2 binding along wild-type autosomes was polarized: chromosome arms were enriched at the INM and centers were depleted. This polarization was reduced for each autosome similarly in both mutants. The integrated LEM-2 signal on each chromosomal extremity was plotted against the signal integrated over each center, to visualize the effects of the mutations (Figure 5B). We conclude that the INM binding of the endogenous repeat-rich domains on chromosome arms requires H3K9 methylation and its recognition by CEC-4. Nonetheless, other positioning pathways likely exist, since chromosome extremities were displaced to different degrees.

In many organisms heterochromatin is also clustered around the nucleolus, the site of rDNA transcription by RNA Pol I (Padeken and Heun, 2014). The *C. elegans* rDNA is found on the

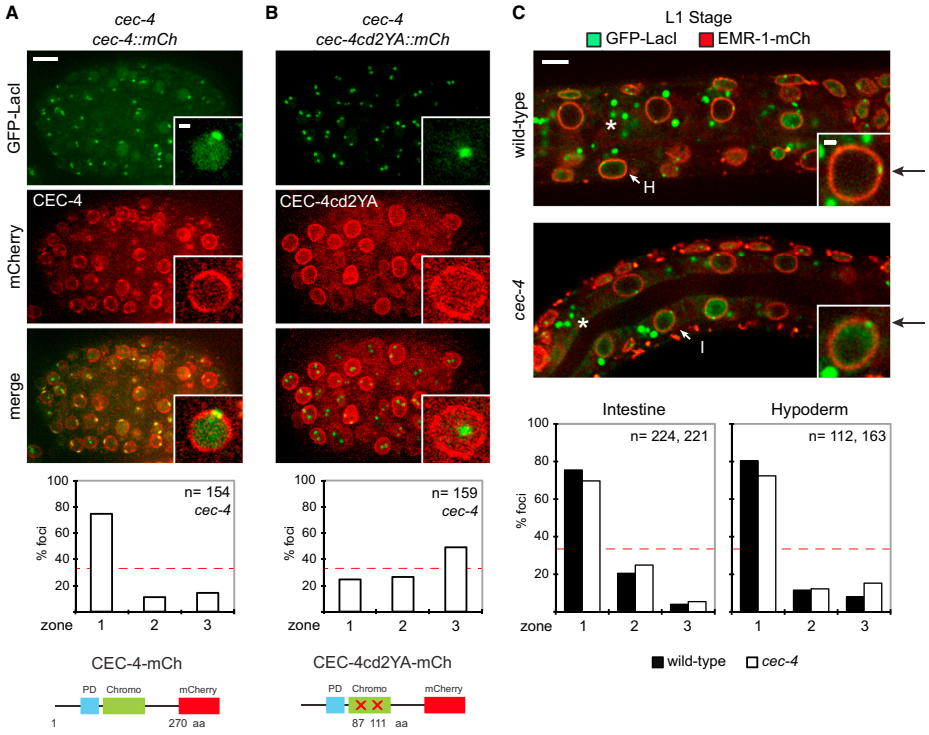

Figure 4. CEC-4 CD-H3K9me Recognition Required for Heterochromatic Array Anchoring in Embryos, while Larvae Have Compensatory Pathway(s)

(A) Z-projections showing co-localization of *gwIs4* GFP-LacI signal with CEC-4-mCh in *cec-4* null embryos. Insets: single nucleus. Zoning assay for array distribution, n = foci scored. Schematic view of transgenic protein expressed.

(B) Same as (A), except that CEC-4 transgene contains CD mutations (CEC-4cd2YA-mCh). Pair-wise comparison of (A) and (B) graphs with p value < 0.001, χ^2 test.

(C) Single plane images of L1 stage worms containing *gwIs4* and EMR-1-mCh in indicated genotypes. White arrows indicate hypoderm (H) or intestine (I) cells; * marks granule intestine foci. Insets: intestine nuclei, black arrows = array foci. Zoning assay on indicated tissues, n = foci scored per condition. Scale bars, 5 μm in embryos/L1 sections and 2 μm in single nuclei.

See also Figure S2.

distal arms of ChrI and ChrV in heterochromatic regions (Figure 5A). We therefore checked whether nucleoli change their radial position in the *cec-4* mutant by staining for a conserved marker of the nucleolus, fibrillarin (Figure 5A). In embryos lacking CEC-4, nucleoli shifted quantitatively away from the perinuclear lamin (Figure 5C), confirming that CEC-4 contributes profoundly to the positioning of endogenous chromatin in embryos.

Monitoring Gene Expression in the Absence of CEC-4

It has long been debated whether nuclear localization is sufficient to influence gene expression. To test this we generated gene expression profiles (RNA-seq) of WT, *met-2 set-25*, and *cec-4* mutant embryos. Pairwise comparison of two independent biological replicas of mutant and WT samples showed a reproducible upregulation (>4-fold) of a large number of genes in embryos lacking H3K9 methylation (*met-2 set-25)*, whereas the loss of CEC-4 led to robust upregulation of a single gene, *srw-85* (Figure 5D). The modest effect of *cec-4* mutation on gene expression is consistent with our results from the array-borne GFP-LacI (Figure 1F). In the case of endogenous genes in early embryos, the lack of derepression might simply reflect the absence of transcription factors needed for tissue-specific gene expression. However, given that the loss of H3K9 methylation does upregulate many genes in embryos, it is more likely that H3K9me-ligands other than CEC-4 mediate gene repression. Analysis of datasets in 500 bp windows across the whole genome, for potential changes in non-genic regions, yielded similar results to the gene-centric analysis; only genomic

windows spanning the *srw-85* locus were reproducibly upregulated in *cec-4(ok3124)* (Figure S5C).

The dramatic induction of *srw-85* (> 16-fold) upon displacement from the INM is a notable exception (Figures 5A and 5D–5F). Its derepression correlates strongly with subnuclear position, and not with H3K9 methylation state, as it was not derepressed in *met-2* or *set-25* single mutant embryos, which retain anchoring (Towbin et al., 2012). SRW-85 is a member of the *C. elegans* chemoreceptor family of seven transmembrane G protein-coupled receptors (7TM-GPCR). The gene sits on ChrV-right, along with 90% of the 145 *srw* family members, and is normally expressed in non-ASE type (gustatory) neurons (Etchberger et al., 2007). Given that surrounding genes are not equally upregulated (Figure S5D), we conclude that *srw-85* is an exception rather than the rule. CEC-4, unlike other H3K9 methylation readers, serves primarily to position chromatin, although the H3K9me2/me3 modification it recognizes also mediates transcriptional silencing.

Perinuclear Anchoring Helps Stabilize an Ectopically Induced Cell Differentiation Program

We examined *cec-4* mutant worms for developmental defects. Surprisingly, we found no drop in brood size nor embryonic lethality (either at 20°C or 26°C). We scored no reproducible differences in the developmental timing of embryonic stages, and except for a slight increase in the proportion of male progeny, proliferation appeared normal under standard laboratory conditions (data not shown). Given that alternative anchoring pathways are induced in L1 larvae, we sought to test the role of CEC-4-mediated chromatin tethering specifically in embryos.

To this end, we used an assay that induces muscle cell specification in embryos in response to a cell-type independent burst of HLH-1 (MyoD) expression, a master regulator for muscle differentiation (Fukushige and Krause, 2005). Induction of HLH-1 is driven by the *hsp-16.2* heat-shock (HS) promoter on a transgene array (*HS::hlh-1*) and is achieved by placing embryos at 34°C for 10 min; about 24 hr after, efficiency of induction can be monitored by morphology and muscle-specific gene expression (Figure 6A). To test whether *cec-4* mutant alters the efficiency of muscle induction, we introduced the *HS::hlh-1* transgene and the *gwIs4* array into WT and *cec-4* mutant, using the latter as a fluorescent reporter for muscle-specific gene expression (*myo-3p::RFP*). At 40 min after HS, *hlh-1* mRNA was expressed at comparable levels in both genotypes, as was the downstream muscle specific myosin, *myo*-3, at 24 hr after HS (Figure 6B).

We induced HLH-1 expression at different time points during synchronized embryonic growth and monitored the outcome by microscopy. A striking difference between WT and mutant embryos was noted when we exposed the bean stage (~560 cells; 300 min growth at 22.5°C) to the HLH-1 pulse (Figure 6C–6F). Whereas 100% of the wild-type embryos turned into lumps of muscle-like cells with muscle-twitching behavior, among the heat-shocked *cec-4* null embryos a reproducible 25% continued to develop, reaching the point of hatching from the eggshell despite their documented HLH-1 expression (Figure 6C and 6D). These hatched larva-like organisms were clearly abnormal, as they were disrupted by the slightest manipulation and failed to survive. Nonetheless, they had progressed well beyond embryonic stages and did not manifest the muscle morphology of their WT counterparts (Figure 6C and 6E). To rule out a general temperature sensitivity of *cec-4* deletion, we exposed the mutant embryos lacking the *HS::hlh-1* to HS, yet observed no effect on development: all embryos yielded normal larvae (Figure 6C).

After HLH-1 induction, the fluorescent reporter *myo-3p::RFP* was detected in patches of cells in both genotypes, with an overall higher intensity in WT cells (Figures 6E and S6A). The subset of *cec-4* mutant embryos that became muscle, like the WT embryos, showed twitching behavior. In contrast, the *cec-4* null hatched larva-like worms had a dispersed *myo-3p::RFP* expression pattern throughout the organism, which was distinct from the usual *myo-3* expression pattern in L1 larvae body wall muscle (Figure 6E). We could complement the *cec-4* deletion by introducing the tagged CEC-4-mCh; indeed, this restored the normal WT response to HLH-1 induction, and 100% of the embryos became muscle cells. In contrast, complementing with CEC-4cd2YA-mCh yielded results reminiscent of the *cec-4* null, albeit less penetrant (Figure S6B).

The inefficiency of the *cec-4* mutant for muscle tissue conversion in response to MyoD, appears to reflect an inability to lock in the muscle specification program and repress other differentiation programs. In other words, despite high level expression of HLH-1, the *cec-4* mutant appeared to remain more permissive to other differentiation signals and therefore continued to develop other tissues while expressing muscle-specific genes. We confirmed this by tracking an intestine cell marker that is not expressed in either genotype at the bean stage when we perform HS. The reporter (kind gift of G.-J. Hendriks and H. Grosshans, personal communication) expresses a GFP-tagged nuclear pore protein from an L1-stage gut-specific promoter (*nhx-2*). At 18 hr after HS, we find that the fluorescent gut marker (*nhx-2p::npp-9::GFP*) was detected in 94.5% of *cec-4* mutant embryos, but significantly less in WT (39.6%; Figure 6F).

Given the fragility of the hatched larvae-like structures, neither immunostaining nor manual isolation for RNA-seq was possible. However, their morphology alone allows one to conclude that a significant fraction of the *cec-4* mutant embryos failed to restrict gene expression to the muscle program. Thus, the perinuclear sequestration of silent genes by CEC-4 in embryonic stages appears to help stabilize the HLH-1-induced muscle cell fate.

DISCUSSION

Perinuclear Chromatin Sequestration through Histone H3K9 Methylation

Heterochromatin, or transcriptionally silenced chromatin, is often juxtaposed to the INM in eukaryotic organisms. Previous work has identified H3K9 methylation as essential for heterochromatin anchoring in worms (Towbin et al., 2012) and important in mammalian cells (Kind et al., 2013; Pinheiro et al., 2012). However, no INM anchor that selectively binds this epigenetic mark was known. Here we describe CEC-4 as a perinuclear *C. elegans* protein which is necessary for the tethering of endogenous chromatin bearing me1-, me2-, or me3-H3K9 histones. Its CD's aromatic cage is necessary for H3K9me binding in vitro and

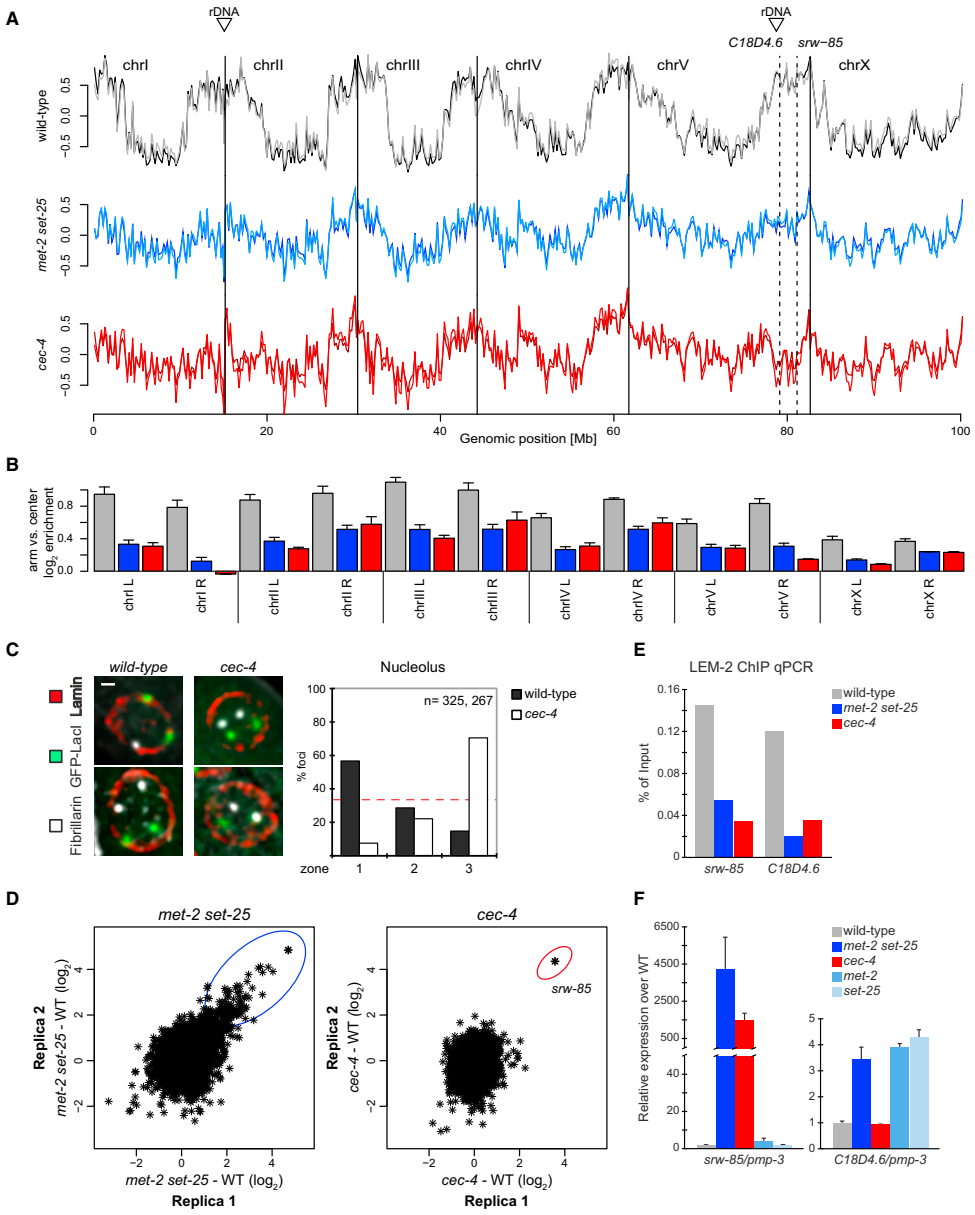

Figure 5. CEC-4 Influences Anchoring of Endogenous Chromatin and Nucleoli, but Not Silencing

(A) LEM-2 ChIP-seq profiles over chromosomes are shown for two independent replicas of early embryos of WT (gray/dark gray), *met-2 set-25* (blue/light blue), and *cec-4* (red/light red) mutants. Dashed line shows *srw-85* and *C18D4.6* genes, and triangles show rDNA clusters.

(legend continued on next page)

in vivo. Ablation of CEC-4 delocalizes heterochromatin, but does not necessarily lead to its derepression, whereas loss of histone H3K9 methylation compromises both. Other H3K9me-ligands (HP1 homologs HPL-1 and HPL-2, or LIN-61) contribute to transcriptional repression by binding H3K9me2 or me3, but do not mediate perinuclear anchoring. This bifurcation in function of a single methylated lysine in a histone tail, through divergent sets of methyl-lysine readers, provides a paradigm for how epigenetic states can coordinate distinct activities. In this case, chromatin can be anchored without silencing and silenced without anchoring, even though the two functions are correlated through H3K9 methylation. H3K9me1/me2 is sufficient for tethering through CEC-4, while H3K9me3 is needed for gene repression mediated by other H3K9me-readers (Figure 7). It remains to be seen if CEC-4 and other H3K9me readers interact.

CEC-4 Contributes to the Robustness of Ectopically Induced Differentiation

This finding gave us the opportunity to examine what happens during development when heterochromatin anchorage is compromised, without loss of H3K9 methylation or the transcriptional repression it mediates. Although *cec-4* mutant embryos yielded normal adult worms when development proceeded unperturbed, we were able to demonstrate a function for heterochromatin anchoring in early development by inducing muscle differentiation with ectopic expression of MyoD (HLH-1). Unlike the WT strain, a significant fraction of *cec-4* deficient embryos (about 25%) did not maintain the muscle fate provoked by HLH-1 induction (Figure 6) and continued to develop. In contrast, the induction of muscle cell fate and repression of alternative programs of differentiation occurred in 100% of the WT bean-staged embryos. The failure of the mutant to sustain an HLH-1-induced muscle program could either mean that CEC-4 actively supports muscle-specific gene expression, or else that it helps repress other tissue-specific programs. Given that muscle markers were expressed in heat-shocked *cec*-4 mutant embryos and that muscles develop normally in the mutant without HS, we favor the latter hypothesis: upon loss of CEC-4-mediated heterochromatin sequestration, non-muscle programs may not be properly repressed during ectopic muscle induction. This is consistent with earlier studies that showed a clear spatial segregation of active and inactive tissue-specific genes in differentiated cells of *C. elegans* larvae (Meister et al., 2010).

Because *cec-4* ablation per se seems to have a very limited effect on normal transcription patterns, we propose that CEC-4-mediated tethering does not control gene repression directly, but instead influences events that prepare genes for tissue-restricted patterns. These events might be the remodeling of epigenetic states (e.g., through histone deacetylases that bind the nuclear envelope [Zullo et al., 2012]), the sequestration of promoters away from their regulators, or the timing of replication of tissue-specific genes (Hiratani et al., 2008). These changes may not directly repress transcription, but rather change the compaction state of chromatin as a prerequisite for stage-specific repression. Indeed, the INM-released arrays in *cec-4* mutants are less compact (Figure 1), although we did not detect less histone H3K9 methylation by genome-wide ChIP (data not shown).

ESC differentiation studies have shown that the timing of replication of genes, and their reassembly into chromatin following replication, are compromised by spatial misorganization (reviewed in Hiratani et al., 2009). Moreover, it has been suggested that altered replication timing precedes commitment to differentiation-related expression patterns (Hiratani et al., 2008). Thus, we propose that CEC-4-mediated chromatin positioning and compaction may contribute to a replication timing program, which in turn reinforces appropriate gene repression. We expect that the compromised commitment of *cec-4* mutant is not restricted to muscle differentiation, but rather is a general mechanism that becomes important when normal development is perturbed. Whereas the ectopic HLH-1 induction is definitely a strong perturbation, less dramatic perturbations during development may rely on spatial sequestration to ensure proper patterns of tissue-specific gene expression.

Extending Nuclear Anchoring Mechanisms to Other Organisms

Although CEC-4 is the first CD protein reported to form a ring at the nuclear perimeter autonomously, CEC-4's anchoring function becomes either redundant or replaced by other mechanisms in L1 larvae, the stage at which most cells reached terminal differentiation. We note that heterochromatin can be anchored in differentiated tissues without H3K9 methylation, and without HPL-1, HPL-2, or LIN-61 (Studencka et al., 2012b; Towbin et al., 2012). Another CD protein, CEC-3, had no impact on embryonic array distribution in our screen, although it appears to restrain the expression of a neuronal specific transcription factor in larvae (Greer et al., 2014; Zheng et al., 2013). Thus, four H3K9me binders—HPL-1, HPL-2, LIN-61 and CEC-3—contribute to transcriptional silencing during development, while CEC-4 specifically sequesters H3K9me-containing chromatin in embryos. CEC-4 may also contribute to heterochromatin anchoring in some differentiated worm tissues, albeit in a redundant manner (data not shown).

(B) LEM-2 ChIP enrichment of arms (left or right) compared with corresponding center plotted for each genotype. Error bars = SEM.
(C) Representative merged color, single plane nuclei are shown for WT and *cec-4* mutant stained for anti-fibrillarin, lamin, and *gwIs4* array (anti-GFP), Scale bar, 2 μm. Zoning assay of nucleolar foci in 50–250 cell stage embryos, n = foci scored; pair-wise comparison p value < 0.001, χ^2 test.
(D) Relative gene expression profiles as scatter plots of *met-2 set-25* and cec-*4* mutants versus WT early embryo extracts. Genes significantly changed are circled, bold star = *srw-85*.
(E) LEM-2 ChIP qPCR for *srw-85* and *C18D4.6* genes. ChIP values as a percentage of respective input DNA.
(F) Gene expression levels of indicated genotypes by qRT-PCR, normalized to *pmp-3* gene and shown relative to WT expression. Error bars = SEM of 3 biological replicas.
See also Figure S5.

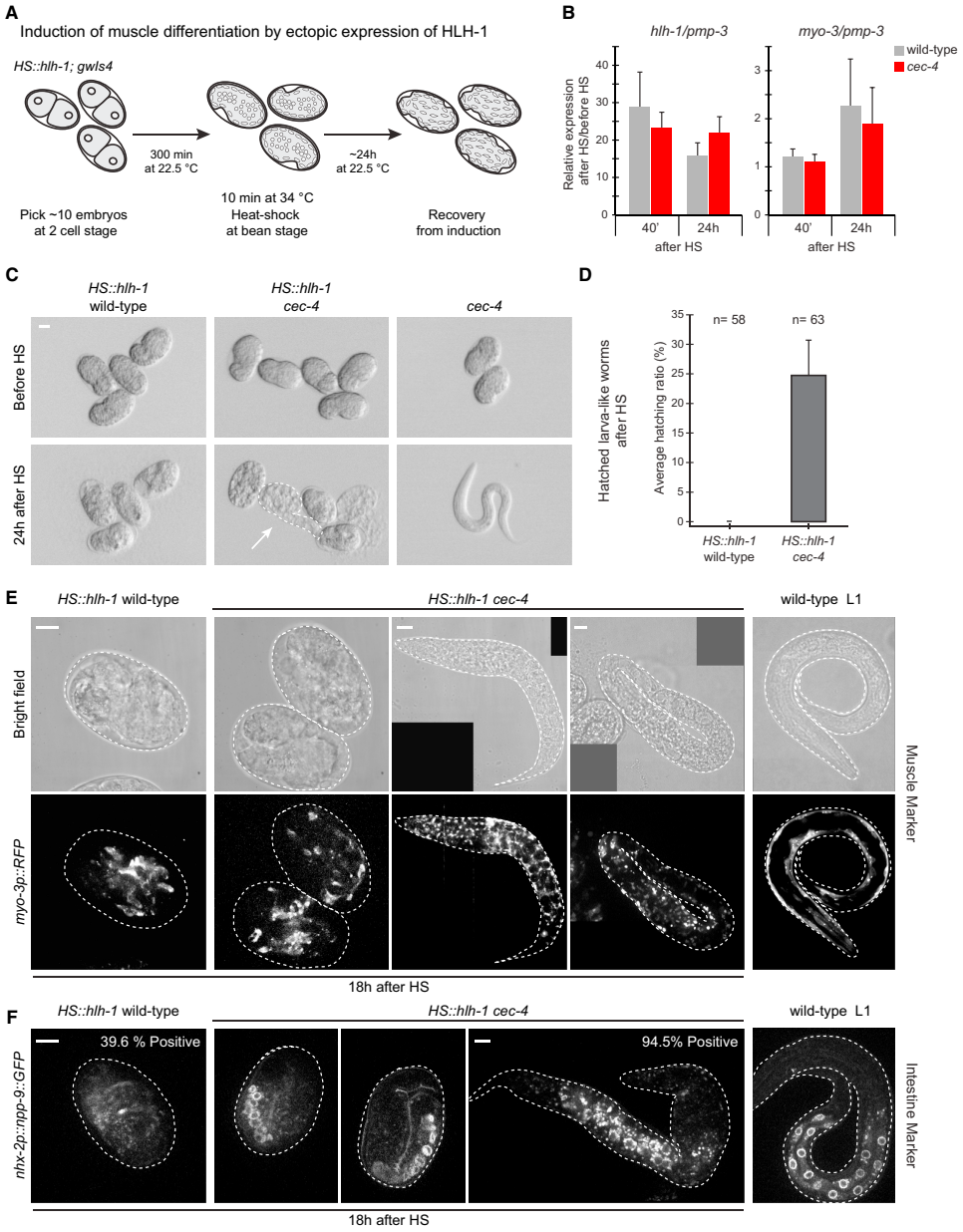

Figure 6. Lack of CEC-4 Impairs the Commitment of Embryos to a Forced Muscle Differentiation

(A) Experimental flow for forced muscle differentiation by HS induction of the master regulator HLH-1. See main text and Supplemental Experimental Procedures.

(legend continued on next page)

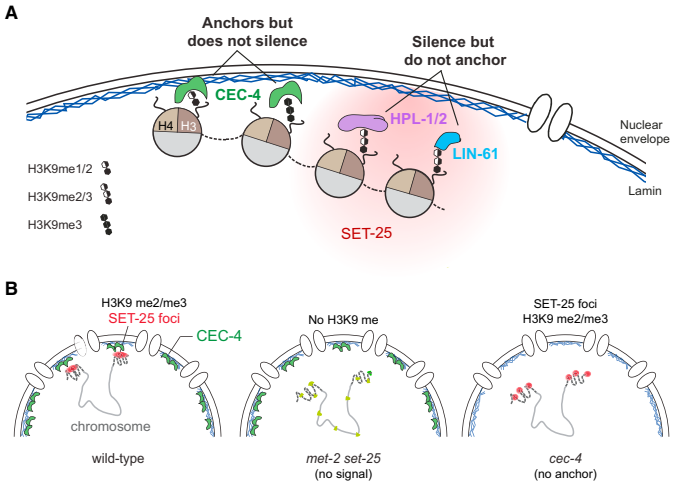

Figure 7. Different H3K9 me1, me2, and/or me3 Ligands Mediate Anchoring and Transcriptional Repression

(A) Model showing the split function of H3K9me for anchoring and repression thanks to different ligands.

(B) Summary of chromosome organization in early embryos in indicated genotypes. In WT embryos H3K9 methylation-enriched chromosome arms (dash lines) bind CEC-4 at the INM and are enriched for SET-25 (red foci). Lack of H3K9 methylation (*met-2 set-25* mutant) releases heterochromatin in embryos and derepresses genes (light green spots). Loss of CEC-4 compromises chromatin position, but does not induce gene expression.

We have not identified a direct homolog of CEC-4 in non-nematode species, and we suspect that this protein's two functions, INM-association and specific H3K9me-recognition, may be embodied in two separate polypeptides in mammals. As mentioned, an example of such split function may be the mammalian nuclear membrane-spanning protein PPR14, which can bind HP1. The interpretation that PPR14 anchors heterochromatin through this ligand is complicated, however, by the pleiotropic effects its loss has on nuclear shape (Poleshko et al., 2013). Similarly, the mammalian LBR may bind HP1 and carries a Tudor domain with a preference for H4K20me2 in vitro (Hirano et al., 2012; Ye and Worman, 1996). Whereas there is no compelling evidence that either H4K20me2 or HP1 mediate perinuclear anchoring in early development, LBR itself is implicated in the spatial organization of the genome in differentiated mammalian cells, particularly in cells that do not express Lamin A/C (Clowney et al., 2012; Solovei et al., 2013). Unfortunately, indirect effects again complicate the interpretation of LBR ablation, since this transmembrane protein has sterol reductase activity that regulates cholesterol metabolism and maintains appropriate spacing between inner and outer nuclear membranes (Holmer et al., 1998). Thus, both indirect effects and redundancy among anchors have made it difficult to characterize chromatin-tethering pathways in mammalian cells. Nonetheless, it is possible that these INM proteins function through chromatin binding proteins that resemble CEC-4. Separation of function mutations that uniquely compromise chromatin positioning will be needed to define these pathways unequivocally.

In other species, repressive epigenetic marks other than H3K9 methylation may contribute to the spatial sequestration of repressed chromatin. In mouse 3T3 embryonic fibroblasts (MEFs), the Polycomb mark H3K27me3 was reported to contribute to perinuclear positioning at the edges of LADs (Harr et al., 2015). In worms, the loss of Polycomb components MES-3 and MES-6 led to derepression of our heterochromatic reporter in embryos (Towbin et al., 2012), but did not trigger release from the nuclear periphery. Moreover, in most species, the H3K27me3-positive foci found in differentiating cells are not perinuclear (Eberhart et al., 2013). This, however, does not preclude the possibility that combinatorial epigenetic signatures target chromatin to the INM.

The relative simplicity of the *C. elegans* system and the conserved nature of its epigenetic and developmental programs has allowed us to dissect nuclear organization with a genetic approach. Given the conserved role H3K9me has in chromatin positioning, it is likely that factors with analogous functions as CEC-4 exist elsewhere. Functional screens in compromised backgrounds will be able to shed light on relevant anchors in differentiated cells. Disruption of specific anchors in differentiated tissues will extend our understanding of the function of heterochromatin sequestration.

(B) Quantitation of *hlh-1* and muscle specific *myo-3* expression by qRT-PCR in indicated genotypes, 40 min and 24 hr after HS relative to before HS; data normalized to *pmp-3* gene. Error bars = SEM of 3 biological replicas.

(C) Stereoscopic representative images of synchronized bean stage embryos before and 24 hr after HS. As control, *cec-4* null embryos lacking *HS::hlh-1* were treated similarly. Hatched larva-like worms highlighted with dashed white line and arrow. Scale bar, 20 μm.

(D) Average hatching ratio after HS according to genotype in bar plot. Error bars = SEM of six independent assays, n = total embryos tested.

(E) Muscle reporter pattern for indicated genotypes. Z-projections of bright field and fluorescent *myo-3p::RFP* (from *gwIs4*) imaging taken 18 hr after HS. Wild-type L1 imaged independently. Scale bars = 5 μm.

(F) Intestine reporter *nhx-2p::npp-9::GFP* pattern for indicated genotypes. Z-projections taken as in (E). n = 3, total number of embryos scored = 53 and 55 respectively. Scale bars,5 μm.

See also Figure S6.

EXPERIMENTAL PROCEDURES

RNAi Screen

RNAi was performed at 22.5°C by placing L1 worms on feeding plates as previously described (Timmons et al., 2001). For the list of genes used (Table S3) in the RNAi screen see Supplemental Experimental Procedures.

Microscopy

Microscopy was carried out on a spinning disc confocal microscope, using 2% agarose pads for live-microscopy or poly-lysine coated slides for fixed samples. Acquisition and analysis of array and nucleolus distribution, array spot volume, expression levels of GFP-LacI and CEC-4-mCh, and enrichment of CEC-4 over array are online, along with a description of super resolution-structured illumination microscopy (SR-SIM; Elyra S.1 [Carl Zeiss]).

AlphaScreen Direct Binding and In Vitro Assays

Purified recombinant His-tagged CEC-4 CD (200 nM) was screened for its binding to modified histone peptides with the ALTA Biosciences peptide array system (Alta Biosciences, UK) and the AlphaScreen assay. Details for protein purification, peptide pull down and ITC are in Supplemental Experimental Procedures.

LEM-2 ChIP-Seq and RNA-Seq

Early embryonic progeny was harvested after synchronization (60–65 hr depending on each strain) for WT, *met-2 set-25,* and *cec-4* mutant strains in two independent biological replicates. LEM-2 ChIP was performed as described (Ikegami et al., 2010). Total RNA was extracted by phenol/chloroform, further purified, and depleted for rRNA. Detailed information about library preparation and data analysis is described in Supplemental Experimental Procedures.

Heat-Shock Induced Muscle Differentiation

Two cell-stage embryos, of different genetic backgrounds containing the *HS::hlh-1* transgene, were allowed to develop until bean stage (300 min at 22.5°C). HS at 34°C for 10 min was performed either on 2% agarose pads or on liquid with a thermal cycler with in situ slide block. After recovery for 24 hr, evaluation of hatching larva-like worms was determined by stereomicroscopy, and reporter markers by spinning disc confocal microscopy. Details for qPCR of HS samples is described in Supplemental Experimental Procedures.

ACCESSION NUMBERS

The accession numbers for the ChIP-seq and RNA-seq data reported in this paper is NCBI Gene Expression Omnibus GEO: GSE74134.

SUPPLEMENTAL INFORMATION

Supplemental Information includes Supplemental Experimental Procedures, six figures, and seven tables and can be found with this article online at http://dx.doi.org/10.1016/j.cell.2015.10.066.

AUTHOR CONTRIBUTIONS

Conceptualization, A.G.-S., B.D.T., and S.M.G.; Methodology, A.G.-S., B.D.T., and D.S.C.; Validation, A.G.-S., V.K., D.S.C.; Formal Analysis, D.G., M.H.H; Investigation, A.G.-S., B.D.T., V.K., D.S.C., M.H.H, L.G., L.W., T.Y., X.W.; Resources, K.Z.; Writing – Review & Editing, A.G.-S., B.D.T., D.S.C., S.M.G.; Supervision, K.Z., S.M.G.; Funding Acquisition, S.G.M.

ACKNOWLEDGMENTS

Some strains were provided by the *Caenorhabditis* Genetics Center (CGC) of the NIH Office of Research Infrastructure Programs (P40 OD010440). We thank G-J. Hendriks, H. Grosshans, R. Thierry, P. Zeller, A. Peters, P. Hein, Y. Gruenbaum, and P. Askjaer for reagents and materials. We thank J. Lieb and K. Ikegami for training A.G.-S. in LEM-2 ChIP. We thank the FMI Worm, Genomics, Protein Structure, Protein Analysis, and Microscopy facilities for valuable advice and support. A.G.-S. was supported by FP7 Marie Curie Network Nucleosome 4D and the SNSF NCCR "Frontiers in Genetics." S.M.G. thanks the FMI and SNSF for support.

Received: July 1, 2015
Revised: October 7, 2015
Accepted: October 27, 2015
Published: November 19, 2015

REFERENCES

Barski, A., Cuddapah, S., Cui, K., Roh, T.-Y., Schones, D.E., Wang, Z., Wei, G., Chepelev, I., and Zhao, K. (2007). High-resolution profiling of histone methylations in the human genome. Cell *129*, 823–837.

Brachner, A., and Foisner, R. (2011). Evolvement of LEM proteins as chromatin tethers at the nuclear periphery. Biochem. Soc. Trans. *39*, 1735–1741.

Clowney, E.J., LeGros, M.A., Mosley, C.P., Clowney, F.G., Markenskoff-Papadimitriou, E.C., Myllys, M., Barnea, G., Larabell, C.A., and Lomvardas, S. (2012). Nuclear aggregation of olfactory receptor genes governs their monogenic expression. Cell *151*, 724–737.

Couteau, F., Guerry, F., Muller, F., and Palladino, F. (2002). A heterochromatin protein 1 homologue in Caenorhabditis elegans acts in germline and vulval development. EMBO Rep. *3*, 235–241.

Eberhart, A., Feodorova, Y., Song, C., Wanner, G., Kiseleva, E., Furukawa, T., Kimura, H., Schotta, G., Leonhardt, H., Joffe, B., and Solovei, I. (2013). Epigenetics of eu- and heterochromatin in inverted and conventional nuclei from mouse retina. Chromosome Res. *21*, 535–554.

Etchberger, J.F., Lorch, A., Sleumer, M.C., Zapf, R., Jones, S.J., Marra, M.A., Holt, R.A., Moerman, D.G., and Hobert, O. (2007). The molecular signature and cis-regulatory architecture of a C. elegans gustatory neuron. Genes Dev. *21*, 1653–1674.

Fischle, W., Wang, Y., and Allis, C.D. (2003a). Binary switches and modification cassettes in histone biology and beyond. Nature *425*, 475–479.

Fischle, W., Wang, Y., Jacobs, S.A., Kim, Y., Allis, C.D., and Khorasanizadeh, S. (2003b). Molecular basis for the discrimination of repressive methyl-lysine marks in histone H3 by Polycomb and HP1 chromodomains. Genes Dev. *17*, 1870–1881.

Fukushige, T., and Krause, M. (2005). The myogenic potency of HLH-1 reveals wide-spread developmental plasticity in early C. elegans embryos. Development *132*, 1795–1805.

Fussner, E., Ahmed, K., Dehghani, H., Strauss, M., and Bazett-Jones, D.P. (2010). Changes in chromatin fiber density as a marker for pluripotency. Cold Spring Harb. Symp. Quant. Biol. *75*, 245–249.

Gerstein, M.B., Lu, Z.J., Van Nostrand, E.L., Cheng, C., Arshinoff, B.I., Liu, T., Yip, K.Y., Robilotto, R., Rechtsteiner, A., Ikegami, K., et al.; modENCODE Consortium (2010). Integrative analysis of the Caenorhabditis elegans genome by the modENCODE project. Science *330*, 1775–1787.

González-Aguilera, C., Ikegami, K., Ayuso, C., de Luis, A., Íñiguez, M., Cabello, J., Lieb, J.D., and Askjaer, P. (2014). Genome-wide analysis links emerin to neuromuscular junction activity in Caenorhabditis elegans. Genome Biol. *15*, R21.

Greer, E.L., Beese-Sims, S.E., Brookes, E., Spadafora, R., Zhu, Y., Rothbart, S.B., Aristizábal-Corrales, D., Chen, S., Badeaux, A.I., Jin, Q., et al. (2014). A histone methylation network regulates transgenerational epigenetic memory in C. elegans. Cell Rep. *7*, 113–126.

Gudise, S., Figueroa, R.A., Lindberg, R., Larsson, V., and Hallberg, E. (2011). Samp1 is functionally associated with the LINC complex and A-type lamina networks. J. Cell Sci. *124*, 2077–2085.

Guelen, L., Pagie, L., Brasset, E., Meuleman, W., Faza, M.B., Talhout, W., Eussen, B.H., de Klein, A., Wessels, L., de Laat, W., and van Steensel, B. (2008). Domain organization of human chromosomes revealed by mapping of nuclear lamina interactions. Nature *453*, 948–951.

Harr, J.C., Luperchio, T.R., Wong, X., Cohen, E., Wheelan, S.J., and Reddy, K.L. (2015). Directed targeting of chromatin to the nuclear lamina is mediated by chromatin state and A-type lamins. J. Cell Biol. *208*, 33–52.

Hirano, Y., Hizume, K., Kimura, H., Takeyasu, K., Haraguchi, T., and Hiraoka, Y. (2012). Lamin B receptor recognizes specific modifications of histone H4 in heterochromatin formation. J. Biol. Chem. *287*, 42654–42663.

Hiratani, I., Ryba, T., Itoh, M., Yokochi, T., Schwaiger, M., Chang, C.W., Lyou, Y., Townes, T.M., Schübeler, D., and Gilbert, D.M. (2008). Global reorganization of replication domains during embryonic stem cell differentiation. PLoS Biol. *6*, e245.

Hiratani, I., Takebayashi, S., Lu, J., and Gilbert, D.M. (2009). Replication timing and transcriptional control: beyond cause and effect–part II. Curr. Opin. Genet. Dev. *19*, 142–149.

Holmer, L., Pezhman, A., and Worman, H.J. (1998). The human lamin B receptor/sterol reductase multigene family. Genomics *54*, 469–476.

Ikegami, K., Egelhofer, T.A., Strome, S., and Lieb, J.D. (2010). Caenorhabditis elegans chromosome arms are anchored to the nuclear membrane via discontinuous association with LEM-2. Genome Biol. *11*, R120.

Kind, J., Pagie, L., Ortabozkoyun, H., Boyle, S., de Vries, S.S., Janssen, H., Amendola, M., Nolen, L.D., Bickmore, W.A., and van Steensel, B. (2013). Single-cell dynamics of genome-nuclear lamina interactions. Cell *153*, 178–192.

Koester-Eiserfunke, N., and Fischle, W. (2011). H3K9me2/3 binding of the MBT domain protein LIN-61 is essential for Caenorhabditis elegans vulva development. PLoS Genet. *7*, e1002017.

Kubben, N., Adriaens, M., Meuleman, W., Voncken, J.W., van Steensel, B., and Misteli, T. (2012). Mapping of lamin A- and progerin-interacting genome regions. Chromosoma *121*, 447–464.

Mattout, A., Aaronson, Y., Sailaja, B.S., Raghu Ram, E.V., Harikumar, A., Mallm, J.P., Sim, K.H., Nissim-Rafinia, M., Supper, E., Singh, P.B., et al. (2015). Heterochromatin Protein 1β (HP1β) has distinct functions and distinct nuclear distribution in pluripotent versus differentiated cells. Genome Biol. *16*, 213.

Meister, P., Towbin, B.D., Pike, B.L., Ponti, A., and Gasser, S.M. (2010). The spatial dynamics of tissue-specific promoters during C. elegans development. Genes Dev. *24*, 766–782.

Meister, P., Mango, S.E., and Gasser, S.M. (2011). Locking the genome: nuclear organization and cell fate. Curr. Opin. Genet. Dev. *21*, 167–174.

Meuleman, W., Peric-Hupkes, D., Kind, J., Beaudry, J.B., Pagie, L., Kellis, M., Reinders, M., Wessels, L., and van Steensel, B. (2013). Constitutive nuclear lamina-genome interactions are highly conserved and associated with A/T-rich sequence. Genome Res. *23*, 270–280.

Minc, E., Allory, Y., Worman, H.J., Courvalin, J.C., and Buendia, B. (1999). Localization and phosphorylation of HP1 proteins during the cell cycle in mammalian cells. Chromosoma *108*, 220–234.

Nestorov, P., Tardat, M., and Peters, A.H. (2013). H3K9/HP1 and Polycomb: two key epigenetic silencing pathways for gene regulation and embryo development. Curr. Top. Dev. Biol. *104*, 243–291.

Nigg, E.A. (1992). Assembly and cell cycle dynamics of the nuclear lamina. Semin. Cell Biol. *3*, 245–253.

Padeken, J., and Heun, P. (2014). Nucleolus and nuclear periphery: velcro for heterochromatin. Curr. Opin. Cell Biol. *28*, 54–60.

Peric-Hupkes, D., Meuleman, W., Pagie, L., Bruggeman, S.W., Solovei, I., Brugman, W., Gräf, S., Flicek, P., Kerkhoven, R.M., van Lohuizen, M., et al. (2010). Molecular maps of the reorganization of genome-nuclear lamina interactions during differentiation. Mol. Cell *38*, 603–613.

Pickersgill, H., Kalverda, B., de Wit, E., Talhout, W., Fornerod, M., and van Steensel, B. (2006). Characterization of the Drosophila melanogaster genome at the nuclear lamina. Nat. Genet. *38*, 1005–1014.

Pinheiro, I., Margueron, R., Shukeir, N., Eisold, M., Fritzsch, C., Richter, F.M., Mittler, G., Genoud, C., Goyama, S., Kurokawa, M., et al. (2012). Prdm3 and Prdm16 are H3K9me1 methyltransferases required for mammalian heterochromatin integrity. Cell *150*, 948–960.

Poleshko, A., Mansfield, K.M., Burlingame, C.C., Andrake, M.D., Shah, N.R., and Katz, R.A. (2013). The human protein PRR14 tethers heterochromatin to the nuclear lamina during interphase and mitotic exit. Cell Rep. *5*, 292–301.

Solovei, I., Wang, A.S., Thanisch, K., Schmidt, C.S., Krebs, S., Zwerger, M., Cohen, T.V., Devys, D., Foisner, R., Peichl, L., et al. (2013). LBR and lamin A/C sequentially tether peripheral heterochromatin and inversely regulate differentiation. Cell *152*, 584–598.

Steffen, P.A., Fonseca, J.P., and Ringrose, L. (2012). Epigenetics meets mathematics: towards a quantitative understanding of chromatin biology. BioEssays *34*, 901–913.

Studencka, M., Konzer, A., Moneron, G., Wenzel, D., Opitz, L., Salinas-Riester, G., Bedet, C., Krüger, M., Hell, S.W., Wisniewski, J.R., et al. (2012a). Novel roles of Caenorhabditis elegans heterochromatin protein HP1 and linker histone in the regulation of innate immune gene expression. Mol. Cell. Biol. *32*, 251–265.

Studencka, M., Wesołowski, R., Opitz, L., Salinas-Riester, G., Wisniewski, J.R., and Jedrusik-Bode, M. (2012b). Transcriptional repression of Hox genes by C. elegans HP1/HPL and H1/HIS-24. PLoS Genet. *8*, e1002940.

Taddei, A., and Gasser, S.M. (2012). Structure and function in the budding yeast nucleus. Genetics *192*, 107–129.

Talamas, J.A., and Capelson, M. (2015). Nuclear envelope and genome interactions in cell fate. Front. Genet. *6*, 95.

Taouji, S., Dahan, S., Bossé, R., and Chevet, E. (2009). Current Screens Based on the AlphaScreen Technology for Deciphering Cell Signalling Pathways. Curr. Genomics *10*, 93–101.

Taverna, S.D., Li, H., Ruthenburg, A.J., Allis, C.D., and Patel, D.J. (2007). How chromatin-binding modules interpret histone modifications: lessons from professional pocket pickers. Nat. Struct. Mol. Biol. *14*, 1025–1040.

Timmons, L., Court, D.L., and Fire, A. (2001). Ingestion of bacterially expressed dsRNAs can produce specific and potent genetic interference in Caenorhabditis elegans. Gene *263*, 103–112.

Towbin, B.D., Meister, P., Pike, B.L., and Gasser, S.M. (2010). Repetitive transgenes in C. elegans accumulate heterochromatic marks and are sequestered at the nuclear envelope in a copy-number- and lamin-dependent manner. Cold Spring Harb. Symp. Quant. Biol. *75*, 555–565.

Towbin, B.D., González-Aguilera, C., Sack, R., Gaidatzis, D., Kalck, V., Meister, P., Askjaer, P., and Gasser, S.M. (2012). Step-wise methylation of histone H3K9 positions heterochromatin at the nuclear periphery. Cell *150*, 934–947.

Unnikrishnan, A., Gafken, P.R., and Tsukiyama, T. (2010). Dynamic changes in histone acetylation regulate origins of DNA replication. Nat. Struct. Mol. Biol. *17*, 430–437.

Wilson, K.L., and Foisner, R. (2010). Lamin-binding Proteins. Cold Spring Harb. Perspect. Biol. *2*, a000554.

Ye, Q., and Worman, H.J. (1996). Interaction between an integral protein of the nuclear envelope inner membrane and human chromodomain proteins homologous to *Drosophila* HP1. J. Biol. Chem. *271*, 14653–14656.

Zheng, C., Karimzadegan, S., Chiang, V., and Chalfie, M. (2013). Histone methylation restrains the expression of subtype-specific genes during terminal neuronal differentiation in Caenorhabditis elegans. PLoS Genet. *9*, e1004017.

Zullo, J.M., Demarco, I.A., Piqué-Regi, R., Gaffney, D.J., Epstein, C.B., Spooner, C.J., Luperchio, T.R., Bernstein, B.E., Pritchard, J.K., Reddy, K.L., and Singh, H. (2012). DNA sequence-dependent compartmentalization and silencing of chromatin at the nuclear lamina. Cell *149*, 1474–1487.

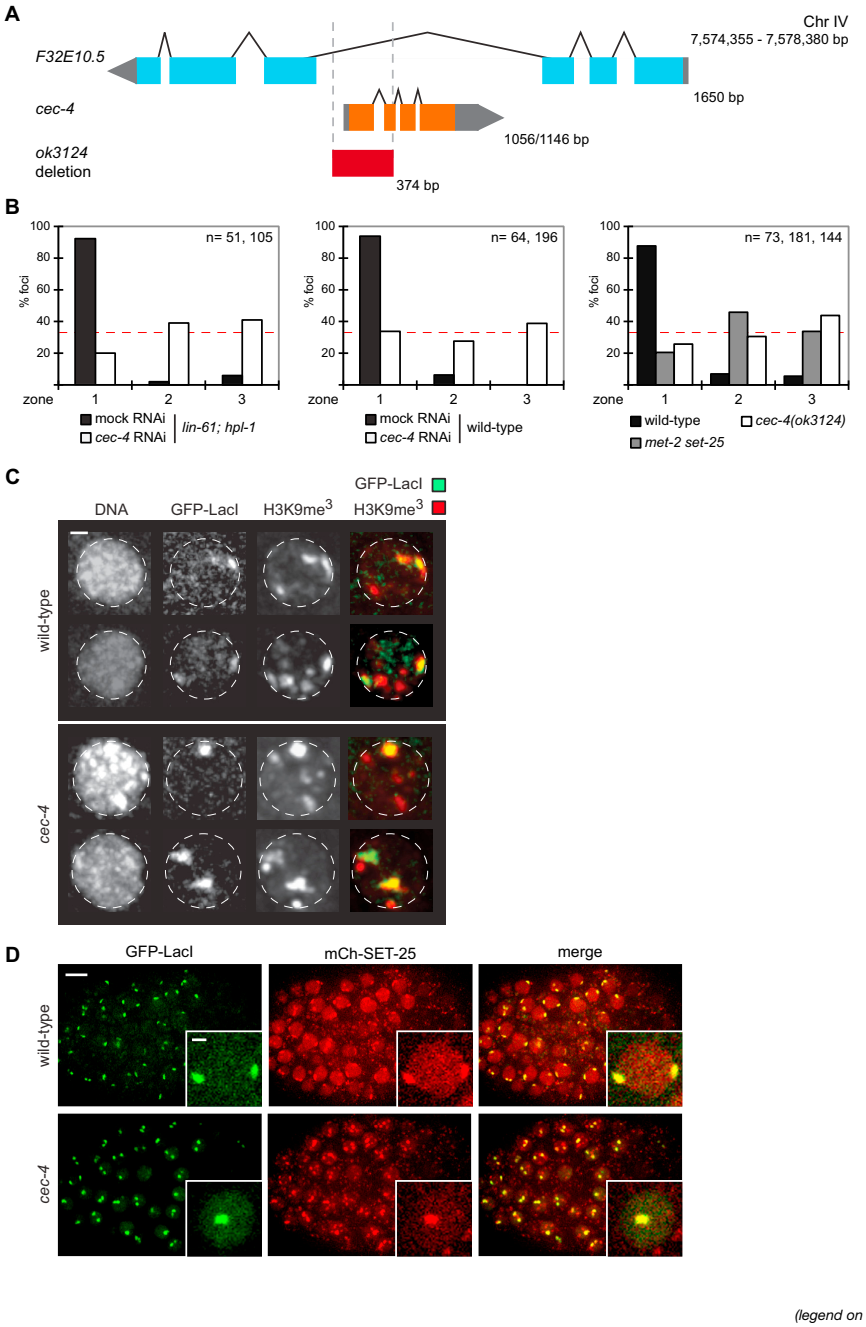

(legend on next page)

Cell

Figure S1. Genomic Context of *cec*-4 and Its Deletion Allele, Related to Figure 1

Heterochromatic array contains H3K9me3 and co-localizes with SET-25 even when it is away from nuclear periphery in *cec-4* mutant.

(A) Schematic representation (not to scale) of genomic region where *cec-4* gene is localized, and deletion allele coverage.

(B) Quantitation of array distribution in different experimental conditions as indicated, n: foci scored in presented order. Pair-wise comparisons of *mock RNAi* and WT conditions with the respective *cec-4 RNAi* and *cec-4* mutant show statistically significant differences with p-value < 0.001 in all comparisons, χ^2 test.

(C) Immunofluorescence (IF) of transgene *gwIs4* array (anti-GFP) and repressive histone mark H3K9me3 in WT and *cec-4* mutant strains. Z-projection of representative nuclei are shown, co-localization observed as yellow signal in merged panels. Scale bar, 2 μm.

(D) Live microscopy of N-terminally tagged SET-25 with mCherry (mCh-SET-25) together with array in indicated genotypes. Z-projection images of embryos in individual and merged colors. Insets: single nuclei. Scale bars, 5 and 2 μm for embryos and insets respectively.

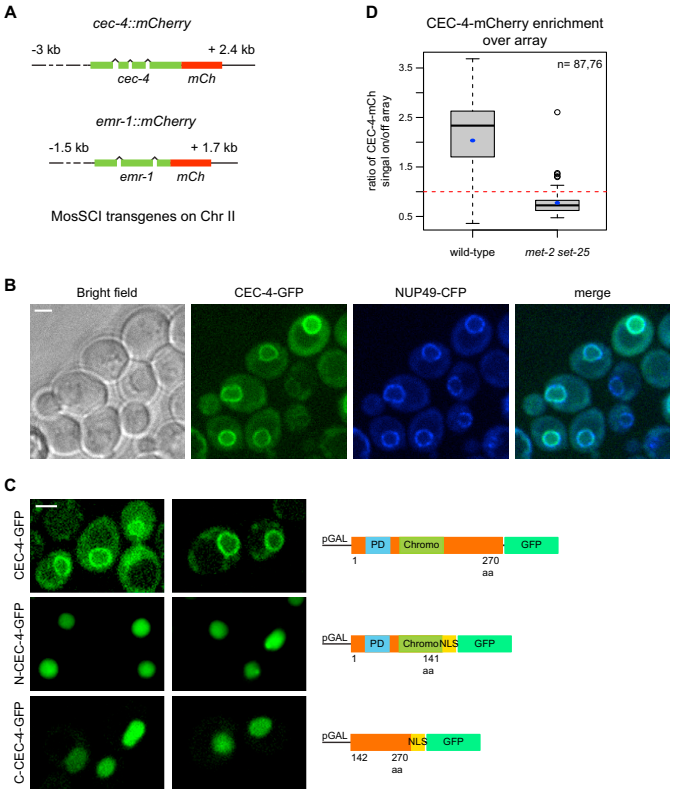

Figure S2. CEC-4 and EMR-1 Constructs Used for This Study, Related to Figures 2 and 4

CEC-4 forms a nuclear ring in *S. cerevisiae*, which is compromised by loss of full-length protein.

(A) Schematic representation of CEC-4 and EMR-1 fusion constructs to mCherry. Both constructs were integrated as single copy on Chr II by MosSCI. *cec-4::mCherry* transgene contains the endogenous promoter (upstream −3kb from transcription start site) and 3′UTR (542bp after stop codon) of *cec-4* gene. *emr-1::mCherry* was kindly provided by Askjer P. and contains the endogenous promoter (upstream −1.567kb from transcription start site) and 3′UTR (300bp after stop codon) of *emr-1* gene.

(B) Expression of intron-less full-length CEC-4 fused C-terminally to GFP in *S. cerevisiae*. Bright field, CEC-4-GFP, NUP-49-CFP (as perinuclear marker) and merged single plane images are shown.

(C) Full-length, N-term and C-term fragments of CEC-4 fused to GFP expressed in yeast. Schematic representation of each construct is presented, in which the GAL1-10 promoter (pGAL) drives CEC-4-mCherry and corresponding fragment fusions. Single plane images of representative patterns are shown. Scale bars on (B) and (C) panel, 2 μm.

(D) Quantitation of CEC-4-mCherry intensity level on array-bound region in contrast to a non-array perinuclear region, as described in Supplemental Experimental Procedures for WT and *met-2 set-25* mutant embryos. Whiskers: 1st and 3rd quartiles, black circles: outliers, black lines: median, blue dots: mean, red dashed line: baseline set as no difference in enrichment, n: total number of arrays per nuclei measured of each genotype.

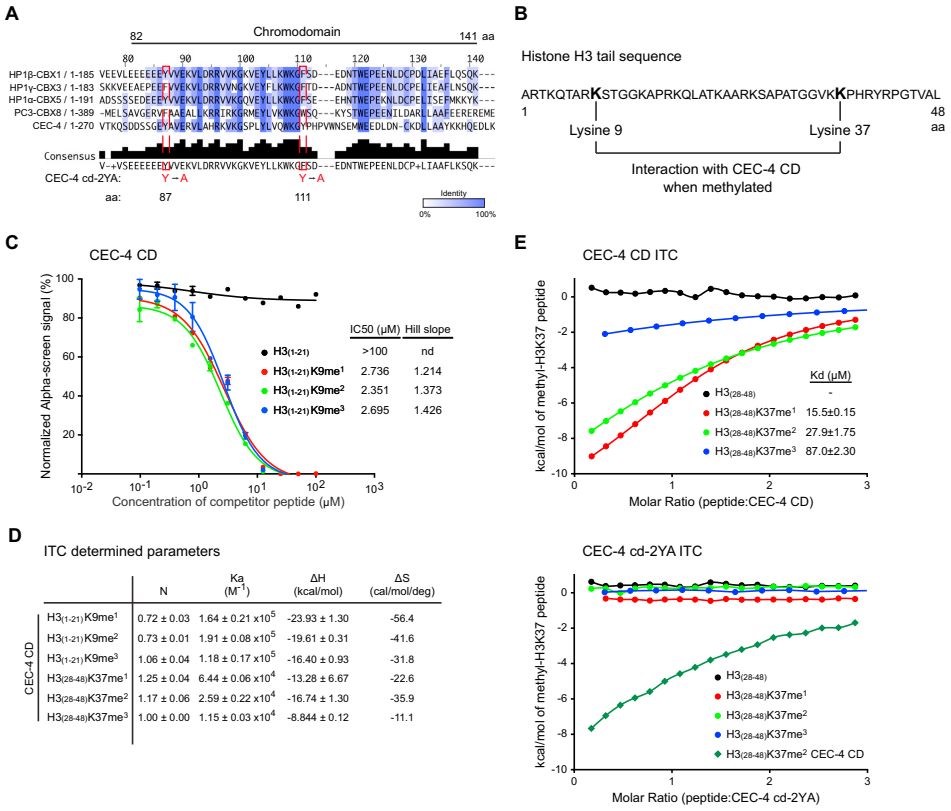

Figure S3. CEC-4 Chromodomain Is Conserved and Binds to All Methylated Forms of H3K9 and to H3K37me with Lower Affinity, Related to Figure 3

CD point mutations impair binding to all substrates tested.

(A) ClustalW multiple sequence alignment of CEC-4's CD (82-141 aa) with different *H. sapiens* CBX proteins as indicated. Blue color range represents percentage of identity, and consensus sequence is displayed. The two highlighted lysines (dashed red boxes) replaced by alanines in the CEC-4 cd 2YA construct.

(B) Histone H3 tail sequence for visualization of amino acid context of lysines 9 and 37, to which CEC-4 CD showed positive.

(C) IC_{50} (half maximal inhibitory concentration) of H3K9 peptides binding to CEC-4 CD measured by AlphaScreen peptide displacement assay. Non-biotinylated H3K9 peptides were used to compete with the binding of CEC-4 CD and biotin-H3K9me2 peptide in AlphaScreen binding assay.

(D) Table showing parameters measured for association of CEC-4 CD and the different methylated states of indicated H3 peptides. N (stoichiometry), K (association constant), ΔH (enthalpic change) and ΔS (entropy change) in Isothermal Titration Calorimetry (ITC) assay.

(E) Quantitation of binding affinities of methylated H3K37 peptides to CEC-4 CD and mutant cd-2YA, determined by ITC. For all graphs solid lines represent a nonlinear least-square fit using one-site fitting equation.

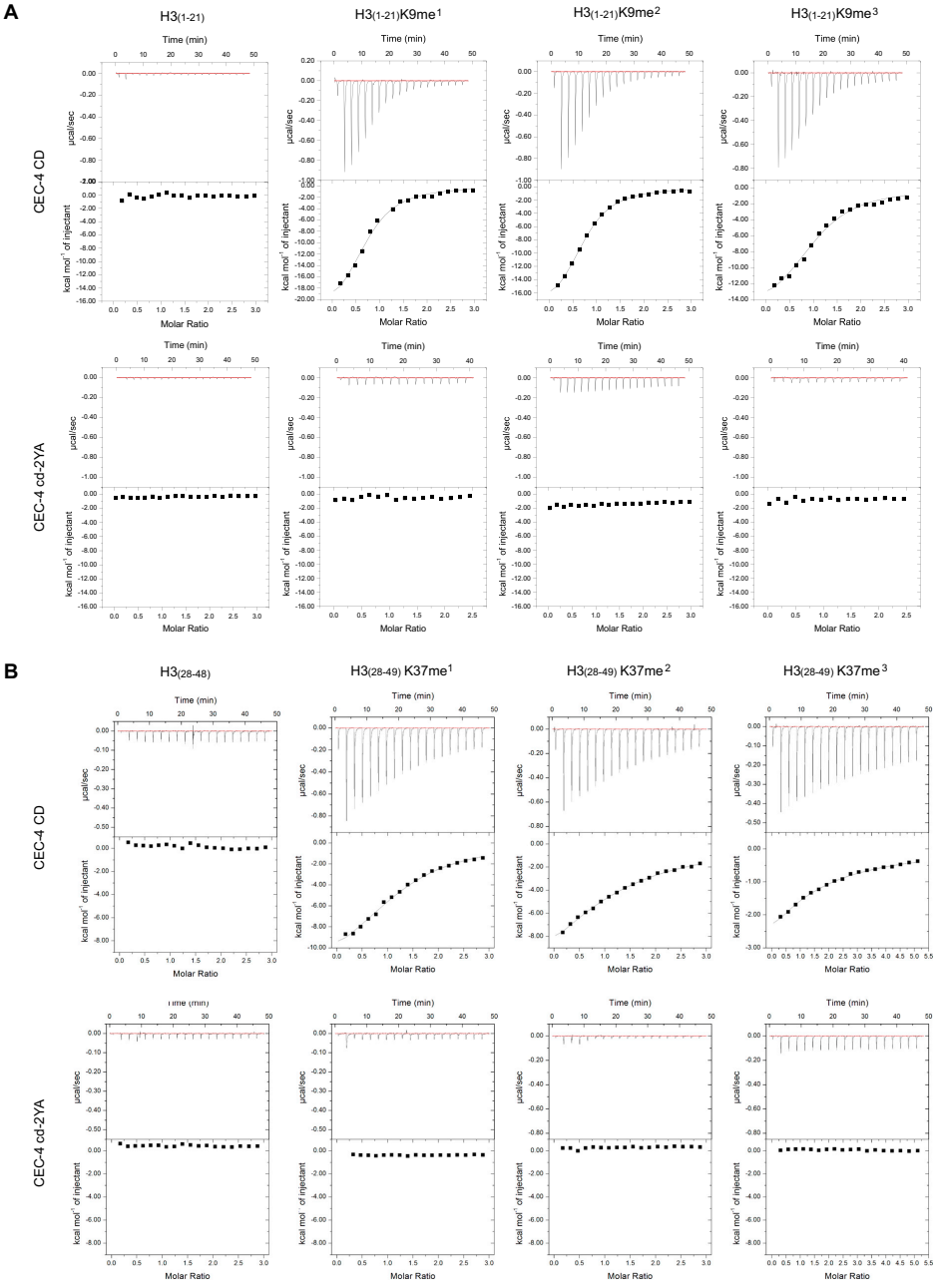

(legend on next page)

Figure S4. Intact CEC-4 CD Binds Preferentially to All Methylated Forms of H3K9 and with Less Affinity for H3K37 (me1 > me2 > me3) as Monitored by ITC, Related to Figure 3

(A) Raw binding data of ITC injections of all methylated forms of H3K9 for both CEC-4 CD and CEC-4cd-2YA is shown. Dissociation constants (Kd) determined are shown in Fig 2E. Kd's with CEC-4cd-2YA were unable to be determined.

(B) Same as in (A) except that the peptides are related to methylation of H3K37. Kd's are shown in Fig S2E.

S6 Cell *163*, 1333–1347, December 3, 2015 ©2015 Elsevier Inc.

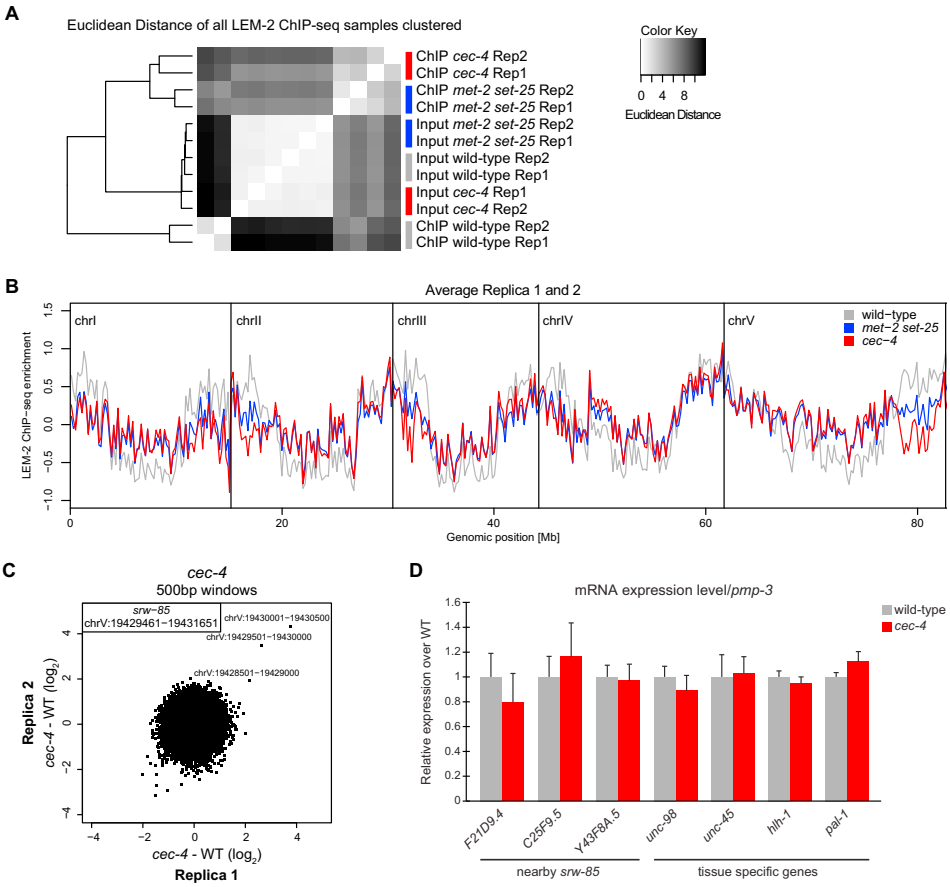

Figure S5. LEM-2 ChIP Enrichment Signals of *met-2 set-25* and *cec-4* Mutants Cluster and Are Different from WT, with a Less Polarized Pattern, Related to Figure 5

Genes *srw-85* and *C18D4.6* are depleted for H3K9me in *cec-4* embryos, while only *srw-85* is derepressed.

(A) Heat-map of hierarchical clustered Euclidean distances of LEM-2 ChIP and Input (total chromatin extracted) normalized reads of WT, *met2 set-25,* and *cec-4* mutants in duplicate.

(B) Average of duplicates of LEM-2 ChIP enrichment plotted over chromosomes. Tracks are shown only for autosomal chromosomes. Averaged signals (*Z* scores of IP – input) are shown in 200 kb windows.

(C) Relative expression profiles in windows of 500 bp (not strand assigned) for the whole genome of cec-*4* mutants to WT levels in early embryos. Scatter plots compare replicas of indicated genotypes.

(D) qRT-PCR mRNA level quantitation for indicated genes in WT and *cec-4* mutant background. Data shown normalized to *pmp-3* gene and relative to the expression in WT. Error bars = SEM of five biological replicas of early embryo extracts.

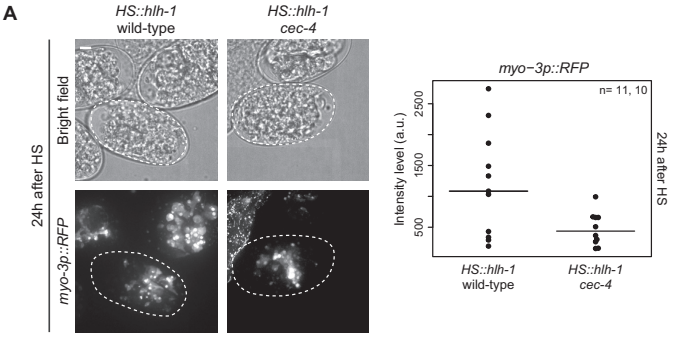

B

Genotype	Embryos	Hatched larva-like worms
HS::hlh-1 CEC-4-mCherry cec-4	33	0
HS::hlh-1 CEC-4cd2YA-mCherry cec-4	32	3
HS::hlh-1 cec-4	63	15
HS::hlh-1	58	0

Figure S6. Muscle-Specific myo3-RFP Expression Occurs in Both Genotypes after HS, Albeit at Higher Levels in WT, Related to Figure 6

Restoration by expression of CEC-4-mCherry, but not the CEC-4 CD-2YA mutant.

(A) Muscle specific *myo-3p::RFP* reporter (contained in *gwIs4* array) for indicated genotypes 24 hr after HS. Z-projection images of bright field and *myo-3p::RFP* are shown. Scale bar, 5 μm. Quantitation of RFP intensity signal 24 hr after HS for indicated genotypes. Intensity levels are plotted in a.u., black line: median, n: number of embryos of respective genotype.

(B) Table showing number of hatched larva-like worms for different strains tested.

Cell

Supplemental Information

Perinuclear Anchoring of H3K9-Methylated Chromatin Stabilizes Induced Cell Fate in *C. elegans* Embryos

Adriana Gonzalez-Sandoval, Benjamin D. Towbin, Veronique Kalck, Daphne S. Cabianca, Dimos Gaidatzis, Michael H. Hauer, Liqing Geng, Li Wang, Teddy Yang, Xinghao Wang, Kehao Zhao, and Susan M. Gasser

Supplemental Experimental Procedures:

Constructs and Strains

Gene synthesis of *cec-4* for protein expression and yeast constructs were from GenScript USA Inc. For the CEC-4 tagged construct, the gene was amplified from N2 worm genomic DNA. All plasmid constructs were generated by MultiSite Gateway® cloning (Invitrogen). The Y87A and Y111A point mutations in the *cec-4* gene, referred to as 2YA, were introduced by multi-site-directed mutagenesis (Agilent Technologies) for both *in vivo* and *in vitro* experiments. All worm and yeast strains used are listed in Table S1 and S2, respectively. The *cec-4(ok3124)* strain received from CGC was out-crossed six times to N2 wild-type strain. CEC-4 tagged wild-type and mutant cd2YA versions, were made using the MosSCI technique (Frokjaer-Jensen et al., 2008). The MosSCI strains were out-crossed twice to N2 wild-type strain. The EMR-1-mCherry strain was kindly provided by P. Askjer; the intestine specific marker strain (*nhx-2p::npp-9::GFP*) in Fig. 6F by Hendricks G.J. and H. Grosshans (Friedrich Miescher Institute for Biomedical Research, Basel, Switzerland, personal communication). Worms for microscopy experiments were grown at 22.5˚C; RNA and LEM-2 ChIP sequencing strains were grown at 20˚C; qPCR strains were grown at 20˚C except for Fig. 6B at 22.5˚C. For yeast experiments, CEC-4 full length (1-270 aa), CEC-4N (1-144 aa) and CEC-4C (142-270 aa) were cloned into Advanced Gateway Destination vector plasmid 14193 (pAG415GAL-ccdB-EGFP); plasmids were transformed using standard transformation protocol in GA-1981 or GA-3628 strains (see Table S2 for strain details). Yeast were grown at 30°C.

RNAi

RNAi was performed by placing larval stage 1 (L1) worms on feeding plates as previously described (Timmons et al., 2001). Table S3 and S6 lists genes tested in RNAi screen and CEC-4-

mCherry localization experiments. All RNAi clones used were sequenced first to confirm target. As a mock RNAi control, the L4440 vector (Fire vector library) was modified by removing an *EcoRV* fragment containing 25bp identical to GFP-LacI.

Immunofluorescence (IF)

IF for Fig. S1C was done as described in (Meister et al., 2010), and for Fig. 2B and 5C IF as described in (Rohner et al., 2013). Antibodies used in pairs: for *gwIs4:* monoclonal anti-GFP (MBL-D153-3) and Alexa-488 anti-rat; for H3K9 methylation: monoclonal anti-H3K9me3 (Wako #303-34832) and Alexa-568 anti-mouse; for nuclear pores: monoclonal mAB414 (Abcam ab24609) and Alexa-555 anti-mouse; for lamin: anti-CeLMN-1 (a gift from Y. Gruenbaum, The Hebrew University of Jerusalem, Jerusalem, Israel) and Alexa-488, -555 or -647 anti-rabbit; for CEC-4-mCherry: monoclonal anti-mCherry (Life technologies M11217) and Alexa-488 anti-rat; for nucleolus: anti-Fibrillarin (kindly provided by P. Heun, Welcome Trust Center for Cell Biology, Edinburgh, UK) and Alexa-555 anti-human.

Microscopy

Except for Fig. 2B and 6C, microscopy was carried out on spinning disk multipoint confocal microscopes: (1) AxioImager M1 [Carl Zeiss] + Yokogawa CSU-22 scan head, Plan-Neofluar 100×/1.45 NA oil objective, EM-CCD camera [Cascade II; Photometrics], and MetaMorph 7.7.2 software or (2) Olympus IX81 + Yokogawa CSU-X1 scan head, PlanApo 100x/1.45 TIRFM or 60x/1.45 NA oil objectives, 2X Back-illuminated EM-CCD EvolveDelta (Photometrics), and VisiView 2.1.4 software. Live microscopy samples were prepared as previously described (Meister et al., 2010). Figs. 1E, 1F, 5C and S1C were de-convolved with Huygens Pro software. Single plane and 3D reconstruction (maximum intensity Z-projections) images and analysis were generated using Fiji/ImageJ software (Schindelin et al., 2012). Quantitation of array and

nucleolus distribution on focal stacks of images was done with plugin PointPicker (http://bigwww.epfl.ch/ thevenaz/pointpicker/) as described (Meister et al., 2010); for proper quantitation in *cec-4(ok3124)* mutant, we used a strain with an additional copy of a lacO free *baf-1p::GFP-LacI* transgene (*gwIs39*), to enhance the GFP signal and be able to identify nuclear periphery.

Quantitation of GFP/RFP signal intensity on focal stack images was done selecting the plane at the embryo middle section and subtracting the average background of corresponding image. In Fig. 1F all strains were compared to average wild-type signal intensity. In Fig. S2D, quantitation of CEC-4-mCherry enrichment over array on focal stacks of images was done measuring, for each nucleus, the mCherry intensity in the nuclear volume occupied by the array and divided by the mCherry intensity in an equivalent region outside the array at the nuclear periphery. In Fig. 2D, quantitation of CEC-4-mCherry and EMR-1-mCherry fluorescent intensity in various tissues of L1 worms was performed on single nuclei, selecting a middle nuclear section plane; the obtained intensity values were normalized on the average background fluorescence of the corresponding image. Zoning assay graphs were done in Microsoft Excel and Intensity signal box-plots in R.

For Fig. 1F Fiji ImageJ was used to change de dynamic range of deconvolved images, giving more value to low intense pixels (same settings applied to all images). Pixel classification in Ilastik 1.1.5 image analysis and classification software (Sommer, 2011)was used to segment the greyscale images in 3D space. With all Ilastik features selected, three individual labels were trained for detecting (1) the background, (2) the nuclei and (3) the GFP foci. A Matlab based function was used analyze the Ilastik probability maps and calculate different nuclei and foci parameters. Spot volume describes the 3D foci dimensions in voxels and Spot distance is

calculated by measuring the minimal 3D distance from the Spot centroid to the nuclear periphery.

For Fig. 2B, high-resolution imaging was performed with a super resolution-structured illumination (SR-SIM) microscope (Elyra S.1 [Carl Zeiss], Plan-Apochromat 63x/1.4 NA objective lens, EM-CCD camera [iXon 885; Andor Technology], and ZEN Blue 2010D software [Carl Zeiss]). Processing was performed with Zen software [Carl Zeiss]. For Fig. 6C, microscopy was carried out on fluorescence stereomicroscope (Leica MZ FL III, PlanApo 2x/0.07 NA, Leica DFC350 FX camera 0.63x lens, and Imagic ims Client V14Q4_p3 software).

For yeast experiments (Fig. S2B and C), cells were cultured overnight at 30°C in a synthetic medium containing 2% raffinose, 0.1% glucose and lacking leucine to prevent the loss of the plasmid. The next day cultures were diluted in the same medium containing raffinose only, and were imaged when cells reached a concentration of 0.2-0.4 $x10^7$ cells/ml. Live yeast cells were mounted on pad of agarose (1.4%) containing raffinose or galactose for imaging.

Multiple sequence alignment

CEC-4 and *H. sapiens* CBX protein sequences were aligned with ClustalW (www.ebi.ac.uk), and visualized by Jalview (Waterhouse et al., 2009).

Recombinant protein purification

The CEC-4 CD (aa 25-141) and CEC-4 cd-2YA (aa 25-141, Y87A-Y111A) constructs were cloned into pOPINF vector using the In-Fusion system (Clontech) (Berrow et al., 2007), proteins were expressed in the *E. coli* strain BL21 Rosetta pLysS and affinity purified through the His tag binding to ProBond Ni-NTA resin (Invitrogen) according to manufacturer's instructions. For ITC experiments His tag was removed by HRV 3C protease digestion (Novagen) and proteins were

further purified by gel filtration on a HiLoad 16/60 Superdex 75 column in 20 mM Tris pH 7.5, 200 mM NaCl, 0.02% NaN3 and 1 mM TCEP. Purity was confirmed by SDS–PAGE and Coomassie blue staining. Protein concentration was measured by UV absorbance (280 nm).

Binding Assay SulfoLink

H3K9me0 and H3K9me3 peptides (aa 1-20 + Cys) (gift from A. Peters, Friedrich Miescher Institute for Biomedical Research, Basel, Switzerland) were reduced and coupled to SulfoLink beads (Thermo scientific) according to manufacturer's instructions. 25μM of recombinant His tagged CEC-4 CD and CEC-4 cd-2YA were incubated with the peptide-beads slurry (7µM peptide concentration) for 2 h at 4ºC on a rotator. After washing three times with 20mM Tris-HCl pH 7.5, 0.2M NaCl and 0.05% Triton X-100 for 1min-5min-1min, respectively, bound proteins were released from the beads, run on an SDS-PAGE gel, and stained by SYPRO® Ruby.

Peptide array library and AlphaScreen direct binding

AlphaScreen direct binding assays were performed in 384-well plate (ProxiPlate^{TM}-384 Plus, Perkin Elmer) with AlphaScreen Histidine Detection kit (Nickel Chelate, PerkinElmer #6760619) in optimized assay buffer (25mM HEPES, 100mM NaCl, 0.1% BSA, 0.05% Tween20, pH=7.5). The binding of CEC-4 CD to histone peptides was performed by AlphaScreen assay with ALTA Biosciences peptide array system (Alta Biosciences, UK). Three different peptide concentrations (62.5, 125 and 250nM) were used to screen histone peptides binding to CEC-4 CD (200nM). Quantitation was based on the intensity readout. The peptides with an intensity of 50-fold more than the control (assay condition without protein) were considered as hits. Table S4 shows raw data generated from AlphaScreen.

AlphaScreen direct binding was further used for confirmation of methylated H3K9 binding to CEC-4 CD. 3μl of 2-fold serial dilutions of N-terminal biotinylated histone $H3_{1-21}$K9 peptides, final concentration 0.5-500nM, were plated in a 384-well plate followed by adding 3μl of N-terminal His-tagged CEC-4 CD (final 200nM). After incubation at room temperature for 1 hour, 3μl of streptavidin-coated donor beads (20ug/ml) and 3μl of nickel chelate acceptor beads (20ug/ml) were then added under low light conditions. The plates were sealed and incubated at room temperature for 1 h, then read on an EnVision multilabel Plate Reader (Perkin Elmer).

Peptide displacement assay

IC50 (half maximal inhibitory concentration) for H3K9 peptides to CEC-4 CD were measured by AlphaScreen peptide displacement assay and done in duplicate. 2-fold series dilution of non-biotinylated H3K9 peptides starting from 100µM were used for competing with the binding of biotin-H3K9me2 (50nM) to CEC-4 CD (25nM). After incubation at room temperature for 1 hour, streptavidin-coated donor beads (20ug/ml) and nickel chelate acceptor beads (20ug/ml) were then added under low light conditions. The plate was then read on the EnVision using the AlphaScreen protocol after 1 hour incubation.

Isothermal Titration Calorimetry (ITC)

ITC was carried out on a MicroCal iTC200 calorimeter (GE Healthcare) at 25°C in 20 mM Tris-HCl pH7.5, 100 mM NaCl. 30 µM recombinant-cleaved CEC-4 CD and CEC-4 cd-2YA proteins were loaded into sample cell, 450μM histone $H3_{1-21}$K9 or $H3_{28-48}$K37 peptide solution was sequentially injected into sample cell; with exception of 800μM for $H3_{28-48}$K37me3 . Thermodynamic parameters N (stoichiometry), Ka (association constant), ΔH (enthalpic change) and ΔS (entropy change) were obtained by nonlinear least-square fitting using Origin software. ITC experiments were performed twice.

LEM-2 Chromatin Immuno-precipitation followed by deep sequ encing (ChIP-seq)

Wild-type, *met-2 set-25* and *cec-4* mutant strains were grown in parallel and in two independent biological replicas. For each strain, 400,000 L1 worms were grown synchronously in 500 ml S-medium containing HB101 *E. coli* strain, as food source, under continuous agitation (180 rpm) at 20ºC until gravid adults with early embryos were observed (between 60-65 hours depending on strain). Embryonic progeny was harvested using hypochlorite treatment. Embryos were cross-linked with 2.16% formaldehyde in M9 buffer for 30 minutes at room temperature, washed twice with M9 and once with FA buffer (50mM HEPES-KOH pH7.5, 1mM EDTA, 1% Triton X-100, 0.1% sodium deoxycholate, 150mM NaCl). LEM-2 ChIP was performed as described (Ikegami et al., 2010) with anti-LEM-2 (Novus Biologicals #48540002). Libraries were prepared from chromatin IP (1.7 -7.4 ng) and input (10 ng) samples using the NEBNext ultra DNA library prep kit for Illumina (NEB # 7370) and the NEBNext Multiplex Oligos for Illumina (NEB # E7335), according to the manufacturer's recommendations. No size selection was performed during sample preparation and the libraries were indexed and amplified using 15 PCR cycles, using the recommended conditions. After a final cleanup with Agencourt AmPure XP beads (Beckman # A63881), the library size distribution and concentrations were determined using a BioAnalyzer 2100 (Agilent technologies) and Qubit (Invitrogen) instrument, respectively. The final pools were prepared by mixing equimolar amounts of all individually indexed libraries and then sequenced on a HiSeq 2500 (Illumina) in Rapid mode (Paired-End 50). Processing of the LEM-2 ChIP-seq data, all paired-end ChIP-seq data (2x50bp) were mapped to the *C. elegans* genome (ce6) with the R package QuasR (Gaidatzis et al., 2015) (http://www.bioconductor.org/packages/3.1/bioc/html/QuasR.html) using the included aligner bowtie (Langmead et al., 2009) allowing only for uniquely mapping read pairs. The command

used to do the alignments was "proj<- qAlign("samples.txt","BSgenome.Celegans.UCSC.ce6")" which instructs bowtie to align using the parameters "--fr -m 1 --best --strata --maxins 500 --phred33-quals". Read density along the genome was calculated by tiling the genome into 200kb windows (non-overlapping) and counting the number of sequence fragments within each window. The command used to create the window count table was qCount(proj,regions,useRead="first"). This instructs QuasR to position each read at the middle of its respective fragment (determined by the two reads) and to only consider the first read (on any strand) for quantitation in order to avoid double counting. To compensate for differences in the read depths of the various libraries, we divided each sample by the total number of mapped reads and multiplied by the average library size. Log2 expression levels were calculated after adding a pseudocount of 1 (y=log2(x+1)). Finally, ChIP-seq signals are displayed as z-scores of IP – input.

RNA followed by deep sequencing (RNA-seq)

Wild-type, *met-2 set-25*, *cec-4* mutant strains were grown in two independent biological replicas. For each strain, 100,000 - 200,000 L1 worms were grown synchronously in 250 ml S-medium containing HB101 *E. coli* strain under continuous agitation (180 rpm) at 20ºC until gravid adults with early embryos were observed (between 60-65 hours depending on strain). Embryonic progeny was harvested using hypochlorite treatment, re-suspended in 500μl Trizol® and snap-freeze in liquid nitrogen. Extraction of RNA was performed according to the WormBook protocol (Stiernagle, 2006). Total RNA was purified using RNeasy kit (QIAGEN 74104) including DNase treatment. Depletion of ribosomal RNA was done for 5 μg of total RNA with Ribo-Zero™ Margnetic Gold Kit (Epicentre MRGZG12324) and further concentrated with RNA Clean & Concentrator™ kit (Zymo Research R1015) according to corresponding manufacturer's

instructions. From the depleted RNA 50ng were used for library preparation with the ScriptSeq v2 RNA-seq Library preparation kit (Epicentre). Equimolar pools of 3 samples were created and loaded on an Illumina HiSeq v3 flowcell using a cBot. Sequencing was performed on a HiSeq 2500 sequencer for 51 cycles running RTA 1.17.21.3. Samples were demultiplexed and FastQ files were generated using blc2fastq-1.8.4. Processing of the RNA-seq data, gene expression levels from RNA-seq data were quantified as described previously (Hendriks et al., 2014) using WormBase (WS190) annotation for coding transcripts and in windows of 500bp (unstranded) for the whole genome, in order to track non-genic changes.

Real-Time Quantitative PCR (RT-qPCR)

For gene expression levels in Fig. 5F same initial RNA extracts were used as for RNA-seq with addition of parallel grown and extracted cultures of *met-2* and *set-25* single mutant strains. For Fig. 6B three independent replicas of mixed stage embryo extracts were collected as described below in the Heat-shock induced muscle differentiation section. For Fig. S5C five independent early embryo extracts were used: starting from 25, 000 synchronized L1 worms of wild-type and *cec-4* mutant grown on peptone-rich (PR) plates with OP50 *E.coli* for 60-65 hours until gravid adults with early embryos were observed; RNA extraction was performed by 4 rounds of freeze cracking, treat with chloroform and transfer aqueous phase to Direct-zol™ column and follow manufacturer's instructions (30 minutes DNase I digestion included). For all RNA extracts cDNA synthesis was done with SuperScript® III First-Strand Synthesis System (Thermo Fisher Scientific 18080-051) according to manufacturer's instructions, starting from 1-2 μg of total RNA and using $(dT)_{20}$ oligos; RNase H treatment was included.

LEM-2 ChIP qPCR samples of corresponding genotypes were produced as described above for LEM-2 Chromatin Immuno-precipitation followed by deep sequencing.

All RT-qPCR reactions were done in 10μl volume, using diluted cDNA to 500ng or total volume of ChIPed and Input (10% of total material used) samples, with SYBR® Green PCR Master Mix (Life technologies 4309155) for Fig. 6B and 5F mRNA or GoTaq® Green Master Mix (Promega M712) for Fig. 5E and S5C according to manufacturer's instructions. Gene-specific primers (see Table S5) were used in 300nM concentration. StepOnePlus™ System (Life technologies 4376600) was used for qPCR run and data collection. Further analysis was done in Microsoft Excel.

All primer pairs were tested and selected for amplification efficiencies ranging from 90-100%, except for *unc-98* with 83%, *C18D6.4* with 73% and *myo-3* with 68%. For gene expression analysis $\Delta\Delta C_T$ method was used, *pmp-3* carried as housekeeping gene for sample normalization. For ChIP-qPCR ChIP sample data was normalized to corresponding input chromatin (reported as percentage input on figures).

Heat-shock induced muscle differentiation

Except for Fig. 6B, two cell stage embryos were isolated from transgenic gravid adults containing heat-shock (HS) expression construct *gvIs[hsp-16.2::hlh-1 rol6(su1006)]* and *gwIs4 [baf-1p::GFP-lacI::let-858 3'UTR; myo-3p::RFP]* or *[nhx-2p::npp-9::BLRP:GFP:3xHA-unc-54 3'UTR]* and different genetic backgrounds as stated in each figure; in Fig. 6C an extra *cec-4* mutant alone was carried as control for HS induction. Isolated embryos were incubated for 300 min at 22.5°C, either directly on agarose slides or in liquid inside humid chamber. All working genotypes reach embryonic bean stage after this incubation period. Embryos were shifted to 34°C for 10 min in a thermal cycler with a In-Situ slide block. Recovery from HS induction was done at 22.5°C in humid chamber and assessment of hatched larva-like worms was done in between 18 to 24 h after HS. Images were taken on stereomicroscope and/or spinning disk

confocal microscope, as appropriate. As controls for myogenic conversion we observed twitching and fluorescent reporter *myo-3p::RFP* bared in *gwIs4* array. For Fig. 6B, synchronized L1 worms of corresponding genotypes were plated on PR-plates with OP50 bacteria, and incubated for 2 days at 22.5°C until gravid adulthood. Embryonic progeny was harvested using hypochlorite treatment. Mixed stage embryos were split into three 1.5ml tubes with equal volumes: one tube was re-suspended in 500μl Trizol® and snap-frozen in liquid nitrogen (before HS condition), the rest were heat-shocked in a thermal cycler for 10 min at 34°C. They recovered at room temperature, one tube for 40 min (40' after HS) and second tube 24 h (24h after HS). Both tubes were re-suspended in Trizol® and snap-frozen like the "before HS" sample.

Supplemental Tables:

Table S2. List of yeast strains. Related to Experimental Procedures

Strain	Background	Genotype	Reference
GA-1340	W303	*can1-100* ***mlp1****::URA3* ***mlp2****::HIS3* ***esc1****::KanMx4*	(Andrulis et al., 2002)
GA-1469	W303	***mlp1****::TRP1*	(Hediger et al., 2002)
GA-1470	W303	***mlp2****::HIS3*	(Hediger et al., 2002)
GA-1526	W303	***mlp1****::TRP1,* ***mlp2****::HIS3*	(Hediger et al., 2002)
GA-1981	W303	*MATa/MATα, leu2-3,112/leu2-3,112, his3-11,15/his3-11,15, trp1-1/trp1-1, can1-100/can1-100, ade2-1/ade2-1, ura3-1/ura3-1 = W303 diploid*	(Thomas and Rothstein, 1989)
GA-2470	W303	***nup133****::HIS3*	(Bucci and Wente, 1998)
GA-3628	W303	*can1-100 NUP49::CFP-NUP49 URA3*	(Taddei et al., 2009)
GA-4887	W303	***mps3::mps3 delta75-150****KanMx6 tel1::URA*	(Schober et al., 2009)
GA-5306	W303	*can1-100* ***nup84****::His3*	(Nagai et al., 2008)
GA-5307	W303	*can1-100* ***nup120****::His3*	(Nagai et al., 2008)
GA-5545	W303	***src1****::hygro NUP49-GFP*	(Ferreira et al., 2011)
GA-5670	W303	***mlp1****::URA3* ***mlp2****::HIS3* ***siz2****::cloNAT*	(Ferreira et al., 2011)

Table S5. RT-qPCR primer pairs used in this study. Related to Figs. 5 and 6

Target	Sequence
srw-85 F	GCGTGTCCCGAAATAAAGTC
srw-85 R	GATCTTCAAGTCTCGAATGCAG
C18D6.4 F	TACAGTGCTCATCAACTTGCC
C18D6.4 R	GCAATAAGAAGAGCATCTTCAAGG
pmp-3 F	GTTCCCGTGTTCATCACTCAT
pmp-3 R	ACACCGTCGAGAAGCTGTAGA
genomic *srw-85* F	GTGAGATGTGCCTGAGGAGT
genomic *srw-85* R	CCTACCGCTATCCATTCACG
genomic *C18D6.4* F	CGGGCTCTGGATGAGGTAAT
genomic *C18D6.4* R	TGCTATTGGCGGGAGGCTTA
hlh-1 F	CAAAGAACGTGTCCGAATCC
hlh-1 R	TGAGAGGAAGTCACATAATCGT
myo-3 F	AGACAGGTTGAGGAGGCTGA
myo-3 R	TCTGATAAGCGCACTGGATG
F21D9.4 F	CAGAGTATACTACAAAGGACTGGAG
F21D9.4 R	AGCCGATTGAGGTTGATGAC
C25F9.5 F	TTTCATCACACGAGATGAGATGG
C25F9.5 R	GTATACGTAGGTAGCAAGTCCTG
Y43F8A.5 F	TTAATGATCCTCAACATGCGCT
Y43F8A.5 R	GAGGTGCTATCCGTAAGTGTG
unc-98 F	TCCAGATACAACAATGGATGACGA
unc-98 R	TGAGCACTTGAACTTCCGACA
unc-45 F	GCTGATGAATTATACACTGAAGC
unc-45 R	GAGCCTCTTTTGCGTCTTGA
pal-1 F	GGAAGTAGCAGTAGTGATAGTGG
pal-1 F	GAATCCCTGAAACTGTTGATAATCC

Table S6. Depletion of nuclear envelope components to address CEC-4-mCherry perinuclear localization in worms. Referred in text section "*CEC-4 is intrinsically localized at the nuclear periphery*"

RNAi of NE related gene	CEC-4-mCh localization
anc-1	Perinuclear ring
baf-1	Perinuclear ring
emr-1	Perinuclear ring
lem-2	Perinuclear ring
lmn-1	Perinuclear ring
sun-1	Perinuclear ring
unc-83	Perinuclear ring
unc-84	Perinuclear ring
zyg-12	Perinuclear ring

Table S7. Yeast mutations in nuclear envelope components used to address CEC-4-mCherry perinuclear localization in yeast. Referred in text section "*CEC-4 is intrinsically localized at the nuclear periphery*"

Mutation Tested	CEC-4-mCh localization
mlp1 mlp2 esc1	Perinuclear ring
mlp1	Perinuclear ring
mlp2	Perinuclear ring
mlp1 mlp2	Perinuclear ring
mlp1 mlp2 siz2	Perinuclear ring
nup133	Perinuclear ring
mps3::mps3 delta75-150 tel1	Perinuclear ring
nup84	Perinuclear ring
nup120	Perinuclear ring
src1	Perinuclear ring

Supplemental References

Andrulis, E.D., Zappulla, D.C., Ansari, A., Perrod, S., Laiosa, C.V., Gartenberg, M.R., and Sternglanz, R. (2002). Esc1, a Nuclear Periphery Protein Required for Sir4-Based Plasmid Anchoring and Partitioning. Mol Cell Biol *22*, 8292-8301.

Berrow, N.S., Alderton, D., Sainsbury, S., Nettleship, J., Assenberg, R., Rahman, N., Stuart, D.I., and Owens, R.J. (2007). A versatile ligation-independent cloning method suitable for high-throughput expression screening applications. Nucleic acids research *35*, e45.

Bucci, M., and Wente, S.R. (1998). A novel fluorescence-based genetic strategy identifies mutants of Saccharomyces cerevisiae defective for nuclear pore complex assembly. Mol Biol Cell *9*, 2439-2461.

Ferreira, H.C., Luke, B., Schober, H., Kalck, V., Lingner, J., and Gasser, S.M. (2011). The PIAS homologue Siz2 regulates perinuclear telomere position and telomerase activity in budding yeast. Nat Cell Biol *13*, 867-874.

Frokjaer-Jensen, C., Wayne Davis, M., Hopkins, C.E., Newman, B.J., Thummel, J.M., Olesen, S.-P., Grunnet, M., and Jorgensen, E.M. (2008). Single-copy insertion of transgenes in *Caenorhabditis elegans*. Nat Genet *40*, 1375-1383.

Gaidatzis, D., Lerch, A., Hahne, F., and Stadler, M.B. (2015). QuasR: quantification and annotation of short reads in R. Bioinformatics *31*, 1130-1132.

Hediger, F., Dubrana, K., and Gasser, S.M. (2002). Myosin-like proteins 1 and 2 are not required for silencing or telomere anchoring, but act in the Tel1 pathway of telomere length control. J Struct Biol *140*, 79-91.

Hendriks, G.J., Gaidatzis, D., Aeschimann, F., and Grosshans, H. (2014). Extensive Oscillatory Gene Expression during C. elegans Larval Development. Molecular cell *53*, 380-392.

Ikegami, K., Egelhofer, T.A., Strome, S., and Lieb, J.D. (2010). Caenorhabditis elegans chromosome arms are anchored to the nuclear membrane via discontinuous association with LEM-2. Genome Biol *11*, R120.

Langmead, B., Trapnell, C., Pop, M., and Salzberg, S.L. (2009). Ultrafast and memory-efficient alignment of short DNA sequences to the human genome. Genome Biol *10*, R25.

Meister, P., Towbin, B.D., Pike, B.L., Ponti, A., and Gasser, S.M. (2010). The spatial dynamics of tissue-specific promoters during C. elegans development. Genes & Development *24*, 766-782.

Nagai, S., Dubrana, K., Tsai-Pflugfelder, M., Davidson, M.B., Roberts, T.M., Brown, G.W., Varela, E., Hediger, F., Gasser, S.M., and Krogan, N.J. (2008). Functional Targeting of DNA Damage to a Nuclear Pore-Associated SUMO-Dependent Ubiquitin Ligase. Science *322*, 597-602.

Rohner, S., Kalck, V., Wang, X., Ikegami, K., Lieb, J.D., Gasser, S.M., and Meister, P. (2013). Promoter- and RNA polymerase II-dependent hsp-16 gene association with nuclear pores in Caenorhabditis elegans. J Cell Biol *200*, 589-604.

Schindelin, J., Arganda-Carreras, I., Frise, E., Kaynig, V., Longair, M., Pietzsch, T., Preibisch, S., Rueden, C., Saalfeld, S., Schmid, B., *et al*. (2012). Fiji: an open-source platform for biological-image analysis. Nat Methods *9*, 676-682.

Schober, H., Ferreira, H., Kalck, V., Gehlen, L.R., and Gasser, S.M. (2009). Yeast telomerase and the SUN domain protein Mps3 anchor telomeres and repress subtelomeric recombination. Genes & development *23*, 928-938.

Sommer, C.S., C.; Köthe, U.; Hamprecht, F. A. (2011). ilastik: Interactive Learning and Segmentation Toolkit. Eighth IEEE International Symposium on Biomedical Imaging (ISBI) Proceedings, 230-233.
Stiernagle, T. (2006). Maintenance of C. elegans. WormBook, 1-11.

Taddei, A., Van Houwe, G., Nagai, S., Erb, I., van Nimwegen, E., and Gasser, S.M. (2009). The functional importance of telomere clustering: Global changes in gene expression result from SIR factor dispersion. Genome Research *19*, 611-625.

Thomas, B.J., and Rothstein, R. (1989). The genetic control of direct-repeat recombination in Saccharomyces: the effect of rad52 and rad1 on mitotic recombination at GAL10, a transcriptionally regulated gene. Genetics *123*, 725-738.

Timmons, L., Court, D.L., and Fire, A. (2001). Ingestion of bacterially expressed dsRNAs can produce specific and potent genetic interference in *Caenorhabditis elegans*. Gene *263*, 103-112.

Waterhouse, A.M., Procter, J.B., Martin, D.M., Clamp, M., and Barton, G.J. (2009). Jalview Version 2--a multiple sequence alignment editor and analysis workbench. Bioinformatics *25*, 1189-1191.

CHAPTER 4: HISTONE DEGRADATION IN RESPONSE TO DNA DAMAGE ENHANCES CHROMATIN DYNAMICS AND RECOMBINATION RATES

Hauer, M. H., A. Seeber, V. Singh, R. Thierry, R. Sack, A. Amitai, M. Kryzhanovska, J. Eglinger, D. Holcman, T. Owen-Hughes and S. M. Gasser (2017). "Histone degradation in response to DNA damage enhances chromatin dynamics and recombination rates." Nat Struct Mol Biol 24(2): 99-107.

Author contributions: M.H.H. and S.M.G. wrote the manuscript. M.H.H. designed experiments and analyzed the data. M.H.H. performed most of the experiments. A.S. contributed to experimental design, data analysis and writing of the manuscript, and performed high-speed live-cell tracking after Zeocin treatment. M.H.H. planned and M.H.H. and A.S. performed the ectopic integration assays and the Rad52-YFP recovery assay. M.K. assisted in ectopic recombination assays. V.S. and T.O.-H. performed and analyzed genome-wide nucleosome mapping. A.A. and D.H. performed biophysical analysis of high-speed tracking data. R.T. performed and maintained the coding for 3D SIM-data analysis. R.S. performed all mass spectrometry measurements and the analysis of label-free experiments. J.E. performed and maintained the coding of tools for 3D interspot distance measurements. All the authors discussed the data and participated in the preparation of the manuscript.

Summary

This chapter presents my main project as a PhD student in the Gasser laboratory. In the following study, we show that cellular levels of histones drop 20–40% in response to DNA damage. Histones were degraded by the proteasomes which was dependent on both both the DNA damage checkpoint and the INO80 nucleosome remodeler. We confirmed reductions in histone levels by stable isotope labeling of amino acids in cell culture (SILAC)-based mass spectrometry, genome-wide nucleosome mapping and fluorescence microscopy. Chromatin compaction and increased fiber flexibility accompanied histone degradation, both in response to DNA damage and after artificial reduction of histone levels. As a result, recombination rates and DNA-repair focus turnover were enhanced. We propose that a generalized reduction in nucleosome occupancy is an integral part of the DNA damage response in yeast that provides mechanisms for enhanced chromatin mobility and homology search.

Histone degradation in response to DNA damage enhances chromatin dynamics and recombination rates

Michael H Hauer[1,2], Andrew Seeber[1,2], Vijender Singh[3], Raphael Thierry[1], Ragna Sack[1], Assaf Amitai[4,5], Mariya Kryzhanovska[1], Jan Eglinger[1], David Holcman[4], Tom Owen-Hughes[3] & Susan M Gasser[1,2]

Nucleosomes are essential for proper chromatin organization and the maintenance of genome integrity. Histones are post-translationally modified and often evicted at sites of DNA breaks, facilitating the recruitment of repair factors. Whether such chromatin changes are localized or genome-wide is debated. Here we show that cellular levels of histones drop 20–40% in response to DNA damage. This histone loss occurs from chromatin, is proteasome-mediated and requires both the DNA damage checkpoint and the INO80 nucleosome remodeler. We confirmed reductions in histone levels by stable isotope labeling of amino acids in cell culture (SILAC)-based mass spectrometry, genome-wide nucleosome mapping and fluorescence microscopy. Chromatin decompaction and increased fiber flexibility accompanied histone degradation, both in response to DNA damage and after artificial reduction of histone levels. As a result, recombination rates and DNA-repair focus turnover were enhanced. Thus, we propose that a generalized reduction in nucleosome occupancy is an integral part of the DNA damage response in yeast that provides mechanisms for enhanced chromatin mobility and homology search.

The genomic DNA of eukaryotes is highly organized and packed into chromatin. The most basic unit of chromatin is the nucleosome, which is formed by 146 bp of DNA that wrap around an octameric core of histone proteins. Chromatin remodelers use the energy from ATP hydrolysis to change the local state of chromatin by sliding/spacing or ejecting nucleosomes. These actions regulate gene transcription[1], replication[2], chromatin structure and DNA repair genome-wide[3,4]. Cellular genomes are constantly exposed to different sources of DNA damage, requiring the repair machinery to both disrupt and restore chromatin structure[5]. Heterochromatic chromatin tends to obstruct protein access to repair sites. Moreover, DNA double-strand breaks (DSBs) found in heterochromatin relocate to the edge of such domains[6–8], a phenomenon that requires a certain degree of physical mobility.

In budding yeast and human cells exposed to DNA damage, an increase in chromatin mobility has been observed both at lesions[9–11] and at undamaged sites where no DSBs could be detected[10,12]. The chromatin remodeler INO80-C and activation of the DNA damage checkpoint (DDC) were implicated in both processes[9,10,12]. Functionally, enhanced local DSB mobility was shown to be correlated with efficient repair by homologous recombination[9]. Modeling algorithms (A.A., A.S., S.M.G. and D.H., unpublished observations) suggest that mobility could enhance the search for the donor sequence required for homology-based repair, and elevated chromatin mobility was shown to result in genomic translocations in human cells[11]. However, the mechanisms that underlie enhanced chromatin mobility have remained elusive. Here we show that nucleosome degradation triggered by remodelers and checkpoint proteins enhances chromatin movement and accessibility, and promotes efficient repair.

RESULTS

DNA damage triggers extensive histone loss from chromatin

To investigate whether DNA damage and DDC activation affect chromatin structure and/or composition genome-wide, we used quantitative SILAC mass spectrometry in *Saccharomyces cerevisiae* and measured histone abundance before and after acute treatment (1 h) with the radiomimetic drug Zeocin. Relative ratios of nonmodified histone peptides (damage versus control, unlabeled ('light' (L)) versus labeled ('heavy" (H)) peptides) indicated a substantial loss of 20% ± 6% of the core histones H2A, H2B, H3 and H4 (**Fig. 1a** and **Supplementary Fig. 1**). Interestingly, levels of the histone variant Htz1 (H2A.Z) remained rather stable. Quantitative immunoblot analysis confirmed our observations and showed robust DDC activation (γH2A signal, Rad53 upshift) along with a dose-dependent relationship between histone H3/H4 loss and Zeocin treatment (**Fig. 1b**). We observed the same effect when we used another source of DNA damage, ionizing radiation (γ-IR) (**Supplementary Fig. 2a–d**).

Despite being highly quantitative for protein abundance, mass spectrometry data do not distinguish between histone pools and nucleosomes, and they lack positional information. To investigate whether entire nucleosomes were lost globally after DNA damage or at specific genomic loci, we carried out genome-wide nucleosome mapping. We found that the positioning of nucleosomes around the promoters

[1]Friedrich Miescher Institute for Biomedical Research, Basel, Switzerland. [2]Faculty of Natural Sciences, University of Basel, Basel, Switzerland. [3]Centre for Gene Regulation and Expression, School of Life Sciences, University of Dundee, Dundee, UK. [4]Institut de Biologie de l'École Normale Supérieure, Ecole Normale Supérieure, Paris, France. [5]Present address: Institute for Medical Engineering & Science, The Massachusetts Institute of Technology, Cambridge, Massachusetts, USA. Correspondence should be addressed to S.M.G. (susan.gasser@fmi.ch).

Received 9 August 2016; accepted 1 December 2016; published online 9 January 2017; doi:10.1038/nsmb.3347

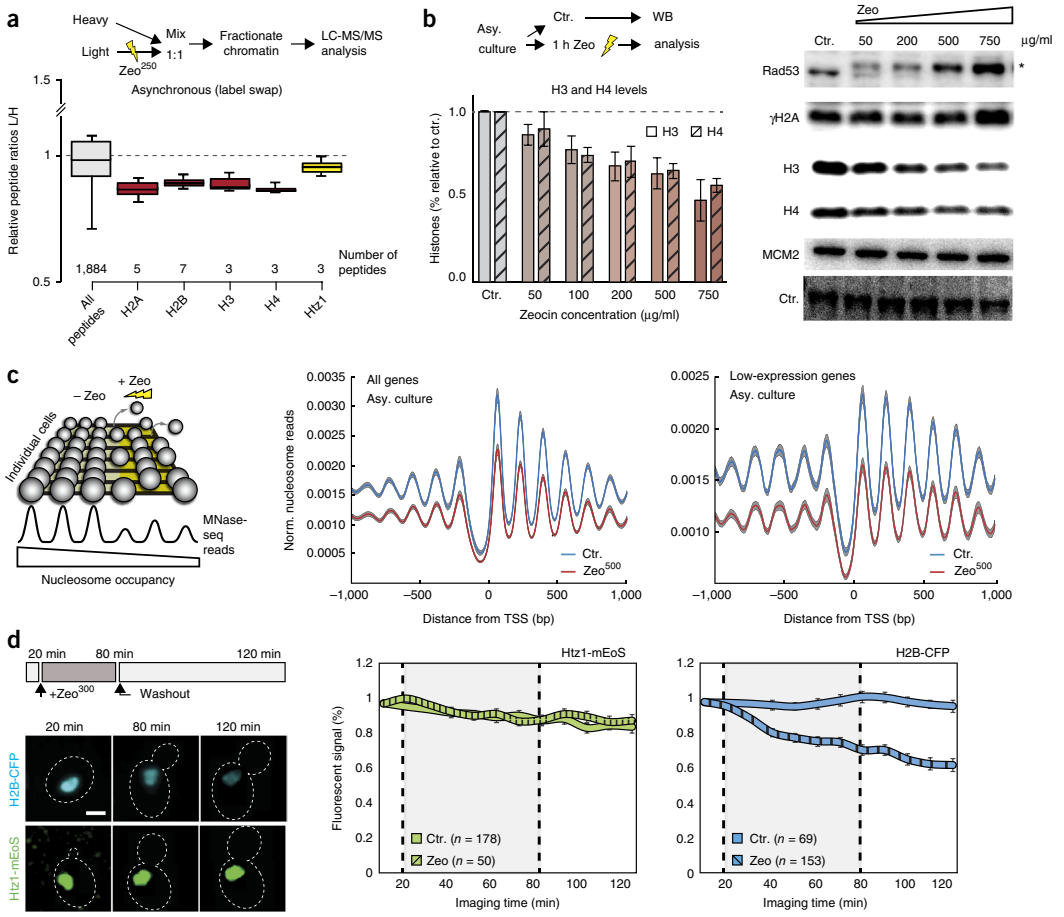

Figure 1 DNA damage triggers a global loss of core histones from chromatin. (**a**) Damage-dependent global histone degradation quantified by SILAC-based mass spectrometry on chromatin fractions from two independent cells pools (for further information see **Supplementary Fig. 1**). Box plots (with median, interquartile ranges and Tukey whiskers) show light/heavy (L/H) histone peptide distribution, indicating the degradation of core histones and, to a lesser extent, Htz1 (H2A.Z). Zeo^{250}, 250 µg/ml Zeocin. (**b**) Right: representative immunoblot analysis using antibodies to H3 and H4 on whole cell extracts from asynchronous (asy.) wild-type cultures in response to Zeocin treatment. Rad53 and γH2A were probed to confirm checkpoint activation. MCM2 was used to control for loading; here the control (Ctr.) represents bands on the Ponceau-stained membrane. The asterisk indicates a phosphorylation-dependent Rad53 mobility shift. Uncropped gel images are shown in **Supplementary Data Set 1**. Left: a schematic illustrating the experimental setup and a bar graph showing mean values and s.e.m. of immunoblot quantification of H3 and H4 blots from at least four independent experiments after Zeocin treatment, relative to the control condition. WB, western blotting. (**c**) Genome-wide nucleosome mapping. The scheme illustrates the effect of histone loss on nucleosome reads. Nucleosomal DNA fragments were sequenced from strain GA-6879 (wild type) grown in the absence (Ctr.) or presence of 500 µg/ml Zeocin (Zeo^{500}). The graphs show the distribution of nucleosome reads over all genes and over the 15% of genes with the lowest expression aligned to the transcription start site (TSS). Results are from four independent experiments (gray shading indicates ±s.d.). Norm., normalized. (**d**) Live single-cell microscopy of H2B-CFP and Htz1-mEos. Scale bar, 2 µm. Graphs show the experimental outline and the mean fluorescent signals and s.e.m. of individual cells (cell numbers indicated) per treatment over time relative to the control condition. The dashed lines in the graphs indicate the beginning and the end of Zeocin treatment. Source data are available online.

of yeast genes changed little after damage induction (**Fig. 1c**). To assess global changes in nucleosome abundance, we implemented internal standardization by mixing defined numbers of *Candida glabrata* cells with the experimental *S. cerevisiae* cells before chromatin preparations[13]. Normalization of the *S. cerevisiae* reads with respect to the *C. glabrata* reads showed a decrease in nucleosome occupancy both within promoters and across coding regions after Zeocin treatment (**Fig. 1c** and **Supplementary Table 1**). This effect was just as strong on a subset of 750 low-expression genes (**Fig. 1c**) as it was on highly transcribed genes (**Supplementary Fig. 2e**), which suggests that transcription is unlikely to regulate or drive the reduction. Finally, we found no preferential depletion in specific structural

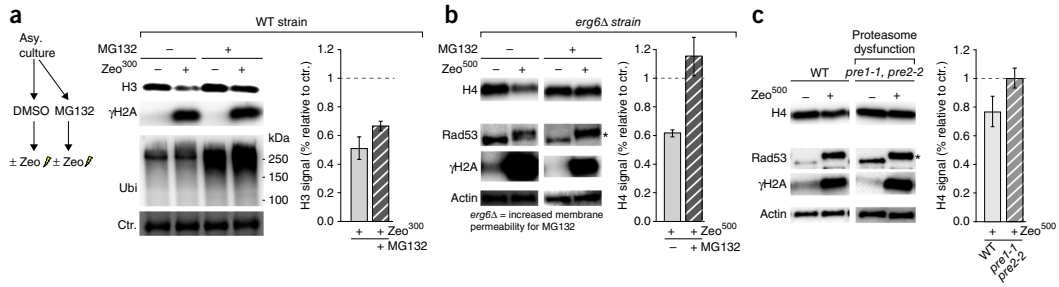

Figure 2 Histones are degraded by the proteasome. (**a**) Left: scheme illustrating the experimental setup. (**a**,**b**) Immunoblot analyses and quantification showing H3 (**a**) and H4 (**b**) levels before and after Zeocin treatment in whole cell extracts from asynchronously growing (Asy.) wild-type cells (**a**) or *erg6*Δ cells (**b**) treated with the proteasome inhibitor MG132 (both experiments were done in triplicate). MG132 permeability is increased in *erg6*Δ cells, which rescues histone H3 from being degraded. Antibodies to ubiquitin (Ubi) indicated proper function of the MG132 inhibitor, validating the experimental protocol. (**c**) Immunoblot analysis and quantification showing H4 levels in response to Zeocin treatment in wild-type and 26S proteasome dysfunctional cells (*pre1-1*, *pre2-2*) (the experiment was done in four replicates). Mutations in *PRE1* and *PRE2* suppress histone H4 degradation. Rad53 and γH2A were probed to confirm checkpoint activation. Actin and control show loading; control represents bands on the original gel (UV-TGX-stained). Uncropped gel images are shown in **Supplementary Data Set 1**. Bar graphs show mean ± s.e.m. Asterisks in **b** and **c** indicate a phosphorylation-dependent Rad53 mobility shift. Source data are available online.

elements such as centromeres or telomeres, in agreement with the idea that the effect is widespread.

To determine the kinetics of histone reduction, we used time-lapse live-cell tracking of functional fluorescently labeled ectopic histone H2B (H2B-CFP) or control Htz1-mEos, along with Nup49-GFP, which labels the nuclear rim (**Fig. 1d**, **Supplementary Fig. 2g** and **Supplementary Video 1**). We used microfluidic chambers to trap cells and pulse-treated the cells for 1 h with Zeocin, which generated roughly 4–7 DSBs per genome[14]. Histone H2B degradation (20% ± 1.7% compared with undamaged cells) occurred within 30 min of Zeocin exposure. We did not observe differential loss of either Nup49-GFP (**Supplementary Fig. 2f**) or the Htz1-mEos control after

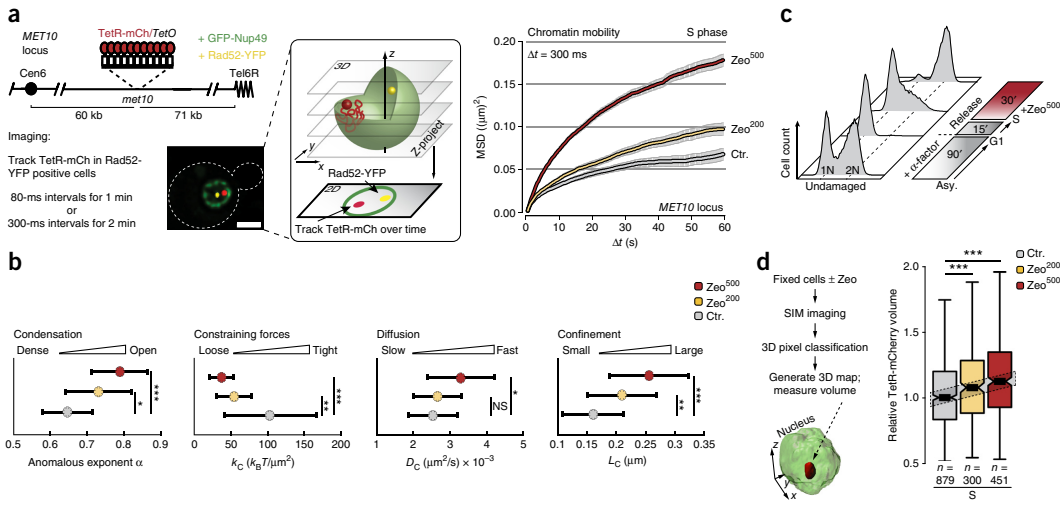

Figure 3 High-speed live-cell imaging and super-resolution microscopy show chromatin expansion and enhanced flexibility after DNA damage. (**a**) Diagram with representative image showing the experimental setup for high-speed imaging. The graph on the right shows mean squared displacement (MSD) analysis (Δt = 300 ms) of the *MET10* locus in response to Zeocin treatment, indicating dose-dependent increases in global chromatin mobility in response to DNA damage (n^{Ctr} = 23, $n^{Zeo^{200}}$ = 15, $n^{Zeo^{500}}$ = 21 different cells from three independent experiments). Scale bar, 2 μm. (**b**) Means (colored dots) and whiskers (±s.d.) of biophysical parameters derived from imaging data predict chromatin expansion and flexibility increases after Zeocin treatment. (**c**) Experimental outline and flow cytometry analysis of cell-cycle stages. (**d**) The 3D super-resolution imaging regime. The box plots show TetR-mCherry focus volume distributions after Zeocin treatment in S-phase cells relative to the control condition of multiple single cells (*n* values in graph) from two different cultures. MSD graph represents the mean ± s.e.m. (gray shaded region) of cells pooled from three independent experiments. Box plot represents median values (black rectangles), interquartile ranges and Tukey whiskers. The dashed rectangle highlights the trend of medians and is not a statistical value). $^*P < 0.05$, $^{**}P < 0.01$, $^{***}P < 0.001$, unequal-variance *t* test (**d**) or Kolmogorov–Smirnov test (**b**); NS, not significant. See **Supplementary Data Set 2** for mobility parameters and numbers of cells analyzed.

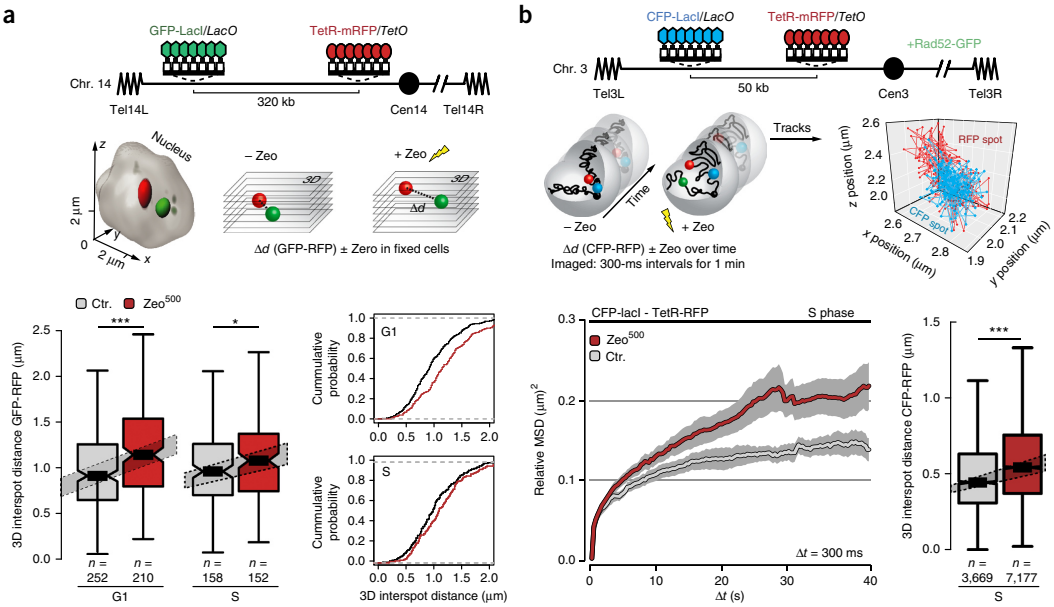

Figure 4 DNA damage increases chromatin flexibility. (**a**) Top: the experimental setup and procedure for 3D intrachromosomal distance measurements between two tagged loci on chromosome 14. Bottom: box plots and cumulative-distribution graphs showing GFP-to-mRFP distance distributions from multiple single cells (*n* values shown in graph) from two different cultures in fixed conditions before and after Zeocin treatment in G1 phase or after release into S phase. The gray dashed rectangles highlight the trend of medians and are not statistical values. (**b**) Top: live-cell imaging regime used to monitor distance changes between two loci on the left arm of chromosome 3 over time and after Zeocin treatment. Exemplary tracks indicate the movement of CFP and mRFP foci over time. Bottom left: relative MSD graph showing mean ± s.e.m. (gray shading) from multiple single (n^{Ctr} = 13, n^{Zeo} = 53) cells from two different cultures, indicating less constrained spot movement after DNA damage. Bottom right: box plots representing median values, interquartile ranges and Tukey whiskers and showing the distribution of all measured CFP-to-mRFP distances. *$P < 0.05$, ***$P < 0.001$; results from unequal-variances *t* tests.

DNA damage, which suggests that the induced histone degradation targets only core histones (**Fig. 1d**). Combined with our mass spectrometry and immunoblotting data, these results suggest the rapid degradation of histones, rather than simple eviction from chromatin. Previously, Gunjan and colleagues[15,16] showed that an excess of nonchromatin-bound histones is phosphorylated by the Rad53 checkpoint kinase and subsequently ubiquitinated and subjected to proteasomal degradation. This prompted us to test whether the proteasome inhibitor MG132 or mutation of the 26S proteasome (*pre1-1*, *pre2-2*)[17] would suppress the loss of histones from chromatin. Consistent with proteasome involvement, both the inhibitor and the mutations in *PRE1* and *PRE2* genes suppressed the DNA-damage-induced H3 or H4 degradation (**Fig. 2**). Moreover, by synchronizing cells in G1 phase before damage, we found that degradation occurred throughout the cell cycle (**Supplementary Fig. 3**).

We considered that the observed histone loss might be accentuated by impaired expression of histone genes, which are tightly regulated and show promoter-dependent upregulation in S phase. To eliminate this confounding factor, we placed the H3 and H4 genes under the control of the galactose promoter in a strain in which both endogenous H3 and H4 copies were deleted (histone-shutdown strain; **Supplementary Fig. 4a**). With constitutive H3/H4 expression (growth in media with low amounts of galactose), we found the same depletion effect after exposure to Zeocin as was noted in cells with endogenous histone genes, in agreement with the idea that DNA damage induces active degradation of histones, and not simply a loss of new histone synthesis (**Supplementary Fig. 4**). The loss of histones was rapid and so substantial that by 1 h after treatment, every third nucleosome could be removed from DNA. It is therefore likely that higher-order chromatin structure changes in response to DNA damage.

Damaged chromatin increases mobility, decompaction and flexibility

The increase in chromatin movement after DNA damage has been well documented, although the mechanisms leading to enhanced mobility remain elusive[12,18,19]. To see whether histone loss might be at the root of this phenomenon, we examined the physical characteristics of yeast chromatin under the same conditions that triggered histone loss. Using improved imaging protocols, we monitored the volume of chromatin domains in three-dimensional (3D) space, the inherent flexibility of the nucleosome polymer and the physical movement of fluorescently tagged sites.

Previous studies in which chromatin mobility was quantified used low sampling rates during live-cell imaging ($\Delta t = 1.5$ s) to determine the trajectory of a moving locus and the area explored (radius of constraint)[9–12,20]. However, such low time-resolved data yield little information on chromatin fiber compaction or flexibility. To resolve this, we used a novel high-speed imaging technique (300-ms or 80-ms imaging intervals) with which we confirmed that increased chromatin mobility can be

monitored at a nondamaged site (*MET10*) in cells responding to widespread DNA damage (**Fig. 3a** and **Supplementary Fig. 5a**). By applying an analysis based on polymer models to our high-speed imaging data (A.A., A.S., S.M.G. and D.H., unpublished), we estimated biophysical parameters that predict both the expansion of chromatin (reflected by an increase in the anomalous exponent α) and the loss of constraining forces that limit chromatin movement (as seen by a decrease in the spring constant K_C) (**Fig. 3b** and **Supplementary Fig. 5b**).

To examine whether the 3D volume of a defined chromatin domain was altered in the nucleus, we used super-resolution microscopy coupled with subsequent machine-learning and 3D pixel-classification analysis. Using this technique, we measured the change in volume of TetR-mCherry-tagged chromosomal loci (chromatin expansion) in cells fixed 30 min after exposure to different amounts of Zeocin (**Fig. 3c**). Indeed, we scored a dose-dependent decompaction of S-phase chromatin: 3D TetR-mCherry foci volumes expanded with increased amounts of damage (**Fig. 3d**).

The second prediction from the polymer modeling of locus dynamics was that the flexibility of the chromatin fiber would be enhanced after DNA damage. Thus, we monitored chromatin flexibility with confocal microscopy and measured the 3D distances between two differentially labeled genomic loci positioned on the same chromosome arm. We used two independent sets of loci spaced at genomic distances of either 320 kb on chromosome 14 or 50 kb on chromosome 3. For the first set, we synchronized cells, fixed them before or after Zeocin treatment and then calculated the average of all distances measured between the lacI-GFP and TetR-mRFP fluorescently tagged loci (**Fig. 4a**). We found that after DNA damage, the average interspot distance increased substantially in both G1-phase (0.97–1.2 μm) and S-phase (0.99–1.12 μm) cells. For the second set of data, we took a similar approach, but we measured the distance between CFP-lacI-tagged and TetR-mRFP-tagged foci on chromosome 3 in real time (**Supplementary Video 2**). In all cases we included Rad52-GFP and ensured that there was no overlap of Rad52-GFP with either of the other two fluorescent signals, thus ensuring that the measured changes did not arise from effects linked to local DNA repair events. Analysis of changes in relative mean squared distance and of the average of all measured distances revealed a robust increase in interspot dynamics and distances after Zeocin treatment (**Fig. 4b**). These data are consistent with a model in which damage-triggered histone degradation reduces the amount of nucleosome-mediated compaction within the chromatin fiber, causing chromatin to expand. The enhanced physical dynamics would thus be a reflection of increased flexibility.

Histone abundance dictates chromatin movement and decompaction

To confirm that increased chromatin mobility and decompaction arise as a consequence of histone loss, we made use of a histone-shutdown yeast strain that expresses H3 and H4 under the control of the *GAL1-GAL10* (*GAL1-10*) promoter, which is susceptible to media-controlled repression as well as induction (**Fig. 5a**). After 1 h in galactose, we released α-factor-arrested cells bearing this shutdown construct into raffinose-containing medium. Depending on the concentration of raffinose, we observed reduced *GAL1-10*-driven expression, which reduced histone levels in a controlled manner by 39% within an hour (**Supplementary Fig. 6a**,**b**). This artificial reduction of histones did not cause DDC activation, even when levels were reduced extensively (**Supplementary Fig. 6b**). By using the appropriate galactose:raffinose mixture, however, we were able to reduce histone levels in a controlled manner, even in the absence of damage (**Fig. 5b**). This reduction

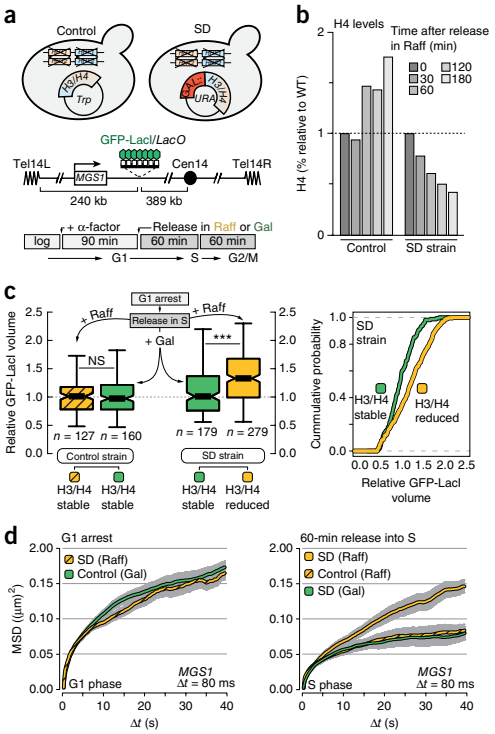

Figure 5 Artificial histone reduction in the absence of damage triggers chromatin expansion and increased motion. (**a**) Schematic showing a method for reducing H3 and H4 levels via transcriptional inhibition by releasing cells into media containing raffinose. A plasmid-borne construct in which the *GAL1-10* promoter drives the only pair of histone H3/H4 genes was used in the shutdown (SD) strain, whereas a plasmid carrying the wild-type *HHT1-HHF1* locus was used in the control strain. (**b**) Quantified immunoblot data showing histone H4 loss at different time points after H3/H4 shutdown in raffinose medium, from one experiment (**Supplementary Fig. 6**). (**c**) Box plots and cumulative-density graph showing volume distributions of data derived from 3D structured illumination microscopy (SIM) on multiple single cells (*n* values in graph) from two different cultures with tagged *MGS1* loci after controlled histone H3/H4 shutdown. Data are presented relative to the control condition (hatched yellow box plot). The lower and upper horizontal dashed lines in the cumulative-density graph indicate 0% and 100%, respectively. Box plots represent median values, interquartile ranges and Tukey whiskers. $^{***}P < 0.001$; NS, not significant; results from unequal-variances *t* tests. (**d**) MSD analysis of the *MGS1* locus in response to controlled histone-level reductions. The graph on the right shows enhanced chromatin movement of the *MGS1* locus after controlled histone shutdown via 60-min release into S phase in raffinose-containing medium ($n^{SD\ (Raff)} = 30$, $n^{Control\ (Raff)} = 34$, $n^{SD\ (Gal)} = 52$ different cells from three independent experiments). The graph on the left shows that G1-phase chromatin was more mobile than S-phase chromatin but did not further increase mobility after H3/H4 repression in raffinose-containing medium ($n^{SD\ (Raff)} = 30$, $n^{Control\ (Gal)} = 97$ different cells from three independent experiments). Both MSD graphs show the mean ± s.e.m. (gray shading) of cells pooled from at least three different experiments. See **Supplementary Data Set 2** for mobility parameters and numbers of cells analyzed. Source data are available online.

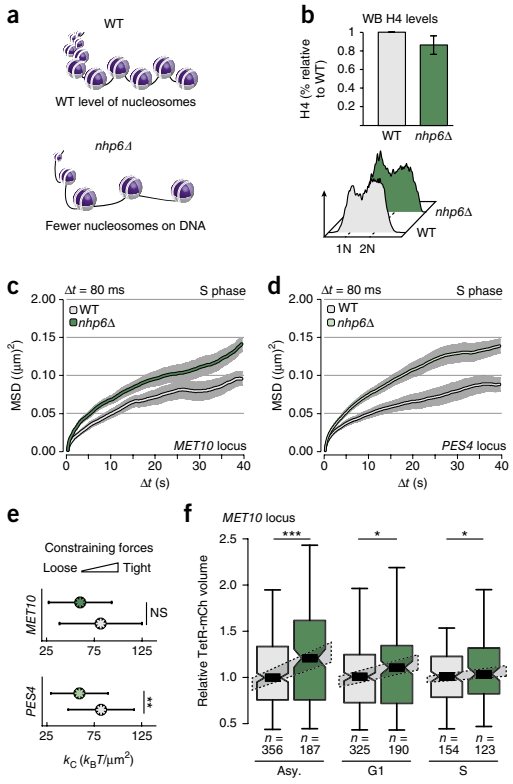

Figure 6 Loss of high-mobility-group proteins NHP6A and NHP6B links reduced nucleosome occupancy to chromatin expansion and enhanced mobility. (**a**) Cells carrying deletions of both *NHP6A* and *NHP6B* (*nhp6*Δ) have fewer nucleosomes on DNA than wild-type cells. (**b**) Immunoblot quantification from three experiments confirmed reduced histone levels in *nhp6*Δ cells, and flow cytometry analysis showed similar cell-cycle profiles for wild-type and *nhp6*Δ cells. (**c**,**d**) MSD graphs derived from high-speed live cell imaging data of *nhp6*Δ cells, highlighting enhanced chromatin mobility at two independent genomic loci, *MET10* (**c**) and *PES4* (**d**) ($n^{MET10,WT}$ = 31, $n^{MET10,nhp6\Delta}$ = 47, $n^{PES4,WT}$ = 35, $n^{PES4,nhp6\Delta}$ = 57 different cells from three independent experiments). (**e**) Graphs showing the means (colored dots) and whiskers (±s.d.) of biophysical parameters derived from imaging data, predicting concurrent loss of constraining forces on chromatin. Color-coded as in **b**. (**f**) Box plots showing *MET10* (TetR-mCherry) foci volumes resulting from 3D-SIM microscopy in multiple asynchronous (asy.) G1-phase or S-phase *nhp6*Δ and wild-type cells (*n* values in graph) from two different cultures, indicating chromatin expansion in *nhp6*Δ cells. Color-coded as in **b**. All bar graphs and MSD graphs (cells pooled from at least three independent experiments) represent the mean ± s.e.m. Box plots in **f** represent median values, interquartile ranges and Tukey whiskers. $^*P < 0.05$, $^{**}P < 0.01$, $^{***}P < 0.001$, Kolmogorov–Smirnov tests (**e**) or unequal-variances *t* tests (**f**). See **Supplementary Data Set 2** for mobility parameters and numbers of cells analyzed. NS, not significant.

provoked both chromatin decompaction (**Fig. 5c**) and a striking increase in chromatin mobility, measured at the *MGS1* locus after 1 h on the defined medium (**Fig. 5d**).

To further validate these findings, we made use of a mutant bearing deletions of two high-mobility group protein 1 (HMGB1) gene orthologs, *NHP6A* and *NHP6B* (*nhp6aΔnhp6bΔ*, for simplicity referred to here as *nhp6*Δ), that was previously described as having reduced levels of core histone proteins[21] (**Fig. 6a**). We observed that *nhp6*Δ did not trigger endogenous damage checkpoints and showed neither an altered flow cytometry distribution (**Fig. 6b**) nor Rad53 activation (**Supplementary Fig. 7a**), yet by tracking chromatin mobility with the high-speed imaging regime we found that the mobility of two labeled foci, *MET10* and *PES4*, was markedly enhanced in *nhp6*Δ cells (**Fig. 6c**,**d** and **Supplementary Fig. 7b**). High-resolution time-lapse imaging of the GFP-LacI-tagged *PES4* or the TetR-mCherry-tagged *MET10* locus further confirmed an increase in chromatin flexibility, reflected in a decrease in the spring constant K_C, and a positive trend in the anomalous exponent α (**Fig. 6e** and **Supplementary Fig. 7c**,**d**). Finally, using super-resolution microscopy we monitored an increase in the 3D volume of the TetR-mCherry-labeled *MET10* locus in *nhp6*Δ cells, which was more pronounced in an asynchronous culture, for unknown reasons (**Fig. 6f**). Combined with the effects observed in the histone-shutdown strain, these manipulations argue for a direct link between histone levels and chromatin movement.

Histone loss depends on checkpoints and INO80-C and modulates recombination efficiency

DNA damage activates the central DDC kinase Mec1 (ATR), which initiates a widespread phosphorylation cascade leading to a global damage response and cell-cycle arrest. Additionally, repair proteins such as Mre11, Exo1, Rad51 and Rad52 act locally on DNA to mediate resection and preparation for either repair by homologous recombination or end-joining. Among Mec1 targets are the downstream effector kinase Rad53 (CHK2)[22] and multiple subunits of the INO80-C remodeler[23,24]. Because both INO80-C and DDC proteins have been implicated in a general increase in chromatin mobility in response to DNA damage[12], we hypothesized that these factors might also regulate histone loss, which we have shown can trigger enhanced chromatin mobility.

Using immunoblotting, we found that in strains lacking checkpoint kinase Mec1 or Rad53, histone degradation after Zeocin treatment was completely abolished (**Fig. 7a**,**b**). More strikingly, the same dependency was observed for three strains with deletion of Arp8, Ies4 or Arp5, respectively, INO80-C subunits that do not contribute to the DDC but are required for nucleosome remodeling (**Fig. 7a**,**b**). Importantly, histone loss occurred independently of Rad51 and Exo1, which shows that local repair events are not necessary for the DDC-triggered degradation of histones. We further confirmed this with two other assays: H2B-CFP fluorescence monitoring over time (**Fig. 7c**) and super-resolution microscopy of tagged locus 3D volumes (**Fig. 7d**). In all cases we found that histone loss and chromatin expansion required the Mec1-mediated checkpoint and intact INO80-C: no histone loss or chromatin expansion was seen in *mec1Δsml1Δ*, *rad53*Δ or *arp8*Δ strains, whereas cells bearing *sml1*Δ (a control for the *mec1Δsml1Δ*) and *rad51*Δ behaved like their wild-type counterparts in response to damage (**Fig. 7c**,**d**).

The main role of the DDC kinase Mec1 is to trigger a cell-wide stress response that helps the cell cope with DNA damage. This seems to be, at least in part, mediated by the remodeler INO80-C[23,24]. The importance of chromatin remodeling in histone degradation is not entirely surprising, given that INO80 was recently shown to interact with CDC48, an AAA^+ ATPase involved in proteasome-dependent protein degradation[25]. Moreover, both MEC1 and INO80-C are linked to RNA polymerase II eviction at sites of replication fork–transcription collision[24]. Thus, these genetic dependencies further validate our hypothesis that histone degradation and chromatin expansion are the key phenomena underlying damage-enhanced chromatin movement (**Fig. 7e**). Our

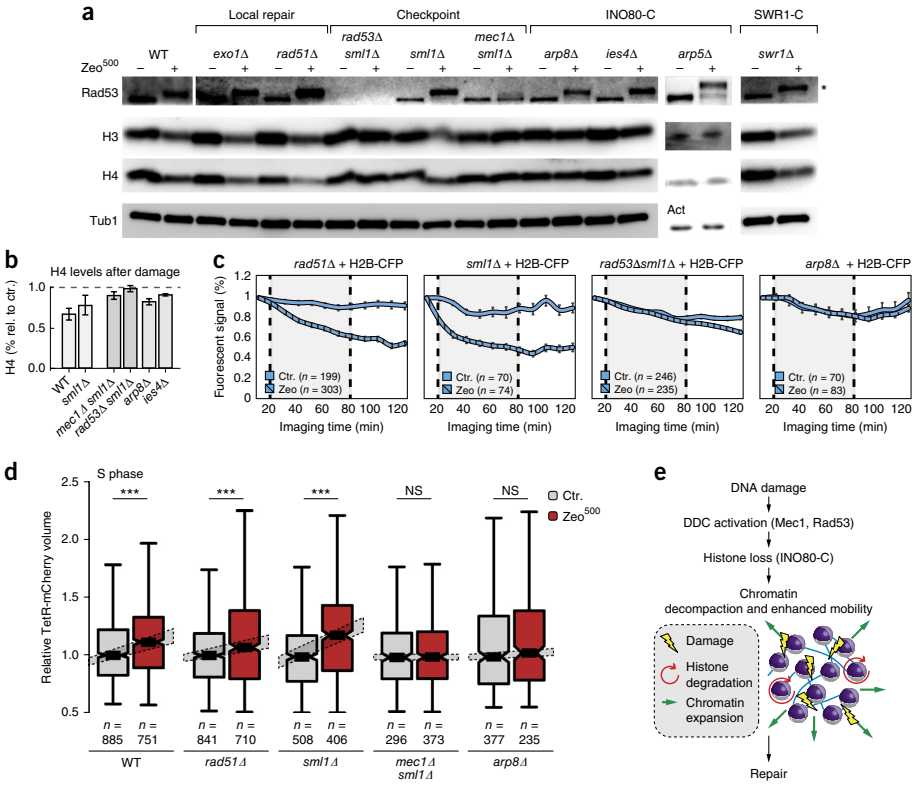

Figure 7 INO80-C and checkpoint proteins regulate histone degradation and chromatin expansion in response to damage. (**a**) Representative results from immunoblotting with H3- and H4-specific antibodies on whole cell extracts from wild-type cells and different mutants in response to DNA damage. Rad53 was probed to confirm checkpoint activation; tubulin (Tub1) or actin (Act) was used as a loading control. Asterisk indicates a phosphorylation-dependent Rad53 mobility shift. Uncropped gel images are shown in **Supplementary Data Set 1**. (**b**) Immunoblot quantification (mean and s.e.m.) of wild-type cells, checkpoint mutants and INO80-C mutants from blots derived from $n^{WT} = 8$, $n^{sml1\Delta} = 3$, $n^{mec1\Delta sml1\Delta} = 3$, $n^{rad53\Delta sml1\Delta} = 3$, $n^{arp8\Delta} = 3$, and $n^{ies4\Delta} = 3$ different experiments. (**c**) Results from live single-cell microscopy of H2B-CFP in local repair, checkpoint and INO80-C mutants after Zeocin treatment. Graphs show the mean fluorescent signals of all individual cells (cell numbers indicated in graph) per treatment over time relative to the control condition. Vertical dashed lines indicate the beginning and end of Zeocin treatment. Graphs show mean ± s.e.m. (**d**) TetR-mCherry focus volume distributions after Zeocin treatment in wild-type and various mutant cells (*n* values in graph) from two different cultures in one experiment that were released into S phase; data shown relative to the control condition. INO80-C and Mec1 are required for chromatin expansion. Box plots show median values, interquartile ranges and Tukey whiskers. $***P < 0.001$; NS, not significant; results from unequal-variances *t* tests. Source data are available online. (**e**) Model suggesting that checkpoint signaling triggers INO80-C-dependent histone loss, thus leading to subsequent chromatin expansion, enhanced mobility and chromatin flexibility, which ultimately enhance repair.

data further suggest that a failure to degrade histones might impair repair proteins' access to chromatin, providing an additional explanation for previously observed repair deficiencies in these mutants[26,27].

To examine the functional relevance of the observed DNA-damage-triggered reduction in nucleosome occupancy, and to test the hypothesis that nucleosome reduction facilitates homologous recombination and thus DNA repair, we made use of a recombination assay that monitors the integration rates of two different *URA3* cassettes (800-bp homology or 82-bp homology) at two independent loci (*MGS1* and *URA3*). In otherwise isogenic haploid strains, we impaired INO80-C activity by disrupting its nucleosome-binding subunit Arp8 (*arp8*Δ) or we deleted both *NHP6* genes, to reduce nucleosome levels genome-wide[21]. Consistent with previously reported recombination defects in *arp8*Δ strains[26,27], we observed reduced recombination rates in this mutant, whereas rates were significantly increased in the *nhp6*Δ strain (**Fig. 8a**). Interestingly, Liang *et al.*[16] showed that deletion of the histone H3-H4 copy-2 genes (*HHT2* and *HHF2*) can confer resistance to DNA-damaging agents and restore the viability of DDC mutants under stress conditions. Thus, we hypothesized that artificially lowering histone levels by removing NHP6 might rescue *arp8*Δ sensitivity and even increase the fitness of wild-type cells under damaging conditions. Using a recovery assay that scores cell survival after a 1-h treatment with increasing amounts of Zeocin, we found that *nhp6*Δ cells recovered better from acute DNA damage than a wild-type strain did, and that reducing nucleosome occupancy by deleting *NHP6* partially rescued the Zeocin sensitivity of an *arp8*Δ strain (**Fig. 8b**).

The observation that increased recombination rates in *nhp6*Δ cells stemmed from changes in nucleosome occupancy prompted us to

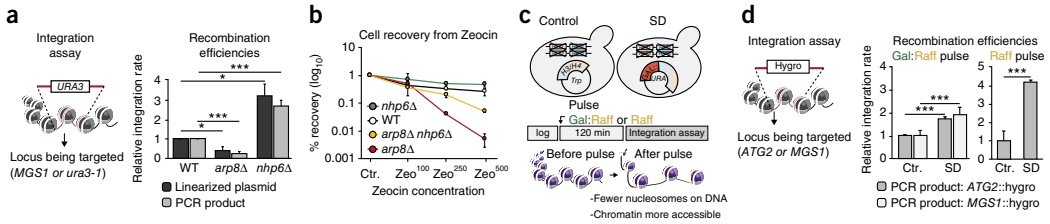

Figure 8 Reduced nucleosome occupancy enhances recombination and rescues *arp8*Δ sensitivity. (**a**) Ectopic recombination assay with two different integrative *URA3* cassettes in wild-type, *arp8*Δ and *nhp6*Δ strains. The diagram on the left shows that recombination takes place in the context of chromatin. The bar graph shows the mean integration frequency (+ s.e.m.) in selected mutants, relative to the wild type, from three independent cultures for each strain. (**b**) The average recovery rate of the wild type and various isogenic mutants from an acute treatment with different amounts of Zeocin; data shown relative to the control condition. Individual points indicate the mean over three independent replicates; error bars show ±s.e.m. (**c**) The workflow and the strains used to reduce H3 and H4 levels by means of transcriptional inhibition as in **Figure 5a**. (**d**) Ectopic recombination assay with two different hygromycin (hphMX4)-based constructs that target either the *ATG2* or the *MGS1* locus. The bar graph shows the mean integration frequency (± s.e.m.) of both constructs in the shutdown strain relative to the control strain after 120 min of pulsed histone H3/H4 reductions in galactose:raffinose (Gal:Raff; 1:20) or raffinose (Raff.) medium. Three independent cultures were tested. SD, shutdown strain. $^{*}P < 0.05$, $^{***}P < 0.001$, two-tailed paired Student's *t* tests. Source data are available online.

test whether gene-targeting rates could also be increased by other approaches that reduce histone levels. Hence, we used the same recombination assay in our histone-shutdown strain and followed the integration of two different hygromycin-resistance markers at either *ATG2* (*ATG2*::hygro) or *MGS1* (*MGS1*::hygro). This was done immediately after a 2-h incubation in raffinose-containing medium (raffinose only or a defined 1:20 galactose:raffinose mixture), which reduces histone H3 and H4 levels (**Fig. 8c**). Consistent with the *nhp6*Δ experiment, we found that a reduction of histone levels by means of transcriptional repression significantly enhanced the integration rates of both *ATG2*::hygro and *MGS1*::hygro PCR products (**Fig. 8d**).

Finally, we used fluorescence microscopy to follow the kinetics of Rad52-GFP focus formation and dissolution during 16 h after a brief exposure to Zeocin. We found fewer Rad52 (BRCA2) foci in *nhp6*Δ cells than in wild-type cells (**Supplementary Fig. 7e**). Given that Rad52 accumulates at sites of damage and disappears once recombination-mediated repair is completed[28], this result suggests that a reduction in histone levels enhances the turnover of the recombination-mediated repair reaction.

DISCUSSION

In a robust combinatorial approach, we used quantitative mass spectrometry, fluorescent live-cell microscopy and genome-wide nucleosome mapping to show that core histone proteins—but not the histone variant Htz1—are degraded from yeast chromatin when the genome is challenged by DNA damage. This requires checkpoint activation and INO80-C function and is mediated through the proteasome. Furthermore, reducing the levels of histones on DNA enhances chromatin mobility, decompaction and fiber flexibility. Proteins that function uniquely in recombination-mediated DNA repair (for example, Rad51 and Exo1) were not involved in histone loss, whereas the Mec1-target INO80-C, a chromatin remodeler implicated in efficient repair, is. Other studies have postulated a release of chromosomal tethers around the centromere as the source of altered chromatin mobility[20,29]. This, however, cannot account for the observed expansion of noncentromeric chromatin or for the observed dependence on INO80-C for these events. Furthermore, there is no evidence to date that centromeres delocalize in response to damage.

Although we cannot rule out that other mechanisms also contribute to nuclear or chromosomal motion, our data irrefutably demonstrate that a reduction in histone levels, even in the absence of DNA damage, is sufficient to decompact chromatin and enhance chromatin mobility. We suggest that histone degradation facilitates the search for donor sequences, an event required for DSB repair by homologous recombination with a nonsister template, and that chromatin decompaction might further enhance the access of DNA (both damage and template) to the repair machinery. However, mobility might also help disrupt improper pairing events during homologous recombination. Recombination assays indicate that a reduction in nucleosome occupancy brought about by *NHP6* deletion or by means of transcriptional histone gene repression increases gene-targeting rates and enhances the turnover rate of repair processes. Although controlled histone loss might facilitate repair, its misregulation and the resulting effects on chromatin structure and dynamics are likely to promote oncogenic translocations that might drive tumorigenesis.

Taken together, our study identifies histone loss as a fairly immediate response to DDC activation and implicates remodeler-dependent histone degradation as a novel and integral part of the yeast DNA damage response. We demonstrate how changes in chromatin composition can affect the physical characteristics of chromatin, and we show that artificial histone-level reduction can be used to increase recombination efficiency. Understanding how the post-translational modification status of histones and the entire chromatin proteome changes after DNA damage will require further investigation. We speculate that gene-targeting rates in mammalian cells can also be improved through manipulation of histone occupancy.

METHODS

Methods, including statements of data availability and any associated accession codes and references, are available in the online version of the paper.

Note: Any Supplementary Information and Source Data files are available in the online version of the paper.

ACKNOWLEDGMENTS

M.H.H. thanks S. Koren-Hauer for critical reading and assistance in preparing the manuscript, and V. Dion and H. Ferreira for fruitful discussions and advice. We thank V. Dion (Center for Integrative Genomics, University of Lausanne, Lausanne, Switzerland; strain GA-5816), J. Haber (Department of Biology and Rosenstiel Medical Center, Brandeis University, Waltham, Massachusetts, USA; strain JKM-179), B. Luke (Institute of Molecular Biology, Mainz, Germany; strain GA-3364), K. Bystricky (University of Toulouse, Toulouse, France; precursor strain for GA-9777, strain GA-9227), J.-M. Galan (Institut Jacques Monod, Paris, France;

strains GA-1364, GA-1365 and GA-1366) and F. Winston (Department of Genetics, Harvard Medical School, Boston, Massachusetts, USA; plasmids 3494 and 3495) for reagents and material. We are grateful for the technical assistance provided by L. Gelman (microscopy), S. Bourke (microscopy) and H. Kohler (FACS). M.H.H. thanks the Bioinformatics facility for help in getting started with R. We thank all members of the FMI Protein Analysis and Microscopy facilities for valuable advice and support. We thank all members of the Gasser laboratory for valuable discussions and technical support. M.H.H. was supported by a PhD fellowship of the Boehringer Ingelheim Fonds. S.M.G. thanks the HFSP, SNSF and the Novartis Research Foundation for support.

AUTHOR CONTRIBUTIONS

M.H.H. and S.M.G. wrote the manuscript. M.H.H. designed experiments and analyzed the data. M.H.H. performed most of the experiments. A.S. contributed to experimental design, data analysis and writing of the manuscript, and performed high-speed live-cell tracking after Zeocin treatment. M.H.H. planned and M.H.H. and A.S. performed the ectopic integration assays and the Rad52-YFP recovery assay. M.K. assisted in ectopic recombination assays. V.S. and T.O.-H. performed and analyzed genome-wide nucleosome mapping. A.A. and D.H. performed biophysical analysis of high-speed tracking data. R.T. performed and maintained the coding for 3D SIM-data analysis. R.S. performed all mass spectrometry measurements and the analysis of label-free experiments. J.E. performed and maintained the coding of tools for 3D interspot distance measurements. All the authors discussed the data and participated in the preparation of the manuscript.

COMPETING FINANCIAL INTERESTS

The authors declare no competing financial interests.

1. Boettiger, A.N. *et al.* Super-resolution imaging reveals distinct chromatin folding for different epigenetic states. *Nature* **529**, 418–422 (2016).
2. Aze, A., Sannino, V., Soffientini, P., Bachi, A. & Costanzo, V. Centromeric DNA replication reconstitution reveals DNA loops and ATR checkpoint suppression. *Nat. Cell Biol.* **18**, 684–691 (2016).
3. Gerhold, C.B., Hauer, M.H. & Gasser, S.M. INO80-C and SWR-C: guardians of the genome. *J. Mol. Biol.* **427**, 637–651 (2015).
4. Seeber, A., Hauer, M. & Gasser, S.M. Nucleosome remodelers in double-strand break repair. *Curr. Opin. Genet. Dev.* **23**, 174–184 (2013).
5. Soria, G., Polo, S.E. & Almouzni, G. Prime, repair, restore: the active role of chromatin in the DNA damage response. *Mol. Cell* **46**, 722–734 (2012).
6. Chiolo, I. *et al.* Double-strand breaks in heterochromatin move outside of a dynamic HP1a domain to complete recombinational repair. *Cell* **144**, 732–744 (2011).
7. Lemaître, C. *et al.* Nuclear position dictates DNA repair pathway choice. *Genes Dev.* **28**, 2450–2463 (2014).
8. Torres-Rosell, J. *et al.* The Smc5-Smc6 complex and SUMO modification of Rad52 regulates recombinational repair at the ribosomal gene locus. *Nat. Cell Biol.* **9**, 923–931 (2007).
9. Dion, V., Kalck, V., Horigome, C., Towbin, B.D. & Gasser, S.M. Increased mobility of double-strand breaks requires Mec1, Rad9 and the homologous recombination machinery. *Nat. Cell Biol.* **14**, 502–509 (2012).
10. Miné-Hattab, J. & Rothstein, R. Increased chromosome mobility facilitates homology search during recombination. *Nat. Cell Biol.* **14**, 510–517 (2012).
11. Roukos, V. *et al.* Spatial dynamics of chromosome translocations in living cells. *Science* **341**, 660–664 (2013).
12. Seeber, A., Dion, V. & Gasser, S.M. Checkpoint kinases and the INO80 nucleosome remodeling complex enhance global chromatin mobility in response to DNA damage. *Genes Dev.* **27**, 1999–2008 (2013).
13. Hu, B. *et al.* Biological chromodynamics: a general method for measuring protein occupancy across the genome by calibrating ChIP-seq. *Nucleic Acids Res.* **43**, e132 (2015).
14. Povirk, L.F., Wübter, W., Köhnlein, W. & Hutchinson, F. DNA double-strand breaks and alkali-labile bonds produced by bleomycin. *Nucleic Acids Res.* **4**, 3573–3580 (1977).
15. Gunjan, A. & Verreault, A. A Rad53 kinase-dependent surveillance mechanism that regulates histone protein levels in *S. cerevisiae*. *Cell* **115**, 537–549 (2003).
16. Liang, D., Burkhart, S.L., Singh, R.K., Kabbaj, M.H. & Gunjan, A. Histone dosage regulates DNA damage sensitivity in a checkpoint-independent manner by the homologous recombination pathway. *Nucleic Acids Res.* **40**, 9604–9620 (2012).
17. Heinemeyer, W., Kleinschmidt, J.A., Saidowsky, J., Escher, C. & Wolf, D.H. Proteinase yscE, the yeast proteasome/multicatalytic-multifunctional proteinase: mutants unravel its function in stress induced proteolysis and uncover its necessity for cell survival. *EMBO J.* **10**, 555–562 (1991).
18. Dion, V. & Gasser, S.M. Chromatin movement in the maintenance of genome stability. *Cell* **152**, 1355–1364 (2013).
19. Krawczyk, P.M. *et al.* Chromatin mobility is increased at sites of DNA double-strand breaks. *J. Cell Sci.* **125**, 2127–2133 (2012).
20. Strecker, J. *et al.* DNA damage signalling targets the kinetochore to promote chromatin mobility. *Nat. Cell Biol.* **18**, 281–290 (2016).
21. Celona, B. *et al.* Substantial histone reduction modulates genomewide nucleosomal occupancy and global transcriptional output. *PLoS Biol.* **9**, e1001086 (2011).
22. Sanchez, Y. *et al.* Regulation of RAD53 by the ATM-like kinases MEC1 and TEL1 in yeast cell cycle checkpoint pathways. *Science* **271**, 357–360 (1996).
23. Morrison, A.J. *et al.* Mec1/Tel1 phosphorylation of the INO80 chromatin remodeling complex influences DNA damage checkpoint responses. *Cell* **130**, 499–511 (2007).
24. Poli, J. *et al.* Mec1, INO80, and the PAF1 complex cooperate to limit transcription replication conflicts through RNAPII removal during replication stress. *Genes Dev.* **30**, 337–354 (2016).
25. Lafon, A. *et al.* INO80 chromatin remodeler facilitates release of RNA polymerase II from chromatin for ubiquitin-mediated proteasomal degradation. *Mol. Cell* **60**, 784–796 (2015).
26. Chen, X. *et al.* The Fun30 nucleosome remodeller promotes resection of DNA double-strand break ends. *Nature* **489**, 576–580 (2012).
27. van Attikum, H., Fritsch, O. & Gasser, S.M. Distinct roles for SWR1 and INO80 chromatin remodeling complexes at chromosomal double-strand breaks. *EMBO J.* **26**, 4113–4125 (2007).
28. Lisby, M., Barlow, J.H., Burgess, R.C. & Rothstein, R. Choreography of the DNA damage response: spatiotemporal relationships among checkpoint and repair proteins. *Cell* **118**, 699–713 (2004).
29. Verdaasdonk, J.S. *et al.* Centromere tethering confines chromosome domains. *Mol. Cell* **52**, 819–831 (2013).

ONLINE METHODS

Yeast growth, cell cycle arrests and flow cytometry. The yeast strains and plasmids used in this study are listed in **Supplementary Tables 2** and **3**. Yeast strains were all haploid and, except for the SILAC strain and the Htz1-mEos imaging control strain, were derived from the W303 background (**Supplementary Table 2**). Unless otherwise stated, yeast cultures were grown at 30 °C until logarithmic (log) growth phase (OD_{600} = 0.7; 1×10^7 cells/ml) before Zeocin (Invitrogen) or γ-IR exposure at 30 °C. Live-cell microscopy was done at 25 °C. Flow cytometry samples were prepared as previously described[30].

For controlled *GAL1-10*::H3/H4 expression experiments coupled with gene-targeting assays, GA-8386 and the relevant control strain culture (GA-8385) were grown overnight to saturation in YP galactose/raffinose (YP Gal/Raff) 1:5 medium. The next morning, cultures were inoculated in the same respective medium and grown until log growth phase (OD_{600} = 0.7; 1×10^7 cells/ml) before being subjected to pulsed histone-level reductions. After reaching log phase, cells were washed once, and pulsed H3 and H4 histone-level reductions were accomplished via growth in either prewarmed 30 °C YP Gal/Raff 1:20 or YP raffinose medium for 120 min before transformation with the respective gene-targeting selection cassettes. For further information about the gene-targeting assay, refer to the section "Ectopic recombination assays."

For cell-cycle arrest and release experiments, 1.5×10^{-8} M alpha factor (Zymo Research) was added to exponentially growing cultures at a density of OD_{600} = 0.5. After 1 h, another half of the initial amount of alpha factor was added for 30 min, and cells were either held in G1 phase or released into prewarmed medium for 15–25 min before Zeocin damage treatment in S phase. Cell fixation in the relevant experiments was done for 2 min at room temperature with 4% paraformaldehyde.

For all Zeocin or γ-IR experiments, saturated yeast overnight cultures were diluted to OD_{600} = 0.1 the next morning and grown to log phase. In all assays, Zeocin was added directly to G1-phase arrested, S-phase released or asynchronously growing log cultures. Cultures were incubated with the drug for 1 h before high-speed tracking microscopy, or for the time periods indicated in figures for other assays and experiments. For γ-IR exposure, 5 ml of cell culture was transferred to a 35 × 10-mm petri dish and irradiated in a Faxitron CellRad cell irradiator until the indicated dose (in grays) was reached. After γ-IR treatment, cells were directly harvested for further downstream western blotting or mass-spectrometry-based analysis. For undamaged conditions, either cells were imaged immediately for high-speed tracking microscopy, or growth was continued along with that of the treated samples for the time periods indicated in the figures. γ-IR undamaged control cells were also spread on petri dishes and harvested after irradiation of treated cells was complete. Further specific growth and treatment conditions for high-speed tracking live-cell microscopy were applied according to the procedure described in ref. 12.

The proteasome-inhibition assay with proteasome inhibitor MG132 (Bachem) was done according to the procedure described in ref. 31. In brief, wild-type GA-6879 (**Fig. 2a**) or *erg6*Δ (ref. 32) GA-1364 (**Fig. 2b**) cells were grown to saturation overnight in SC proline (wild-type, synthetic complete medium without ammonium sulfate but with 0.1% L-proline) or YPAD medium (GA-1364). The next morning, cells were inoculated to OD_{600} = 0.1 in SC (wild-type) or YPAD (GA-1364) proline medium supplemented with 0.003% SDS and grown to OD_{600} = 0.5 before the addition of 75 μM MG132, or of the same volume of DMSO for the control condition. After 30 min of incubation with the inhibitor, Zeocin treatment or no-damage control growth was carried out for 1 h at 30 °C before cell harvesting for western blotting.

For H2B-CFP (strain GA-3364 and derivatives) and two-foci (strain GA-9777) live-cell fluorescent microscopy, log-phase cells were trapped with three pulses of 5 p.s.i. pressure in CellASIC plates of the ONIX microfluidic perfusion system (Merck Millipore). All perfusions were done at a continuous flow rate of 2 p.s.i. pressure. After a 20–30-min recovery phase, cells were treated for 30 min with Zeocin before high-speed CFP-RFP tracking microscopy. The recovery phase of H2B-CFP-tagged cells was 20 min, after which they were treated with a pulse of Zeocin for 1 h, and H2B-CFP fluorescence was followed for an additional 40 min after treatment.

For constitutive H3/H4 expression or reduction experiments, GA-8386 and the relevant control strain culture (GA-8385) were grown overnight to saturation in YP galactose (YP Gal) or YP Gal/Raff medium and inoculated in the same respective media before Zeocin treatment and cell collection. For controlled H3/H4 shutdown experiments, overnight growth and growth to OD_{600} = 0.5 were done with the same strains in YP Gal/Raff (Gal/Raff 1:5 ratio) medium, which confers wild-type H3/H4 expression levels. After G1-phase arrest at 25 °C with alpha factor in YP Gal/Raff medium, cells were released into either prewarmed 25 °C YP Gal or YP Raff medium for 60 min before fixation for structured illumination microscopy (SIM) or high-speed live-cell imaging.

In all other western blotting and label-free mass spectrometry experiments, cells were grown in full medium (YPD), and cell growth for microscopy experiments was done in either synthetic complete medium or sterile, filtered, non-autoclaved YPD medium.

Genome-wide nucleosome mapping. Strains tested for changes in nucleosome occupancy (GA-6879 and GA-8386) were grown in appropriate media to OD_{600} = 0.8. Cultures were split in two, and one of the two was treated with Zeocin (500 μg/ml) for 1 h. At this point the OD_{600} absorbance of each sample was measured and *C. glabrata* cells were spiked in at 1/10 according to the sample OD_{600}. Cells were washed three times with ice-cold TBS (20 mM Tris-HCl, pH 8.0, and 150 mM NaCl) and lysed by bead-beating in micrococcal nuclease (MNase) digestion buffer (10 mM Tris, pH 8.0, 50 mM NaCl, 5 mM $MgCl_2$, 1 mM $CaCl_2$, 1 mM β-mercaptoethanol, 0.5 mM spermidine, 0.075% NP-40). The obtained chromatin samples were MNase digested to isolate mononucleosomes, and sequencing libraries were prepared according to the method described by Wiechens *et al.*[33]. Paired-end libraries of MNase-digested chromatin were sequenced using Illumina HiSeq technology. Fastq files containing raw reads were aligned to the *S. cerevisiae* and *C. glabrata* reference genomes by Bowtie2 with the option of a maximum fragment length of 500 for nucleosome fragments. The nucleosome dyads at each position were calculated in a defined window flanking the transcription start site (TSS). The sum of dyads at a given position across all TSSs was then normalized by the total number of nucleosome dyads across all positions flanking ~6,000 TSSs in the given window. We normalized the reads further against the number of *C. glabrata* reads in the sample. For low- and high-expression gene plots, the TSSs of 15% high-expression genes and 15% low-expression genes were chosen. The data were smoothed using a 50-bp sliding window for graphical representation. Plots were generated with Python's plotting modules matplotlib and pylab.

Quantitative western blot analysis. The total protein content in the relevant samples was determined with the Quant-iT protein assay kit (Thermo Fisher Scientific), and 8.75 μg of total protein was loaded and run on Criterion TGX Stain-Free 8–16% (Bio-Rad) gels under SDS denaturing electrophoresis conditions. Rapid fluorescent detection of all proteins in the gel or on the membrane was done according to the manufacturer's specifications, and protein transfer on PVDF membranes was done with the Trans-Blot Turbo system. All antibodies used for subsequent immunodetections are listed in **Supplementary Table 4**. Rad53 protein was detected with a custom-made mouse monoclonal antibody (GenScript) to the FHA2 domain of Rad53. Anti-γH2A was similarly a custom-made polyclonal antibody specific for phospho-S129 in yeast H2A. Titration curves of histone H3 and histone H4 antibodies were generated to work within the linear detection range before use (data not shown).

Chromatin fractionation and quantitative mass spectrometry. For SILAC-based mass spectrometry, lysine and arginine double-labeling of the *lys2*Δ *arg4*Δ strain yAG-06A was achieved by growth for at least ten generations in 'heavy' medium as described previously[34]. After growth to log phase or at G1 cell-cycle arrest, heavy-labeled cells (or 'light'-labeled cells for label-swap controls) were treated for 1 h with Zeocin and mixed 1:1 based on the exact cell count with light-labeled (or heavy-labeled for label-swap control), nontreated control cells. Prior to mixing, FACS and western blotting samples were taken to test for cell-cycle distribution and DDC activation.

Chromatin fractionation was carried out as previously described[35], with the modification that chromatin obtained from SILAC-labeled yeast samples was resuspended in urea buffer (50 mM Tris-HCl, pH 7.5, 6 M urea, 1% SDS, 5 mM EDTA) sonicated for optimal solubilization of proteins followed by a TCA protein-precipitation step before downstream mass spectrometric analysis. To avoid carbamylation in urea buffer, samples were kept below 20 °C and quickly processed. Control samples from whole cell extract, supernatant and the chromatin fraction were analyzed with SDS-PAGE (Novex 8–16% Tris-glycine gel, Invitrogen) gel electrophoresis followed by Coomassie staining.

doi:10.1038/nsmb.3347

Samples for label-free histone quantification came from log-phase or G1-phase arrested cells grown in YPD medium. After γ-IR treatment, 5 ml of culture was fixed with 10% TCA on ice. Whole cell lysates were obtained by bead-beating at 4 °C in urea buffer (50 mM Tris, pH 7.5, 6 M urea, 1% SDS, 5 mM EDTA). 100–150 µg of total protein was precipitated for downstream MS analysis.

For both SILAC and label-free samples, we carried out reduction and alkylation of cysteines in 20 µl of RCM buffer (0.5 M Tris, pH 8.6, 6 M GnHCl) by adding 4 µl of 100 mM TCEP (tris(2 carboxyethyl)phosphine) for 30 min followed by 4 µl of 250 mM iodoacetamide for another 30 min (in the dark), both at room temperature. Prior to the addition of 20 µl of 1 mg/ml LysC (Wako, Japan), the extracts were diluted two-fold to keep a final HEPES concentration of 20 mM. The first digestion was carried out overnight at 25 °C. After two-fold dilution, 100 µl of 0.5 mg/ml trypsin was added, and the second digestion was carried out at 37 °C overnight. Samples were desalted using SepPak C18 columns (Waters), and eluates were dried to completion in a SpeedVac (Thermo Fisher Scientific).

Both SILAC and label-free LC-MS/MS analyses were done on an Easy-nLC 1000 pump coupled to an LTQ Orbitrap Velos mass spectrometer (Thermo Fisher Scientific) using a Digital PicoView ion source (New Objective). Peptides were separated on a New Objective analytical column (75 µm × 25 cm, Reprosil, 3 µm) with a 150-min 0.1% formic acid–acetonitrile gradient. The flow rate was 200 nL/min, and injection volumes were adapted accordingly for 1 µg of peptides on column. Data were acquired in a Top20 data-dependent analysis mode. MS scans were acquired at a resolution of 60,000 over a range of m/z 350–1,200. We identified label-free peptides by searching Swiss-Prot using Mascot 2.4 (Matrix Science) and compiled them in Scaffold 3.0 (Proteome Software). SILAC peptides were identified with MaxQuant 1.4.1.2 via a search of the SGD database. Two missed cleavage sites were allowed.

We carried out label-free relative quantification of histones by generating the extracted ion chromatogram for the peptide precursor mass, integrating the peak areas (using QuanBrowser (Thermo Fisher Scientific)), which we then used to calculate the peptide ratios. The average of those ratios determined the ratio of the histones (reference untreated or wild-type sample). This method is more precise than the Top3 TIC method used in Scaffold. Untreated or wild-type references were set to 1. We used two peptides from each ALF, KPK1, IF4A and IFSA1 protein as internal references for the quantification of relative histone abundances in each run. Histone-level ratios in SILAC samples are shown as the average from all non-label-swap or label-swap replicas. Ratios were derived from the MaxQuant peptide list, with only core histone peptides reported as not being subject to post-translational modifications taken into account[21]. We addressed significance by blotting the distribution of all protein ratios from the MaxQuant protein-groups list together with the protein intensities. Core histones were always the most abundant proteins measured and resided within the first significant interval. We filtered the MaxQuant protein-groups list by removing all contaminants, all reverse hits, and proteins quantified with less than two peptides. The cutoff for variability was set to 30%. Normalization was done manually with the 35 most abundant proteins (histones excluded). The MaxQuant peptide list (excluding the G1 experiment) was filtered accordingly without a variability cutoff and with only peptides that had an H/L or L/H count greater than 3 taken into account. Normalization was done manually with the top 10% most abundant peptides (histone peptides excluded).

Live-cell microscopy and image analysis. Live microscopy was done on a temperature-controllable Olympus IX81 microscope with a Yokogawa CSU-X1 scanning head equipped with two EM-CCD EvolveDelta (Photometrics) cameras, an ASI MS-2000 Z-piezo stage and a PlanApo 100×/1.45-NA (numerical aperture) total internal reflection fluorescence microscope oil-immersion objective and Visiview software. For mRFP-GFP or mRFP-CFP high-speed tracking, fluorophores were excited with lasers at 561 nm (mCherry or mRFP) and 491 nm (GFP) or 440 nm (CFP), and emitted fluorescence was acquired simultaneously on separate cameras (Semrock FF01-617/73-25 filter for mCherry/mRFP and Semrock FF02-525/40-25 filter for GFP or Semrock FF01-475/42-25 for CFP). High-speed time-lapse series were conducted, taking eight optical slices per stack either every 80 ms for 1 min or every 300 ms for 2 min, with 10-ms exposure times per slice. Time-lapse image stacks were analyzed as in ref. 9, using a custom-made ImageJ (FIJI) plugin[36] to extract coordinates of locus position from the movies. We tested phototoxicity by exposing wild-type cells (GA-6879) to standard imaging conditions and following outgrowth for 5 h by morphological analysis, comparing them with unexposed cells. Time series acquired from strains GA-9227 and GA-9777 (two-spot data) were deconvolved using Huygens Remote Manager, channel-aligned, and cropped to contain one single cell per nucleus with the two respective fluorescent spots. Spot tracking over time was done with the ImageJ plugin TrackMate included in Fiji[37]. We generated box plots by plotting all measured distances of treated or untreated cells. Relative MSD analysis was performed with KNIME[38] using the workflow provided in **Supplementary Data Set 3**. For each frame, we measured the distance vector of tracks in two channels by selecting the two spots with minimal distance. We performed an MSD analysis on the distance vectors for all frames, and tracks with a maximum MSD(t) value greater than 10 µm^2 were considered as outliers (due to mismatching of two distant tracks) and removed from the analysis. Relative MSD versus t was averaged over all tracks and plotted using R.

For H2B-CFP (GA-3364 and derivatives) live-cell microscopy, cells trapped in CellASIC plates were mounted on the same microscopic setup, and different stage positions of the whole field of view were excited with a 440-nm laser. The emitted fluorescence was acquired on an EM-CCD EvolveDelta (Photometrics) camera using a Semrock FF01-475/42-25 emission filter. The Htz1-mEos (GA-9594) and Nup49-GFP (GA-5816) control strains were excited at 491 nm, and fluorescence was recorded through a Semrock FF02-525/40-25 filter. Time-lapse series (120 min total) of 100 optical slices per stack (200-nm intervals) were acquired for 12 time points at 10-min intervals, with each slice being exposed for 10 ms per laser line. Bright-field images were acquired using a CoolLED diode. Images were deconvolved using the Huygens Remote Manager software. For image analysis, deconvolved maximum-intensity projections were analyzed as a merged stack in ICY. Nuclei were detected and segmented using hierarchical k-means and active contours and followed through the time series. The integrated nuclear intensity was calculated for each cell nucleus, and the average intensity of all single cells per condition was plotted over time. In figures, the t_0 time point to 100% intensity (via averaging of the first two time points) and the Zeocin treatment condition of each strain are shown relative to the respective control.

Structured illumination microscopy and image analysis. Structured illumination images were acquired on a Zeiss Elyra S.1 microscope with an Andor iXon 885 EM-CCD camera using an HR diode 488 100-nW solid state laser, a BP 525-580 + LP 750 filter and a PLAN-APOCHROMAT 63×/1.4-NA oil DIC objective lens. Cells were fixed in 4% paraformaldehyde, washed three times in PBS and then attached to a thin SIM-grade Zeiss 1.5 glass coverslip using concanavalin A. Cells were fully sectioned into 50–65 slices at 0.1-nm intervals taken at 60-ms exposures per slice with five rotations of the illumination grid. Bright-field images of the cells were also acquired with an X-Cite PC 120 EXFO Metal Halide lamp. ZEN Black was used to process the images with the automatic settings and with the "Raw Scale" option selected. We then analyzed 3D stacks by using pixel classification and a custom Matlab script to determine the spot volumes and other features as follows: We used a fully automated nucleus and spot-segmentation workflow that allowed for individual detection and feature extraction where a manual or even a semi-automated delineation would be unfeasible. The image-processing software was realized within the Matlab environment and supported by the supervised learning-based pixel-classification toolkit Ilastik[39]. The voxels corresponding to the nucleus, the inner spot and background regions are annotated interactively by brush strokes during the training phase. Features calculated at the labeled pixels and their local neighborhood are then used to train a pixel classifier based on a random Forest ensemble learning method. The processing software provides an automated whole segmentation of all the nuclei and spots present in the scene. The image-processing function is later used in a parallelized batch process on multiple processors. After detection and segmentation of nuclei and spots, the program produces a graphical output in the form of a maximum-intensity projection with delineation of the nucleus, the spots and the unique ID integer that identifies the nucleus candidate. In addition, 3D logical masks corresponding to the classes "spot" and "nucleus" are computed. Finally, the program generates an ASCII file in which key features such as volume and solidity 3D and descriptive statistics are listed for all detected nuclei and foci. The solidity factor is calculated as the proportion of pixels in the 3D convex hull. For statistical analysis and data representation, raw volumes were filtered to exclude spots smaller than 200 and greater than 4,000 voxels, and the control

doi:10.1038/nsmb.3347

condition was set to 1. In figures, Zeocin-treated spot or nuclei volume distributions are shown relative to the untreated control. The distributions were plotted with R as box plots or as cumulative-density functions.

Microscopy and image analysis of fixed samples. Microscopy of fixed GA-9777 samples was done with the same Olympus IX81 microscope setup mentioned before. Cells were fixed with paraformaldehyde and attached to a thin SIM-grade Zeiss 1.5 glass coverslip using concanavalin A. We acquired 70 optical slices in 100-nm intervals with the 561-nm and 491-nm laser lines (130-ms exposure each). Bright-field images were acquired using a CoolLED diode. Images were deconvolved using Huygens Remote Manager and channel-aligned. Then, interspot distances (Δ*d*) between the GFP and mRFP centroids were measured with the Imaris software. The distribution of all measured distances per condition was plotted with R as a box plot or as a cumulative-density function.

Ectopic recombination assays. *For **Figure 8a**: as used in wild-type cells, arp8Δ cells and cells bearing NHP6A/NHP6B deletions*. For specific growth conditions, please consult the "Yeast growth, cell-cycle arrests and flow cytometry" section. Equal amounts of exponentially growing wild-type (GA-6879) *arp8*Δ (GA-8132) and *nhp6*Δ (GA-9771) strains were transformed via the transformation protocol either with a linearized *URA3* plasmid (pRS406 cut with *Stu*I) presenting 800-bp homology to the W303 *ura3-1* locus or with an *mgs1::caURA3* PCR fragment (template plasmid #1050) presenting 40-bp and 42-bp upstream and downstream homology, respectively, to the *MGS1* locus. As a control, centromeric circular plasmid #2422 (ADE2, hphMX4, Cen/ARS), which is maintained in yeast cells ectopically, was transformed alongside with the URA3 integration cassettes. Primers were #7297 (GTTTTTTTACGCTTGAGGCGCATTGCATTGCTGGCACGTTTTTGTGCGGATCC CCGGGTTAATTAA) and #7298 (CGTATATGTTCTAATATATCTCAGATGGGCCCGCGAGACTTTGCGCGTTGGCCGATTCATTA).

After transformation, we split cells and plated them on SC-URA plates (100 µl) to select for transformants resulting from integration, and on and YPD$^+$ hygromycin B plates to select for cells containing the plasmid. We compared the numbers of Ura$^+$ and Leu$^+$ transformants obtained from each reaction to calculate the integration rate for each strain relative to that of a wild-type strain arbitrarily set to 1 as a reference. Growth was scored in biological quadruplicates, and each transformation was done with four technical replicates; results were averaged.

*For **Figure 8c**,**d**: control cells and Gal:H3/H4 'histone shutdown' cells*. For specific growth conditions, please consult the "Yeast growth, cell-cycle arrests and flow cytometry" section. After pre-growth in YP Gal/Raff 1:5 medium, equal amounts of exponentially growing control (GA-8385) and Gal:H3/H4 'histone shutdown' (GA-8386) cells were pulse-reduced for histone H3 and H4 levels via 2 h of growth in either YP Gal/Raff 1:20 or YP raffinose medium. After the histone-reduction pulse, transformations were done with either an *atg2::hphMX4* PCR fragment (PCR product *ATG2::hygro*, template plasmid #1049) presenting 40-bp homology (both upstream and downstream) to the *ATG2* locus or an *mgs1::hphMX4* PCR fragment (PCR product *MGS1::hygro*, template plasmid #1049) presenting 40-bp and 42-bp upstream and downstream homology, respectively, to the *MGS1* locus. As a control, centromeric circular plasmid #282 (LEU2, Cen/ARS), which is maintained in yeast cells ectopically, was transformed alongside with the hphMX4 PCR integration cassettes.

Primers for PCR product *ATG2::hygro* were #6302 (ATAGCCTTGGCGAGTTTTCCGTACATTGAAGAATTCGCCAAGCGGATGCCGGGAGCAGAC) and #6303 (GGGATTTTTGGCTCAAGGTGTGGTGGCCCCTTTTCTAAGGGTGAGCTGATACCGCTCGCC). Primers for PCR product *MGS1::hygro* were #7297 (GTTTTTTTACGCTTGAGGCGCATTGCATTGCTGGCACGTTTTTGTGCGGATCCCCGGGTTAATTAA) and #7298 (CGTATATGTTCTAATATATCTCAGATGGGCCCGCGAGACTTTGCGCGTTGGCCGATTCATTA).

After transformation, cells were split and plated on YP Gal + hygromycin B plates (100 µl plated) to select for transformants resulting from integration of *ATG2::hygro* or *MGS1::hygro* and on and SCGal –Leu plates (10 µl plated) to select for cells containing the plasmid. The numbers of hphMX4$^+$ and Leu$^+$ transformants obtained from each reaction were compared to calculate the integration rate for each strain relative to that of a wild-type strain arbitrarily set to 1 as a reference. Growth was done in biological quadruplicates, and each transformation was done with four technical replicates; results were averaged.

Recovery assay. Equal amounts of exponentially growing (YPAD medium, cell density ~1 × 10^7 cells/ml) wild-type (GA-6879), *arp8*Δ (GA-8132), *nhp6*Δ (GA-9771) and *arp8*Δ*nhp6*Δ cells (GA-9815) were treated in triplicates with increasing amounts of Zeocin (100, 250 and 500 µg/ml). After 1 h of treatment, cells were washed once with fresh, prewarmed (30 °C) YPAD medium and grown for an additional hour in YPAD without Zeocin. After this step, the cell density was accurately determined in three technical replicates and used later as a correction factor for cell growth within the 1 h of Zeocin treatment and the 1 h of growth in YPAD of the control versus the Zeocin-treated cultures (Zeo^{100} – Zeo^{500}). Aliquots were removed and plated in a dilution row. Growing colonies versus plated cells were quantified; the control situation served as reference point and was set to 100%.

Rad52-YFP recovery assay. Cells grown to saturation overnight in sterile, filtered, non-autoclaved YPD medium were diluted the next morning, and the experiment was started when OD_{600} reached 0.6. Wild-type (GA-9772) and *nhp6*Δ cells (GA-9771) were treated with 250 µg/ml Zeocin for 30 min. Zeocin was washed away and Rad52-YFP foci formation was followed over a total time course of 16 h, with microscopic images acquired at the following time points: 0 min, 20 min, 40 min, 1 h, 2 h, 4 h, 6 h, 8 h, 10 h, 12 h, 14 h and 16 h. Rad52-YFP foci were imaged with the same microscopic setup as mentioned above, with 50 optical slices acquired in 200-nm intervals with a 50-ms exposure time using a 514-nm laser with appropriate emission filters. Images were deconvolved as described above and maximum-intensity projected, and the binary (+ or –) content of Rad52-YFP foci of all living cells at each time point in each strain was counted. The average amount of cells containing Rad52-YFP foci per time point was plotted and is shown in figures together with a logarithmic fit.

Estimating the anomalous diffusion exponent α and the diffusion coefficient. Please refer to **Supplementary Note 1**.

Estimating the effective spring coefficient K_c. Please refer to **Supplementary Note 1**.

Statistics and reproducibility. All chromatin mobility data (spot tracking) are pooled from three independent experiments (**Figs. 3a**, **5d** and **6c**,**d**, and **Supplementary Fig. 5a**). Statistical analyses testing the significance of the biophysical parameters derived from the imaging data were performed with Matlab using the Kolmogorov–Smirnov test (**Figs. 3b**, **5d** and **6e**, and **Supplementary Figs. 5b** and **7c**,**d**). All SIM microscopy data from individual single cells were pooled and were derived from one experiment. The data were analyzed with RStudio using unequal-variance *t* tests (**Figs. 3d**, **5c**, **6f** and **7d**). For H2B-CFP single-cell fluorescent microscopy analysis, the integrated nuclear intensity was calculated for each cell nucleus, and the average intensity of all single cells per condition was plotted over time. All data from single cells originated from three independent cultures on three different days (**Fig. 1d**, H2B-CFP), two independent cultures on two different days (**Fig. 1d**, Htz1-mEos; **Fig. 7c**, *rad51*Δ/*sml1*Δ/*arp8*Δ), or two independent cultures on the same day (**Fig. 7c**, *rad53*Δ*sml1*Δ). Recombination efficiency and cell recovery experiments were performed in triplicates (three independent cell cultures), and Excel was used to perform two-tailed Student's *t* tests (**Fig. 8a**,**b**,**d**). Chromatin fractionations were repeated with three independent cultures (**Supplementary Fig. 1f**,**g**) or two independent cultures (**Fig. 1a** and **Supplementary Figs. 1h** and **3i**,**j**). Nucleosome mapping data for the wild-type strain (GA-6879) was performed on four independent cultures (**Fig. 1c** and **Supplementary Fig. 2e**); for the H3/H4 transcription independent strain (GA-8386) the experiment was done once (**Supplementary Fig. 4b**), but new data derived from four independent cultures showed the same effect (data not shown). The kinetics of the Rad52-YFP recovery assay on wild-type and *nhp6*Δ cells (12 different time points) was performed once but done on the single-cell level.

Data availability. The EBI project ID for the nucleosome-seq data in this study is PRJEB14701. Source data for **Figures 1b**,**d**, **2a–c**, **5b**, **7b**,**c** and **8a** and for **Supplementary Figure 2g**, as well as mass spectrometry data (**Supplementary Data Sets 4–9**), are available online. Other data supporting the findings of this study are available from the corresponding author upon request.

doi:10.1038/nsmb.3347

30. Haase, S.B. & Lew, D.J. Flow cytometric analysis of DNA content in budding yeast. *Methods Enzymol.* **283**, 322–332 (1997).
31. Liu, C., Apodaca, J., Davis, L.E. & Rao, H. Proteasome inhibition in wild-type yeast *Saccharomyces cerevisiae* cells. *Biotechniques* **42**, 158–162 (2007).
32. Lee, D.H. & Goldberg, A.L. Selective inhibitors of the proteasome-dependent and vacuolar pathways of protein degradation in *Saccharomyces cerevisiae*. *J. Biol. Chem.* **271**, 27280–27284 (1996).
33. Wiechens, N. *et al.* The chromatin remodelling enzymes SNF2H and SNF2L position nucleosomes adjacent to CTCF and other transcription factors. *PLoS Genet.* **12**, e1005940 (2016).
34. Gruhler, A. *et al.* Quantitative phosphoproteomics applied to the yeast pheromone signaling pathway. *Mol. Cell. Proteomics* **4**, 310–327 (2005).
35. Pasero, P., Duncker, B.P., Schwob, E. & Gasser, S.M. A role for the Cdc7 kinase regulatory subunit Dbf4p in the formation of initiation-competent origins of replication. *Genes Dev.* **13**, 2159–2176 (1999).
36. Sage, D., Neumann, F.R., Hediger, F., Gasser, S.M. & Unser, M. Automatic tracking of individual fluorescence particles: application to the study of chromosome dynamics. *IEEE Trans. Image Process.* **14**, 1372–1383 (2005).
37. Schindelin, J. *et al.* Fiji: an open-source platform for biological-image analysis. *Nat. Methods* **9**, 676–682 (2012).
38. Dietz, C. & Berthold, M.R. KNIME for open-source bioimage analysis: a tutorial. *Adv. Anat. Embryol. Cell Biol.* **219**, 179–197 (2016).
39. Sommer, C. & Gerlich, D.W. Machine learning in cell biology—teaching computers to recognize phenotypes. *J. Cell Sci.* **126**, 5529–5539 (2013).

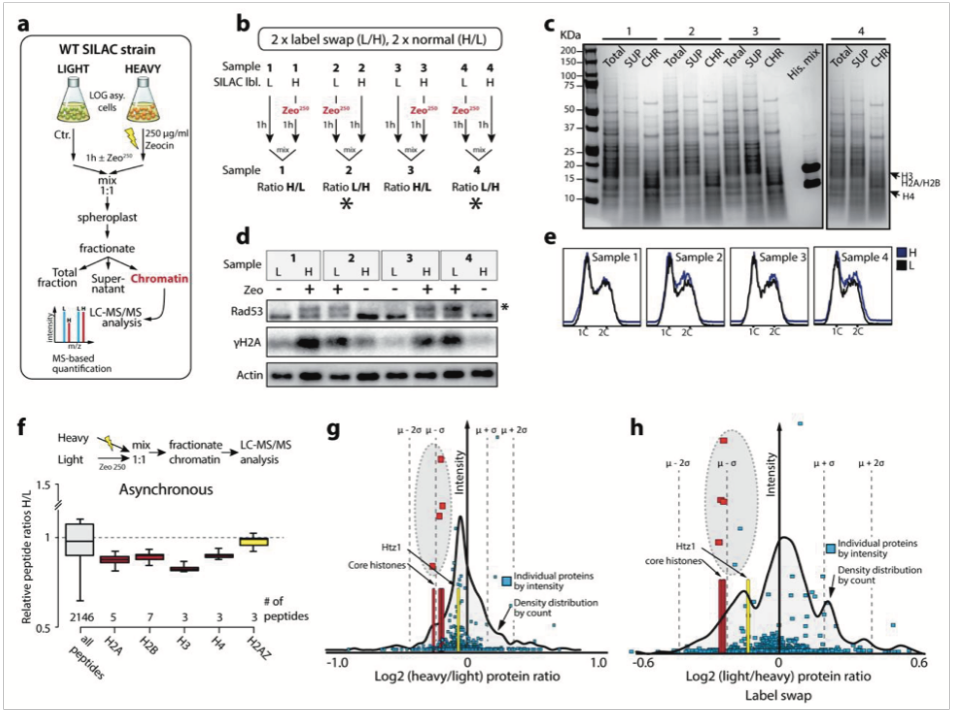

Supplementary Figure 1

SILAC mass spectrometry of pre-enriched chromatin depicts core histone loss.

(**a**) Experimental workflow for SILAC mass spectrometry after Zeocin treatment. (**b**) Labeling and mixing of samples from 4 individual experiments. Asterisks indicates label swap (**c**) Colloidal Commassie stained SDS-PAGE of SILAC experiment replicas showing total protein, supernatant (SUP), and chromatin (CHR) fractions from **a**. His. mix is an equimolar mixture of recombinant Histone H2A, H2B, H3 and H4. (**d**) Control Immunoblot analysis using anti-γH2A anti-Rad53 antibodies to show that checkpoint is activated after Zeocin treatment in the SILAC samples from **bc. (e**) FACS analysis showing that all samples from **b-d** have similar cell cycle profiles. Actin was used as loading control. Asterisks indicate the phosphorylation-dependent mobility shift of Rad53. (**f**) SILAC mass spectrometry on chromatin fractions from three independent cell pools. Boxplots show heavy/light histone peptide distribution indicating the degradation of core histones and, to a lesser extent, Htz1 (H2A.Z). (**g**) Distribution of measured protein ratios in the non-label swap experiment or (**h**) label swap experiment. Core histones are labelled red and reside within the μ-σ range. Htz1 is labelled yellow and resides closer to the mean ratio of all proteins. Boxplots in **f** represent median values, interquartile ranges and whiskers.

Nature Structural & Molecular Biology: doi:10.1038/nsmb.3347

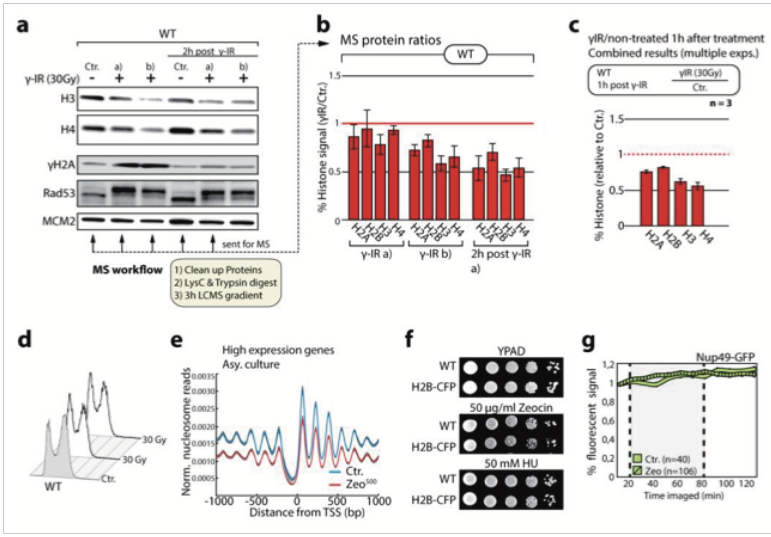

Supplementary Figure 2

Gamma irradiation triggers degradation of core histones, Zeocin reduces nucleosome occupancy, and H2B-CFP tagging does not interfere with cell viability.

(**a**) Immunoblot analysis from one experiment using H3 and H4 specific antibodies on whole cell extracts of asynchronous WT cells exposed to 30 Gy gamma irradiation (γ-IR). Rad53 and γH2A were probed to confirm checkpoint activation. MCM2 was used to control for loading. Arrows indicate samples sent for label-free quantitative mass spectrometric analysis. (**b)** Label-free quantitative mass spectrometry results of samples depicted in **a**. Bar graphs show mean peptide ratios ± s.e.m for the indicated histone proteins upon γIR exposure relative to the control condition. (**c**) Combined label-free mass spectrometry results of sample γ-IR a), γIR b) and an additional experiment. Bar graphs represent the mean peptide ratios (γIR/Ctr.) ± s.e.m. for core histones over all samples. (**d**) FACS analysis showing that all samples have similar cell cycle profiles. (**e**) Genome-wide nucleosome mapping graph shows the distribution of nucleosome reads over 750 highly expressed genes aligned to their TSS from four independent experiments (±s.d. is shaded). (**f**) Drop assay control showing that the H2B-CFP fusion complements the absence of H2B in response to genotoxic agents. (**g**) Live single-cell microscopy of Nup49-GFP. Graph shows the the mean fluorescent signals of of all individual cells (cell numbers indicated in graph) per treatment over time relative to the control (Ctr.) condition. Dotted lines indicate the duration of Zeocin treatment. Graphs show mean ± s.e.m..

Nature Structural & Molecular Biology: doi:10.1038/nsmb.3347

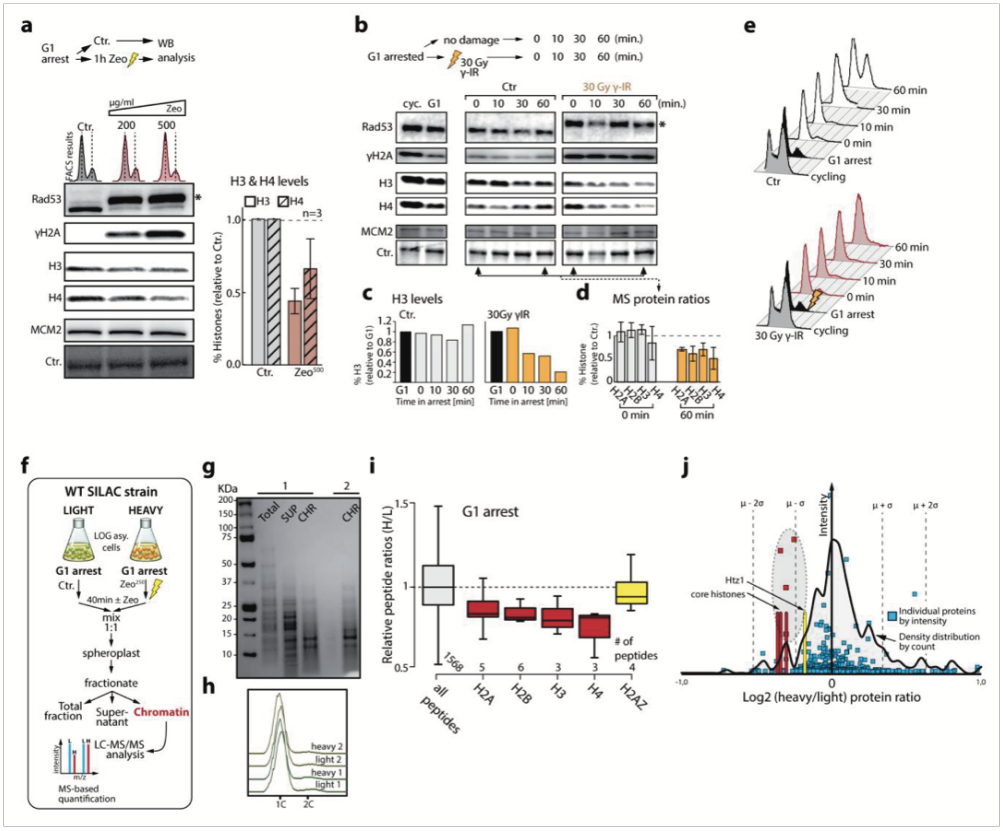

Supplementary Figure 3

Damage-induced histone loss occurs in G1 phase.

(**a-b**) Representative immunoblot analysis of whole cell extracts from G1-arrested cells treated with Zeocin **a** or after exposure to γIR **b**. Histone H3 and H4 levels were probed using histone specific antibodies. Rad53 and γH2A were probed to confirm checkpoint activation. MCM2 was used to control for loading and Ctr. represents bands on the ponceau stained membrane. Bar graphs in **a** show the mean ± s.e.m. over three independent replicates relative to the control condition. FACS results of Zeocin treated samples are shown above immunoblots in **a**. Arrows in **b** indicate samples sent for label-free quantitative mass spectrometric analysis. (**c**) Immunoblot quantifications of irradiated samples from one experiment marked with arrows. (**d**) Label-free quantitative mass spectrometry results of samples depicted with arrows. Bar graphs show mean peptide ratios ± s.e.m. for the indicated histone proteins upon γIR exposure relative to the control condition. (**e**) FACS analysis showing cell cycle profiles of all samples from **b**. (**f**) Experimental workflow for SILAC mass spectrometry of G1 arrested cells after Zeocin treatment. (**g**) Commassie stained SDS-PAGE of samples showing total protein, supernatant (SUP), and chromatin (CHR) fractions. (**h**) FACS analysis showing similar G1 arrest efficiency for all samples. (**i**) SILAC mass spectrometry on chromatin fractions from two independent cells pools. Boxplots show heavy/light histone peptide distribution indicating the degradation of core histones and, to a lesser extent, Htz1. (**j**) Distribution of measured proteins ratios. Core histones are labelled red and reside within the µ-σ range. Htz1 is labelled yellow and residues closer to the mean ratio of all proteins. Boxplots in **i** represent median values, interquartile ranges and whiskers. Asterisk indicates phosphorylation-dependent Rad53 mobility shift.

Nature Structural & Molecular Biology: doi:10.1038/nsmb.3347

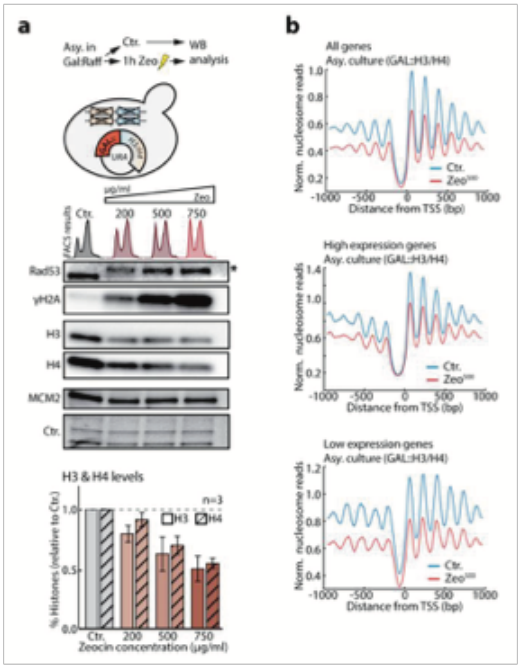

Supplementary Figure 4

Damage-induced histone loss is independent of histone transcription.

(**a**) Top panel shows the experimental procedure and strain used for constitutive histone H3 and H4 transcription in cells grown in YPGal:Raff medium (strain GA-8386). A *URA3* plasmid borne construct in which the *GAL1-10* promoter drives the only pair of histone H3/H4 genes is used. Mid panel shows representative immunoblot analysis using anti-H3 and anti-H4 antibodies on whole cell extracts from the strain depicted in **a** after Zeocin treatment and growth in YPGal:Raff medium. Rad53 and γH2A were probed to confirm checkpoint activation. MCM2 was used to control for loading and Ctr. represents bands on the original gel (UV-TGX stained). Bar graphs in bottom panel show the mean ± s.e.m. over three independent replicates relative to the control condition. Asterisk indicates phosphorylation-dependent Rad53 mobility shift. (**b**) Zeocin treatment causes a genome-wide decrease in nucleosome occupancies. Data represents nucleosome occupancies over the total pool of 5014 protein coding genes, 750 high expression genes and 750 low expression genes aligned to their transcriptional start site (TSS) from one experiment using the strain depicted in **a**.

Nature Structural & Molecular Biology: doi:10.1038/nsmb.3347

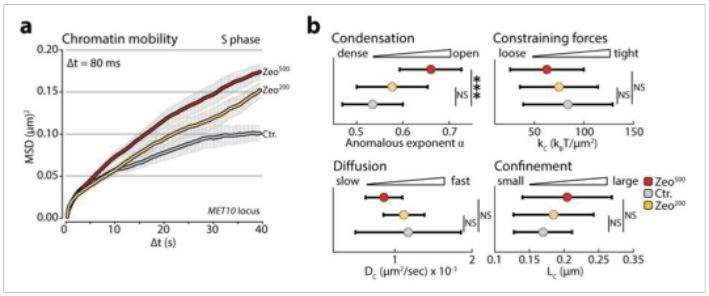

Supplementary Figure 5

High-speed, live-cell imaging reveals increased chromatin movement and a loss of constraining forces after DNA damage.

(**a**) High-speed (Δt=80 ms) imaging of the undamaged *MET10* locus (as in **Fig. 3a-b**) showing that chromatin mobility increases with Zeocin concentration. Average MSD graphs indicate dose-dependent increases in global chromatin mobility in response to DNA damage ($n^{Ctr.}$=39, n^{Zeo200}=31, n^{Zeo500}=29 different cells from three independent experiments). (**b**) Graphs show the means and whiskers (±s.d.) of biophysical parameters derived from imaging data and predict chromatin decompaction after Zeocin treatment. P-values, ***P<0.001, NS=not significant, result from Kolmogorov-Smirnov-tests. All MSD graphs represent the mean ± s.e.m. of cells pooled from three independent experiments. Additionally, consult Supplementary Dataset 2 for mobility parameters and the number of cells analyzed.

Nature Structural & Molecular Biology: doi:10.1038/nsmb.3347

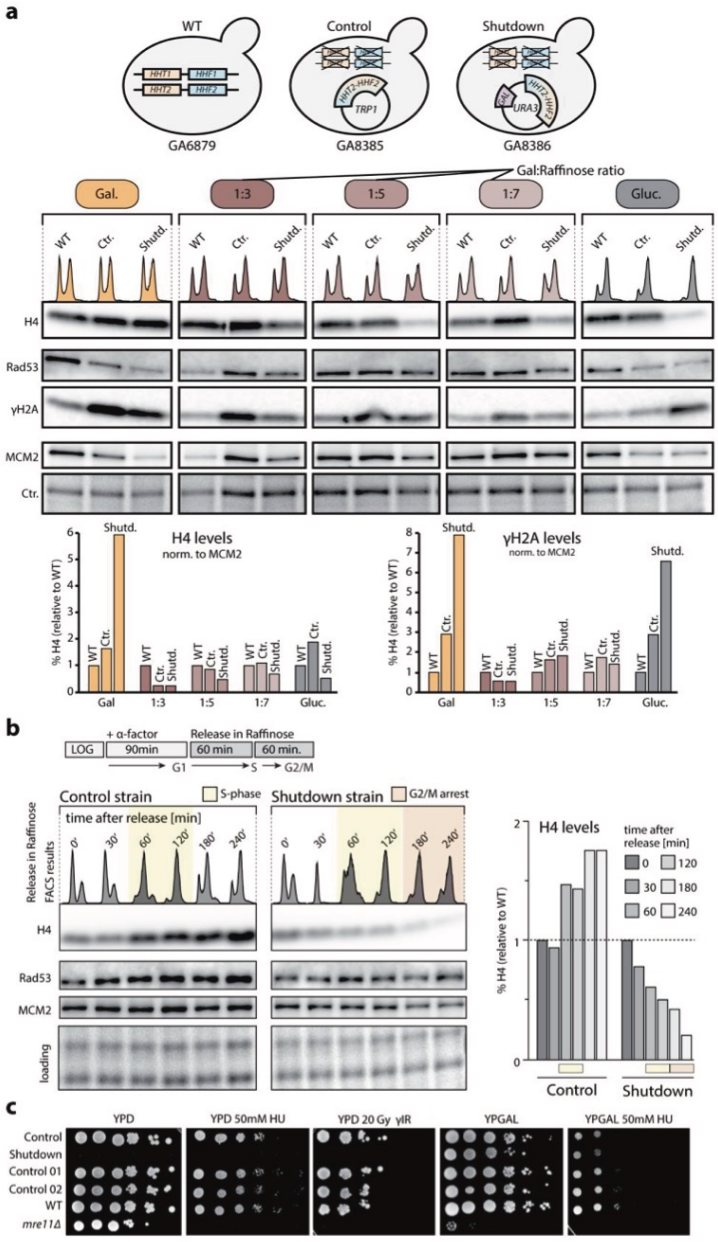

Supplementary Figure 6

Nature Structural & Molecular Biology: doi:10.1038/nsmb.3347

GAL::H3/H4 strain as a tool for *in vivo* artificially controlled histone-level reductions.

(**a**) Schematic representation of wild-type, control and shutdown strains grown in the indicated media. Gal. = galactose, gluc. = glucose. Immunoblot analysis of whole cell extracts of the indicated conditions and strains were performed using an antibody directed against Histone H4. Rad53 and γH2A were probed to confirm checkpoint activation. MCM2 was used to control for loading. Bar graphs from quantified immunoblot derived from one experiment shows overexpression or reduction of H3/H4 in the shutdown strain grown in gal. or gluc. medium respectively. Growth of the shutdown strain in Gal:Raff 1:5 confers H3/H4 levels similar to WT. (**b**) Experimental workflow of the arrest-release experiment used to reduce histone levels in S phase (as in **Fig. 5**). Bar graphs from quantified immunoblot data derived from one experiment shows reductions of H3 and H4 upon release into raffinose medium. (**c**) A defined number of exponentially growing cells (fivefold dilutions) was spotted on different YP or YPD plates containing the indicated dose of hydroxyurea (HU). Cells exposed to 20 Gy γIR were spotted onto YPD plates. Drop assays show functionality of shutdown and control strains. Control = control from **a**, control 1 and 2 = similar to control 1 but expressing HHT2-HHF2 from a *URA3* plasmid (**a**).

Nature Structural & Molecular Biology: doi:10.1038/nsmb.3347

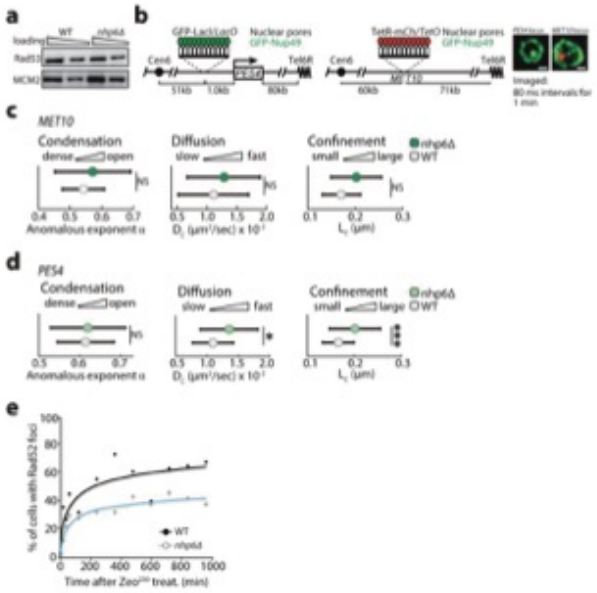

Supplementary Figure 7

Biophysical parameters of *nhp6*Δ tracking data and results from Rad52-YFP recovery assay.

(**a**) Control Immunoblot from one experiment (loading 1x and 2x the volume) showing that *nhp6Δ* strains do not have constitutive checkpoint activation. Rad53 was probed to test for checkpoint activation and MCM2 was used as loading control. (**b**) Schematics of the strains used for imaging the *PES4* and *MET10* loci (**Fig. 6c-e**) with representative images. Scale bar is 2 µm. (**c-d**) Graphs show the means and whiskers (±s.d.) of biophysical parameters derived from imaging data of *PES4* **c** and *MET10* **d** (**Fig. 6c,d**). P-values, *P<0.05, ***P<0.001, NS=not significant, result from Kolmogorov-Smirnov-Tests. (**e**) Rad52-YFP foci recovery assay. Graph shows the overall percentage of Rad52-YFP foci containing cells for each of the 12 time-points from one experiment plotted against the time and shown together with a logarithmic fit.

Nature Structural & Molecular Biology: doi:10.1038/nsmb.3347

Supplementary Tables

Nucleosome mapping sequencing reads

Supplementary Table 1: Information on sequencing reads obtained for each nucleosome mapping replicate. The strain column indicates the strains used. GA-6879 is the wild type and GA-8386 the shutdown strain grown in galactose:raffinose medium. A-C in the strain column indicates the four independent experiments with or without Zeocin treatment for 1h prior to MNase digestion. Column A shows the *S. Cerevisiae* reads and column B the reads from the *C. glabrata* spike-in control.

	A	B	C=(A+B)	E=(A/C)	F=(B/C)*100
Strain	***S. ce.***	***C. glab.***	**total**	**Read fraction *S. cer.***	**Read fraction *C. glab.***
GA-6879_A	50692473.00	9866228.00	60558701.00	0.84	0.16
GA-6879_A_Zeocin	46090144.00	13483686.00	59573830.00	0.77	0.23
GA-6879_B	38787017.00	7282715.00	46069732.00	0.84	0.16
GA-6879_B_Zeocin	36619974.00	10714730.00	47334704.00	0.77	0.23
GA-6879_C	34427922.00	6626795.00	41054717.00	0.84	0.16
GA-6879_C_Zeocin	29746798.00	7722737.00	37469535.00	0.79	0.21
GA-6879_D	25931187.00	4679458.00	30610645.00	0.85	0.15
GA-6879_D_Zeocin	43185379.00	12185328.00	55370707.00	0.78	0.22
GA-8386_A	82089867.00	21788485.00	103878352.00	0.79	0.21
GA-8386_A_Zeocin	53677477.00	20342128.00	74019605.00	0.73	0.27
GA-8386_B	41546073.00	9859227.00	51405300.00	0.81	0.19
GA-8386_B_Zeocin	32786223.00	12332953.00	45119176.00	0.73	0.27
GA-8386_C	25328106.00	6741373.00	32069479.00	0.79	0.21
GA-8386_C_Zeocin	27560758.00	10640545.00	38201303.00	0.72	0.28
GA-8386_D	30336089.00	7284044.00	37620133.00	0.81	0.19
GA-8386_D_Zeocin	31958581.00	12219914.00	44178495.00	0.72	0.28

Yeast strains used in this study

Supplementary Table 2: Yeast strains used in this study. All strains are haploid and all except the SILAC strain and the Htz1-mEos imaging control are derived from the W303 background.

Strain number	Genotype	Source
BY	*MATa; his3del200; leu2del0; met15del0; trp1del63; ura3del0;* (BY4733)	exemplary genotype
W303	*MATa; ade2-1; trp1-1; his3-11; his3-15; ura3-1; leu2-3; leu2-112;* (W303)	exemplary genotype
JKM179	*MATa; hml::ADE1; hmr::ADE1; ade3::GALHO; leu2-3; lys5 trp1::hisG; ura3-52* (JKM179)	exemplary genotype
yAG-06A	*YHR018c::kanMX4; YIR034c::kanMX4* (BY4733)	1
GA-6879	*MATa, RAD52-YFP; NUP49-GFP; ADE2::TetR-mCherry; lys5::LacI-CFP::TRP; leu2::LoxP; ZWF1:cutsite(Lmn::lys5::IsceIcs::LEU2::LacO array::Lmn); met10::lmn adaptamers::HIS3::TetOps-LexA* (W303)	1
GA-9773	*MATa; PES4::4xLexA-lacO::TRP1; his3-15::GFP-LacI-HIS3; NUP49-GFP*	This study
GA-9774	*nhp6a::kanMX4; nhp6b::kanMX4*, same as GA-9773	This study
GA-9771	*nhp6a::kanMX4; nhp6b::kanMX4*, same as GA-6879	This study
GA-9815	*arp8::NAT*, same as GA9771	
GA-9772	Isogenic to GA-6879	This study
GA-7553	*sml1::HIS3*; same as GA-6879	This study
GA-8132	arp8::NAT; same as GA-6879	This study
GA-8182	ies4::NAT; same as GA-6879	This study
GA-8185	swr1::NAT; same as GA-6879	This study
GA-8202	arp5::NAT; same as GA-6879	This study
GA-7551	*rad51::NAT*; in GA-6879	This study
GA-7552	*rad53::NAT*; same as GA-7553	This study
GA-7556	*mec1::NAT*; same as GA-7553	This study
GA-8385	*MATa; Nup49-GFP; GFP-LacI::HIS3; hht2-hhf2Δ hht1-hhf1Δ(no marker) + [#3495 pDM18 pRS415; HHT2-HHF2; CEN/ARS, TRP1]* (W303)	This study
GA-8386	*MATa; Nup49-GFP; GFP-LacI::HIS3; hht2-hhf2Δ hht1-hhf1Δ(no marker) + [#3484 pRM102 pUK420; GAL10-HHT2 GAL1-HHF2; CEN/ARS, URA3]* (W303)	This study
GA-8387	*MATa; Nup49-GFP; GFP-LacI::HIS3; hht2-hhf2Δ hht1-hhf1Δ(no marker) + [#3494 pDM9 pRS416; HHT1-HHF1; CEN/ARS; URA3]* (W303)	This study
GA-9775	*LacO::LEU2::MGS1*, same as GA8385	This study
GA-9776	*LacO::LEU2::MGS1*, same as GA8386	This study
GA-3364	*MATa; HTB2-CFP::kanXM* (W303)	Brian Luke
GA-9700	*rad51::URA3*; same as GA-3364	This study
GA-9698	*sml1::URA3*; same as GA-3364	This study
GA-9695	*arp8::natMX*; same as GA-3364	This study
GA-9712	*Rad53::natMX*; same as GA-9712	This study
GA-9594	*MATa; Htz1-Eos::URA3*; same as JKM179	This study
GA-5816	*MATa; Rad52-YFP; NUP49-GFP; HIS3::LacI-GFP* (W303)	This study
YMB08 (GA-9227)	*MATa; ura3-1::LacI-GFP-URA3; 515kb-XIV::lacO-TRP1; YGL117::tetR-mRFP-NATMX; 196kb-XIV::tetO-LEU2* (W303)	Kerstin Bystricky
GA-9777	*MATa; YGL117(ARS714)::TetR-mRFP-NAT; ade2-1::His3p-CFP-lacI-URA3p-Lambdacl-YFP-ADE2; leu2-3,112 :: tetO-LEU2; 74kb :: LambdaO-HIS3; 40kb :: LacO-TRP1; RAD52-EGFP-CaURA3*	This study
GA-1365	*MATa, pre1-1, pre2-2*	3
GA-1366	*Mata*, WT strain isogenic to GA-1365 and GA-1366	3
GA-1364	*Mata, erg6::LEU2*	4

Nature Structural & Molecular Biology: doi:10.1038/nsmb.3347

Plasmids used in this study

Supplementary Table 3: Plasmids used in this study

Plasmid number	Description	Type	Yeast selection	Bacterial selection	Source
#3484	pUK420-GAL10-HHT2 GAL1-HHF2	CEN/ARS	URA3	AMP	Addgene [5]
#3494	pRS416-HHT1-HHF1	CEN/ARS	URA3	AMP	[6]
#3495	pRS414-HHT2-HHF2	CEN/ARS	TRP1	AMP	[7]
#279	pRS406	integrating	URA3	AMP	Addgene [8]
#1049	pAG32	see source	see source	see source	[8]
#1050	pAG60	see source	see source	see source	[8]
#2422	pWJ132-hphMX4-Gal1-10	2μ plasmid	ADE2/hphMX4	AMP	This study

Antibodies used in this study

Supplementary Table 4: Antibodies used in this study

Antibody	Supplier	Conditions used
Mouse α Rad53	Custom made antibody (GenScript)	1:200 in milk
Rabbit α H4	Abcam AB 10158	1:5000 or 1:7500 in BSA
Mouse α actin	MAB1501	1:10,000 in milk
Goat α MCM2	Santa Cruz (SC 6680)	1:3000 in BSA
Rabbit α γH2A	Custom made antibody	1:3000 i BSA
Rabbit α H3	Abcam AB1791	1:10,000 in BSA
Rabbit α Ubiquitin	Abcam (AB19247)	1:2000 in milk

Nature Structural & Molecular Biology: doi:10.1038/nsmb.3347

Supplementary Table References

1. Gruhler, A. et al. Quantitative phosphoproteomics applied to the yeast pheromone signaling pathway. *Mol Cell Proteomics* **4**, 310-27 (2005).
2. Seeber, A., Dion, V. & Gasser, S.M. Checkpoint kinases and the INO80 nucleosome remodeling complex enhance global chromatin mobility in response to DNA damage. *Genes Dev* **27**, 1999-2008 (2013).
3. Richterruoff, B., Wolf, D.H. & Hochstrasser, M. Degradation of the Yeast Mat-Alpha-2 Transcriptional Regulator Is Mediated by the Proteasome. *Febs Letters* **354**, 50-52 (1994).
4. Heese-Peck, A. et al. Multiple functions of sterols in yeast endocytosis. *Mol Biol Cell* **13**, 2664-80 (2002).
5. Mann, R.K. & Grunstein, M. Histone H3 N-terminal mutations allow hyperactivation of the yeast GAL1 gene in vivo. *EMBO J* **11**, 3297-306 (1992).
6. Duina, A.A. & Winston, F. Analysis of a mutant histone H3 that perturbs the association of Swi/Snf with chromatin. *Molecular and Cellular Biology* **24**, 561-572 (2004).
7. Park, J.H., Cosgrove, M.S., Youngman, E., Wolberger, C. & Boeke, J.D. A core nucleosome surface crucial for transcriptional silencing. *Nature Genetics* **32**, 273-279 (2002).
8. Goldstein, A.L. & McCusker, J.H. Three new dominant drug resistance cassettes for gene disruption in Saccharomyces cerevisiae. *Yeast* **15**, 1541-1553 (1999).

Nature Structural & Molecular Biology: doi:10.1038/nsmb.3347

Supplementary Notes

Estimating the anomalous diffusion exponent α and the diffusion coefficient

We computed the cross-correlation (CC) function using [1]:

$$C(t) = \frac{1}{N_p - t} \sum_{k=1}^{N_p - t} (\mathbf{R}_c(k\Delta t) - \mathbf{R}_c((k+t)\Delta t))^2, \quad (6)$$

for $t = 1, T-1$, where N_p is the number of points in the trajectory. In many studies the CC is referred to as the MSD function [2,3] although these two functions are distinct[1]. The MSD is defined as the squared displacement with respect to the initial trajectory position, averaged over time:

$$\mathrm{MSD(t)} = \left\langle \left(R_c(t) - R_c(0) \right)^2 \right\rangle.$$

For short times, $C(t)$ increases as a power law

$$C(t) = Ct^{\alpha}. \quad (7)$$

where $C > 0$. To extract the coefficient α, we computed $C(t)$ from empirical trajectories and fitted the first seven points of the curve to a power law. A chromatin or DNA locus is characterized experimentally by $\alpha < 1$ [4,5], while for normal diffusion $\alpha = 1$. In the Rouse polymer model[6], the anomalous exponent is $\alpha = 0.5$ computed for intermediate time regime (see [6]).

To compute the diffusion coefficient of the tagged monomer, we use the following empirical estimator described in [1]:

$$D_c = \frac{1}{4\Delta t} \sum_{k=1}^{N_p - 1} (\mathbf{R}_c(k\Delta t) - \mathbf{R}_c((k+1)\Delta t))^2, \quad (8)$$

For short time interval $\Delta t = b^2/D$, the locus motion is Brownian and the diffusion coefficient is well approximated by eq.(8).

Nature Structural & Molecular Biology: doi:10.1038/nsmb.3347

Estimating the effective spring coefficient k_c

Because the chromatin interacts locally with its environment, we estimated this interaction using a polymer model[7], by a harmonic well of strength k acting on a single monomer $\mathbf{R}_n$. The potential energy of the interaction is

$$U(\mathbf{R}_n) = \frac{1}{2}k(\mathbf{R}_n - \boldsymbol{\mu})^2, \tag{9}$$

where $\boldsymbol{\mu}$ is the fix position of the interaction. The velocity of an observed monomer c, averaged over many trajectories is driven by this interacting force, following the relation described in [7]:

$$\lim_{\Delta t \to 0} E\{\frac{\mathbf{R}_c(t+\Delta t) - \mathbf{R}_c(t)}{\Delta t} \mid \mathbf{R}_c(t) = \mathbf{x}\} = -Dk_{cn}(\mathbf{x} - \boldsymbol{\mu}), \tag{10}$$

where $\mathbf{R}_c(t)$ is the position of locus c at time t and D the diffusion coefficient and $E\{. \mid \mathbf{R}_c(t) = \mathbf{x}\}$ means averaging over trajectory realizations such that the condition $\mathbf{R}_c(t) = \mathbf{x}$ is satisfied. Relation (18) links the average velocity of the observed monomer c to the force applied at a distance $|c-n|$. For a Rouse polymer, with a potential well of type (17), the effective spring coefficient is given by

$$k_{cn} = \frac{k\kappa}{\kappa + |c-n|k}, \tag{11}$$

where κ is the monomer-monomer spring coefficient. We estimated k_c from the empirical locus trajectories $\mathbf{R}_c(t)$ by

$$k_c \approx \frac{1}{2(N_p - 1)} \sum_{i=1}^{2} \sum_{h=1}^{N_p - 1} \frac{R_c^i((h+1)\Delta t) - R_c^i(h\Delta t)}{D_c \Delta t (R_c^i(h\Delta t) - \langle R_c^i \rangle)}, \tag{12}$$

where i is the spatial direction (in two dimensions, we sum over the x and y components) and N_p is the number of points in the trajectory. In practice, the quantity $\langle R_c^i \rangle$ is computed by averaging over the trajectory. The diffusion coefficient D_c can be computed by using eq. 8.

Nature Structural & Molecular Biology: doi:10.1038/nsmb.3347

Supplementary Notes References

1. Schuss, Z. Diffusion and Stochastic Processes. An Analytical Approach. *Springer-Verlag, New York, NY* (2009).
2. Dion, V., Kalck, V., Horigome, C., Towbin, B.D. & Gasser, S.M. Increased mobility of double-strand breaks requires Mec1, Rad9 and the homologous recombination machinery. *Nat Cell Biol* **14**, 502-9 (2012).
3. Mine-Hattab, J. & Rothstein, R. Increased chromosome mobility facilitates homology search during recombination. *Nat Cell Biol* **14**, 510-7 (2012).
4. Kepten, E., Bronshtein, I. & Garini, Y. Improved estimation of anomalous diffusion exponents in single-particle tracking experiments. *Physical Review E* **87**(2013).
5. Weber, S.C., Theriot, J.A. & Spakowitz, A.J. Subdiffusive motion of a polymer composed of subdiffusive monomers. *Phys Rev E Stat Nonlin Soft Matter Phys* **82**, 011913 (2010).
6. Doi, M., Edwards, S. F. The Theory of Polymer Dynamics. . *Oxford: Clarendon Press.* (1986).
7. Amitai, A., Toulouze, M., Dubrana, K. & Holcman, D. Analysis of Single Locus Trajectories for Extracting In Vivo Chromatin Tethering Interactions. *PLoS Computational Biology* **11**, e1004433 (2015).

Nature Structural & Molecular Biology: doi:10.1038/nsmb.3347

Fig. 1b

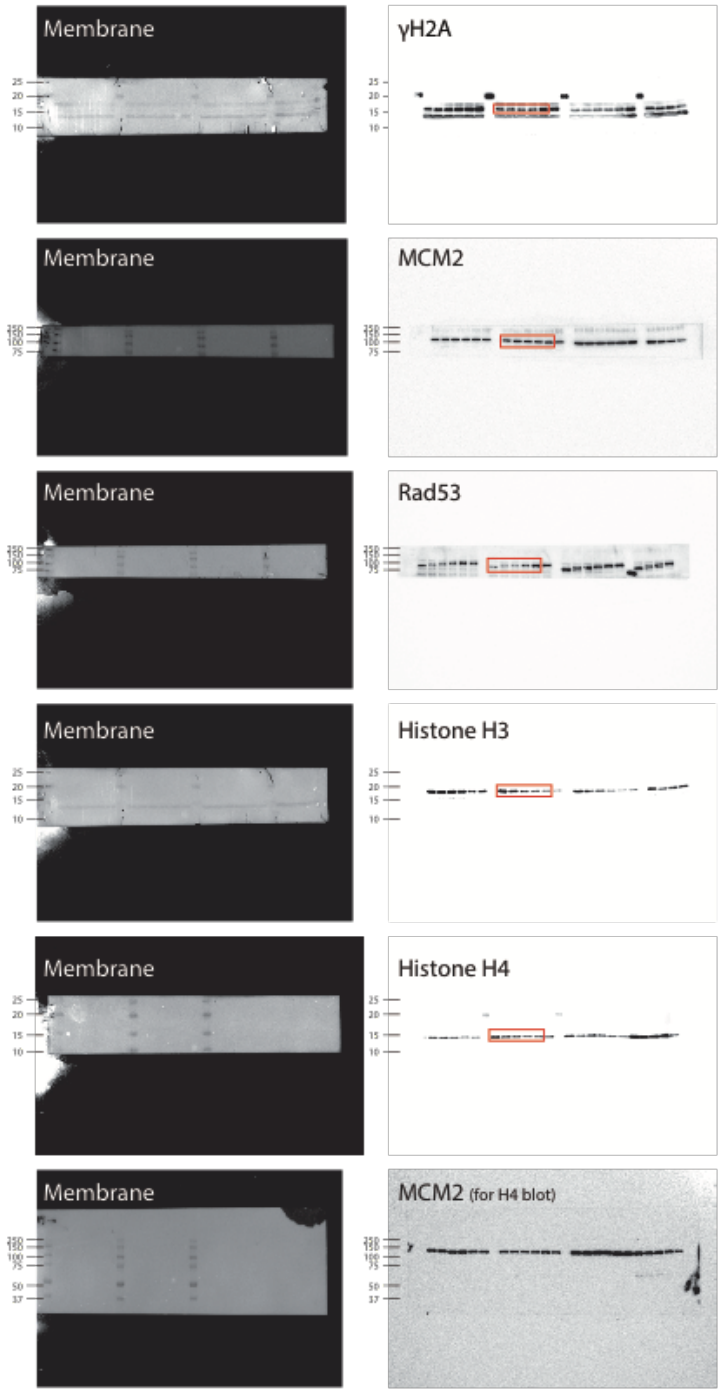

Nature Structural & Molecular Biology: doi:10.1038/nsmb.3347

Fig. 1b

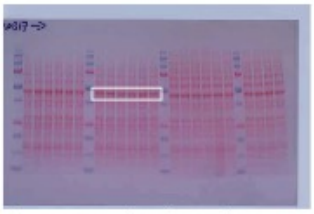

Ponceau stained membrane
after transfer

Nature Structural & Molecular Biology: doi:10.1038/nsmb.3347

Fig. 2a

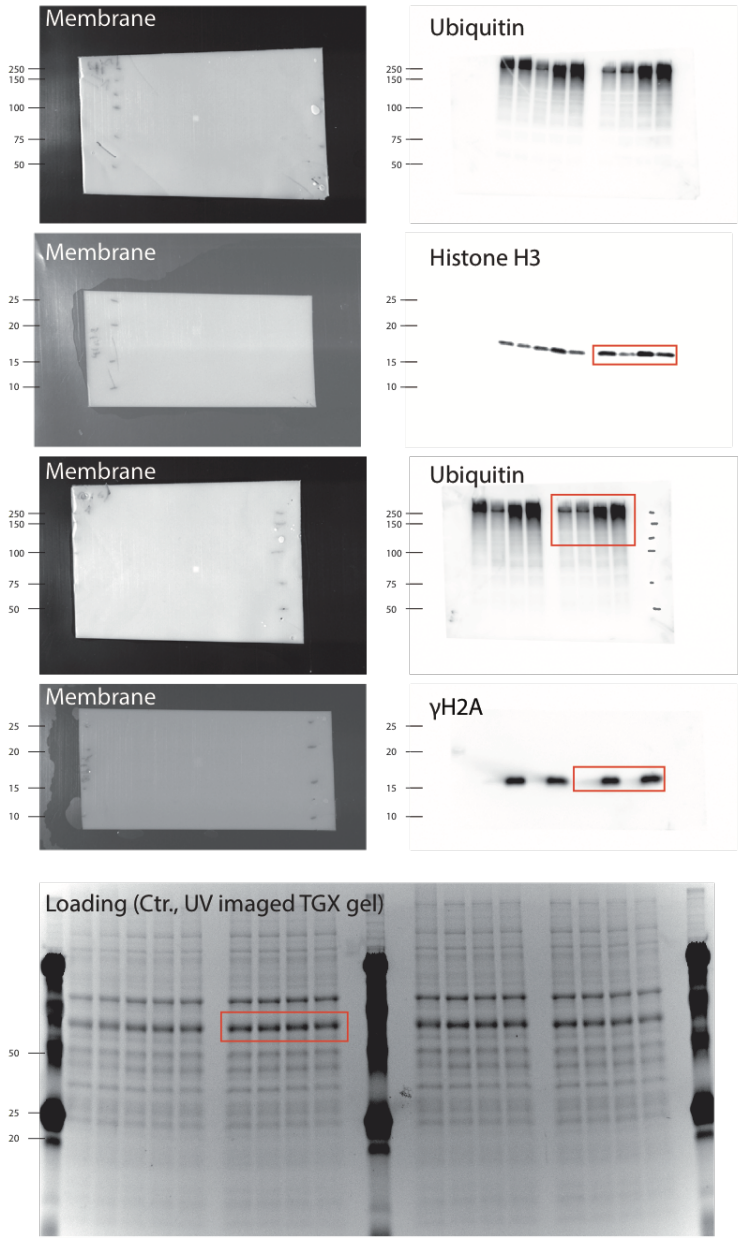

Nature Structural & Molecular Biology: doi:10.1038/nsmb.3347

Fig. 2b

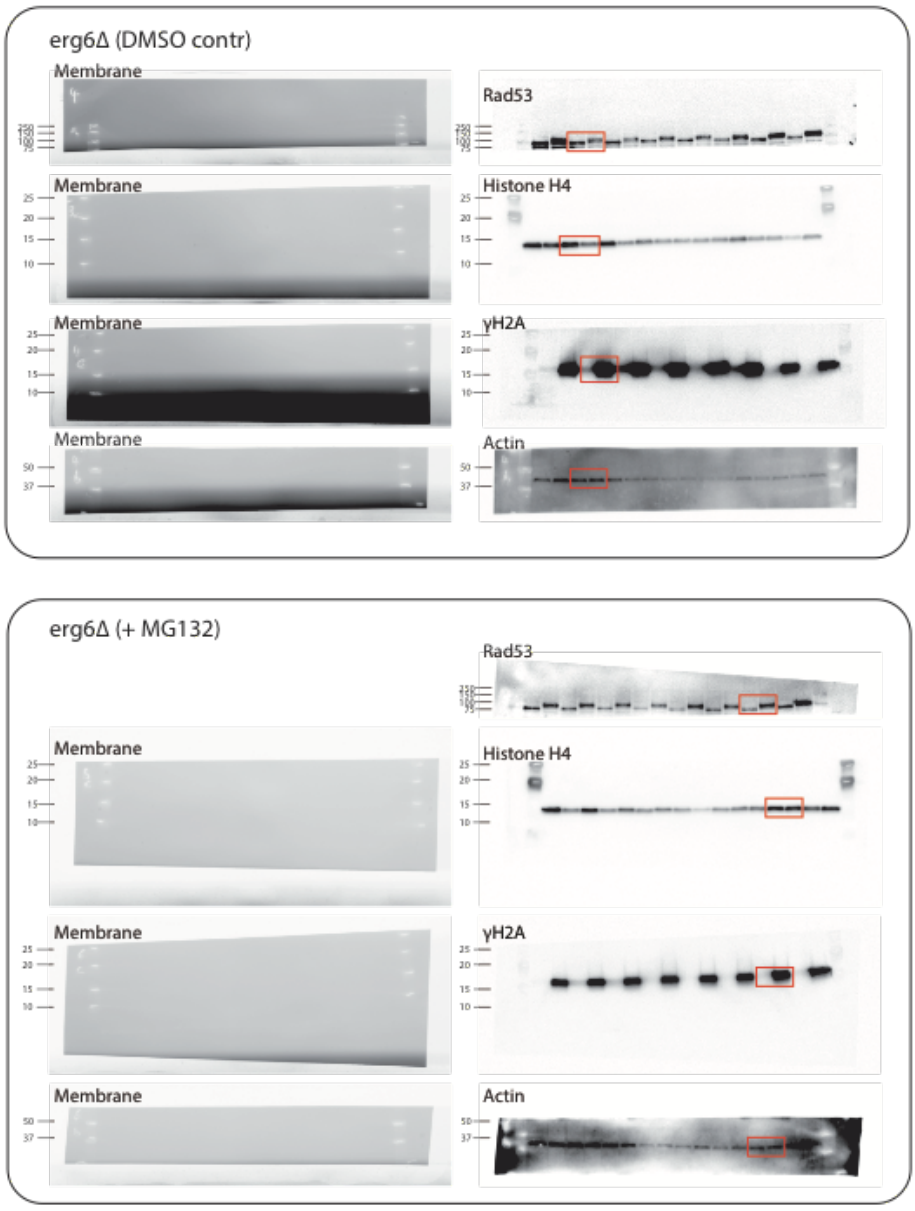

Nature Structural & Molecular Biology: doi:10.1038/nsmb.3347

Fig. 2c

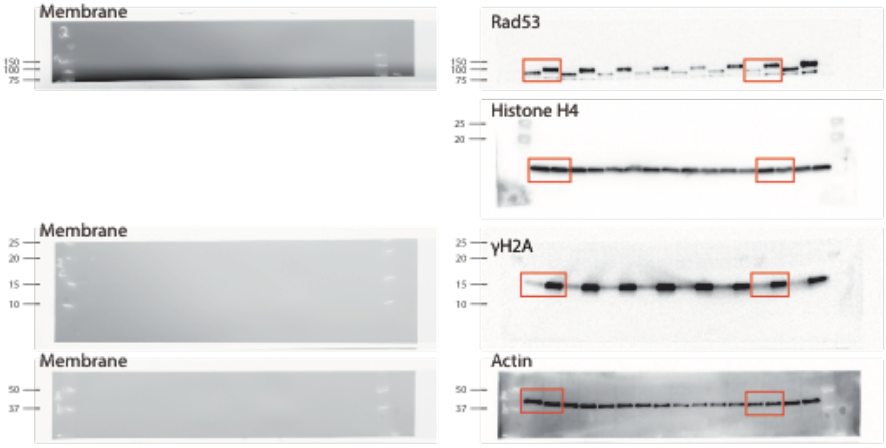

Nature Structural & Molecular Biology: doi:10.1038/nsmb.3347

Fig. 7a

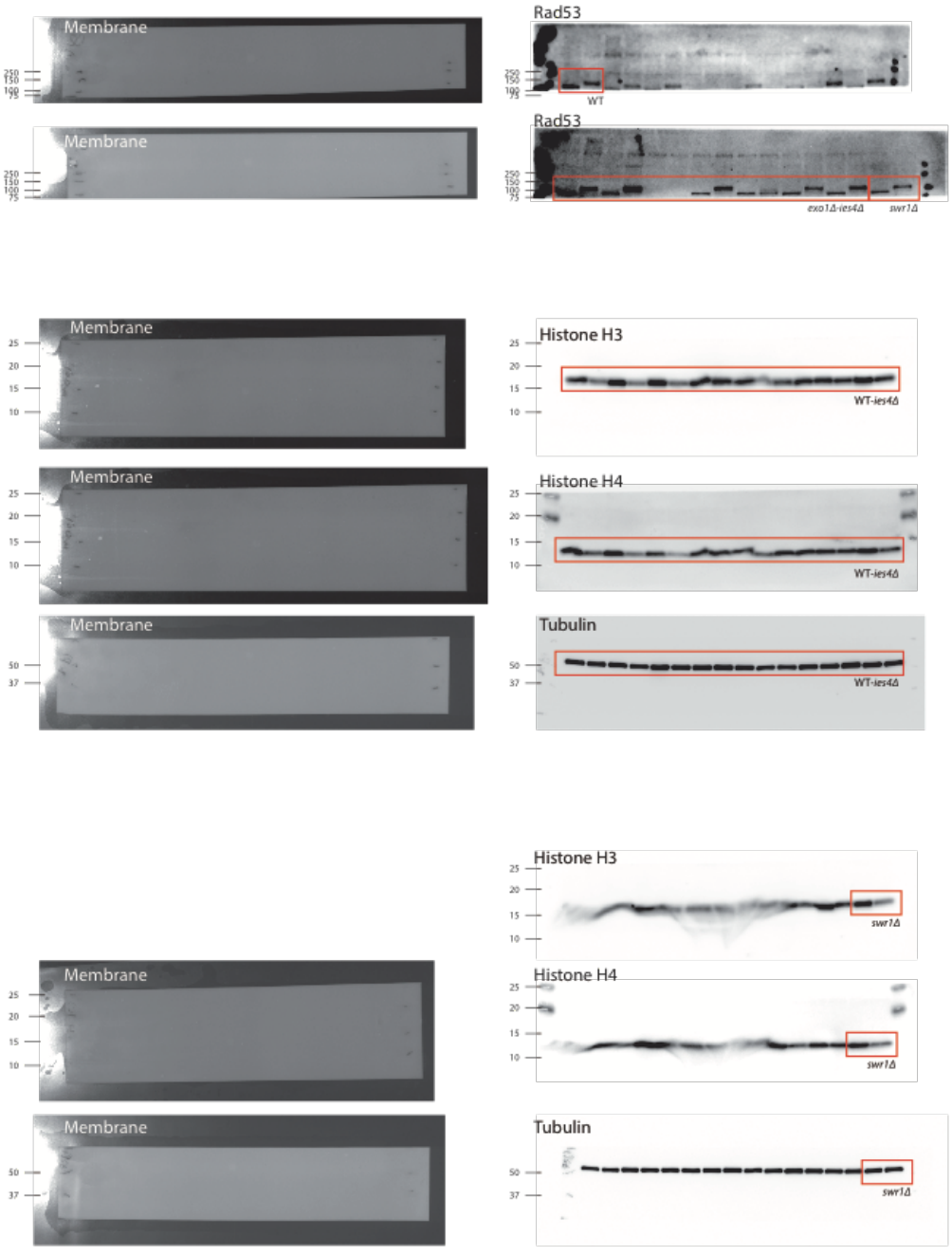

Nature Structural & Molecular Biology: doi:10.1038/nsmb.3347

Fig. 7a

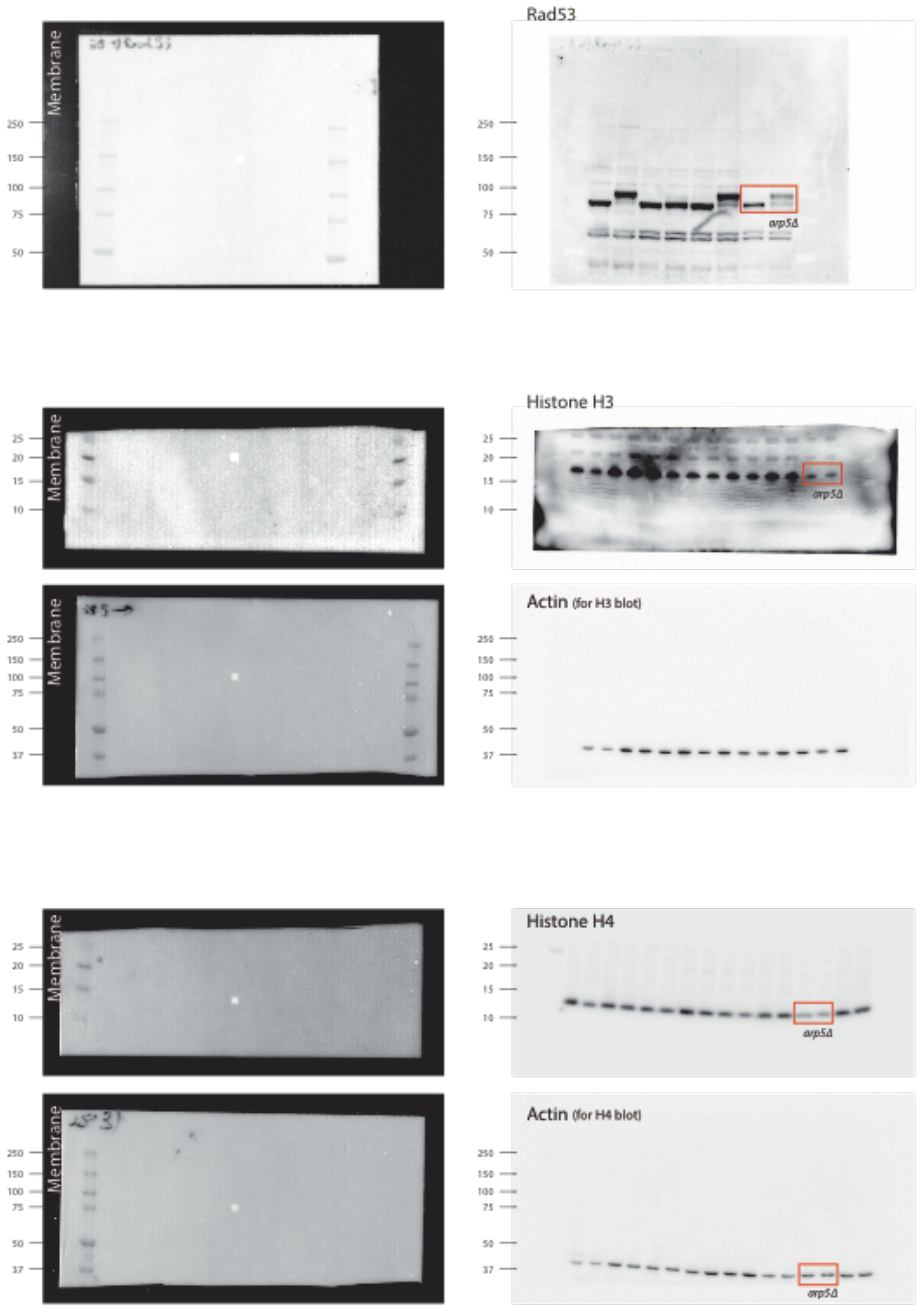

Nature Structural & Molecular Biology: doi:10.1038/nsmb.3347

CHAPTER 5: PROBING GLOBAL CHROMATIN COMPOSITION WITH MASS SPECTROMETRY

Summary

Assessing all chromatin bound proteins at once is of special interest and can answer the question how global chromatin composition changes in response to genotoxic insults (**Fig. 6a**). This chapter describes our progress in developing a mass spectrometry (MS) based workflow to examine the global protein composition of chromatin (chromatome) in yeast. Previously described techniques were developed for mammalian systems (Paul Ginno & Dirk Schübeler, unpublished data)(Kustatscher, Hegarat et al. 2014) and provided a basis for our approach. However, they awaited refinement to allow for application to yeast. We used TMT (Tandem Mass Tag)(McAlister, Huttlin et al. 2012) labeling based MS to unambiguously compare different chromatin purification methods and devise a robust workflow for yeast. This work has been done in close collaboration with Mariya Kryzhanovska, (a Master student in the Gasser laboratory who worked under my guidance) and Paul Ginno (a postdoctoral researcher in the Schübeler laboratory).

Rationale

Several MS studies have used different cell fractionation approaches to quantify the proteome of the entire nucleus (Dundr and Misteli 2002, Mosley, Florens et al. 2009, Wuhr, Guttler et al. 2015) or its different subcompartments (Andersen, Lyon et al. 2002). Fractionation is necessary because highly abundant cytoplasmic proteins otherwise mask the signal of the relatively low abundance nuclear proteins. Currently, much effort has been put into developing proteomic techniques which address local or global chromatin composition following formaldehyde crosslinking of proteins to DNA, coupled with DNA, protein or peptide immunoprecipitation (IP) (Wierer and Mann 2016)). A recent study has devised a novel method to quantitatively determine all chromatin-bound proteins (chromatome) in mammalian cells (Kustatscher, Hegarat et al. 2014, Kustatscher, Wills et al. 2014). This technique is based on formaldehyde crosslinking and subsequent chromatin fractionation. First, whole cells are crosslinked with formaldehyde followed by nuclear extraction, lysis and subsequent chromatin fractionation. As chromatin is a dense meshwork of DNA-protein crosslinks, it is largely insoluble and precipitates in aqueous solutions. Importantly, Kustatscher *et al.* implemented two key steps in this protocol which could both lower sample complexity and reduce unspecific binding. First, RNA was digested from crosslinked chromatin which reduced highly

abundant ribosomal protein signals. Secondly, high concentrations of the chaotrope urea were used to eliminate unspecifically-bound/non-crosslinked proteins from the precipitated chromatin sample.

Work in the Schübeler laboratory (Paul Ginno & Dirk Schübeler, unpublished results) devised another method that allows for MS based quantification of the chromatome. This technique exploits the unique property of cesium chloride (CsCl) gradients to separate DNA-protein crosslinks from free DNA and protein upon ultracentrifugation, a process called isopycnic focusing (Solomon, Larsen et al. 1988, Orlando, Strutt et al. 1997). Given the unique density of protein-DNA complexes, it can be used to separate mammalian chromatin from other cellular components. To this end, nuclei are extracted from mammalian cells, crosslinked and solubilized in a high concentration CsCl solution by sonication. Following ultracentrifugation, the CsCl creates a self-forming gradient, and the chromatin-containing fractions band with a buoyant density of ϱ = 1.39 g/cm^3. The fraction is recovered, dialyzed against physiological buffer and prepared for MS. Both of these techniques (by Kustatscher & by Ginno) were developed for mammalian cell systems in which histone-DNA complexes (nucleosomes) form a major component that is readily isolated from other cellular components.

In **chapter 4**, we used simple chromatin fractionation techniques coupled with SILAC-based MS analysis to assess chromatin composition in response to DNA damage in budding yeast. Using this, were were not able to make definitive statements about the presence of chromatin proteins other than histones. The measured intensity values of other proteins were often very low and we observed variability between replicates. Furthermore, the presence of cytoplasmic proteins in the chromatin sample made us doubt whether this approach achieves sufficient purity to determine an entire chromatome. We therefore set out to develop a robust workflow that would allow us to monitor changes in chromatin bound proteins in yeast, in response to DNA damage.

Results

We first tested whether the CsCl gradient-based, chromatin purification protocol developed in the Schübeler laboratory would be applicable in yeast (**Fig. 6b**). Due to the difficulty of lysing yeast cells without spheroplasting, the nuclear extraction step was omitted. In brief, we crosslinked cells with formaldehyde during exponential growth, lysed them with detergents and subjected the lysate to CsCl fractionation. Following the workflow illustrated in **Fig. 6bc**, we collected CsCl gradient fractions and visualized DNA with Hoechst. We found DNA enriched at a buoyant density of ϱ=1.39 g/cm^3 which is indicative for DNA-protein crosslinks, or chromatin (Solomon, Larsen et al. 1988, Orlando, Strutt et al.

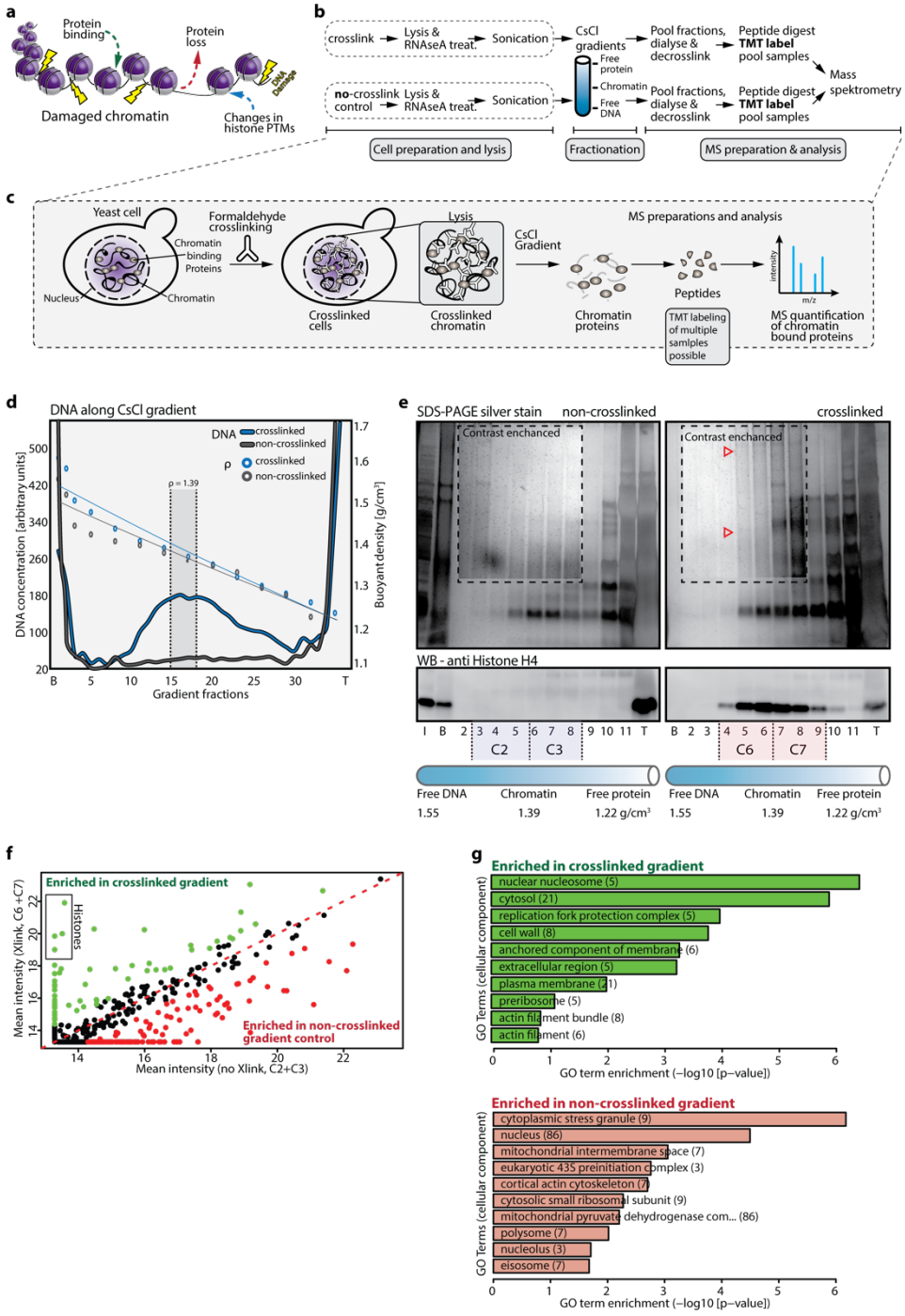

Figure 6 Probing chomatin-wide protein composition with the CsCl approach. (**a**) General objective: developing a method which would allow to proge chromatin-wide protein composition in response to DNA damage. (**b-c**) Experimental workflow for CsCl based chromatin enrichment combined with TMT labeling and subsequent mass spectrometry. The control was done without formaldehayde crosslinking. Whole cells are subjected to formaldehyde crosslinking. After cell lysis, samples are treated with RNAseA and DNA is sheared and solubilized via sonication. Protein-DNA crosslinks are fractionated via isopycnic focusing during ultracentrifugation on a self-forming CsCl gradient. DNA content along the gradient fractions is measured via Hoechst staining and chromatin containing fractions are dialyzed against a physiological buffer. After crosslink reversal and DNA digestion with Benzonase, samples are send for mass spectrometric measurements. (**d**) DNA concentration along CsCl gradient fractions derived from non crosslinked vs. crosslinked whole cell lysates. An enrichment of DNA-protein crosslinks is seen in the crosslinked sample only at the expected density of $\rho = 1.39$ g/cm³.

(**e**) Silver stained SDS-PAGE and histone H4 Western blot of further pooled fractions from the two gradients visualized in d. An enrichment of DNA-histone crosslinks is only detected in the gradient, derived from crosslinked whole cells (fractions 4-9). Fractions 5-7 further show high molecular weight bands on a silver stained SDS-PAGE, suggesting the presence of other proteins apart from histones in the chromatin peak. (**f**) Scatterplot showing proteins either enriched in the crosslinked gradient or the control situation. Log2 mean intensities from C2+C3 and C6+C7 fractions (e) were plotted. Green dots represent proteins enriched upon crosslinking, whereas red marked proteins were significantly enriched in the control situation. (**g**) GO term analysis of proteins enriched in the crosslinked gradient (green) or in the control (red) reveals that except nuclear nucleosome and replication fork protection complexes no other chromatin specific proteins could be enriched upon crosslinking.

1997). Free nucleic acids with a density of approximately ϱ = 1.7 g/cm3 were found at the bottom and free proteins (ϱ =1.28–1.35 g/cm3) formed a proteinaceous band at the top of the gradient (ϱ=1.7g/cm^3) (**Fig. 6d**). This indicated that chromatin should have been well separated from other cellular components.

To estimate protein composition within gradient fractions, we dialyzed them against a physiological buffer and visualized proteins by silver staining on SDS-PAGE gels (**Fig. 6e**). Histone H4 distribution within the gradient was followed with immunoblotting (**Fig. 6e**). Immunoblots showed a clear peak of DNA-nucleosome crosslinks that were separated from the free histones at the top the gradient (**Fig. 6e**, C6 and C7). As expected, the control sample (no crosslinking) showed neither DNA (**Fig. 6d**, fractions 10-25) nor histone signals (**Fig. 6e, C2 and C3**) at the respective density of ϱ=1.39 g/cm^3. Interestingly, histone H4 peak fractions showed high molecular protein bands on the SDS-PAGE, probably deriving from chromatin-bound non-histone proteins (**Fig. 6e**). We thus combined the respective gradient fractions from non-crosslinked and crosslinked cells (**Fig. 6e**, 3-8 and 4-9 respectively), prepared TMT labeled peptides and send those for MS analysis. Unfortunately, we could not detect a specific enrichment for any chromatin proteins other than histones upon crosslinking (**Fig. 6f**). This became even more apparent after a GO term analysis of all significantly enriched proteins in both the crosslinked and control samples (**Fig. 6g**). Apart from histones, only one other chromatin related protein group (replication fork protection complex) was found to be enriched after crosslinking.

Against our expectations, nucleolar proteins were found in the control fractions and cytoplasmic proteins were recovered in the crosslinked samples. This is in contrast to what Ginno & Schübeler observed with the same method in mammalian cells. As we had omitted the nuclear fractionation step, which is a lengthy and error prone procedure in yeast, we hypothesized that the impurities in the gradient might arise from whole cell crosslinking. This hypothesis is further strengthened by a study which used crosslinking combined with CsCl gradients to isolate proteins bound to the yeast mitochondrial genome. Here, it was necessary to purify mitochondria before crosslinking and successful CsCl enrichments (Kaufman, Newman et al. 2000). In addition, two other studies in yeast successfully used insolubility-based chromatin purification methods (Kubota, Hiraga et al. 2011, Kubota, Nishimura et al. 2013). These latter

methods were similar to the chromatin fractionation procedure described in **Chapter 4**. We therefore developed four additional workflows with three of them including an additional spheroblasting and chromatin pre-fractionation step (**Fig. 7a**).

Pre-fractionated yeast chromatin was either crosslinked (**Fig. 7b**) or directly prepared for MS. The two crosslinked chromatin samples were further used for CsCl gradient fractionation or subjected to urea washes as described by Kustatscher *et al.* (Kustatscher, Hegarat et al. 2014). After repeating each workflow twice, we used TMT-based MS to compare them side by side for reproducibility and chromatin protein enrichment.

Clustering of all eight samples by log2 peptide intensities showed high correlation within replicates (R>0.8) (**Fig. 7c**). The reproducibility was further addressed with scatterplots, which showed correlation coefficients higher than 0.87 in all cases. This confirms that our workflow is robust (**Fig. 7d**). Interestingly, all pre-fractionated (PF) chromatin samples formed a supercluster that was clearly distinct from the two non-pre-fractionated, whole cell extract (WCE) samples (**Fig. 7d**). This indicated that the protein composition was largely similar in between pre-fractionated chromatin, but was clearly distinct from that of directly crosslinked cells.

After showing that all workflows were reproducible, our next goal was to see which of these allowed for the best enrichment of chromatin proteins. We thus first extracted the intensities of all histone and transcription factor (TF) derived peptides within each of the two replicates from the four workflows and visualized them as boxplots (**Fig. 7e**). Remarkably, pre-fractionated chromatin, which was washed by urea (**Fig. 7e,** PF_Urea_r1&r2), showed the highest histone intensity signal and the lowest TF signal. We next performed a GO term analysis to address the enrichment of chromosome, nucleus or cytosol related proteins (**Fig. 7f**). After summing up the signal intensities of all proteins which fall into one of these categories, we calculated their proportion with respect to the total protein signal. This gave us a measure for the percentage these categories occupy within in each sample. Strikingly, almost 20% of the total protein signal in pre-fractionated chromatin samples further purified with CsCl (PF_CsCl) or washed with urea (PF_Urea) was derived from chromosome-related proteins. The same was true for proteins annotated as "nuclear": this yielded nearly 65% in both workflows, while "cytosolic proteins" made up only 5%. Taken together with the high histone signal intensity (**Fig. 7e**, PF_Urea_r1&r2), this clearly shows that pre-fractionating chromatin and subsequently subjecting it to urea washes was the best way to enrich for chromatin-bound proteins.

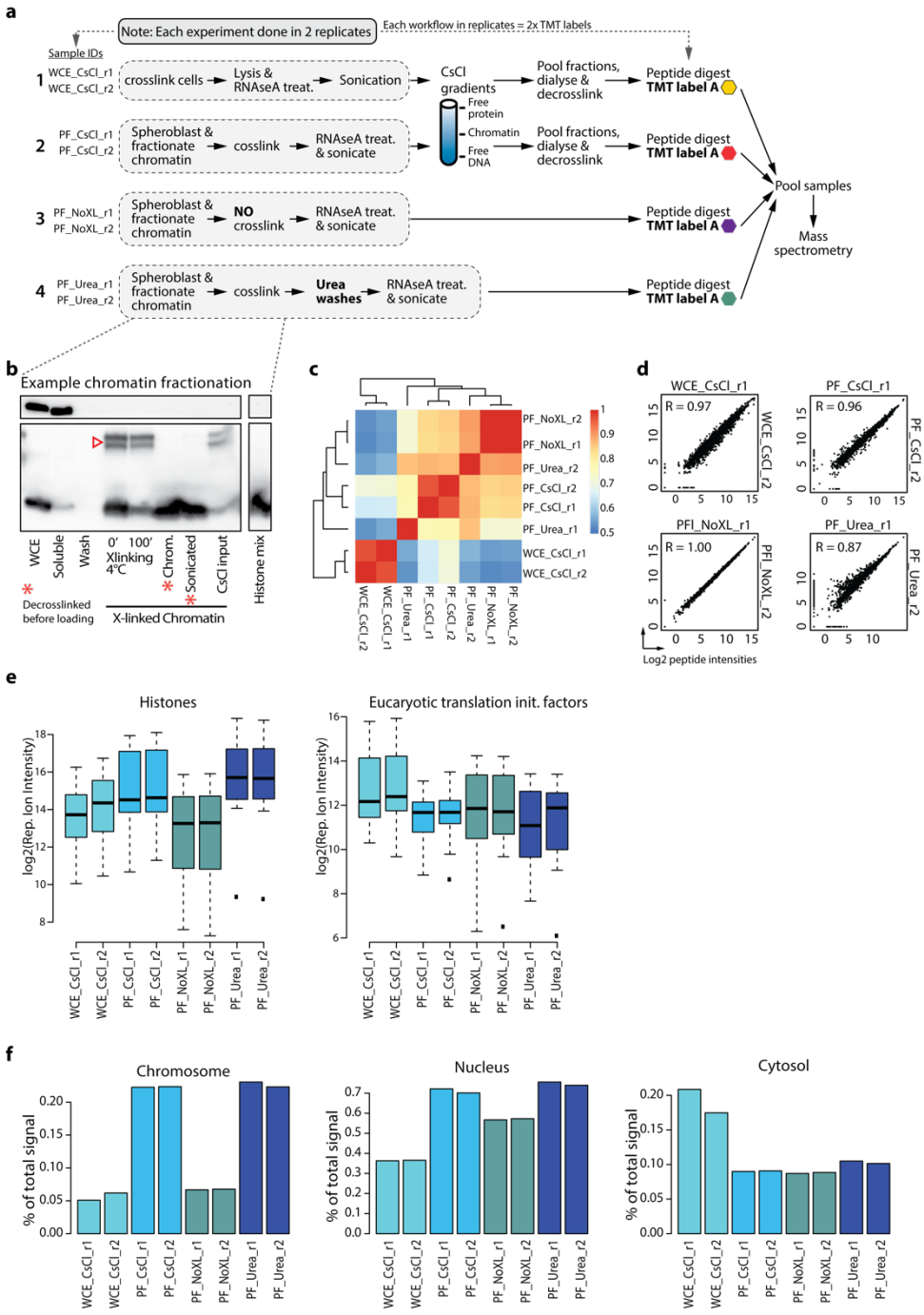

Figure 7 Four different approaches for chromatome enrichment. (**a**) Four different workflows were tested for efficient enrichment of chromatin-related proteins. Each workflow was done in duplicates and the total of 8 samples were mulitplexed via TMT labeling and subsequent MS analysis. 1; WCE_CsCl describes crosslinking of whole cells followed by CsCl gradients of whole cell extracts. 2; PF_CsCl indicates chromatin prefractionation followed by crosslinking and coupled to CsCl gradients. 3; is a classic chromatin fractionation workflow without crosslinking. 4, is equal to 3 but chromatin was crosslinked subsequent to fractionation and washed with urea. (**b**) Western plots following the pre-fractionation and crosslinking procedure of chromatin as shown in workflow 2 (see in a). WCE = whole cell extract. Soluble = soluble fraction after precipitating chromatin. Wash = fraction used to wash precipitated chromatin. 0' and 100' Xlinking = 0 min. and 100 min. time-points of precipitated chromatin in buffer with formaldehyde at 4°C. Red triangles show a crosslinking depended upshift of histone H4. Sonicated = chromatin after sonication. CsCl input = sample loaded on the CsCl gradient. (**c**) Heatmap of log2-intensities for all eight reporters shows good correlation (R>0.8) within replicates.

(**d**) Log2-intensities of all reporter (TMT) channels within replicates were plotted against each other. The correlation coefficient for each combination is shown. (**e**) Histone and translation factor signal distribution within different chromatin precipitation methods. Intensities of either histones or translation factor (TFs) peptides were extracted from the total intensity of every sample. Distributions of log2 transformed histone or TFs intensities are shown. (**e**) Proportion of specific GO term signal to total reporter signal per sample. Bargraphs "Chromosome", "Nucleus" and "Cytosol" represent the proportion of each GO term category in relation to the total protein signal.

References

Andersen, J. S., C. E. Lyon, A. H. Fox, A. K. Leung, Y. W. Lam, H. Steen, M. Mann and A. I. Lamond (2002). "Directed proteomic analysis of the human nucleolus." Curr Biol **12**(1): 1-11.

Dundr, M. and T. Misteli (2002). "Nucleolomics: an inventory of the nucleolus." Mol Cell **9**(1): 5-7.

Kaufman, B. A., S. M. Newman, R. L. Hallberg, C. A. Slaughter, P. S. Perlman and R. A. Butow (2000). "In organello formaldehyde crosslinking of proteins to mtDNA: identification of bifunctional proteins." Proc Natl Acad Sci U S A **97**(14): 7772-7777.

Kubota, T., S. Hiraga, K. Yamada, A. I. Lamond and A. D. Donaldson (2011). "Quantitative proteomic analysis of chromatin reveals that Ctf18 acts in the DNA replication checkpoint." Mol Cell Proteomics **10**(7): M110 005561.

Kubota, T., K. Nishimura, M. T. Kanemaki and A. D. Donaldson (2013). "The Elg1 replication factor C-like complex functions in PCNA unloading during DNA replication." Mol Cell **50**(2): 273-280.

Kustatscher, G., N. Hegarat, K. L. Wills, C. Furlan, J. C. Bukowski-Wills, H. Hochegger and J. Rappsilber (2014). "Proteomics of a fuzzy organelle: interphase chromatin." EMBO J **33**(6): 648-664.

Kustatscher, G., K. L. Wills, C. Furlan and J. Rappsilber (2014). "Chromatin enrichment for proteomics." Nat Protoc **9**(9): 2090-2099.

McAlister, G. C., E. L. Huttlin, W. Haas, L. Ting, M. P. Jedrychowski, J. C. Rogers, K. Kuhn, I. Pike, R. A. Grothe, J. D. Blethrow and S. P. Gygi (2012). "Increasing the multiplexing capacity of TMTs using reporter ion isotopologues with isobaric masses." Anal Chem **84**(17): 7469-7478.

Mosley, A. L., L. Florens, Z. Wen and M. P. Washburn (2009). "A label free quantitative proteomic analysis of the Saccharomyces cerevisiae nucleus." J Proteomics **72**(1): 110-120.

Orlando, V., H. Strutt and R. Paro (1997). "Analysis of chromatin structure by in vivo formaldehyde cross-linking." Methods **11**(2): 205-214.

Solomon, M. J., P. L. Larsen and A. Varshavsky (1988). "Mapping protein-DNA interactions in vivo with formaldehyde: evidence that histone H4 is retained on a highly transcribed gene." Cell **53**(6): 937-947.

Wierer, M. and M. Mann (2016). "Proteomics to study DNA-bound and chromatin-associated gene regulatory complexes." Hum Mol Genet **25**(R2): R106-R114.

Wuhr, M., T. Guttler, L. Peshkin, G. C. McAlister, M. Sonnett, K. Ishihara, A. C. Groen, M. Presler, B. K. Erickson, T. J. Mitchison, M. W. Kirschner and S. P. Gygi (2015). "The Nuclear Proteome of a Vertebrate." Curr Biol **25**(20): 2663-2671.

Material and Methods

Media and growing conditions for SILAC yeast strain

Unless otherwise stated, yeast cultures were grown at 30 °C until logarithmic (Horlbeck, #52) growth phase (OD600 = 0.7; 1 × 107 cells/ml).

Materials

Physiological buffer:

1 x PB	Stock solutions	For 40ml
10mM Tris pH 8	1M	400ul
1 mM EDTA	0.5M	80ul
0.5 mM EGTA	0.5M	40ul

Dialysis Buffer:

1 x DB	Stock solutions	5L
10 mM Tris pH 8	1M	50ml
5% Glycerol	100%	250ml
1 mM EDTA	0.5M	10ml
0.5 mM EGTA	0.5M	5ml
H20		4685ml

Buffer A (store at 4°C):

10 x Buffer A	Stock solutions	For 100ml
200mM HEPES pH7.5	1M	20ml
800mM KCl	2M	40ml
80mM EDTA-KOH	0.5M	16ml
5mM Spermidine	0.5M	1ml
2mM Spermine	0.5M	0.4ml
H2O		to 100ml

Buffer B (prepare fresh):

1 x Buffer B	Stock solutions	For 100ml
100mM PIPES-KOH pH 9.4	0.5M	20ml
0.1M EDTA-KOH	0.5M	20ml
0.1% Na-Azide	10%	1ml
10mM DTT	1M	1ml
H2O		to 100ml

Buffer C:

1 x Buffer C	Stock solutions	For 100ml
50mM K-Phosphate pH7.0	1M	5ml
1.1M Sorbitol	2M	55ml
1mM ß-Mercaptoethanol	14.3M	7ul
0.5mM MgCl2	1M	50ul
H2O		to 100ml

Wash buffer (prepare fresh):

1 x WB	Stock solutions	For 80ml
0.25x (10x BufferA)	10 x Buffer A	20ml
1M Sorbitol	2M	40ml
0.5mM PMSF	200mM	200ul
Roche protease inhibitor 1x		2 maxi tablets
H2O		to 80ml

E buffer (prepare fresh):

1 x EB	Stock solutions	For 100 ml
30mM KCl	1M	3 ml
50mM HEPES-KOH pH7.5	1M	5ml
2.5mM MgCl2	1M	250ul
0.1mM ZnSO4	10 mM	1ml
2mM NaF	200mM	1ml
0.5mM Spermidine	0.5M	100ul
0.2mM PMSF	200mM	100 ul
Roche protease inhibitor 1x		2 maxi tablets
Phosphatases inhibitor 1x	(100x)	1 ml
with or without:		

0.25% TritonX-100	100%	250ul
0.5% TritonX-100	100%	500ul
H2O		to 100 ml

Chromatin stabilization by crosslinking of whole yeast cells and preparation of WCE for chromatin enrichment

Log-phase yeast cells were fixed for 1 hour at 25°C by addition of formaldehyde (37% formaldehyde solution, Sigma-Aldrich) to a final concentration of 3%. Quenching was carried out with glycine (final 0,125M) for 10 min at 25°C. Cells were harvested by short centrifugation (3500 x g) and washed once with 1 x PBS. Washed cell pellets were resuspended in physiological buffer (PB). The homogeneous cell suspension was flash frozen in droplets. Mechanical lysis was performed by cryo-grinding (Retsch grinder) applying 5 cycles of 30 Hz for 2 min. Frozen cell powder was transferred to falcon tubes and left to thaw on ice. The volume of WCE was adjusted to 5 ml by ice-cold PB. Sonication was performed on a Branson sonifier, applying 30% amplitude power for 6 cycles of 30 sec ON and 15 sec OFF. The sample was cooled in an ethanol/dry ice bath during the sonication process. Elimination of RNA from the WCE was achieved by 15 min RNAse (home-made) digestion (final 0.05 mg/ml) at 37°C. After this step, sample volumes were adjusted to 12 ml with ice-cold PB. Incubation with sarcosyl (sodium lauroyl sarcosinate, FLUKA) at final concentration of 0.5% was carried out at 4°C and continued for 30 min. Finally, samples were cleared by short centrifugation (2000 x g, 2 min, 4°C). Cleared lysate was stored on ice until further processing as described in the enrichment protocol.

Chromatin yielding by pre-fractionation and subsequent cross-linking

One liter of log-phase yeast culture (OD600 = 0.7) was harvested by centrifugation (2000 x g, 5 min, RT) and washed once with 1 x PBS. Cell pellets were resuspended in 45 ml Buffer B and incubated at RT on a rolling device. Buffer B was exchanged by brief centrifugation (2000 x g, 2 min, RT) and resuspension in 12 ml of Buffer C. Zymolase 100T (US Biologicals) digestion was carried out at 30°C and final concentration of 0,75 mg/ml. The digestion was stopped when the spheroplasting was efficiently achieved followed by microscopy testing. After a brief centrifugation step (1500 x g, 2 min, 4°C), spheroblast pellets were carefully washed twice with ice cold wash buffer. First, spheroblasts were carefully resuspended in 2 ml of E buffer without Triton X-100, before 2,25 ml E buffer + 0,25% Triton X-100 was added. For mixing, slow invertion on ice was performed untill the lysis of spheroplasts was complete. The total lysis mixture was overlaid on 9 ml of 30% sucrose in E buffer + 0.25% TritonX-100 (with 1.5% formaldehyde) in a Ultra Clear Beckman Coulter 14 ml tube. After ultracentrifugation (18000 x g, 15 min, 4°C) supernatant

was removed and chromatin pellet was gently resuspended in 5 ml of E buffer + 0,25% Triton X-100 with 1% formaldehyde. Chromatin was cross-linked for 60 min on ice, inverting from time to time and further cross-linked at RT for 25 min on a rolling device. Addition of final 0,125 M glycine quenched free formaldehyde and stopped the crosslinking reaction. The final chromatin sample was centrifuged at 14 000 x g at 4°C for 15 min and carefully resuspended in 4 ml PB. Chromatin pellet was kept on ice till further chromatin enrichment protocol either by CsCl or Urea wash.

Chromatin enrichment by CsCl gradient purification

Cesium chloride (SIGMA) was added to cleared lysates or pre-fractionated chromatin to a final buoyant density of 1.4 g/cm^3 and loaded in Beckman Coulter polyallomer ultracentrifuge tubes. Ultracentrifugation in an SW41 rotor was carried out for 90 h, 29 000 rpm, 20 °C. Gradients were harvested by picking a needle at the bottom of gradient and collecting drops in nearly equal fractions of 500 µl. DNA content in each of fraction was determined by Hoechst stain and DNA containing fractions were collected. Fractions were dialyzed overnight in against dialysis buffer (DB). Dialyzed fractions were de-crosslinked at 95°C for 45 min and addition of 1 ul Benzonase® (250 units) was sufficient to digest DNA within 20 min incubation at 37°C. Proteins were precipitated over night by trichloracetic acid (TCA) at a final concentration of 20%. Protein pellets were washed once with 10 % TCA/ddH2O solution and additionally washed by 70% ethanol solution. Dried protein pellet were stored at -80°C until further trypsin digestion for mass spectrometric analysis.

DNA content determination by Hoechst stain

For each of the CsCl gradient fractions (10 µl) were mixed with 200 µl of freshly prepared assay solution in a black 96 well plate. Fluorescence was measured with a Spectra Max GEMINI EM microplate reader. All fractions were measured at least in duplicates.

1 mg/ml Hoechst 33258 (Eugene) in ddH2O
10 x TNE buffer (store at 4°C)
100 mM Tris-HCl, pH 7.5 (Hoechst stock 1M)
10 mM EDTA, pH 8 (stock 0.5M)
2M NaCl (stock 5M) pH 7.4

H 33258 stock solution (1000 x)	10 ul
TNE buffer (10 x)	10 ml
H2O	90 ml
Total	100 ml

Chromatin enrichment by urea-washes

RNA in pre-fractionated chromatin was digested with RNAse for 20 min at 37°C. The chromatin pellet (after centrifugation 14000 x g, 15 min, 4°C) was resuspended carefully, but completely in PB + 2% SDS (sodium dodecyl sulfate). Urea buffer (1.5 ml) was added and mixed thoroughly by inverting the tube several times. Urea wash steps were repeated twice spinning for 15 min at 14 000 x g at RT. Finally, the resulting chromatin pellet was washed once in PB + 2% SDS and resuspended in 1 ml PB. Sonication was performed with a Bioruptor® at 4°C for 15 min, 15 sec ON, 15 sec OFF (max power). Sample volume was increased to 2 ml PB and sarcosyl was added to final 1%. After 30 min incubation at 4°C on a rotating device and centrifugation step (14 000 g, 15 min, RT), the soluble fraction was de-crosslinked at 95°C for 45 min. Chromatin samples were snap frozen and stored at -80°C until further processing such as DNA digestion by Benzonase® and standard TCA protein precipitation procedure.

Immunoblotting

The total protein content in the relevant samples was determined with the Quant-iT protein assay kit (Thermo Fisher Scientific), and 8.75 μg of total protein was loaded and run on Criterion TGX Stain-Free 8–16% (Bio-Rad) gels under SDS denaturing electrophoresis condi- tions. Rapid fluorescent detection of all proteins in the gel or on the membrane was done according to the manufacturer's specifications, and protein transfer on PVDF membranes was done with the Trans-Blot Turbo system. Rad53 protein was detected with a custom-made mouse monoclonal antibody (GenScript) to the FHA2 domain of Rad53. Anti-γH2A was similarly a custom- made polyclonal antibody specific for phospho-S129 in yeast H2A. Titration curves of histone H3 and histone H4 antibodies were generated to work within the linear detection range before use (data not shown).

Trypsin digestion

Equal amounts (nearly total 100 ug) of each protein sample were resuspended in RCM buffer (0.5 M Tris pH 8.6/ 6 M GnHCl, 0.45 μm filtered) and incubated at RT for 30 min after addition of 20 ul 100 mM TCEP. Addition of 20 ul 250 mM iodoacetamide (prepare 46 mg/mL of iodoacetamide in ddH2O) and incubation at RT in darkness for 30 min were followed by sample dilution with 500 ul trypsin digestion buffer (50 mM Tris/HCl pH 8.6, 5 mM CaCl2). Protein digestion was carried out by the addition of trypsin (final 3 ng/ul) and 100 % acetonitrile (HPLC grade, final 3.125%) to each sample and an overnight incubation at 37°C. The next day, half of the initial trypsin portion was added and digestion was continued for another 3-4 hours at 37°C.

Desalting

Peptides were desalted using 50 mg C18 solid phase extraction cartridges (Waters). Approx. 630 ul of eluate were obtained. 30 ul (max. 5 ug) aliquots were transferred into auto sampler glass vials for quality control MS analyses and dried together with the remaining 600 ul (max. 95 ug) aliquots in a speed vac.

TMT9plex labeling and desalting

Samples were labeled with channels 126 – 130C of TMT 10plex reagent (Label reagent set, Thermo Fischer, Lot# PI202555). According to the facility's standard TMT labeling protocol, we mixed in equal volumes and then desalted. 40 ul of labeling buffer (2M Urea/0.2M HEPES, pH = 8.3) was added to dried peptide pellets followed by the addition of 6 ul of the respective TMT reagent solution (TMT reagents 126-130C in anhydrous DMSO). The reactions were stopped by adding 3 ul of stop solution (1.5 M hydroxylamine). Finally, samples were mixed and empty reaction vials were washed with 20 ul high pH buffer (1M potassium phosphate buffer, pH = 12). Mixed solutions were acidified with 230 ul of 2M HCl and 80 ul of 5% trifluoroacidic acid (final TFA conc. 0.5%). This mixture was desalted on 50 mg C18 SepPak Waters SPE cartridges. After elution, peptides were mixed with 50 ul 50% acetonitrile, 0.15% TFA. An approximate of 5 ug of the eluted TMT peptide mix was transferred to an autosampler glass vial and dried the remaining 900 ug were dried for subsequent peptide fractionation.

LC-MS acquisition

TMT-labeled peptide samples were analyzed using an LC-MS3 method by nano liquid chromatography tandem mass spectrometry with an EASY-nLC 1000 pump using a two column set up (Thermo Fisher Scientific). The peptides were loaded in buffer A onto a trap column (Acclaim PepMap 100, 75μm x 2cm, C18, 3μm, 100Å) and separated using a PepMap RSLC analytical column (50 μm x 15 cm, C18, 2 μm) column at 45C mounted on a modified DPV ion source (New Objective) connected to an Orbitrap Fusion mass spectrometer (Thermo Scientific) at a flow rate of 150 nl/m with a linear gradient of 3-8% buffer B in 3 minutes followed by a linear increase from 8-22% B in 40 minutes, 22-40% B in 5 min, 46-80% B in 5 min followed by 8 min wash at 80% B (buffer A: 0.1% formic acid in water, buffer B: 0.1% formic acid in acetonitrile). Data was acquired using an MS3 method as described by McAlister et al. (Mcalister et al. 2014). Briefly, MS1 full scans were acquired with a cycle time of 1 second in the Orbitrap analyzer at 120k resolution followed by CID fragmentation and detection in the ion trap of the top 10 MS1 peptide precursors, synchronous precursor selection of the top 6 MS2 fragment ions followed by HCD fragmentation and detection of the TMT10plex reporter ions at 60k resolution in the Orbitrap analyzer.

CHAPTER 6: CONCLUSIONS AND FUTURE PROSPECTIVES

This last chapter is divided into two parts. The first part summarizes my findings and discusses the relevant results. The second part highlights the future directions arising from these results.

Discussion

In this thesis I have explored global chromatin changes that arise in response to DNA damage. The majority of my work was focused on chromatin in the broad sense – specifically focused on histones. During my time in the Gasser laboratory, I have used multiple techniques such as quantitative mass spectrometry, fluorescence microscopy and image analysis workflows to examine chromatin changes in response to DNA damage. This led to the main contributions discussed in **Chapters 2 – 5**. We found that the DNA damage response causes widespread changes in the physical structure and protein composition of chromatin. Our work on this subject uncovered a previously unappreciated pathway which triggers proteasomal degradation of histone proteins in response to DNA damage (**Chapter 4**). During the course of this study, we further developed a semi-automated image analysis workflow that was successfully used to measure the expansion and nuclear position of fluorescently labeled chromatin domains both in yeast and *C. elegans* (**Chapters 2 & 3**). In addition, we have devised a mass spectrometry-based workflow for the quantitative analysis of global chromatin composition (**Chapter 5**). Finally, we found that forced changes in endogenous nucleosome occupancy can impact repair events in yeast. If transferred to mammalian cells, this effect might have interesting applications in the future.

Nucleosome degradation and chromatin expansion at the basis of global chromatin mobility

In **Chapter 4**, I have outlined and discussed my main PhD project which uncovered the mechanism by which remodeling enzymes are able to increase chromatin mobility in response to DNA damage.

We used quantitative mass spectrometry, fluorescent live-cell microscopy and genome-wide nucleosome mapping to show that core histone proteins are degraded in response to damage in a checkpoint, remodeler and proteasome-dependent manner. This caused chromatin to expand globally, become more flexible and enhance its mobility. These findings were further validated in a recent publication from the Gasser and Holcman laboratories which showed that INO80-C-dependent chromatin expansion and relaxation also occurred at site specific DSBs (Amitai, Seeber et al. 2017). Our results thus implicate histone degradation in both local and global damage-provoked chromatin mobility

(**Fig. 8ab**). Furthermore, we suggest remodeler-dependent histone degradation as a novel and integral part of the DNA damage response in yeast (**Fig. 8c**).

Forcing nucleosome loss from DNA led to enhanced chromatin mobility, unfolded chromatin and

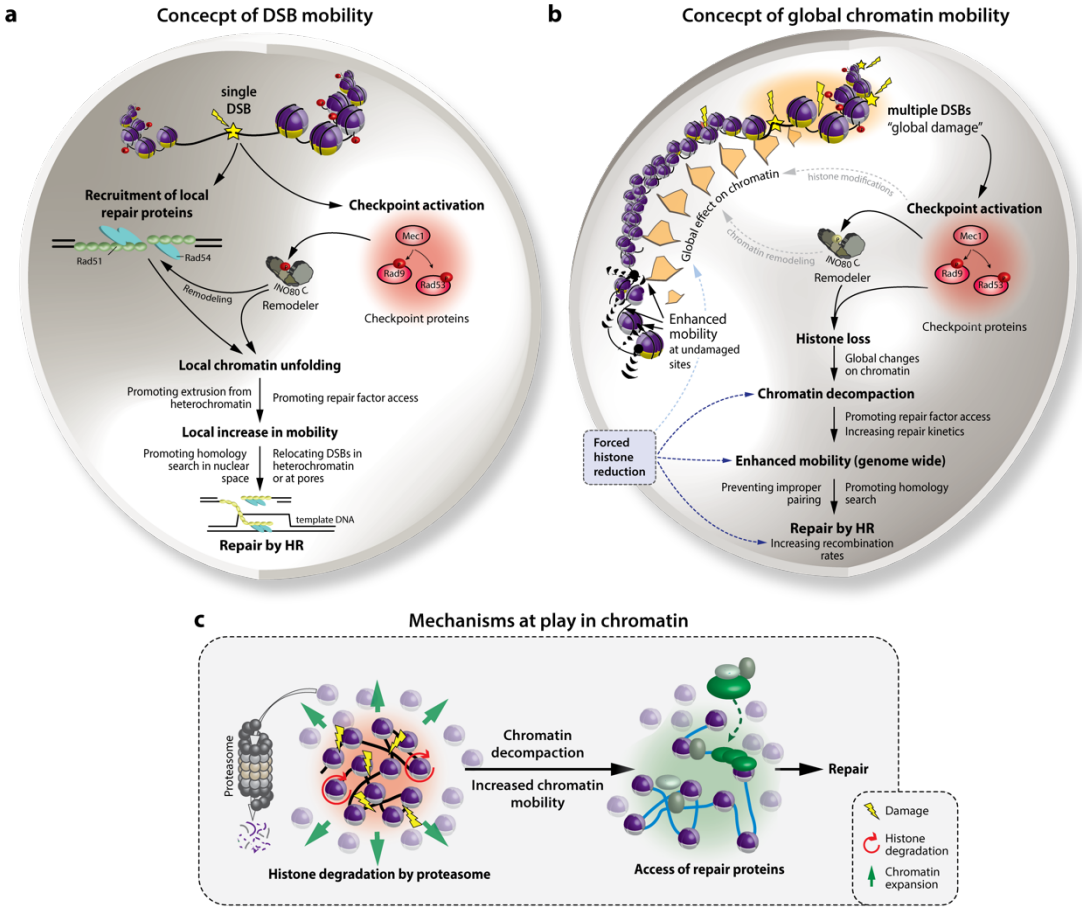

Figure 8 Concepts of local and global chromatin mobility in response to DNA damage. (**a**) Recapitulation of DSB mobility. For detailed information see Fig. 4. (**b**) Model for global chromatin mobility. Zeocin is used to induce random DSBs and SSBs to the genome. This damage activates the key DDR kinase Mec1. Mec1 targets checkpoint proteins Rad9 and Rad53. Furthermore, it phosphorylates subunits of the chromatin remodeling complex INO80. Non-damaged loci in this scenario will be four times more mobile as compared to the undamaged condition. This global increase in chromatin movement requires Mec1, Rad53 and the INO80-C complex. Both the checkpoint and INO80-C trigger proteasome dependend degradation of core histones in response to DNA damage. This decompacts chromatin, enhances global mobility and facilitates repair. The impact of forced histone reductions is highlighted in blue. (**c**) Mechansims which are thought to be at play in chromatin upon DNA damage.

increased fiber flexibility (**Fig. 8c**). This directly linked chromatin composition to physical DNA movement and placed nucleosomes at the basis of damage-related mobility. Notably, this result contradicts an earlier report where transcriptional shutdown of histone H3 was found to decrease locus mobility (Verdaasdonk, Vasquez et al. 2013). The difference may reflect that enhanced chromatin flexibility requires the loss of both H3 and H4. Another explanation might be that the prolonged H3 repression workflow used by Verdaasdonk et al. caused an extended G2 cell cycle arrest and apoptosis even before data

acquisition. Furthermore, it was shown that H4 (but not H3) shutdown lead to a declustering of kinetochores (Bouck and Bloom 2007). Yet, another report by the Durocher group has recently postulated a release of chromosomal tethers around the centromere as the source of both altered local as well as global chromatin mobility (Strecker, Gupta et al. 2016). The authors identified Cep3, an inner kinetochore protein in yeast, as a target of the DDC kinase Rad53 and showed that damage-induced phosphorylation of Cep3 triggers a release of centromeres from their SPB tether. This was proposed to generally promote chromatin movement in response to damage, an effect that seem to be abrogated in a phospho-dead (S575A) Cep3 mutant. Strikingly, the cep3-S575A mutation had no effect on repair by homologous recombination which would suggest that chromatin mobility is dispensable for repair (Strecker, Gupta et al. 2016). These effects, however, cannot account for the expansion of non-centromeric chromatin or for the INO80-C dependencies observed in our study. Therefore, two independent hypotheses on how DNA damage increases chromatin movement exist: either through centromere declustering or through a change in chromatin fiber structure. Here I will discuss our current interpretation of the present data and how these hypotheses may potentially overlap.

As mentioned earlier, Bouck *et al.*, 2007, showed that complete transcriptional shutdown of H4 leads to kinetochore declustering. Therefore, the observed mobility increase in our *NHP6* deletion or the artificial transcriptional histone gene repression strains may arise not from a genome-wide loss of histones but rather a coincident loss of histone-H3 like centromere protein Cse4 at yeast centromeres. This raises the question whether damage-dependent histone loss is a cause or consequence to centromere declustering? An unpublished study from the Gasser laboratory currently addresses this question (Anais Cheblar & Andrew Seeber, personal communication). In this work, *NHP6* deletions were used to lower nucleosome occupancy in yeast cells containing a fluorescently tagged version of the essential kinetochore protein Mtw1 in combination with a tagged nuclear pore protein (Nup49). Both the nuclear position of Mtw1 as well as Mtw1 declustering (as in Strecker et al., 2016) was scored in either G1 or G2/M cells. Similar experiments were done after Zeocin treatment. Importantly, the microtubule poison Nocodazole was used as a positive control for kinetochore detachment (Bystricky, Heun et al. 2004). Surprisingly, neither kinetochore declustering nor detachment was observed in nhp6Δ cells or upon Zeocin treatment in either cell cycle stage. As expected, Nocodazole treatment led to kinetochore detachment. This contradicts the data from Strecker et al. and unambiguously shows that kinetochore declustering is not induced by DNA damage or in nhp6Δ. Furthermore, Amitai et al. found that the actin cytoskeleton impacts chromatin mobility through actin-driven nuclear oscillations which can be removed by treating cells with the actin polymerization inhibitor Latrunculin A. These oscillations were not required for enhancing the

mobility of a DSB. Therefore, it appears that DNA damage induced chromatin mobility is a result of direct changes to the chromatin fiber involving the INO80 complex.

Chromatome proteomics – a method to measure chromatin-wide protein abundances in yeast

Chromatin is a "fuzzy organelle" and subject to constant changes. This makes it especially challenging to access dynamic changes in protein abundances and modifications. Two recent mass spectrometry techniques were used to crosslink, purify and quantitatively analyze chromatin from mammalian cells (Kustatscher, Hegarat et al. 2014, Paul Ginno & Dirk Schübeler - unpublished results). In **Chapter 5**, we have compared and modified these techniques and adapted them for chromatome analysis in yeast. During the course of this study, we found that CsCl gradient-based purification of chromatin from crosslinked cells is incompatible with yeast. It did not enrich chromatin-related proteins other than histones. We thus further tested four different workflows for successful chromatin enrichment. Out of these four, pre-fractionating chromatin from yeast cells before crosslinking and combined with subsequent washes urea washes performed best. It showed the highest amount of chromatin enrichment and the lowest amount of cytoplasmic protein contamination. We found that urea wash steps probably caused slightly higher variation within replicates, but was nevertheless essential to reduce non-specifically bound proteins. Purifying pre-fractionated chromatin over CsCl gradients showed comparable result. However, we do not recommend this technique because sample preparation times are substantially longer (up to five days as compared to two). We therefore recommend the "pre-fractionation, urea wash" workflow to address the chromatome in yeast. Coupled with TMT based labeling of peptides, up to nine different conditions can be quantified in parallel (multiplexed).

Future directions

In **Chapter 4**, I have shown that INO80-C plays a major role in damage-induced histone degradation. This is not surprising as the Ies3 and Ies4 subunits of INO80-C are targets of the Rad53 DDC checkpoint kinase and phosphorylated in response to DNA damage (Morrison, Kim et al. 2007). We further showed that histones were largely degraded by the proteasome. This suggests that histones need to be targeted for degradation by ubiquitination. Interestingly, INO80 was recently shown to interact with CDC48, an AAA+ ATPase involved in proteasome-dependent protein degradation (Lafon, Taranum et al. 2015). Moreover, both the DDC kinase Mec1 and INO80-C are linked to RNA polymerase II eviction at sites of replication fork–transcription collision, another process which most probably requires ubiquitin-mediated protein degradation (Poli, Gerhold et al. 2016). However, it remains to clarify what triggers histone degradation in yeast and how this process is related to the DDR. To answer this question, it would be interesting to

monitor histone PTMs before and after DNA and in damage in the absence and presence of proteasomal inhibition. This could be achieved by combining MS based chromatome measurements (described in **Chapter 5**) with histone PTM profiling. Given the involvement of the proteasome, we expect histones to acquire ubiquitination. In a simpler approach, histones could be first immunoprecipitated and subsequently investigated for ubiquitin-related upshifts on immunoblots. The Gunjan laboratory has recently identified multiple E2 and E3 ubiquitin-conjugating enzymes that regulate the degradation of excess histone levels in yeast (Singh, Kabbaj et al. 2009, Singh, Gonzalez et al. 2012). It is of interest to test the involvement of these enzymes in the damage-depended histone degradation pathway.

Using genome-wide nucleosome mapping, we identified a global reduction in nucleosome occupancy in response to DNA damage induced with Zeocin (**Chapter 4**). Up to now, we could not link this depletion to any structural elements or genomic regions such as centromeres or telomeres. As nucleosome occupancy equally dropped in high and low-level transcribed genes, this effect was independent from gene transcription. It would be interesting to determine the role of INO80 in this process and further examine whether nucleosomes are preferentially lost at INO80-binding sites and/or at genes which are activated in response to DNA damage. To this end, ChIP-sequencing could be used to identify INO80-C binding sites before and after Zeocin treatment. These sites could then be correlated to genome-wide nucleosome positioning data in WT and INO80-C mutant cells in the absence or presence of DNA damage. Finally, there is no study which addressed global transcriptional changes in response to Zeocin treatment. Therefore, RNA sequencing experiments would have to be done to correlate histone loss with gene transcription.

Using mass spectrometry and nucleosome mapping, we showed that core histones are degraded and lost from chromatin generally, i.e. genome-wide. However, it is not clear whether local histone loss at Zeocin-induced SSBs and DSBs could have contributed to this effect. There is the possibility that the global effect could just reflect the accumulation of random local losses in the cell population. This raised the question whether the damage checkpoint triggers a truly global nucleosome loss. Notably, we found that depletion of the exonuclease Exo1 did not inhibit nucleosome loss. This excluded a role of local DSB resection. Furthermore, calculating the amount of resected DNA at 10 DSBs (approximate number of breaks caused by the Zeocin concentrations used) within one hour after damage at a resection speed of 5 kb/h (Saad, Gallardo et al. 2014) could only account for 0.8% of the genome (100 kb). As we observed core histone losses of 20-30%, this provided another reason to neglect the effect of resection during global histone loss. However, probing nucleosome occupancy in response to artificial DDC activation (Bonilla, Melo et al. 2008) in the absence of DNA damage could provide definitive proof. To this end, multiple

DSBs could could be induced away from bulk chromatin by galactose-driven I-SceI cuts on a 2μ plasmid. Each cell harbors up to 150 copies of such plasmids and I-SceI induction should thus trigger a strong checkpoint response without introducing actual damage to chromatin. Genome-wide nucleosome mapping could then be used to specifically address nucleosome occupancy along chromosomes. Furthermore, it is tempting to couple such experiments with the proteomic approach discussed in **Chapter 5**.

In **Chapter 4**, we have shown that histone loss brought about by *NHP6* deletion or by transcriptional repression of histone genes, is sufficient to increase the rate of gene targeting, presumably by making chromatin more accessible. Similar to our results, work from the Bianchi laboratory showed that depletion of HMGB1 (the human homologue to Nhp6) equally triggers histone loss, reduced nucleosome occupancy and increased chromatin accessibility (Celona, Weiner et al. 2011). HMGB1 and Nhp6 belong to the family of high mobility group proteins which are found abundantly on chromatin where they bind to the minor grove of DNA (Malarkey and Churchill 2012). Recent biochemical studies complement our work and show that nucleosomes constrain the activity of CRISPR-Cas9 (Horlbeck, Witkowsky et al. 2016, Isaac, Jiang et al. 2016) which requires access to naked DNA to make its guide-RNA-directed cut (Jinek, East et al. 2013). This suggests that chromatin accessibility is a rate-limiting step for CRISPR-Cas9 related gene editing technologies and that its efficiency might be enhanced in a manner similar to the one we used in yeast. It is thus of interest to test whether artificially reducing nucleosome levels in mammalian cells would increase CRIPR-Cas9 cutting and gene editing rates. This is of special interest as the efficiency of gene editing by HR remains poor and the major challenge to overcome for many practical applications of CRISPR-Cas9 editing (Mali, Yang et al. 2013, Wang, Yang et al. 2013, Chu, Weber et al. 2015, Maruyama, Dougan et al. 2015). A number of molecules exist that bind to and block HMGB1 function such as the anti-inflammatory drug Glycyrrhizin (Mollica, De Marchis et al. 2007) (**Fig. 9a**). We now obtained initial indications that treating either yeast or human cells with this HMGB1 antagonist is sufficient to decrease histone levels in a dose dependent manner (**Fig. 9b-e**). Together with Andrew Seeber and Susan Gasser, I now plan to move on with expanding our previous work from yeast to human cells and test whether more accessible DNA increases the efficiency of CRISPR-Cas9 gene editing.

As mentioned in the introduction, the Neefjes laboratory showed that the chemotherapeutic agent doxorubicin caused histone eviction from open chromatin and contributed to chemotherapeutic effects (Pang, Qiao et al. 2013). Similar to HMGB1, doxorubicin binds to the minor groove of DNA (Frederick, Williams et al. 1990) where it is likely to compete for histone binding (Pang, Qiao et al. 2013). This raises

the idea of testing small molecules which can sterically antagonize HMGB1 in chemotherapeutic combination treatments.

Last, but not least, it should not be forgotten, that controlled histone proteolysis has additional roles in a variety of cellular processes including developmental transitions, spermatogenesis, the immune response and neuronal plasticity (Maze, Wenderski et al. 2015). An interesting article by Dhaenens et recently summarized these facts and put an end to the "step-motherly fashion" by which histone proteolysis had "consistently been treated by the scientific community" (Dhaenens, Glibert et al. 2015).

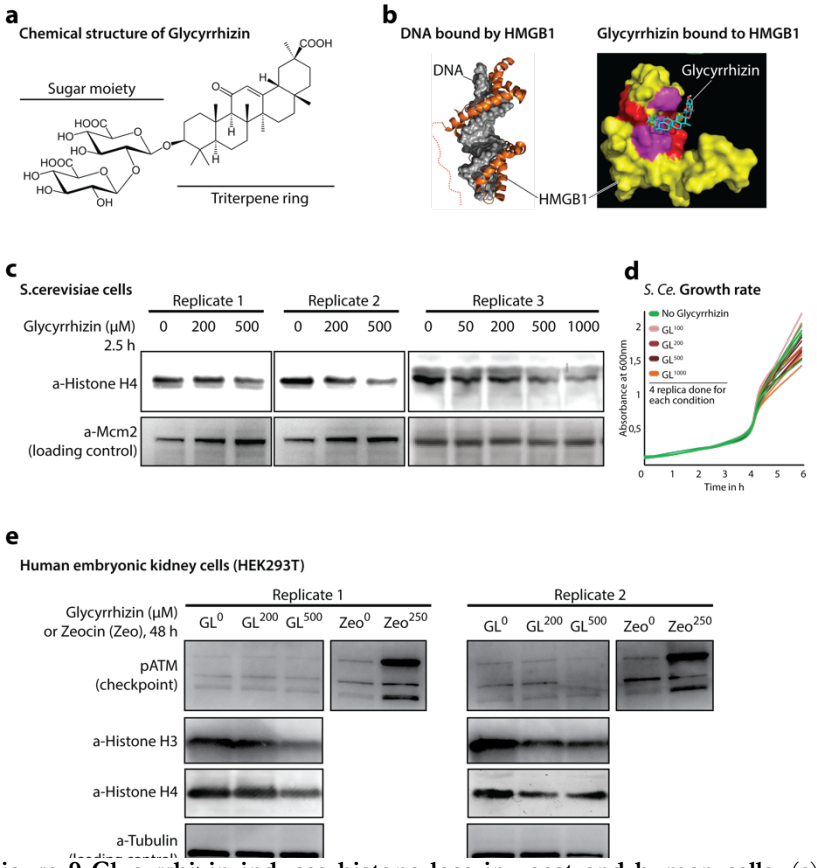

Figure 9 Glycyrrhizin induces histone loss in yeast and human cells. (**a**) Structure of HMGB1 antagonist, Glycyrrhizin, showing the sugar moiety and the triterpene ring. (**b**) HMGB1 binds to the minor groove of DNA. Molecular modelling indicates that the triterpene ring is important for antagonism of HMGB1 (Mollica, De Marchis et al. 2007). (**c**) Immunoblot blot of whole protein content extracted from S. cerevisiae cells after treatment with Glycyrrhizin. (**d**) Groth curve of WT yeast treated with increasing amounts of Glycyrrhizin. No change is seen upon Glycyrrhizin treatment. (**e**) Immunoblots showing H3 and H4 levels in whole cell extracts from HEK293T cells treated with increasing concentrations of Glycyrrhizin dissolved in DMSO or DMSO alone. Interestingly, no checkpoint activation is seen in response to Glycyrrhizin treatment (pATM).

References

Amitai, A., A. Seeber, S. M. Gasser and D. Holcman (2017). "Visualization of Chromatin Decompaction and Break Site Extrusion as Predicted by Statistical Polymer Modeling of Single-Locus Trajectories." Cell Rep **18**(5): 1200-1214.

Bonilla, C. Y., J. A. Melo and D. P. Toczyski (2008). "Colocalization of sensors is sufficient to activate the DNA damage checkpoint in the absence of damage." Mol Cell **30**(3): 267-276.

Bouck, D. C. and K. Bloom (2007). "Pericentric chromatin is an elastic component of the mitotic spindle." Curr Biol **17**(9): 741-748.

Bystricky, K., P. Heun, L. Gehlen, J. Langowski and S. M. Gasser (2004). "Long-range compaction and flexibility of interphase chromatin in budding yeast analyzed by high-resolution imaging techniques." Proc Natl Acad Sci U S A **101**(47): 16495-16500.

Celona, B., A. Weiner, F. Di Felice, F. M. Mancuso, E. Cesarini, R. L. Rossi, L. Gregory, D. Baban, G. Rossetti, P. Grianti, M. Pagani, T. Bonaldi, J. Ragoussis, N. Friedman, G. Camilloni, M. E. Bianchi and A. Agresti (2011). "Substantial histone reduction modulates genomewide nucleosomal occupancy and global transcriptional output." PLoS Biol **9**(6): e1001086.

Chu, V. T., T. Weber, B. Wefers, W. Wurst, S. Sander, K. Rajewsky and R. Kuhn (2015). "Increasing the efficiency of homology-directed repair for CRISPR-Cas9-induced precise gene editing in mammalian cells." Nat Biotechnol **33**(5): 543-548.

Dhaenens, M., P. Glibert, P. Meert, L. Vossaert and D. Deforce (2015). "Histone proteolysis: a proposal for categorization into 'clipping' and 'degradation'." Bioessays **37**(1): 70-79.

Frederick, C. A., L. D. Williams, G. Ughetto, G. A. van der Marel, J. H. van Boom, A. Rich and A. H. Wang (1990). "Structural comparison of anticancer drug-DNA complexes: adriamycin and daunomycin." Biochemistry **29**(10): 2538-2549.

Horlbeck, M. A., L. B. Witkowsky, B. Guglielmi, J. M. Replogle, L. A. Gilbert, J. E. Villalta, S. E. Torigoe, R. Tjian and J. S. Weissman (2016). "Nucleosomes impede Cas9 access to DNA in vivo and in vitro." Elife **5**: e12677.

Isaac, R. S., F. Jiang, J. A. Doudna, W. A. Lim, G. J. Narlikar and R. Almeida (2016). "Nucleosome breathing and remodeling constrain CRISPR-Cas9 function." Elife **5**: e13450.

Jinek, M., A. East, A. Cheng, S. Lin, E. Ma and J. Doudna (2013). "RNA-programmed genome editing in human cells." elife **2**: e00471.

Kustatscher, G., N. Hegarat, K. L. Wills, C. Furlan, J. C. Bukowski-Wills, H. Hochegger and J. Rappsilber (2014). "Proteomics of a fuzzy organelle: interphase chromatin." EMBO J **33**(6): 648-664.

Lafon, A., S. Taranum, F. Pietrocola, F. Dingli, D. Loew, S. Brahma, B. Bartholomew and M. Papamichos-Chronakis (2015). "INO80 Chromatin Remodeler Facilitates Release of RNA Polymerase II from Chromatin for Ubiquitin-Mediated Proteasomal Degradation." Mol Cell **60**(5): 784-796.

Malarkey, C. S. and M. E. Churchill (2012). "The high mobility group box: the ultimate utility player of a cell." Trends Biochem Sci **37**(12): 553-562.

Mali, P., L. Yang, K. M. Esvelt, J. Aach, M. Guell, J. E. DiCarlo, J. E. Norville and G. M. Church (2013). "RNA-guided human genome engineering via Cas9." Science **339**(6121): 823-826.

Maruyama, T., S. K. Dougan, M. C. Truttmann, A. M. Bilate, J. R. Ingram and H. L. Ploegh (2015). "Increasing the efficiency of precise genome editing with CRISPR-Cas9 by inhibition of nonhomologous end joining." Nature biotechnology **33**(5): 538-542.

Maze, I., W. Wenderski, K. M. Noh, R. C. Bagot, N. Tzavaras, I. Purushothaman, S. J. Elsasser, Y. Guo, C. Ionete, Y. L. Hurd, C. A. Tamminga, T. Halene, L. Farrelly, A. A. Soshnev, D. Wen, S. Rafii, M. R. Birtwistle, S. Akbarian, B. A. Buchholz, R. D. Blitzer, E. J. Nestler, Z. F. Yuan, B. A. Garcia, L. Shen, H. Molina and C. D. Allis (2015). "Critical Role of Histone Turnover in Neuronal Transcription and Plasticity." Neuron **87**(1): 77-94.

Mollica, L., F. De Marchis, A. Spitaleri, C. Dallacosta, D. Pennacchini, M. Zamai, A. Agresti, L. Trisciuoglio, G. Musco and M. E. Bianchi (2007). "Glycyrrhizin binds to high-mobility group box 1 protein and inhibits its cytokine activities." Chemistry & biology **14**(4): 431-441.

Morrison, A. J., J. A. Kim, M. D. Person, J. Highland, J. Xiao, T. S. Wehr, S. Hensley, Y. Bao, J. Shen, S. R. Collins, J. S. Weissman, J. Delrow, N. J. Krogan, J. E. Haber and X. Shen (2007). "Mec1/Tel1 phosphorylation of the INO80 chromatin remodeling complex influences DNA damage checkpoint responses." Cell **130**(3): 499-511.

Pang, B., X. Qiao, L. Janssen, A. Velds, T. Groothuis, R. Kerkhoven, M. Nieuwland, H. Ovaa, S. Rottenberg, O. van Tellingen, J. Janssen, P. Huijgens, W. Zwart and J. Neefjes (2013). "Drug-induced histone eviction from open chromatin contributes to the chemotherapeutic effects of doxorubicin." Nat Commun **4**: 1908.

Poli, J., C. B. Gerhold, A. Tosi, N. Hustedt, A. Seeber, R. Sack, F. Herzog, P. Pasero, K. Shimada, K. P. Hopfner and S. M. Gasser (2016). "Mec1, INO80, and the PAF1 complex cooperate to limit transcription replication conflicts through RNAPII removal during replication stress." Genes Dev **30**(3): 337-354.

Saad, H., F. Gallardo, M. Dalvai, N. Tanguy-le-Gac, D. Lane and K. Bystricky (2014). "DNA dynamics during early double-strand break processing revealed by non-intrusive imaging of living cells." PLoS Genet **10**(3): e1004187.

Singh, R. K., M. Gonzalez, M. H. Kabbaj and A. Gunjan (2012). "Novel E3 ubiquitin ligases that regulate histone protein levels in the budding yeast Saccharomyces cerevisiae." PLoS One **7**(5): e36295.

Singh, R. K., M. H. Kabbaj, J. Paik and A. Gunjan (2009). "Histone levels are regulated by phosphorylation and ubiquitylation-dependent proteolysis." Nat Cell Biol **11**(8): 925-933.

Strecker, J., G. D. Gupta, W. Zhang, M. Bashkurov, M. C. Landry, L. Pelletier and D. Durocher (2016). "DNA damage signalling targets the kinetochore to promote chromatin mobility." Nat Cell Biol **18**(3): 281-290.

Verdaasdonk, J. S., P. A. Vasquez, R. M. Barry, T. Barry, S. Goodwin, M. G. Forest and K. Bloom (2013). "Centromere tethering confines chromosome domains." Mol Cell **52**(6): 819-831.

Wang, H., H. Yang, C. S. Shivalila, M. M. Dawlaty, A. W. Cheng, F. Zhang and R. Jaenisch (2013). "One-step generation of mice carrying mutations in multiple genes by CRISPR/Cas-mediated genome engineering." Cell **153**(4): 910-918.

APPENDICES

List of abbreviations

53BP1: p53 binding protein 1, a critical DSB repair protein that antagonizes DNA end resection to promote repair by non-homologous end joining and plays a critical role in the DNA damage checkpoint

alt-NHEJ: alternative non-homologous end joining, a mutagenic pathway in which previously resected DNA ends are ligated together, also called microhomology-mediated NHEJ (MM-NHEJ)

ATR: ataxia telangiectasia and Rad3-related protein, a critical protein kinase in the DNA damage response pathway. Mec1 in *S. cerevisiae.*

D-loop: displacement loop, the DNA structure caused by strand invasion that displaces one strand of the duplex DNA that serves as the template for HR

DSB: DNA double-strand break, a DNA lesion in which both strands of DNA are broken

HC: heterochromatin, highly condensed, and predominantly repetitive and transcriptionally repressed chromatin region that reside at the nuclear periphery and/or in intranuclear depots.

HP1: heterochromatin protein 1, a chromodomain-containing protein that associates with heterochromatin

HR: homologous recombination, a major pathway of DSB repair that requires a homologous template

IR: ionizing radiation consisting of particles, X-rays, or gamma rays with sufficient energy to cause ionization in the medium through which it passes.

KASH: Klarsicht/Anc-1/Syne1 homology, a family of orthologous tail-anchored outer nuclear membrane proteins that make up the cytoplasmic aspect of the LINC complex

LINC complex: linker of nucleoskeleton and cytoskeleton, a complex of inner nuclear membrane SUN proteins and outer nuclear membrane KASH proteins that spans the nuclear envelope

LOH: loss of heterozygosity

MRX(N): Mre11-Rad50-Xrs2 (Nbs1 in mammals) complex, important for DSB repair and stabilization of stalled replication forks

MSD: mean squared displacement

NHEJ: non-homologous end joining, a major pathway of DSB repair that involves direct ligation of the DSB

NPC: nuclear pore complex, the massive protein complex that stabilizes nuclear pores and controls the bidirectional traffic of macromolecules in and out of the nucleus

NORs: nucleolar organization regions, the regions of the genome that give rise to nucleoli, later established as being the rDNA

OB fold: oligonucleotide binding fold.

rDNA: ribosomal DNA, the repetitive region of the genome that is composed of repeats of the genes encoding the ribosomal rRNA subunits. It resides in the nucleolus

R-loops: an R-loop is a three-stranded nucleic acid structure, composed of a DNA:RNA hybrid and the associated non-template single-stranded DNA (ssDNA).

rRNA: the RNAs produced from the rDNA that make up the bulk of the ribosomes

RPA: replication protein A, a trimeric (Rfa1,2,3) complex that binds ssDNA, coating it during replication and DNA repair and acting as a major protein recruitment scaffold

SDSA: synthesis-dependent strand annealing, a template-dependent repair mechanism that proceeds without Holliday junction intermediates and leads to non-crossover products

SMC5/6: a cohesin-related protein complex important for genome integrity, linked to SUMOylation activity

SSA: single-strand annealing, a template-independent (but homology-dependent) repair mechanism in which the copy number of tandem repeats can be reduced after DSB resection

ssDNA: single strand DNA

STUbL: SUMO-targeted ubiquitin ligase, a family of proteins that induce ubiquitination of target proteins and require prior SUMOylation

SUMO: small ubiquitin-like modifier, a small protein that can be conjugated to lysine residues on target proteins

SUN: Sad1/Unc84, a family of orthologous integral inner nuclear membrane proteins that make up the nuclear aspect of the LINC complex

TRF2: telomere repeat (binding) factor, a component of the shelterin complex that protects chromosome ends

Non-thesis related contributions

This is a summary of contributions that I made during my PhD to other bodies of work not directly related to my thesis. Where necessary I state my contribution.

Peer-reviewed Publications

Horigome, C., Y. Oma, T. Konishi, R. Schmid, I. Marcomini, **M. H. Hauer**, V. Dion, M. Harata and S. M. Gasser (2014). "SWR1 and INO80 chromatin remodelers contribute to DNA double-strand break perinuclear anchorage site choice." Mol Cell 55(4): 626-639.

Horigome showed that the Htz1 incorporation by SWR1 shifts DSBs to the nuclear periphery. In this work, I was investigating whether direct SWR1 targeting via Arp6-LexA fusion proteins would impact chromatin mobility (Fig. 4).

Jinek, M., F. Jiang, D. W. Taylor, S. H. Sternberg, E. Kaya, E. Ma, C. Anders, **M. Hauer**, K. Zhou and S. Lin (2014). "Structures of Cas9 endonucleases reveal RNA-mediated conformational activation." Science 343(6176): 1247997.

Jinek, M., K. Chylinski, I. Fonfara, **M. Hauer**, J. A. Doudna and E. Charpentier (2012). "A programmable dual-RNA–guided DNA endonuclease in adaptive bacterial immunity." Science 337(6096): 816-821.

Before I joined Susan Gasser's laboratory, I was working together with Martin Jinek (now Prof. at the University of Zuerich, Switzerland) in Jennifer Doudnas lab in Berkeley (in 2011). During this time, I initiated the biochemical characterization and crystallization of the Cas9 protein (at that time called Csn1) which is now used in the CRISPR/Cas9 genome editing system.

Patent

"Methods for increasing the frequency of gene targeting by chromatin modification"

Inventors: Hauer, M., **Seeber, A**. and Gasser, S.M.,

ACKNOWLEDGEMENTS

First of all, I want to thank Susan Gasser for the guidance and the support throughout my time in her laboratory. I have learned a lot! I am grateful for the fruitful discussions in each of my PhD committee meetings and want to thank all members of my committee. Tom Owen-Hughes (my co-referee), Carl Wu, Dirk Schübeler and Kenji Shimada. I especially thank Tom and Vijender Sighn for our collaboration and the dedication in pushing my project forward. I also thank Nancy Hynes for chairing my PhD thesis defense. Many thanks also go to my external collaborators David Holcman and Assaf Amitai.

During my time as a PhD student in Susan Gasser's laboratory, I was working together with a lot of very talented and helpful colleagues. The beginning of my PhD studies would have been a lot rougher without Vincent Dion and Helder Ferreira. I thank you both for the guidance, tips, tricks and discussions. A big "thank you" also goes to Andrew Seeber. We collaborated closely, discussed regularly, climbed to the highs, fell to the downs and will be tied to each other for some more time in the future. Thanks Andrew. Especial thanks also go to Mariya Kryzhanovska, an unusually talented master student.

I want to express my gratitude to Monika Tsai, Veronique Kalck and Razel Arpagaus. Without your support, my PhD would have probably been twice as long. Many thanks also go to the whole Gasser Laboratory – past and current. Without you guys, daily work, coffee breaks and all the other things would not have been the same.

The FMI microscopy and the FMI protein analysis facilities have been essential to my PhD research. Without the help, input and experience of Laurent Gelman, Steve Bourke, Ragna Sack, Jan Seebacher and Daniel Hess, it would have been a lot more difficult or even impossible to pursue the questions I was asking. Especial, image-analysis-thank-you-very-muches go to Raphael Thierry and Jan Eglinger. I want to thank all the other groups in the FMI for supplying me with advice and material.

Finally, and saving the most important "thank-you's" and hugs for last: Thank you Jenia & Leo. Thank you for your love, the support and the strength I find in the both of you (soon the three of you). I am grateful for the constant support from my parents Monika and Hermann.